TABLE OF CONTENTS

Page

LIST OF TABLES

Page

LIST OF FIGURES

Page

LIST OF ABBREVIATIONS

AC	Adaptive Control
ADMIRE	Aero Data Model In Research Environment
AFTC	Active Fault-Tolerant Control
AFTI	Advanced Fighter Technology Integration
ASIR	Aviation Safety Investigation Report
ASMC	Adaptive Sliding Mode Control
AVIO	Avionic
CRIAQ	Consortium for Research and Innovation in Aerospace in Quebec
CA	Control Allocation
CG	Center of Gravity
cos	Cosines
deg	Degree
DI	Dynamic Inversion
DOF	Degree Of Liberty
EA	Eigenstructure Assignment
ECEF	Earth Centered Earth Fixed
EFM-AG	European Flight Mechanism - Action Group
EKF	Extended Kalman Filter
EMMAE	Extended Multiple Model Adaptive Estimation
ERL	Exponential Reaching Law
FBW	Fly-By-Wire
FCC	Flight Control Computer

FC	Flight Control
FDD	Fault Detection and Diagnosis
FDI	Fault Detection and Isolation
FlightGear	Flight software simulator
FPGA	Field Programmable Gate Array
FT	Foot/Feet
FTC	Fault-Tolerant Control
FTFC	Fault-Tolerant Flight Control
GARTEUR	Group for Aeronautical Research and Technology in Europe
GRÉPCI	Group for Power Electronics and Industrial Control
GUI	Graphical User Interface
IFAC	International Federation of Automatic Control- Secretariat
IP Core	Intellectual Property Core
IRM	International Reference Meridian
KF	Kalman Filter
Kg	Kilogram
lb	Pound
LASSENA	Laboratory of Space, Embedded Systems, Navigation and Avionics
LLA	Longitude Latitude Altitude
LQR	Linear-Quadratic Regulator
MATLAB	Matrix Laboratory
MethoRad	Methodology Radiation
MBU	Multiple-Bit Upset

MDA	MacDonald, Dettwiler and Associates Ltd
MITACS	Mathematics of Information Technology and Complex Systems
MMC	Multiple Model Control
MMST	Multiple Model Switching and Tuning
MPC	Model Predictive Control
MR	Mechanism of Reconfiguration
MRAC	Model Reference Adaptive Control
ms	Millisecond
N	Newton
N-M	Newton-Meter
NASA	National Aeronautics and Space Administration
NDI	Nonlinear Dynamic Inversion
NED	North East Down
NTSB	National Transportation Safety Board
NSERC	Natural Sciences and Engineering Research Council of Canada
PFTC	Passive Fault-Tolerant Control
PIM	Pseudo-Inverse Method
rad	Radian
RC	Reconfigurable Control
REF	Reference
RFC	Reconfigurable Flight Control
RSMC	Reconfigurable Sliding Mode Control
s	Second

SEE	Single Event Effect
SEM	Soft Error Mitigation
SET	Single Event Transient
SEU	Single Event Upset
Sign	Signe
sin	Sine
SIMULINK	Simulation and Model-Based Design
SMC	Sliding Mode Control
SRAM	Static Random Access Memory
SWAP	Space, Weight and Power
tan	Tangent
UART	Universal Asynchronous Receiver Transmitter
UAV	Unmanned aerial vehicle
US	United States
USSR	Union of Soviet Socialist Republics
VSC	Variable Structure Control
VTOL	Vertical Take-Off Landing
XILINX	American Technology Company
XILINX-ISE	Integrated Synthesis Environment

LIST OF SYMBOLS AND UNITS OF MEASUREMENTS

A_{proj}	Geometric approach matrix
$\bar{A}_{proj}$	Modified geometric approach matrix
A^{i}_{proj}	Geometric approach matrix associated to the i^{th} possible output set
A, A_{lat}, A_{long}	Linear dynamic matrices
a (m)	Earth equatorial axis dimension
b (m)	Earth vertical axis dimension
B, B_{lat}, B_{long}	Linear input matrices
$B_{0,i}$	Modified linear input matrix
b_i	Column i of the linear input matrix
b (ft or m)	Wing span
C	Linear output matrix
C_Y	Coefficients inducing a force along the y axis
C_{Y_i} (rad^{-1} or deg^{-1})	C_Y coefficient derivative with respect to i
C_L, C_D	Lift and drag coefficients
C_{L_0}, C_{D_0}(rad^{-1} or deg^{-1})	Lift and drag reference coefficients
C_{L_i} (rad^{-1} or deg^{-1})	Lift coefficient derivative with respect to i
C_{D_i} (rad^{-1} or deg^{-1})	Drag coefficient derivative with respect to i
C_l, C_m, C_n	Rolling, pitching and yawing moments coefficients
C_{l_i} (rad^{-1} or deg^{-1})	Rolling moment coefficient derivative with respect to i
C_{m_i} (rad^{-1} or deg^{-1})	Pitching moment coefficient derivative with respect to i
C_{n_i} (rad^{-1} or deg^{-1})	Yawing moment coefficient derivative with respect to i

$\bar{c}$ (ft or m)	Wing mean aerodynamic chord
e	Eccentricity
EKF_i	The i^{th} Extended Kalman Filter
$f(x)$	Nonlinear dynamic function
F	Fault parameter matrix
F_A (N)	Aerodynamic forces
F_X, F_Y, F_Z (N)	Aerodynamic forces in the x, y, z direction of $\mathcal{F}_B$
F_g (N)	Force of gravitation
F_L, F_D (N)	Lift and drag forces
F_M	The linear map
F_i	$\frac{\partial f(x)}{\partial x}$ evaluated at sample time $t = iT_s$
$\mathcal{F}_I$	Inertial reference frame
$\mathcal{F}_N$	Navigation reference frame
$\mathcal{F}_B$	Fixed-body reference frame
$\mathcal{F}_W$	Wind reference frame
g (ft/s^2 or m/s^2)	Gravitational acceleration
$g(x)$	Nonlinear input function
$\overline{g}$	Modified nonlinear input function
G_i	$\frac{\partial g(x)}{\partial x}$ evaluated at sample time $t = iT_s$
G	Set of augmented dummy inputs
H_i	$\frac{\partial h(x)}{\partial x}$ evaluated at sample time $t = iT_s$
h (ft or m)	Altitude

$h(x)$	Nonlinear output function
i, j, k	Positive integer numbers
i_h(rad or deg)	Horizontal stabilizer incidence angle
$I_{m\times m}$	Identity matrix of size $(m \times m)$
I_x (Kg-m^2)	x direction inertia
I_y (Kg-m^2)	y direction inertia
I_z (Kg-m^2)	z direction inertia
I_{xz} (Kg.m^2)	xz direction inertia
K	Positive gain of the Sliding Mode Controller
K_{EKF_i}	Matrix gain of the i^{th} EKF
$ker\ C$	The kernel function of C
$L_{f(x)}^{r_i-1} h_i(x)$	Lie Derivative
M (N-m)	Pitching moment
Mac	Flight Mach number
m (lbs or Kg)	Mass
m	Input vector size
n	State vector size
$\mathbb{N}$	Set of integer numbers
ox, oy, oz	Longitudinal, lateral and vertical body axis
p	Output vector size
p, q, r (rad/s or deg/s)	Roll, pitch and yaw rates
$P_{i/i}$	The updated error covariance matrix

XXX

$P_{i/i-1}$	The last predicted state error covariance matrix
$P_{0/-1}$	The initial state error covariance matrix
$P_{i+1/i}$	The predicted state error covariance matrix
p_i	The conditional probability of the i^{th} fault scenario
p_{nf}	The conditional probability of no fault scenario
$\bar{q}$ (lb/ft^2 or N/m^2)	Dynamic pressure
R_{W_i}	The discrete matrix of the process noise $\eta_w(t)$
R_i	The residual covariance matrix computed using the i^{th} EKF
R_w	Process noise covariance matrix
R_v	Measurement noise covariance matrix
$\lvert R_{i,t} \rvert$	The determinant R_i calculated using the i^{th} EKF at the time step t
$\{r_i\}$	Set of derivative degrees
$r_{i,t}$	The residual signal generated by the i^{th} EKF at the time step t
r_{nf}	The residual signal generated by the no fault scenario EKF
$\mathbb{R}$	Set of real numbers
$\mathcal{R}(B)$	The column space (range space) of B
R_N^I	Transformation matrix from $\mathcal{F}_I$ to $\mathcal{F}_N$
R_B^N	Transformation matrix from $\mathcal{F}_N$ to $\mathcal{F}_B$
R_B^W	Transformation matrix from $\mathcal{F}_W$ to $\mathcal{F}_B$
$s(x,t)$	The sliding vector
$\dot{s}(x,t)$	Time derivate of the sliding vector
S	Sliding surface

S_b	Sub-manifold surface
S_b^i	Sub-manifold surface for the i^{th} possible output set
S_w (ft^2 or m^2)	Total wing area
T_s (s)	Sampling time
t (s)	Time
t_f (s)	Fault occurrence time
t_i (s)	Time evaluated at iT_s
t_{reach} (s)	The time required to reach the sliding surface
$u(t)$ (rad or deg)	Controller output vector
$\hat{u}_{f_{long}}$ (rad or deg)	Estimated faulty longitudinal controller output vector
$\hat{u}_{f_i}$ (rad or deg)	Estimated faulty controller output vector using the i^{th} EKF
$\dot{u}_f^i(t)$	Time derivate of the reconstructed faulty controller output using Π^i
$\bar{u}_i(t)$ (rad or deg)	Fault occurring on the i^{th} actuator
$\bar{u}_k$ (rad or deg)	Fault occurring on the k^{th} actuator
u_{f_i} (rad or deg)	Reconstructed faulty inputs for the i^{th} actuator
$u_{f_{lat}}$ (rad or deg)	Reconstructed faulty inputs for lateral actuators
$u_{f_{long}}$ (rad or deg)	Reconstructed faulty inputs for longitudinal actuators
$\bar{u}$ (rad or deg)	Actuator fault vector
$\hat{\bar{u}}$ (rad or deg)	Reconstructed actuator fault vector
u_{disc} (rad or deg)	Discrete SMC output
u_{eq} (rad or deg)	Continuous SMC output
$u_f(t)$ (rad or deg)	Faulty input vector

$\hat{u}_f(t)$ (rad or deg)	Reconstructed faulty input vector
$\hat{u}_f^i(t)$ (rad or deg)	Reconstructed faulty input vector using the sub-projector $\Pi^i(x)$
$\hat{u}_f^k(t)$ (rad or deg)	Set of k reconstructed faulty input vectors $u_f^i(t)$
u_i (rad or deg)	u evaluated at $t = iT_s$
$U(t)$ (rad or deg)	Reconfigured SMC output vector
V_L	Lyapunov function candidate
V_T (ft/sec)	Trim velocity
V(ft/s or m/s)	Forward velocity vector
V_{x_0}(ft/s or m/s)	Reference flight speed in the x direction
W (lb)	Weight
$x(t)$	State vector
$x^{(n)}$	(n) order time derivate of the state vector
$\dot{x}(t)$	First order time derivate of the state vector
$\hat{x}(t)$	Estimated state vector
$\tilde{x}(t)$	Tracking error vector
$x_d(t)$	Desired state vector
$\dot{x}_d(t)$	First order time derivate of the desired state vector
$\hat{x}_i$	Estimated state vector using EKF number i
$\dot{x}^i(t)$	Time derivate of the reconstructed state vector using Π^i
$\hat{x}_{i/i}$	The updated estimate state vector
$\hat{x}_{i/i-1}$	The last extrapolated state estimate
$\hat{x}_{0/-1}$	The initial state estimate vector

$\hat{x}_{i+1/i}$	The predicted state estimate vector
$\hat{x}_{nf}$	The state estimate vector for no fault scenario
x_N (m)	North position
x_E (m)	East position
x_D (m)	Down position (Altitude)
X_i, Z_i, M_i	Longitudinal aerodynamic coefficients
Y_i, L_i, N_i	Lateral aerodynamic coefficients
$y(t)$	Output vector
$\dot{y}(t)$	Time derivate of the output vector
y_i	y evaluated at time $t = iT_s$
$\dot{y}^i(t)$	Time derivate of the reconstructed output vector using Π^i
Y_t	Set of previous output vectors y_i
z_i	Augmented state vector
$\nabla\sigma^T$	Gradient of the σ^T matrix
$\nabla{\sigma^T}^i$	Gradient of the σ^T matrix using the sub-projector Π^i
$(\cdot)^{-1}$	Inverse
$(\cdot)^*$	Pseudo-inverse
$(\cdot)^T$	Transpose
T, δ_{Th} (lb or N)	Engine thrust
δ_{LTh} (lb or N)	Left engine thrust
δ_{RTh} (lb or N)	Right engine thrust
$\hat{\delta}_{LTh}$ (lb or N)	Estimated left engine thrust

$\hat{\delta}_{RTh}$ (lb or N)	Estimated right engine thrust
δ_a (rad or deg)	Aileron deflection
$\hat{\delta}_a$ (rad or deg)	Estimated aileron deflection
$\dot{\delta}_a$	Time derivate of the aileron deflection
$\hat{\delta}_e$ (rad or deg)	Estimated elevator deflection
$\hat{\delta}_r$ (rad or deg)	Estimated rudder deflection
$\dot{\delta}_r$	Time derivate of the rudder deflection
α_T (rad or deg)	Trim angle of attack
δ_c (rad or deg)	Canards deflections
δ_{eL} (rad or deg)	Left elevator deflection
δ_{eR} (rad or deg)	Right elevator deflection
δ_{fL} (rad or deg)	Left flaperon deflection
δ_{fR} (rad or deg)	Right flaperon deflection
δ_r (rad or deg)	Rudder deflection
$\eta_v(t)$	Measurements white noise
$\eta_w(t)$	Process white noise
$\Pi^i(x)$	Geometric sub-projector associated to the i^{th} possible output set
ϕ_i	Discrete transition matrix evaluated at $t = iT_s$
$\frac{\partial f(x)}{\partial x}$	Partial derivate of $f(x)$ respect to $x(t)$
α (rad or deg)	Angle of attack
β (rad or deg)	Sideslip angle
η	Positive real number

λ	Positive real number
$\Pi(x)$	Geometric projector
$\Pi^i(x)$	Geometric sub-projector using the possible set output i
σ (rad or deg)	White noise deviation
φ, θ, ψ (rad or deg)	Roll, pitch and yaw angles
Ω (rad/s or deg/s)	Angular velocity vector
μ (rad or deg)	Latitude
γ (rad or deg)	Longitude
ε	The boundary layer thickness
$\mathcal{W} \subseteq \mathbb{R}^n$	Largest controlled-invariant subspace

INTRODUCTION

Conventional flight controller scheme has been evolved from simple feedback structures in which unexpected scenarios - such as actuator faults, failures, and malfunctions occurring suddenly during the flight - are not generally considered. These scenarios can be introduced by design errors, wrong operation or components aging. They are the initial event which can dramatically change the configuration of the aircraft and may cause severe performance degradation. Furthermore, they can even cause a loss of control leading to a catastrophic instability and result in an unfortunate loss of human lives (Noura et al., 2009).

As the maintenance or repair cannot be achieved immediately in avionic systems, it is required to design more sophisticated and more advanced strategies issues capable of maintaining nominal performance, reducing the risks and increasing the survivability of the aircraft in the presence of such scenarios. Furthermore, these strategies must include the important safety technologies to allow the aircraft to preserve stability, to execute a safety landing and to save passengers' lives.

The challenge of ensuring and improving the required safety levels for aircraft survivability and reducing the risks that critical failures occur has motivated the development of two principal strategies during the last few decades. The first one is known as the hardware redundancy. It is a strategy in which critical components are doubled, tripled or even quadrupled. Then, a selected algorithm is used to determine the correct output value by comparing the redundant outputs. The majority voting approach is one of them and it is widely used in such situation (Danecek et Silhavy, 2011). However, these strategies lead to extra weight and costs thus affecting the overall space, weight and power of the avionic system (Alwi, Edwards et Tan, 2011).

The second one is known as the analytical redundancy and it consists of the design of a modern avionic control system able to adapt to such sudden faults and preserve the stability and the maneuverability of the aircraft for continued safe fly while keeping avionics systems

lighter and less expensive. This can be achieved by a smart control law design, taking into account a unique combination of detection and diagnosis faults/failures and real-time control reconfiguration (Tomayko et Gelzer, 2003). This strategy is widely known in the literature as Fault-Tolerant Control (FTC) systems.

The FTC system can be designed either using passive or active schemes (Christopher, Thomas et Hafid, 2010). Passive schemes are based on a robust control which can operate independently of any fault information. These kinds of schemes do not require reconfiguration or adaptation, but they are expected to be insensitive to some known faults. Although such techniques are simple and less complex, they are not efficient in the presence of worst fault cases as unknown and abrupt faults. In addition, aircraft performance will be degraded even in the no-fault situation. However, active schemes, which are the subject of this thesis, differ from those passive. They are more adaptive for real situations and represent a more advantageous and flexible architecture. Unlike in the case of passive schemes, all the faults that may affect the aircraft cannot be known a priori in real situations. Furthermore, they are designed based on explicit faults' parameters generated by a so-called Fault Detection and Diagnosis (FDD) process and an online Reconfigurable Controller (RC).

The FDD process, known also in the literature as Fault Detection and Isolation (FDI), deals with various kinds of faults. Based on sensors' measurements data and controller outputs, the FDD process generates correct information on the faulty system behavior, on the degradations produced by the fault and on the performance of the degraded system. Then, a so-called Mechanism of Reconfiguration (MR) makes a decision about when and how a reconfiguration action should be taken. The RC is then designed based on the explicit information generated from the FDD process, by adjusting and reconfiguring the controller parameters already designed. The new reconfigurable control then allows real-time compensation of the fault effect which results in avoiding the loss of control, preserving aircraft dynamics and stability and so maintaining nominal performances.

Motivation for Fault-Tolerant Control Systems

The comfort and the safety of passengers were and still are the important requirements in the commercial aircraft industry. However, the loss of aircraft control during a flight is considered among the most important occurrences and involve the most fatalities and disasters in civil aviation history (Kinnersley et Roelen, 2007). Avoiding loss of control, preserving stability and maintaining nominal performances are then considered three of the most important motivating factors for the design of FTC systems. Since aircraft dynamics, control and stability are totally based on critical components so-called control surfaces such as ailerons, elevators and rudders, the behaviour of these components must be supervised at each time.

One of the main reasons leading to loss of control of aircraft is the totally or partially operational failure of one or more of actuators that act on these control surfaces. In 1977, on the Delta flight 1080, captain Jack Mc Mahan has successfully landed his aircraft, despite his left elevator's actuator was stuck at 19 degrees (Abzug et Larrabee, 2005). This event prompted the National Aeronautics and Space Administration (NASA) in 1982 to trigger the first funding program work on possible methods that can be applied in real time to compensate for such faults and therefore preserve stability and maintain nominal performance in such a situation (Montoya et al., 1983). These methods are to be basically able to ensure two requirements: a better quality of behavior of the aircraft under normal conditions and survivability of the aircraft with acceptable performance in the presence of actuators' faults.

Captain Jack Mc Mahan was not the unique example who avoided disaster. There are other pilots who have successfully landed theirs crippled aircrafts such as the DC-10 of the flight 232 in Sioux City, Iowa 1989 (Barnett, Menighetti et Prete, 1992), the Boeing 747-132 of Kalita air freighter in Detroit, Michigan on October 2004 (Smaili et al., 2006) and the Airbus A300B4-203F DHL freighter in Baghdad on November 2003 (Lemaignan, 2005). These events convince that in such cases, the faulty aircraft is still maneuverable. Unfortunately, it

does not always finish as good as well. Indeed, on September 8, 1994, 133 people were dead in an aircraft crash when a rudder's actuator fault occurred in the Boeing 737 of US air flight 427 (Benoit et Czerwinski, 1997). On February 16, 2000, a McDonnell Douglas DC-8-71F lost its elevator's actuator on takeoff, resulting in a crash and the three flight crew members were dead (NTSB/AAR-03/02, 2003). The last example is a crash on January 8, 2003, of the Beechcraft 1900D aircraft of US airways express flight 5481. 19 passengers and 2 pilots aboard were dead. The reason was a failure in elevator's actuator (NTSB/AAR-04/01, 2004). A list of aviation accidents and incidents which occurred between 1994 and 2001 are briefly described by (Kinnersley et Roelen, 2007).

These series of events have attracted the interest of many researchers worldwide, and several programs have been created on the topic of fault-tolerant control. Among others, the most important are the US Air Force program begun in mid-1980s (Eslinger et Chandler, 1988) and the European Flight Mechanics Action Group (EFM-AG) on FTC, established in 2004 under the Group for Aeronautical Research and Technology in Europe (GARTEUR) (Christopher, Thomas et Hafid, 2010), where several control techniques based on dynamic models, capable of detecting and diagnosing the effects of external faults and disturbances have been developed and various interesting bibliographical reviews and books have been published on the topic of FTC systems.

Problem Statement

From the above motivation, the objective of this thesis is to develop an Active Fault-Tolerant Controller (AFTC) that can preserve the stability and maintain the desired performances of the aircraft in the presence of simple and simultaneous actuators' faults without degrading the normal performances. Three aspects are carried out in the present thesis. The first aspect is to investigate the method of designing of FDD process that will be able to handle both simple and simultaneous actuators' faults. For simple faults, residual generating methods based FDD processes are efficient. These techniques are based on a so-called residual signal which depends only on faults and can diagnose a simple actuator fault.

In the case of simultaneous faults, the residual signal will be affected by more than one fault. In this case, geometric methods based FDD processes are more advantageous. Operating as health supervision, the FDD process designed will be at each time able to fast generate accurate faults' parameters which are the time of faults occurrence, the time-varying behaviour of faults and the locations of faults. In some cases when the number of sensors is greater than the number of actuators, more than one set of faults' parameters is generated. In such cases, an algorithm of data fusion is needed to estimate the optimal faults' parameters based on all sets of faults' parameters previously generated.

The second aspect deals with the reconfiguration feature. This mechanism uses information generated by the FDD process to compute faults' parameters and to make a decision on when and how the action of reconfiguration should be taken.

The third aspect is to develop a FTC system that can tolerate both simple and simultaneous actuators' faults without degrading performances when the aircraft operates in normal conditions. In this thesis, the sliding mode control (SMC) is used to develop a Reconfigurable Sliding Mode Controller (RSMC). Based on the faults' parameters generated by the FDD process, and the reconfiguration mechanism, the RSMC reconfigures online the remaining healthy actuators control signals to compensate for the faulty actuators. The RSMC designs first a discontinuous control law to drive the aircraft error dynamics onto a specified surface called sliding surface. Then, it designs a continuous law to let the aircraft error dynamics sliding on this surface for the remaining flight time. This approach has two main advantages. Firstly, while the aircraft error dynamics are on the sliding surface, the aircraft behavior becomes a reduced order system. Secondly, the aircraft dynamics, while in sliding mode, is insensitive to modeling uncertainties and to external disturbances. However, this approach suffers from a major drawback which is the chattering phenomenon resulting when high-frequency actuators' dynamics neglected in system modeling are excited. Thus the performance of the system will be degraded and may even lead to instability. To deal with chattering, some existing methods are used to minimize this phenomenon.

Thesis contributions

In summary, the contributions of this thesis are as follows:

- Deals with partial and total actuator faults;
- Simultaneous faults detection and diagnosis using the geometric approach;
- Accurate faults' parameters identification using a reconfiguration mechanism;
- Estimate the optimal faults' parameters using a data fusion algorithm;
- Simultaneous fault compensation using the reconfigurable sliding mode controller.

List of Papers published in refereed journals

Ghodbane, Azeddine, Maarouf Saad, Jean-François Boland et Claude Thibeault. 2014. « Applied Cosmic Rays Fault Accommodation in Flight Control Systems using Fault Reconstruction based FDD and SMC Reconfiguration ». *International Journal of Computer, Information, Systems and Control Engineering,* vol. 8, n^{o} 7, p. 1141-1146.

Ghodbane, Azeddine, Maarouf Saad, Christelle Hobeika, Jean-François Boland et Claude Thibeault. 2016. « Design of a Tolerant Flight Control System Capable of Reconfiguring in Response to Multiple Faults Induced by Cosmic Rays ». *IEEE Transactions on Aerospace and Electronic Systems,* vol. 52, n^{o} 2, p. 981-697.

Ghodbane, Azeddine, Maarouf Saad, Jean-François Boland et Claude Thibeault. « Reconfigurable Flight Control System Using Multi-Projector-Based Geometric Approach and Sliding Mode technique ». *Journal of the Franklin Institute, Elsevier,* submitted on May 2016.

Thesis outlines

The rest of this thesis is organized as follows:

In chapter 1, some basic knowledge of primary and secondary aircraft control surfaces and redundancy are introduced. Then, definitions of actuators' faults, failures and malfunction are clarified. Next, a general overview is made on FTC, FDD and RC systems. At the end, a literature review on the recent work made in the field of FTC is presented.

Chapter 2 introduces the nonlinear model of a standard aircraft and its equations of motion and navigation. Then the aircraft model linearization and the longitudinal and lateral motions are introduced.

Chapter 3 presents the design of a tolerant flight control system in response to multiple actuator control signal faults induced by cosmic rays. This chapter is the result of a published scientific journal paper. The paper proposes a novel architecture for a fault-tolerant flight control system able to detect and compensate for a new type of faults. The faults are the cause of cosmic-ray-induced multiple-bit upsets that affect actuator control signals in modern Fly-By-Wire (FBW) avionics systems. In this type of faults, the actuator itself remains healthy. A reconfigurable sliding mode control is used to compensate for such errors. A linear military Advanced Fighter Technology Integration (AFTI-F16) aircraft model is used for performing Matlab®/Simulink® simulation and validation (Barfield et D'Azzo, 1983). FlightGear software simulator is used to show the performance and the behavior of the AFTI-F16 aircraft on a Graphical User Interface (GUI).

Chapter 4 presents an applied actuator fault accommodation in flight control systems using fault reconstruction based FDD and SMC reconfiguration. This chapter is the result of a published scientific journal paper and demonstrates the successful real-time implementation of a proposed FTC system by performing Matlab®/Simulink® simulations on a non-linear 6 degrees of freedom (DOF) standard aircraft model generated from the Aero Data Model In a

Research Environment (ADMIRE) (Forssell et Nilsson, 2005), (Bates et Hagström, 2007). FlightGear software simulator is used to show the performance and the behavior of the 6 DOF aircraft on a Graphical User Interface (GUI).

Chapter 5 presents the simultaneous fault reconfigurable flight control system using a multi-projector based geometric approach and an Extended Kalman Filter (EKF) for data fusion (Jassemi-Zargani et Necsulescu, 2001). This chapter is the result of a submitted scientific journal paper and treats the case where the number of sensors is greater than the number of control surfaces. In such case, a multi-projector geometric approach based on several sub-projectors combined with an EKF filter is used to design the fault detection and diagnosis process. Matlab®/Simulink® simulations are performed on a linear Boeing 767 aircraft model (Fossen, 2011). FlightGear software simulator is used to show the performance and the behavior of the Boeing 767 aircraft on a Graphical User Interface (GUI).

At the end of the thesis, the work accomplished and conclusions are summarized and finally some recommendations and suggested future works that can expand the presented study are listed.

CHAPTER 1

THE STATE OF THE ART

The first section of this chapter summarizes the basic knowledge on aircraft control surfaces, the concept of redundancy and introduces definitions and modeling on actuators' faults and failures and several other terms and expressions frequently used throughout this thesis. Different methods used to monitor control surfaces are then introduced briefly. In the second section, a general overview of the FTC systems and their objectives, concepts and principles are presented. In the third and last section, relevant works published in the literature in the field of FTC systems are reviewed and summarized.

1.1 Primary and secondary control surfaces

To fly and move in the three axes directions of the space, a standard aircraft requires control surfaces. These control surfaces make it possible for the aircraft to roll, pitch and yaw. Figure 1.1 shows the three axes and the corresponding aircraft motions and control surfaces. Two main control surfaces exist in a standard aircraft. The primary control surfaces are ailerons, elevators and rudder. They are considered as critical control surfaces. The secondary control surfaces include flaps, slats, spoilers and air brakes. They are considered as less critical control surfaces (Venkata et Chaitanya, 2009). In some literature, control surfaces are called also actuators. In this thesis, actuators are not referred to control surfaces but to components (mechanical, hydraulics or electrical) that act on the control surfaces via the pilot or the autopilot. Later, when faults, failures and malfunctions will be introduced, that will be referred to actuators themselves.

1.1.1 Primary control surfaces

In a standard aircraft, there are three primary control surfaces that control the aircraft motion along three axes. The ailerons are incorporated along the lateral axis on each wing. The elevators are included along the longitudinal axis on the horizontal stabilizer of the tail unit.

The rudder is included along the vertical axis on the vertical stabilizer of the tail unit. These surfaces are instantly checked to maintain the aircraft flight safety and to steer it along its 3D desired flight path. In such standard aircraft, thrust is considered a fourth control. It can be obtained using the engines.

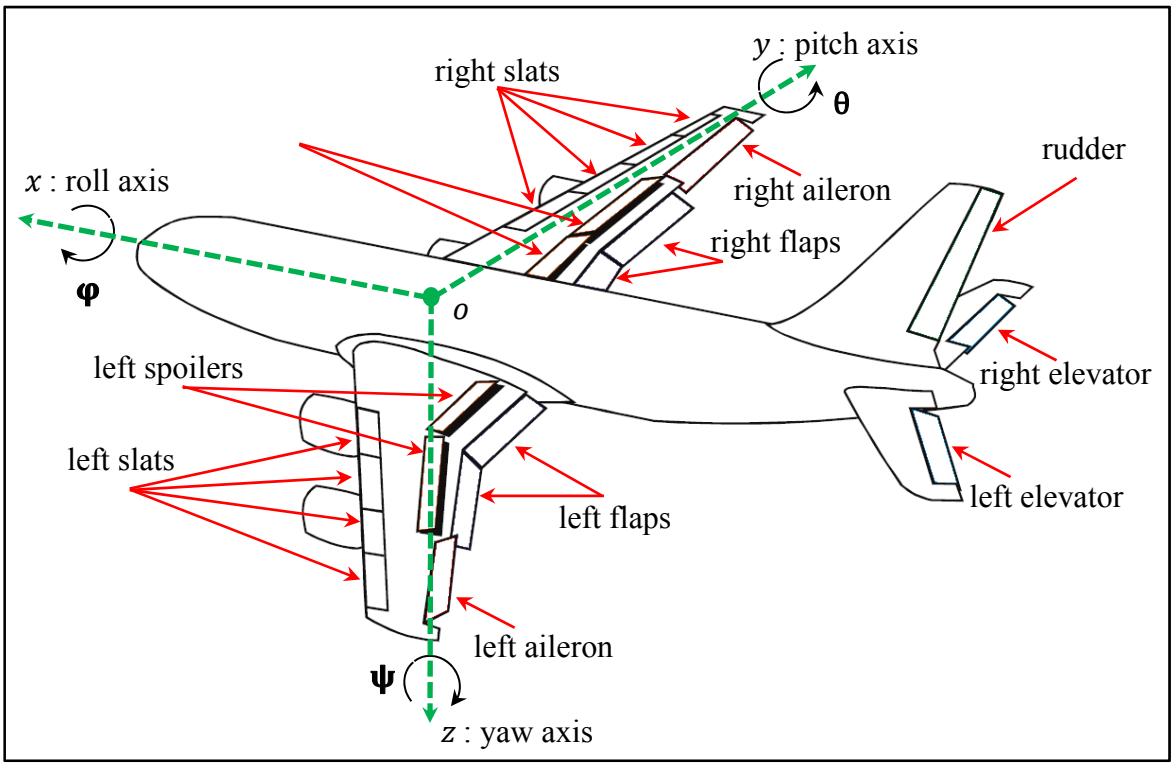

Figure 1.1 Axes and control surfaces of a standard aircraft and the corresponding motions
Adapted from Bennet (2010)

The ailerons control the aircraft to roll around the longitudinal body axis ox. To control aircraft to roll, the motion of the aileron incorporated on one wing must be simultaneous complemented by the opposite motion of the aileron incorporated on the other wing. If the aileron on the left wing is lowered, the aileron on the right wing is raised. The wing with the raised aileron goes down because the force required to lift it through a stream of air is decreased. The wing with the lowered aileron goes up because the force of lift is increased (Venkata et Chaitanya, 2009). Thus, the aircraft is rolled to the left. The roll angle is defined by φ. By convention, it will have a positive roll angle if the right wing is pivoted upwardly

and the left is rotated down. Otherwise, there will be a negative roll angle (McLean, 1990). Figure 1.2 illustrates the ailerons motions effect on the aircraft motion.

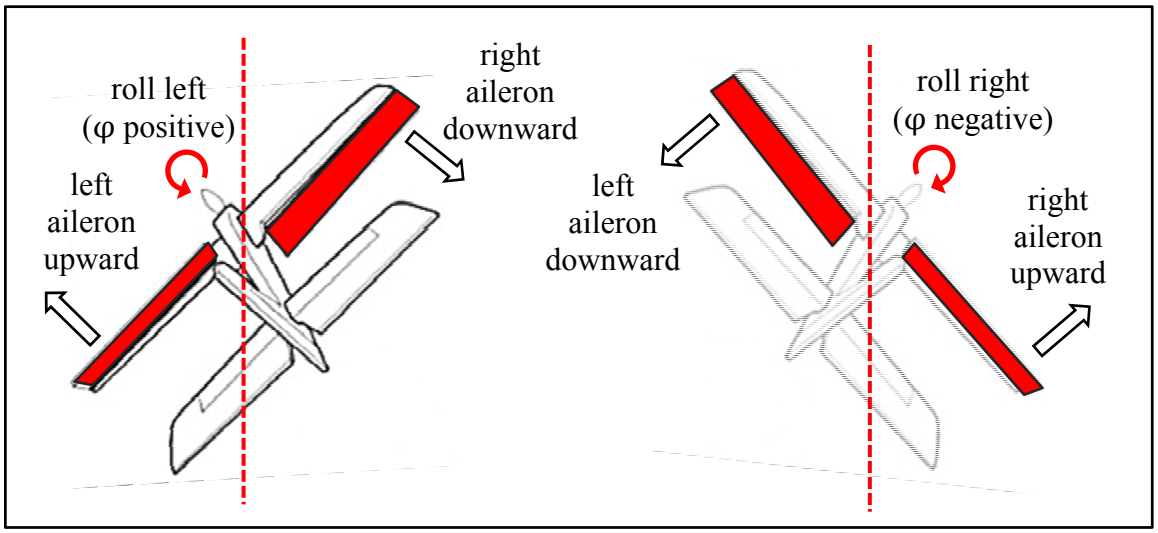

Figure 1.2 The ailerons' effects on the aircraft motion
Adapted from Venkata et Chaitanya (2009)

The elevators control the aircraft to pitch around the lateral body axis oy. Two elevators are located on both sides of the horizontal stabilizer of the aircraft tail unit. By changing the position of the elevators the force of lift increases or decreases. They can move simultaneously and in the same direction. When they move upward, the force of lift is decreased. Then the nose is forced upward and the tail is forced down. Similarly when the elevators move downward, the force of lift is increased. The nose is forced to drop and the tail is forced upward (Venkata et Chaitanya, 2009). The pitch angle is defined by θ. By convention, when the elevators are raised so it will have a positive pitch angle, otherwise there will be a negative pitch angle (McLean, 1990). Figure 1.3 illustrates the elevators motions effect on the aircraft motion.

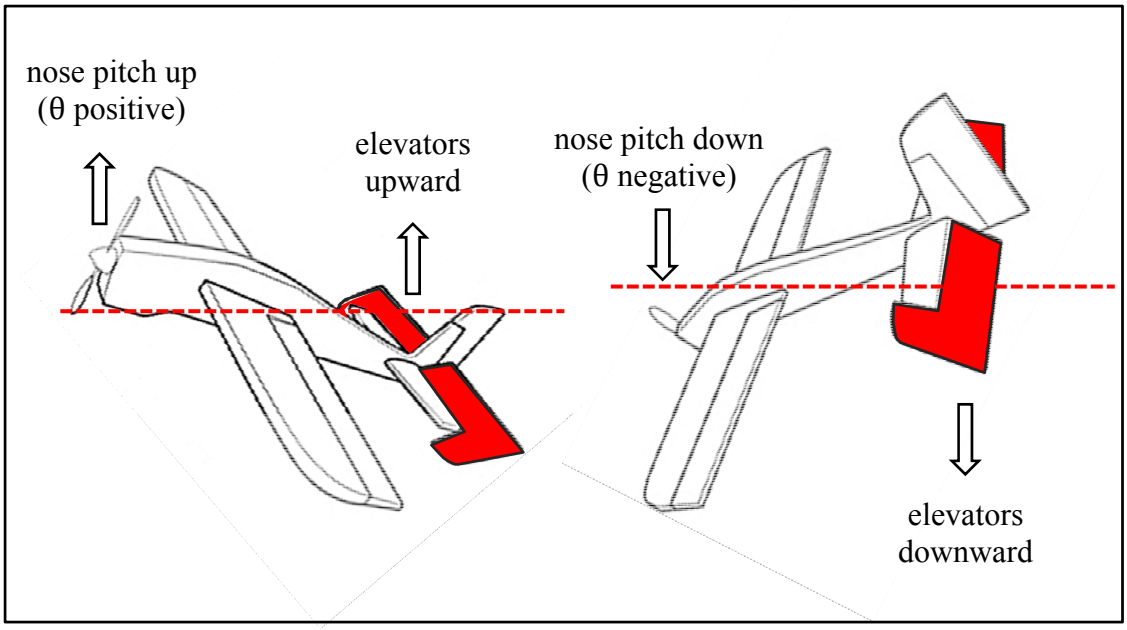

Figure 1.3 The elevators' effects on the aircraft motion
Adapted from Venkata et Chaitanya (2009)

The rudder controls the aircraft to yaw around the vertical body axis oz. The rudder is a movable surface located on the vertical stabilizer of the tail unit. By changing the position of the rudder the aircraft change direction from side to side by redirecting the air fluid past the fuselage.

If the rudder pivots laterally to the left, the nose of the aircraft turns to the left. Similarly, if the rudder pivots laterally to the right, the nose of the aircraft turns to the right (Venkata et Chaitanya, 2009). Alone, the rudder will turn an aircraft, but much more slowly than if ailerons are also used in conjunction. In practice, both ailerons and rudder are used together to co-ordinated turns of an aircraft. Operating as well, ailerons and the rudder are compensating for the adverse yaw phenomenon. The yaw angle is defined by ψ. Conventionally, when the aircraft turns right, the yaw angle is positive. Otherwise, it is negative (McLean, 1990). Figure 1.4 illustrates the rudder motions effect on the aircraft direction.

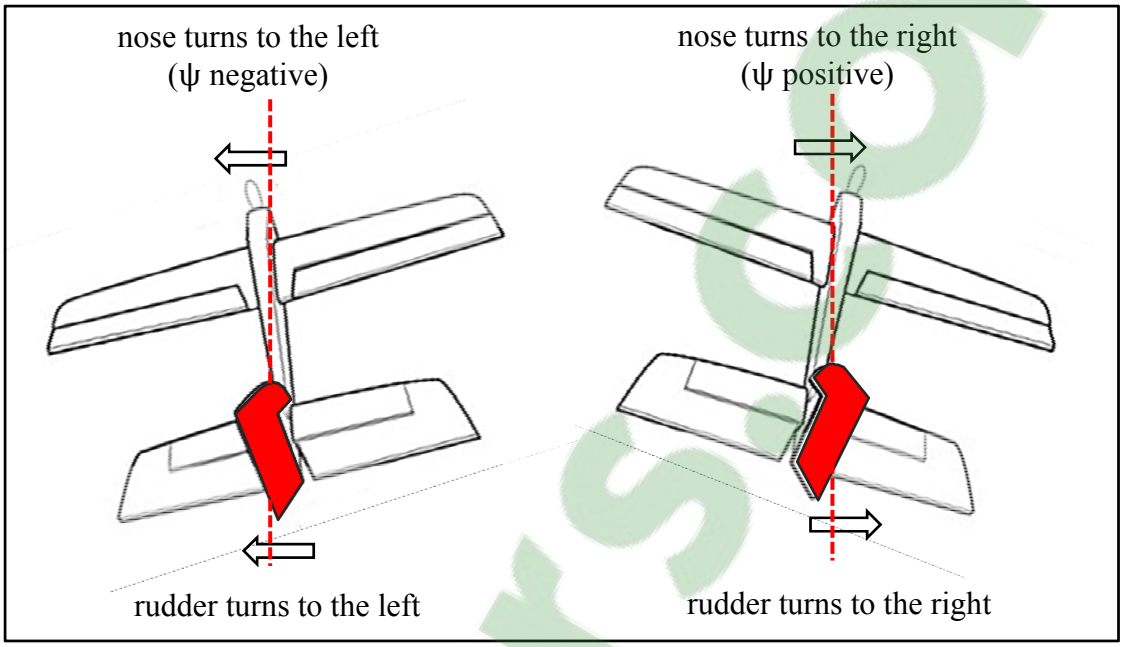

Figure 1.4 The rudder's effects on the aircraft motion
Adapted from Venkata et Chaitanya (2009)

1.1.2 Secondary control surfaces

In a standard aircraft, the main secondary control surfaces are flaps, slats, spoilers and air brakes. Several flap sections located on the inboard two-thirds of the wing trailing or leading edges. The simple flaps called also split flaps pivot only. The complex flaps called also slotted flaps extend and come down. The Krueger flaps extend and camber. Flaps are deployed during the take-off or the landing approach to improve the aerodynamic characteristics of the wing. Unlike flaps, slats have a nozzle like a slot between the high-lift device and the wing. They are usually located on the wing leading edge. Slats extend the wing edge and they sit like a glove on the edge. Spoilers, also called lift dumpers, are used to reduce the force of lift leading to a loss of altitude without increasing airspeed. Also, they can be used asymmetrically to contribute in the aircraft's roll. Air brakes are designed elsewhere on the aircraft and are usually deflect symmetrically outwards from the fuselage in opposite sides to decrease the aircraft speed (Venkata et Chaitanya, 2009).

1.2 Concept of redundancy and FTC

Hardware redundancy is very important for the purpose of FTC systems, to deal with faults, failures and malfunctions (Isermann, 2006). When a fault, failure or malfunction occurs, the control law will be reconfigured among the faulty original actuators and redundant actuators if the faulty original actuators cannot tolerate the fault by themselves. The use of these redundant control surfaces provides the possibility to maintain the desired performance in the case when original control surfaces become faulty. An example for a redundant actuator is the horizontal stabilizers which can be used in the case of elevators' failures. Also, engines can replace a failed rudder, by using them differentially to create yaw (Alwi, Edwards et Tan, 2011). Secondary control surfaces can also be used as redundant control surfaces. The spoilers for example, which are originally deployed to reduce aircraft speed, can also be used asymmetrically to contribute in the aircraft's roll, which is normally ensured in principle by the ailerons (Alwi, Edwards et Tan, 2011).

1.3 Avionic systems history

Otto Lilienthal (1848-1896) was the first pilot that successfully used the vertical tail of his self-made glider for lateral stabilization in Germany, 1894 (Christopher, Thomas et Hafid, 2010). Since that, the technology of Flight Control (FC) Systems has continued to grow. During the 1920s, and for many of the decades that followed, most aircrafts were designed to be statically stable, and the process of automated aircraft stability was further improved by using mechanical and mechanical-hydraulic systems. Around the 1950s, the first concept of Fly-By-Wire (FBW) systems using analog Flight Control Computer (FCC) was introduced. In 1972, with the increasing complexity and speed of aircraft, digital FBW systems are performed by NASA, and then it was made commercial in 1987.

Mechanical systems were designed using only mechanical devices as cables and pulleys. They were used in early aircraft and are still used in recent light aircraft, as in the control system used in the Cessna Skyhawk (Yoney, 2010). However, the control loads become too excessive for such systems in the case of larger aircraft. To overcome this problem, so-called

control tabs are added to provide aerodynamic relief, as those used in the Boeing 707 (Christopher, Thomas et Hafid, 2010). Figure 1.5 illustrates the principle of the mechanical flight control system.

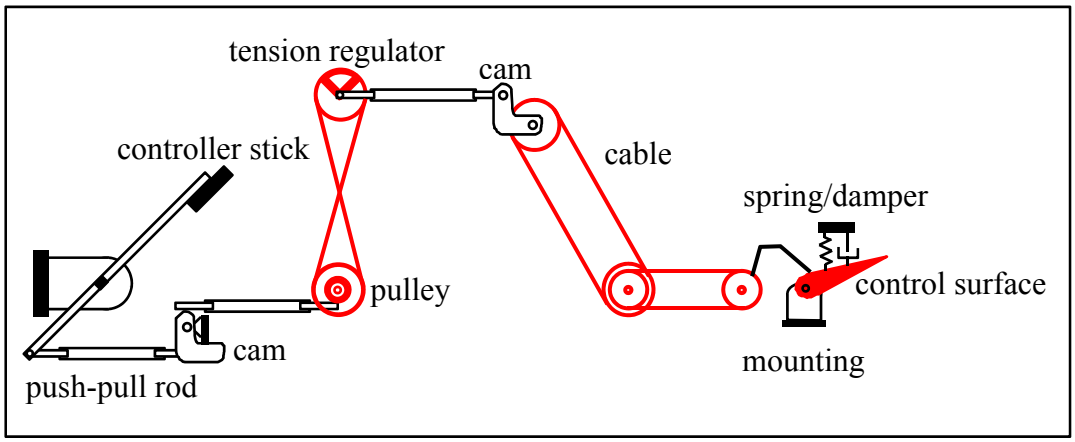

Figure 1.5 The principle of the mechanical flight control system
Adapted from Collinson (2013)

Mechanical flight control systems prove not reliable when size, speed and flight envelopes of the aircraft are increased. This led to add hydraulic power systems. The hydraulic power system links between the mechanical device and the pilot. The resulted hydro-mechanical flight control systems increase the effectiveness of the control surface. However, the main drawbacks are the structural complexity and the weight of the hydraulic power. The hydro-mechanical system was implemented for the first time on the De Havilland Comet in 1949 and on the Boeing 707 in 1954. In 1969, the Boeing 747 and Concord were the first commercial aircrafts to have a complete hydro-mechanical system (Christopher, Thomas et Hafid, 2010), (Atul Garg, 2013). Figure 1.6 illustrates a mechanical-hydraulic flight control system.

In recent FBW systems, the mechanical devices, linking between the pilot and the hydraulic power, have been replaced by electrical wirings connected to each other using the Flight Control Computer (FCC).

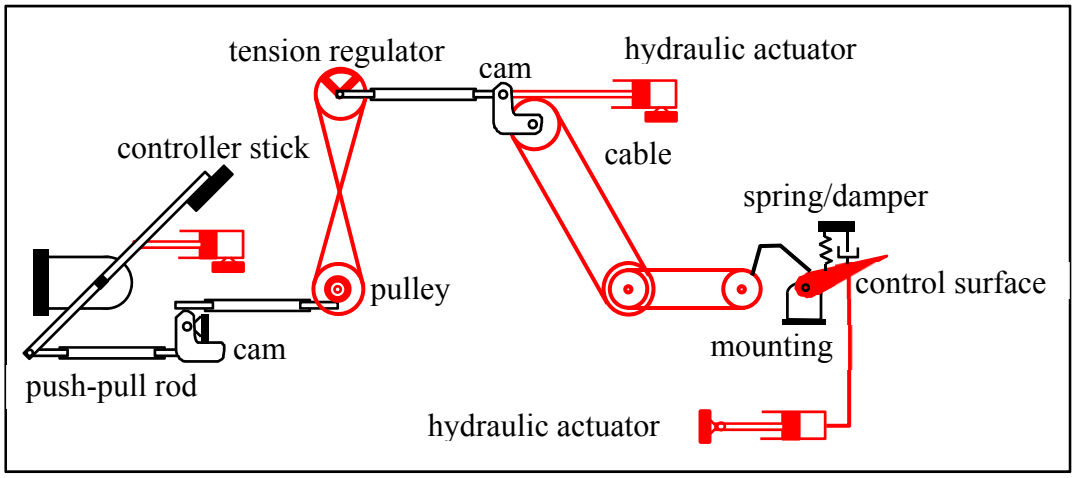

Figure 1.6 The mechanical-hydraulic type of a flight control system
Adapted from Collinson (2013)

Based on the desired trajectory and the sensors' measurements, the FCC computes the required control surface deflections and gives the associated control signals to the actuators. The FBW systems have less weight than those used heavy mechanical devices and hydraulic power, which significantly reduces the aircraft weight. The design and maintenance of the FBW systems are much simpler. The analog FBW systems are designed in the 1950's, followed by the digital FBW in the 1970's. FBW systems are used in most recent civil and military aircrafts (Christopher, Thomas et Hafid, 2010), (Atul Garg, 2013). Figure 1.7 illustrates a FBW flight control system.

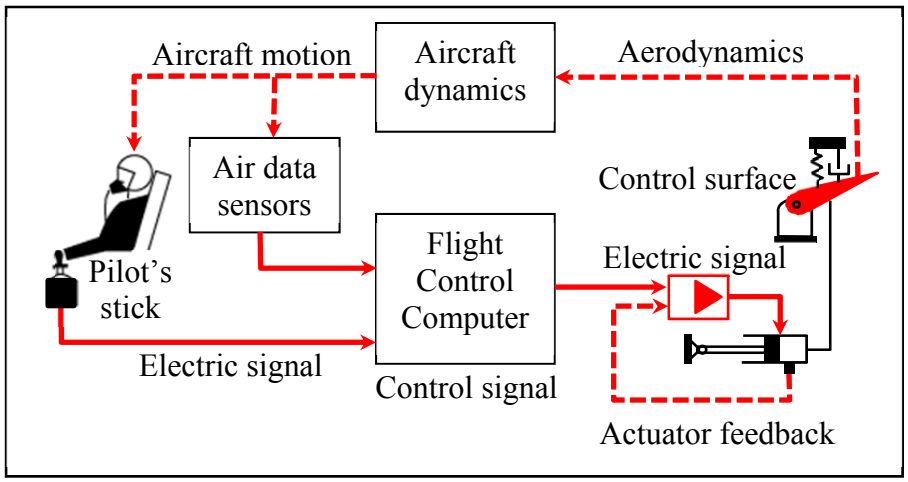

Figure 1.7 The FBW type of a flight control system
Adapted from Collinson (2013)

1.4 Actuator faults, failures and malfunctions

In the field of fault diagnosis, different technological terminologies such as fault, failure and malfunction are used. To avoid confusion between these terminologies, the distinction between them must be clarified. Based on Isermann definition (Isermann, 2006), The IFAC technical committee (Isermann et Ballé, 1997) makes the following definitions: "*A fault is an unpermitted deviation of at least one characteristic property (feature) of the system from the acceptable, usual, standard condition.*" Based on the above statement, an actuator fault is associated with an abnormal behavior of the control surface, which may not necessary affect the overall function of the control surface. It may be small or hidden and abrupt or intermittent. This makes it very hard to online detect and diagnose. When an actuator fails, it is still usable but becomes less effective. The loss of hydraulic fluid is considered one of the reasons for the occurrence of actuators' faults. Figure 1.8 illustrates examples of an actuator fault which corresponds to a loss of effectiveness.

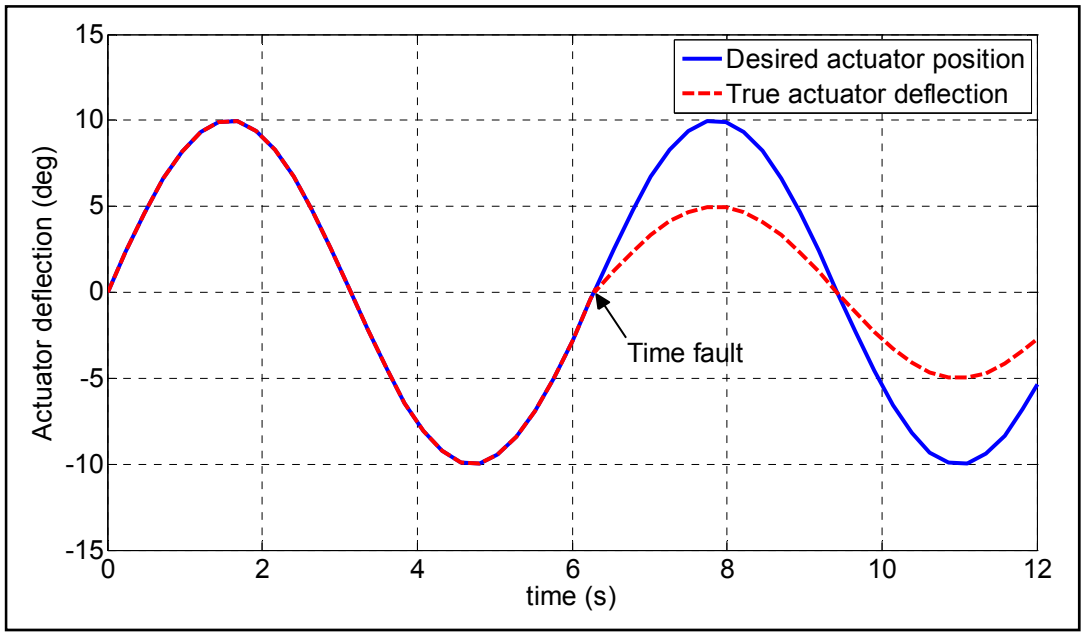

Figure 1.8 A type of an actuator fault: The loss of effectiveness
Adapted from Isermann (2006)

Based on the same reference, the failure has allowed the following definition: "*A failure is a permanent interruption of a system's ability to perform a required function under specified operating conditions.*" Based on the above definition, the failure can be considered as the result of one fault or a set of faults. Therefore the resulted failure compromises the actuator operation, and the actuator will be not usable and its replacement is emergently needed. There are two major types of actuator failures. The control surface may float freely at the zero position and do not provide any aerodynamic effect on the aircraft dynamics as illustrated in the top of Figure 1.9. It can also be jammed at an unknown position or at the actuator limit position and becomes stuck and immovable for the remaining flight time as illustrated in the bottom of Figure 1.9. These failures are the results of the break of one or many mechanical devices which ensure the link between the control surface and the associated actuator.

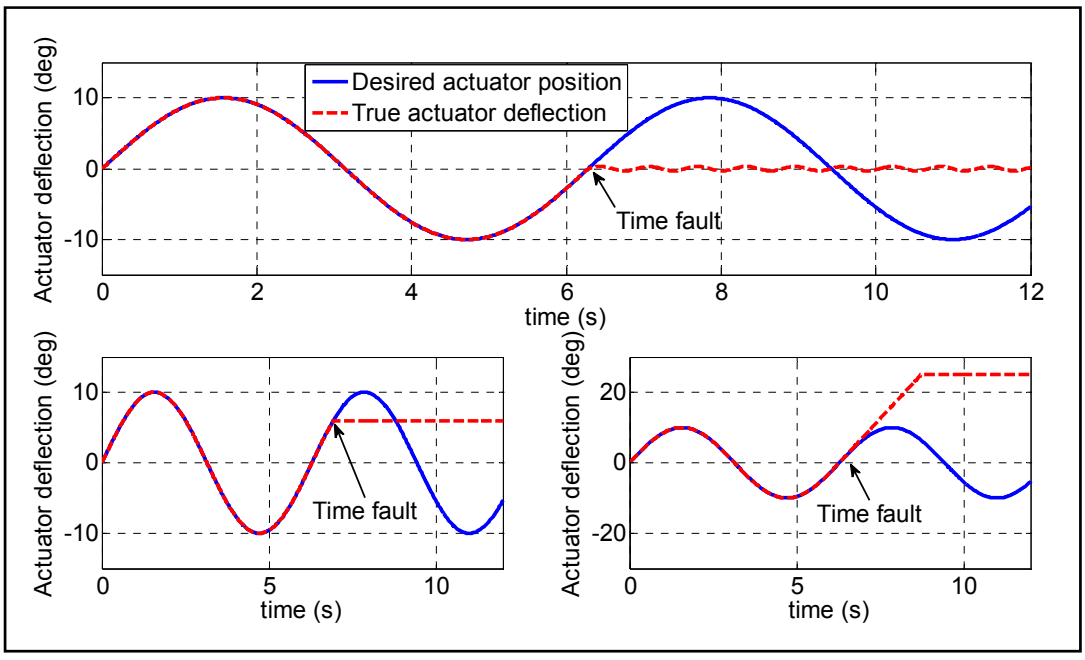

Figure 1.9 The different types of existing actuator failures
Adapted from Isermann (2006)

Finally, the actuator malfunction is an event that causes an intermittent deficiency in the accomplishment of the actuator overall function. It interrupts temporarily the actuator's function resulting from increased actuator stress (Isermann, 2006). As well as the failure, the

malfunction results also from one fault or from a set of faults, except that the malfunction takes less time than the failure. Figure 1.10 shows the development of the failure and the malfunction from the fault and their features.

New types of faults have been introduced when Taber and Normand found that neutrons generated by cosmic rays are capable of causing Single-Event Upsets (SEUs) in modern FBW avionics systems responsible for producing actuator control signals during flight (Taber et Normand, 1995). The resulting inappropriate actuator deflection affects aircraft dynamics and stability.

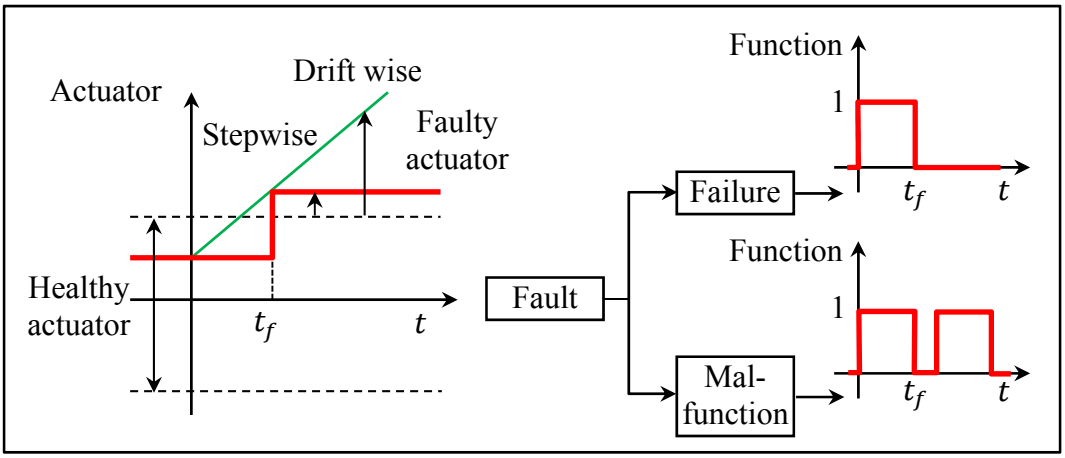

Figure 1.10 Development of the failure and the malfunction from the fault and their features Adapted from Isermann (2006)

Research on the effects of such faults has been grown in the avionics community since 2002. Therefore, NASA and other research centers formed a research partnership to study the effects of cosmic rays on the flight systems (Belcastro, Eure et Hess, 2006).

In 2006, NASA has tested new computer architecture under the impact of neutrons. This architecture was able to detect failure caused by a neutron by comparing the bits. Once the failure is detected, the designed architecture uses and remain using the last computed control law until the failure disappearance (Belcastro, Eure et Hess, 2006). In 2013, new model types of cosmic rays are developed based on the fault emulation process which is based

mainly on the use of the SEU controller of Xilinx® (Hobeika et al., 2013). This study revealed that about 10 % of the faulty outputs fit existing models such as locked in place, loss of effectiveness, floating around trim and hard over. The other 90 % displayed new faults behaviors and they are illustrated in detail in chapter 3.

For the rest of the thesis, the term fault is used because it is widely recognized that faults are unwanted malfunctions of a system, whereas a failure is the result of the total loss of a function (Christopher, Thomas et Hafid, 2010). In addition, a focus on actuator faults is done because, in fact, sensors' failures do not degrade the performance and the stability of commercial aircrafts. Furthermore, the sensor failure can be handled either by using redundant sensors or by estimating the faulty sensors' measurements using some existing techniques (Chen et Speyer, 2004). However, the FDD process developed in this thesis is capable of handling faulty actuators' signals as well as faulty sensors' measurements.

1.5 Fault-Tolerant systems: General overview

In the context of overall flight computer structure environments, three major types of fault-tolerant systems can be designed depending on the type of occurred faults. When faults occur in the hardware or software of the flight computer, then a Fault-Tolerant Computing system will be required to handle this kind of faults. When faults occur in actuators, sensors or structure of the aircraft, then a Fault-Tolerant Control system will be required to handle this kind of faults. Finally, if the faults affect the communication links, a Fault-Tolerant Communication system will be required. This thesis elaborates the Fault-Tolerant Control (FTC) systems and especially in the case of actuators' faults. Figure 1.11 illustrates a basic flight computer system and its faults (Pastor, Lopez et Royo, 2007).

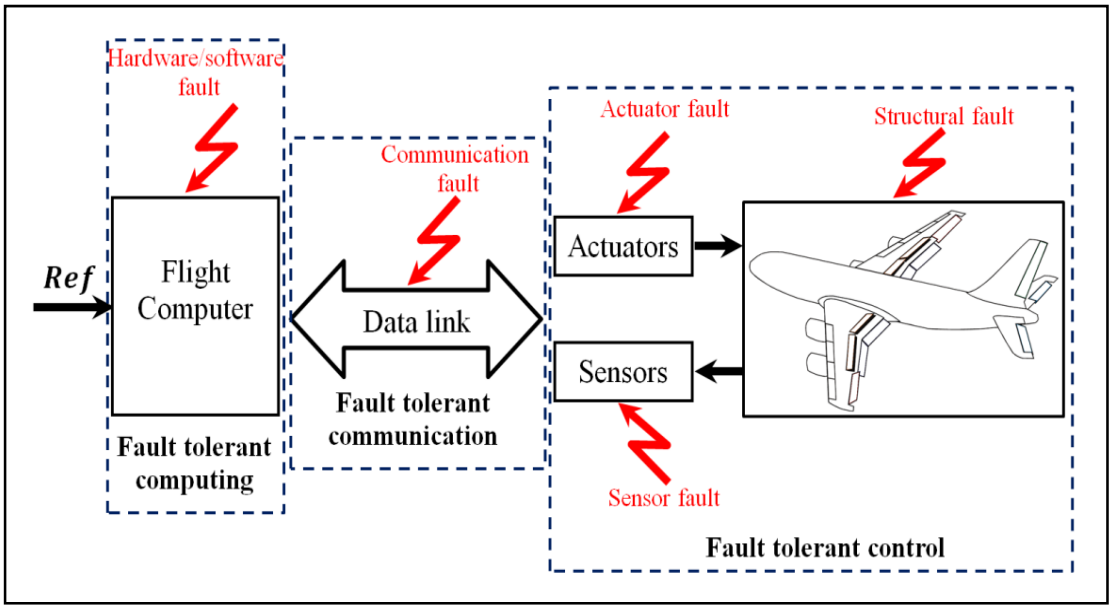

Figure 1.11 A basic flight computer system and its faults
Adapted from Pastor, Lopez et Royo (2007)

1.5.1 Objective of a Fault-Tolerant Control system

A simple conventional feedback control can be very limited, and brings the system to undesired behaviors or even to instability in the presence of an actuator failure. Therefore, the FTC systems have the ability to automatically accommodate the fault to preserve aircraft stability and maintain desired performance in the presence of such faults. The main task of a FTC system is to reconfigure control laws to ensure stability and maintain the desired performance of the system, not only in the normal situation but also when some actuators become failed. FTC systems are classified into two main classes: Passive Fault-Tolerant Control (PFTC) systems and Active Fault-Tolerant Control (AFTC) systems.

1.5.2 Passive and Active Fault-Tolerant Control system

PFTC systems are usually closely related to robust control without requiring any information on faults' parameters nor controller reconfiguration or adaptation. They have the drawbacks that they are reliable only for a closed class of faults and they degrade system performance

even when no faults occur. However, AFTC systems react against component failures using online reconfiguration so that aircraft stability can be preserved and the desired aircraft performance can be maintained. AFTC systems depend on online explicit knowledge of faults' parameters generated from the so-called FDD process. The FDD process operates as a health supervision module of the system and decides to reconfigure the flight controller when faults occur. In some practical applications, PFTC systems are considered as a complement of AFTC systems. Indeed, PFTC systems are required during execution of the fault detection and diagnosis functions (Zhang, Parisini et Polycarpou, 2004), where they are solicited to preserve the stability of the faulty system until AFTC systems are adapted to the new faulty scenario. A main critical criterion in AFTC systems is the FDD process speed constraint which can be defined by the time required to detect and diagnose a fault. Furthermore, the accuracy of the identified fault information and the robustness of the FDD process to external disturbances are considered important issues. Figures 1.12 and 1.13 illustrate the two main families' architectures.

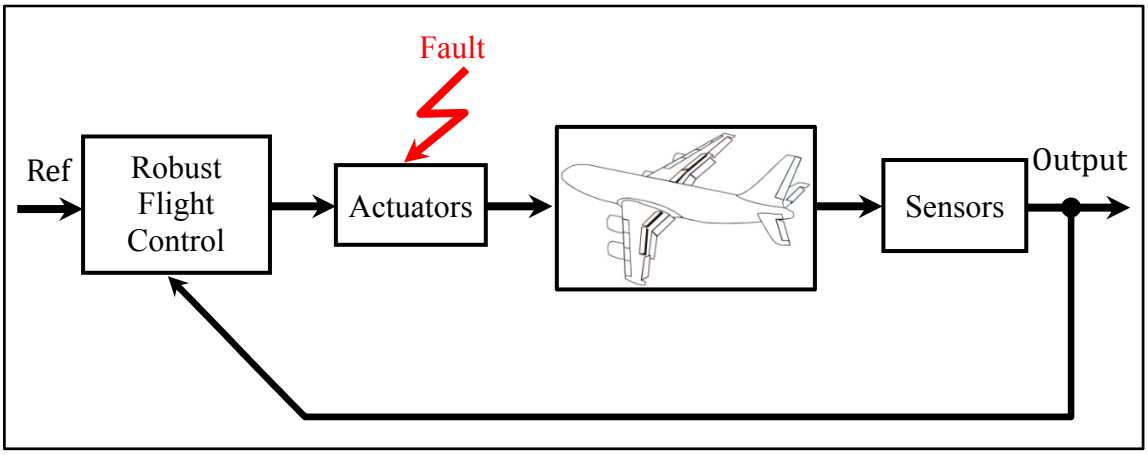

Figure 1.12 PFTC system architecture
Adapted from Blanke et Schröder (2006)

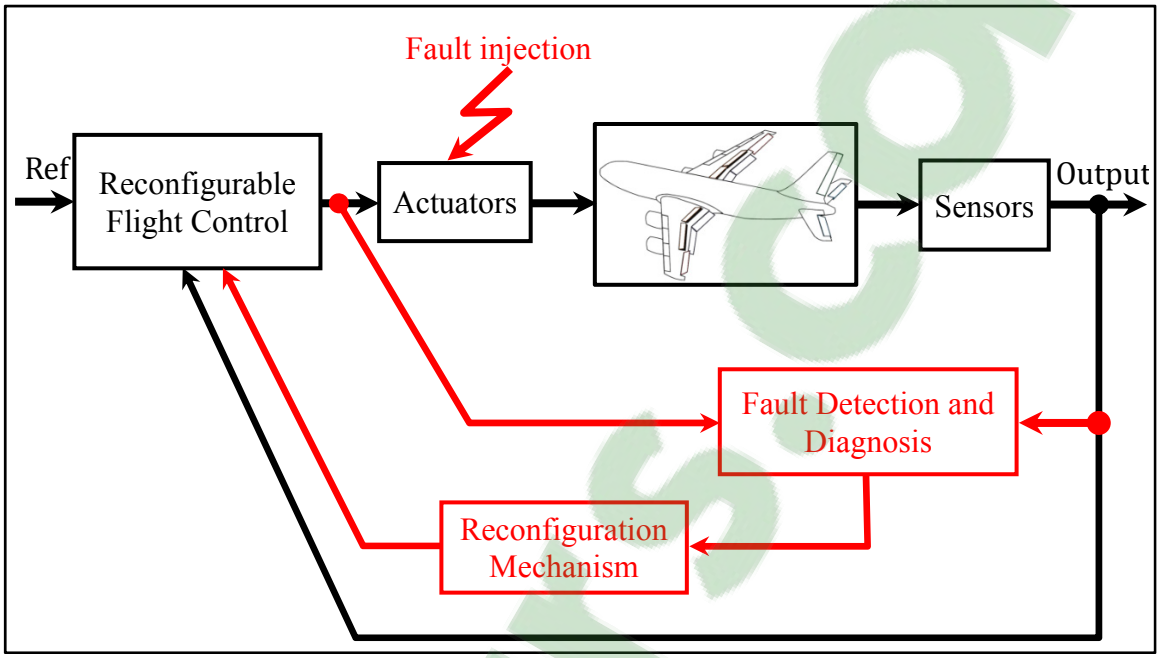

Figure 1.13 AFTC system architecture
Adapted from Zhang et Jiang (2008)

1.6 AFTC systems: Literature review

In general, AFTC systems can deal with linear aircraft models (Zhang et Jiang, 2008) or nonlinear aircraft models (Benosman et al., 2009). They require online explicit knowledge of faults' parameters which are generated by the FDD process. The main objective of an AFTC system is to maintain some acceptable level of performance and stability not only when all control surfaces are fully operational, but also in the case when a fault, failure or malfunction occurs in the system. The idea is to detect and isolate actuators' faults appropriately and then switch to healthy redundant actuators. In this context, the real problem of system reconfiguration becomes a diagnostic problem. When using redundant healthy actuators is not possible, the issue is then to accommodate actuators' faults to completely or partially compensate for their effects.

The general scheme of an AFTC system contains three main components: the Fault Detection and Diagnosis (FDD) process, the mechanism of reconfiguration and the Reconfigurable Controller (RC). The interaction between these three main components allows the overall

control system to be operational in a very systematic manner. It has been demonstrated that the development of each component affects the development of the overall control system (Blanke et al., 1997). Since AFTC systems involve a significant amount of online detection, fault decision-making and controller reconfiguration, one of the key problems in AFTC systems is the combination of these three parts in an overall real-time environment. In the next subsections, FDD, RM and RC will be introduced.

1.6.1 Fault Detection and Diagnosis process

Before introducing the terminology commonly used in the field of fault-tolerant systems which refer to such process, a list of functions that should be executed and combined together are defined such as (Isermann, 2006):

- Fault detection function: Determines the time of occurrence of faults in a system;
- Fault isolation function: Follows fault detection function and determines the location of faults;
- Fault identification function: Follows fault isolation function and determines the time-variant behavior of faults;
- Fault diagnosis function: Follows fault detection function and determines the time-variant behavior and the location of faults.

The terminology of Fault detection and diagnosis (FDD) is used to refer to a fault detection and isolation with identification (Zhang et Jiang, 2008). In other literature, the terminology of Fault Detection and Isolation (FDI) is referred to the same process as in (Ducard, 2009) and in (Chaib et al., 2009b). However, according to (Isermann, 2006), the FDI process does not identify the time-variant behaviour of the fault. Due to the field's lack of consistent terminology, these terms are often used interchangeably in the literature. For the remainder of the thesis, the term FDD will be used because it goes slightly further than the FDI term by covering the capability of identifying a fault, and because of the preference for the use of this term in aeronautic and aerospace fields (Christopher, Thomas et Hafid, 2010).

The FDD process uses the relation between the computed controller output signal and sensors' measurements to extract information on possible behaviour changes caused by actuators' faults to supervise the health status of the aircraft. This information is extracted by comparing observed values of special features, as parameters, state variables or residual signal with their nominal values (Isermann, 2006). The FDD process should be robust and still be sufficiently sensitive to detect the faults in the presence of external disturbances, model uncertainties and sensor noise (Shin, Belcastro et Khong, 2006). For aircraft and aerospace systems, the development of FDD processes' techniques that can be applied to real situations is still an open issue and it is considered an important area for practical research. Figure 1.14 illustrates the principle of the FDD process.

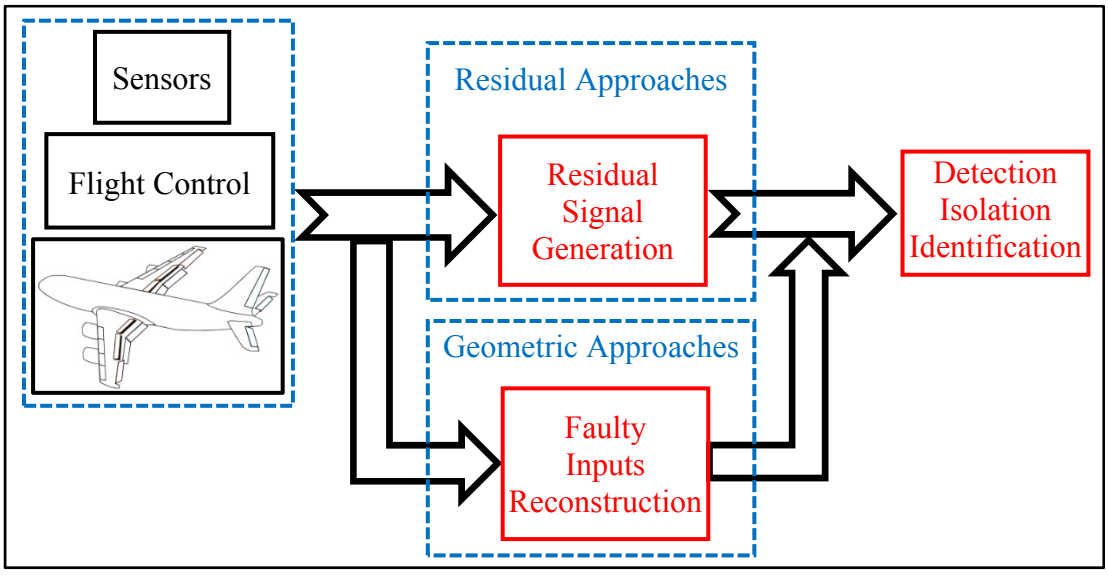

Figure 1.14 The principle of the FDD process
Adapted from Meskin et Khorasani (2011)

In AFTC systems, FDD processes play a vital role in providing information about faults in the system to enable appropriate reconfiguration action to take place. A wide variety of methods based on mathematical models of systems and using modern control theories exist in the literature. These methods can be classified into two main categories: residual generation methods and geometric methods.

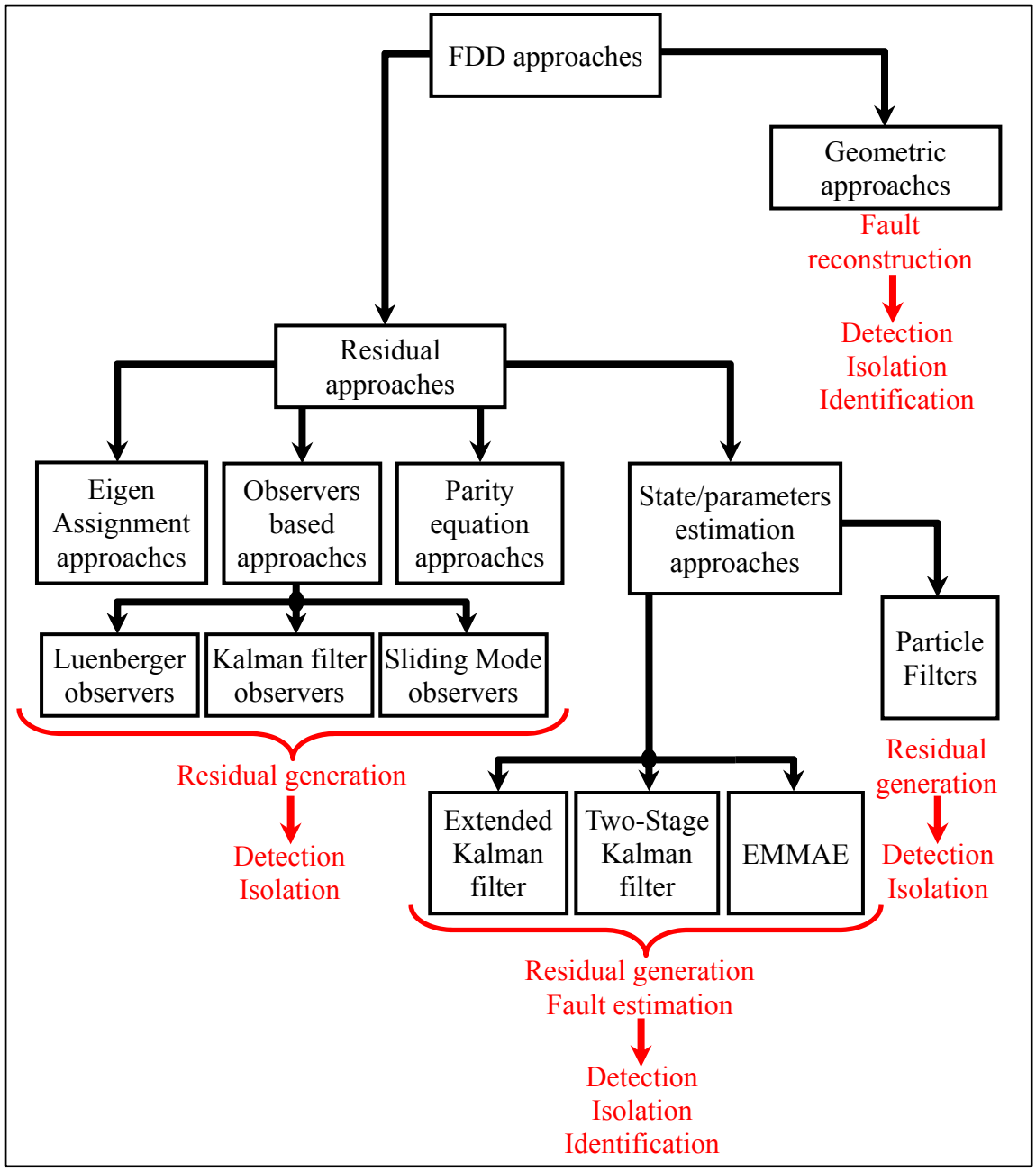

Figure 1.15 The most residual methods cited in the literature
Adapted from Zhang et Jiang (2008)

Residual methods use a so-called residual signal for decision making. This residual signal is expected to be dependent only on actuators' faults. In normal conditions, the residuals should be closed to zero and nonzero when faults occur. To avoid external disturbances false alarms, a designed threshold is usually compared with the residual signal. In such methods, the fault

is detected and isolated, but there is no further information on the time-varying aspect of the fault. However, for some AFTC schemes, further information about the nature and behaviour of the fault is required. Various such methods have been developed in the literature. Residual generation techniques have been categorized by (Patton, Frank et Clark, 2013) as observer-based approaches, parity equation approaches and state/parameter estimation approaches. There are other approaches cited in the literature as eigenstructure assignment (EA), the particle filters method, and the sliding mode observers. Figure 1.15 illustrates the most residual methods cited in the literature. Among the existing residual methods, there are those using the parity equation concept. These methods are increasingly used in aerospace applications. They are used to detect and isolate faults by generating a residual signal based on consistency checks on system input and output data over a given time window. These methods can be found in the work of (Gertler, 1998), (Chow et Willsky, 1984) and (Patton et Chen, 1994).

The eigenstructure assignment (EA) is another popular approach used to design FDD process. In (Patton et Chen, 1991) and (Xiong et Saif, 2000) authors made a number of applications on this approach. A further FDD approach has been designed based on state estimation using particle filters method. The particle filtering approach, so-called Markov Chain Monte Carlo Method, is a probabilistic technique that aims to jointly estimate the state vector and the discrete fault modes at each time. This method can be found in the work of (Liu et Chen, 1998), (Pitt et Shephard, 1999), (Cheng, Varshney et Belcastro, 2008) and (Zhang et al., 2005).

Other existing residual methods are designed based on observers. They consist on the rebuild of the state vector and system output vector using observers which are designed based on either Luenberger observers (White et Speyer, 1987) in the case of deterministic systems or based on the concept of Kalman filter (KF) published by (Kalman, 1960) in the case of stochastic systems. The basic idea is that the parameters of the actual process are estimated on-line and the results are compared with the parameters of the reference model which are obtained initially under the normal conditions. The error generated by comparing the system

output and the output observed will immediately be used as a residual signal to detect the actuator fault. These methods can be found in (Ren, Wang et Shen, 2011), (Alexander, Rarick et Dong, 2008) and (Shijie, 2008). However, these researches were concentrated more on detecting and compensating for faults' effects without isolating or identifying them. Therefore, they limit the FDD process to the detection function. The isolation and identification functions are not treated. For fault detection, a single residual signal is sufficient. However, for fault isolation, a set of structural residuals is required. Each structured residual signal is designed to be sensitive to a subset of faults while remaining insensitive to other faults (Gertler, 1991). However, it is difficult to design such restructured residual sets for many practical systems (Meskin et Khorasani, 2011).

To overcome this limitation, the basic concept of the KF has been extended to be able to estimate the nature and behavior of the fault by incorporating these features in an augmented state vector. In (Chowdhary et Jategaonkar, 2010) and (Zhang et Jiang, 2002) authors used the Extended Kalman Filter (EKF) concept to estimate and identify the aerodynamic parameters. In (Qiu, Zhang et Sun, 2005) and (Hsieh, 2000), authors used another variant called the two-stage adaptive Kalman filter technique for estimating both states and parameters of a dynamic system, in the presence of sensor noise and also in the presence of actuators' faults. However, the fault models used in these works are partial loss of actuators. The total loss and stuck at a position that includes a large class of actuators faults are not treated. Other studies (Ducard, 2009), (Rupp et al., 2005) and (Ducard et Geering, 2006) use the Extended Adaptive Multiple Model estimated (EMMAE) method which is essentially based on a set of Extended Kalman Filters (EKF). Unlike previous works, this method gives the ability to simulate several types of actuators' faults including partial and total failures. Also, it gives the possibility of ensuring the three functions of the FDD processes: the detection, isolation and identification. However, the case of multiple faults is not treated.

Other types of the residual methods are the sliding mode observers which have been used for the design of FDD processes in the last decade. This method uses the residual signal which is generated based on the system sliding motion concept and can be found in (Yang et Saif,

1995), (Tan et Edwards, 2002) and (Wang, 2012) works. The idea is to supervise the sliding motion of the system when faults occurred in the system. When the fault occurs this motion will be broken and a residual signal containing information about the fault is generated. This approach has the ability to detect and isolate the fault and also provide further information about the fault. This information can be used especially for fault accommodation.

Since the fault time-varying behavior information is very useful for on-line reconfiguration in the AFTC systems, geometric methods are more appropriate than residual methods. A new nonlinear FDD scheme providing both detection and diagnosis functions are designed based on geometric methods developed by (De Persis et Isidori, 2001). The new proposed FDD scheme can be applied only if the fault detectability condition is satisfied (De Persis et Isidori, 2000) and some new constraints are respected (Bonfe et al., 2009). This method was applied to a simulation study of a Vertical Take-Off and Landing (VTOL) aircraft (De Persis, De Santis et Isidori, 2001). The main objective is the design of a FDD process able to reconstruct the unknown inputs through a geometric decomposition of the system dynamics into two parts (tangential and transverse dynamics) results in an inverse dynamic computation. This method is detailed in the works of (Hammouri, Kinnaert et El Yaagoubi, 1999), (Chaib et al., 2007), (Chaib et al., 2009b) and (Chaib et al., 2009a). The advantageous of this method is that a large class of actuators' faults can be estimated as well as simultaneous faults can be detected and diagnosed.

1.6.2 Comparison between popular existing FDD approaches

In Table 1.1 some criteria were considered to evaluate and make the choice on the most appropriate method for this thesis. According to the defined thesis objectives, the geometric approach is the best candidate. In some situations, where multiple faults case is not considered, the EMMAE approach is developed.

Table 1.1 Comparison between popular existing FDD approaches

Popular existing FDD methods		**function**	**Simple fault / Multiple faults**
Residual approaches	EA	Detection / Isolation	Simple fault
	Observers		
	Parity equation		
	State/parameter estimation	Detection / Isolation / Identification	Simple fault
Geometric approaches	One projector	Detection / Isolation / Identification	Simple fault / Multiple faults
	Multi-projector		
This thesis	**EMMAE**	**Detection / Isolation / Identification**	**Simple fault / Multiple faults**
	One projector		
	Multi-projector		

1.6.3 Reconfiguration mechanism

The reconfiguration mechanism is required in the design of AFTC systems to determine whether a reconfiguration action is required. In the reconfiguration mechanism, faults' parameters generated by the FDD process are introduced in different forms of selection logic and system management to select the most suitable control function after a fault has occurred. Figure 1.16 illustrates the principle of the reconfigurable mechanism.

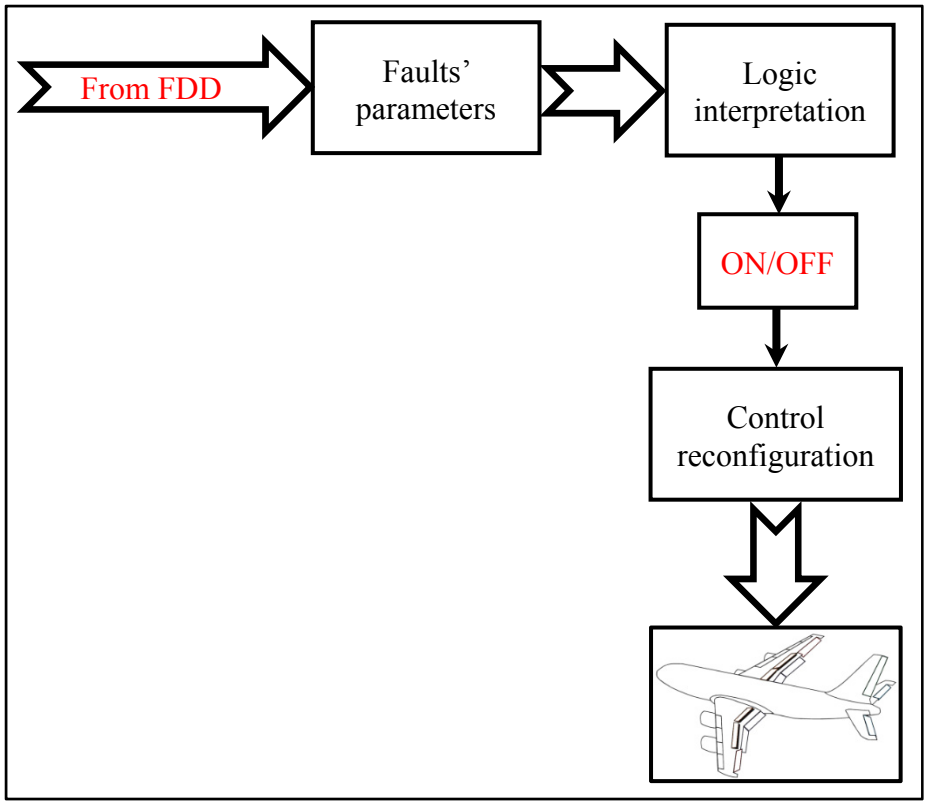

Figure 1.16 The principle of the reconfigurable mechanism

1.6.4 Reconfigurable Controller (RC)

Over the past two decades, various classifications of AFTC systems according to different criteria such as design methodologies and applications have been investigated. According to (Staroswiecki, 2003), AFTC systems can be divided into two main categories: projection based AFTC systems and online reconfiguration based AFTC systems. In projection based AFTC systems, a set of predesigned controllers is used to compensate for a set of possible faults that might occur in the system. When a fault among the possible fault's set occurs, the projected controller selected will be activated to compensate for it. However, online reconfiguration based AFTC systems are based on online redistributing or adaptation of the control laws at the same time when the fault occurs. In this kind of AFTC systems, the control law structure and the controlled system are modified through a change in the parameters. Figure 1.17 summarizes the main AFTC techniques which will be detailed in the following paragraphs.

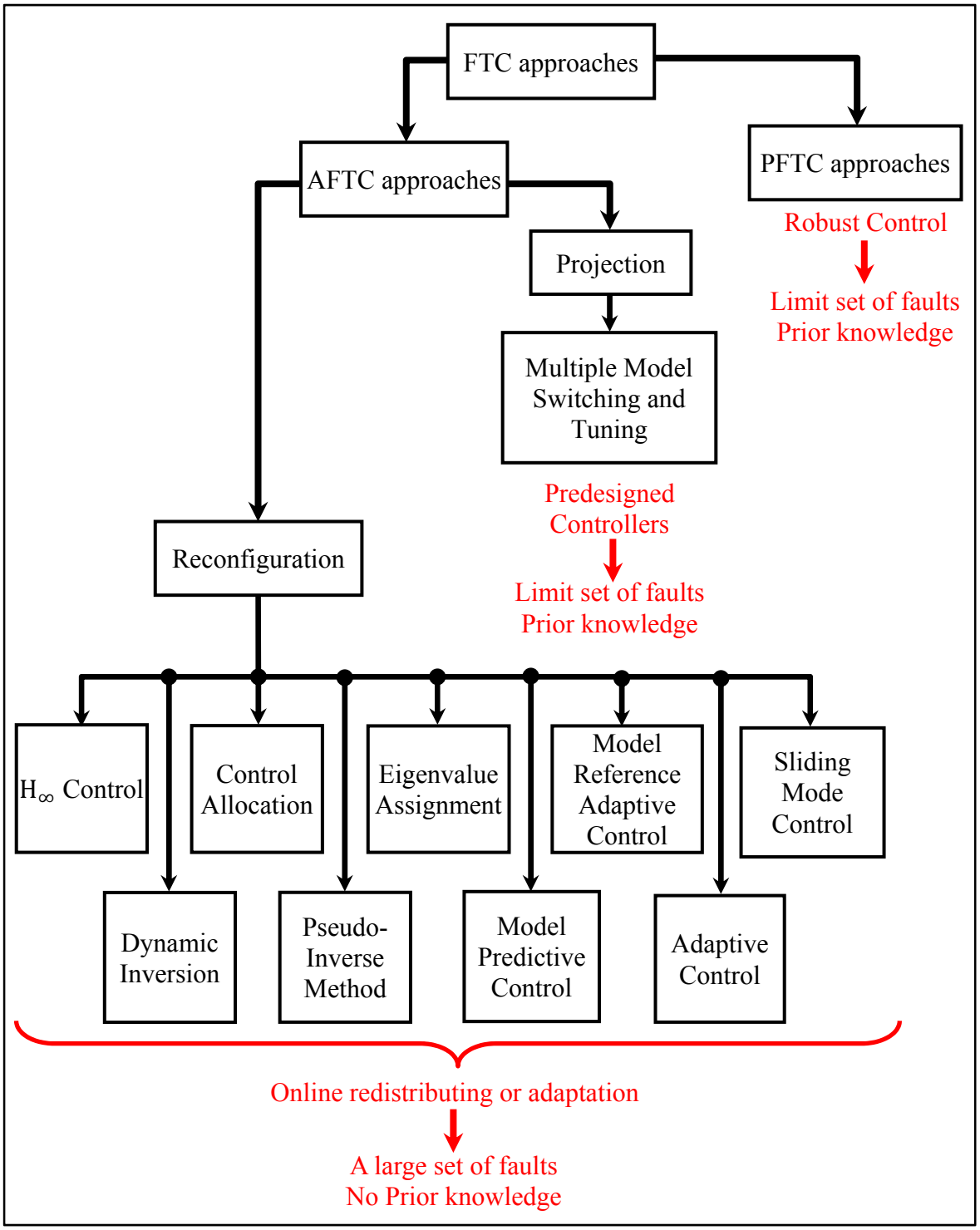

Figure 1.17 AFTC techniques
Adapted from Zhang et Jiang (2008)

(Zhang et Jiang, 2008) gives a review on the main methodologies used for the design of AFTC systems which are summarized as follows:

Pseudo-Inverse Method (PIM): The PIM is a popular reference in the field of AFTC for linear systems, due to its simplicity of design and its ability to handle a very large class of predefined faults. The idea is to place the poles of the post faulty system as close as possible to the nominal closed-loop poles. The main drawback of the PIM is the closed-loop stability, which cannot be always ensured, the assumption that the state feedback is always available and the assumption that faults are predefined which do not reflect real situations. The details of this method can be found in (Gao et Antsaklis, 1991), (Gao et Antsaklis, 1992), (Staroswiecki, 2005), (Staroswiecki, 2005) and (Yang, Blanke et Verhaegen, 2007).

The Eigenvalue Assignment (EA): The main idea of the EA method is to preserve the stability and performance of the system by matching the nominal and the faulty closed-loop eigenvalues and eigenvectors. The objective is to have a faulty closed-loop eigenstructure that will be as close as possible to that of the healthy closed-loop system. Unlike the case of PIM, the stability is guaranteed in EA method. In addition, EA maintains the maximum performance by placing eigenvectors very close as possible to those of the original system. However, EA has two major drawbacks. It requires linear dynamic systems and a perfect knowledge of the fault behavior and of the faulty dynamic model. The details of this method can be found in (Konstantopoulos et Antsaklis, 1996) and (Wang et Lin, 2000).

Model Predictive Control (MPC): MPC has been demonstrated as an efficient control strategy which is well suited to solve complex problems. Based on the optimal control theory, it is widely applied in the industry. The objective of MPC is to obtain predicted state trajectories in the future using the current states and the predictive computed control signals. The main motivation of the use of MPC in the field of FTC system is its capacity of handling many limits and constraints. Indeed, MPC has the ability to handle the actuator limits in an explicit way by including them in the optimization process which is used to obtain the predictive control laws. A fundamental limitation of MPC is its robustness to model

uncertainties and measurement noise. The details of this method can be found in (Maciejowski et Jones, 2003), (Magni, Bennani et Terlouw, 1997), (Kale et Chipperfield, 2004) and (Abdolhosseini, Zhang et Rabbath, 2012).

Model Reference Adaptive Control (MRAC): MRAC so-called the model following method is defined as a controller with adjustable parameters. The purpose of this method is to force the outputs of the system to follow those of a reference model and have the same dynamic for both systems. It can be used when tolerance to damage or structural failures is required. Despite the simplicity of computing the control law, it has two major drawbacks. The first one involves the design of a perfect reference model that requires zero error between the two systems for a long period of time. The second refers to the stability of the system, which will not always be guaranteed after fault occurrence even after designing a suitable reference model. The details of this method can be found in (Morse et Ossman, 1990), (Maciejowski et Huzmezan, 1997), (Ciubotaru, Staroswiecki et Christophe, 2006), (Tao, Chen et Joshi, 2002), (Kim, Lee et Kim, 2003) and (Tao et al., 2013).

Multiple Model Switching and Tuning (MMST): MMST method is based on a finite set of linear models that describe the faulty system in different fault scenarios. For each model, a suitable controller is designed. The control system is reconfigured by choosing the suitable model/controller pair that is the most appropriate for each scenario. This is designed using a weighted combination of control laws already designed. The weights are determined based on Kalman filters which are designed for each model. MMST also includes a tuning part, which is a separate identification algorithm that updates the parameters of the chosen model/controller pair. The MMST is considered to be fast and the stability is ensured. It suffices only that the actual fault scenario matches the predefined fault scenario. However, it has three major limitations. The first one is that MMST requires prior knowledge of different types of faults that can occur. This requirement is not guaranteed in real situations because these faults occur abruptly and have are unknown in nature. The second one is that if the occurred fault scenario is not included in the set of predefined faulty systems, it can lead to instability. The last limitation is that only a simple fault is considered and therefore one

model is selected. So, it cannot, however, deal with multiple faults. The details of this method can be found in (Boškovic et Mehra, 2002), (Yen et Ho, 2003) and (Narendra et al., 2003).

Adaptive Control (AC): AC so-called self-reconfigurable because it often doesn't require a reconfiguration mechanism and FDD process. It deals with a wide range of flight conditions. This type of control has the ability to automatically adapt the parameters of the controller based on changes occurred in the system to keep the desired performance. However, convergence problems when estimating parameters may appear. AC is efficient, stable and even robust for systems with slowly varying parameters. This assumption presents a limitation for such method. Because usually faulty systems have a nonlinear behavior with sudden parameters' faults or structure changes. Another limitation of AC method is that it is designed for a fixed faulty system structure. This assumption also cannot be met in the case of a time-varying fault. To overcome some of these limitations, AC method is combined with other existing techniques such as sliding mode control (SMC). Adaptive SMC (ASMC) makes AC more suitable for AFTC systems. The details of this method can be found in (Slotine et Li, 1991), (Chen, Tao et Joshi, 2004) and (Tao et al., 2013).

Control Allocation (CA): CA strategy so-called restructuring strategy is used when some actuators totally lose their effectiveness. The idea is to reallocate control efforts to remaining healthy actuators. As in PIM, CA uses the pseudo-inverse technique. However, in CA the control law is separated from the control allocation task. The controller law is designed based firstly on a so-called virtual control signal which will be distributed after that by the control allocator to the actuators control demand in terms of desired performances. The first advantage of the CA technique is that actuators' faults compensation is guaranteed without the need for modifying the flight control laws. The second one is that actuators' mechanical limits can be taken into account. However, the major drawback of AC technique is that an online optimization like linear or quadratic programming is required. This requirement presents a weakness even with high computational power computer. The details of this method can be found in (Tao et al., 2013), (Alwi et Edwards, 2006), (Alwi et Edwards,

2008); (Zhang et Theilliol, 2007), (Benosman et al., 2009), (Zhou et al., 2010), (Hamayun, Edwards et Alwi, 2012) and (Ducard, 2009).

Dynamic Inversion (DI): The DI method so-called feedback linearization is a special case of the control linearization, which is based on a nonlinear control law that can remove dynamic nonlinearities of a system to become a linear system. The main idea of DI method is that the nonlinear control law designed will remove undesired dynamics and replace them by desired dynamics. The nonlinear control law can be designed without the need of a model neither switching nor technique nor a gain scheduling. This is considered as the main advantageous of the DI method. However, DI method presents two major drawbacks. The first one is that it requires a perfect knowledge of the system dynamics in order to be able to cancel the plant dynamics perfectly, which is not met in realistic situations. The second drawback is the assumption that all states are observables. This assumption presents an issue for many systems since full state measurement is not always available. The details of this method can be found in (Ito, 2001), (Fisher, 2005), (Tandale et Valasek, 2005), (Lombaerts et al., 2007), (Holzapfel et Sachs, 2004) and (Landry, 2012).

H_∞ Control: H_∞ so-called robust control is developed in both industrial and aerospace applications. In some references, H_∞ control is classified as a PFTC system due to the fact that it doesn't require to get faults' information. Furthermore, H_∞ works in normal conditions as well as in faulty conditions, uncertainties and disturbances. The idea is based on a predesigned controller by minimizing the fault effect on the system since actuator partial loss can be seen as a kind of uncertainty. As many other robust control techniques, one of the main drawbacks of this method is the performance degradation in normal conditions. In addition, the designed controller resulted is usually of a higher order than the system which makes it difficult to implement. The details of this method can be found in (Zhou et Doyle, 1998), (Marcos, Ganguli et Balas, 2005) and (Magni, Bennani et Terlouw, 1997).

Sliding Mode Control (SMC): SMC is applied to the design of systems presenting high uncertainty in the dynamics and requiring high performances. Unlike H_∞ and other robust

control techniques, SMC can accommodate significant uncertainties without losing of performance in normal conditions. The principle of the design of this control technique is separated into two steps. A so-called sliding surface is firstly designed such that the dynamic state motion on this surface converges to the steady state. The performance of the controlled system depends on the choice of the sliding surface. Then a control law is designed to drive the dynamic state motion towards the sliding surface and remains on it once it is reached using a high-speed switching function. To ensure this objective, the control law designed must include both continuous and discontinuous components. The discontinuous component drives the state dynamic motion towards the sliding surface. And once on the surface, the continuous component becomes more dominant than the discontinuous one and drives the state dynamic motion to the steady state. Instead of its robustness, SMC has a major drawback which is the chattering phenomenon resulting from actuators' delays. Indeed, the discontinuous component uses a high-speed switching function. However, this is feasible in ideal systems but not in real situations since in practical mechanical or electrical systems, there is always delay in the actuators. The use of a high-speed switching function leads to exciting high-frequency dynamics neglected in system modeling, which degrades the performance of the system and may even lead to instability. Furthermore, chattering phenomenon decreases the control accuracy and leads to damages in electrical and mechanical components. Chattering phenomenon is unavoidable but it can be attenuated and works to minimize this problem already exist. The details of this method can be found in (Slotine et Li, 1991), (Hess et Wells, 2003), (Utkin, 1992), (Perruquetti et Barbot, 2002), (Edwards, Fossas Colet et Fridman, 2006), (Bartolini et al., 2008), (Boiko et al., 2009), (Bandyopadhyay, Deepak et Kim, 2009), (Fridman, Davila et Levant, 2011), (Brambilla et al., 2008) and (Fallaha et al., 2011).

1.6.5 Comparison between popular existing RC approaches

Also in this section, some criteria have been established to allow us to evaluate, select and design the most appropriate method for this thesis. Indeed, the sliding mode control method

was the best choice to fulfill the objectives of the thesis. The comparison between the most popular RC approaches is illustrated in Table 1.2.

Table 1.2 Comparison between popular existing RC approaches

Popular existing RC methods			**Required Model reference**	**Required prior fault knowledge**	**Type of faults**	**Simple fault / Multiple faults**
PFTC approaches	Robust Control		No	Yes	Limited	Simple
AFTC approaches	Projection	MMST	Yes	Yes	Limited	Simple
		H_∞	No	No	Limited	Simple
	Reconfiguration	PIM	No	Yes	Large	Simple
		EA	No	Yes	Limited	Simple
		MPC	No	No	Limited	Simple
		MRAC	Yes	No	Large	Simple
		AC	No	Yes	Large	Simple
		CA	No	No	Large	Simple / Multiple
		DI	No	No	Large	Simple / Multiple
		SMC	No	No	Large	Simple / Multiple
This thesis	**Reconfiguration**	**SMC**	**No**	**No**	**Large**	**Simple / Multiple**

1.7 AFTC systems using Sliding Mode Controller: Review

The idea of the SMC is evolved from works on the Variable Structure Control (VSC) systems of Emel'Yanov and Barbashin in the Union of Soviet Socialist Republics (USSR) in the 1950s. The SMC appears outside Russia in the 1970s after the publication of Itkis and Utkin works in English (Edwards et Spurgeon, 1998). SMC becomes after that a topic of great interest in control theory and practice in many applications (Utkin, 1992). However, it was not introduced in the FTC systems field until 1989 (Hsu et Costa, 1989). In this reference, authors combined SMC with AC to design a FTC system with little or even no information about uncertainties and faults' parameters. The designed controller was able to accommodate significant uncertainties without causing great degradation in performance. The same strategy was introduced in (Hsu et Costa, 1990), (Hsu, de Araújo et Costa, 1994), (Hsu, Lizarralde et De Araújo, 1997), (Tao et al., 2013), (Alwi et Edwards, 2005), (Oliveira et al., 2007), (Shin, Moon et Kim, 2005), (Qinglei et al., 2011) and (Xu, 2008). In these works, it has been demonstrated that SMC designed alone can only accommodate partial loss faults and cannot accommodate total failures and severe partial loss faults which saturate the actuator. It has shown also that SMC technique combined with AC is considered as a PFTC system because of a priori knowledge of faults is not required. This makes SMC more suitable for FTC system purpose.

In (Tao et al., 2013), authors designed an adaptive SMC to accommodate stuck failures which are considered as total loss of actuators. This method needs knowledge of the structure of both healthy and faulty systems. In (Alwi et Edwards, 2006), (Hamayun, Edwards et Alwi, 2012), (Alwi et Edwards, 2008) and (Alwi, Edwards et Tan, 2011) authors designed an SMC combined with CA and applied on a linear model. The authors assumed that the effectiveness level of the actuators is assumed coming from FDD process.

Since SMC is vulnerable to the chattering phenomenon which leads to parasitic dynamics generated by existing actuators' high-frequency dynamics often neglected when systems are modeled, authors in (Wells, 2002), (Hess et Wells, 2003) and (Vetter, Wells et Hess, 2003)

have designed an asymptotic observer to eliminate such undesired effect. However, these works don't trait total loss actuators' faults. In (Shtessel, McDuffie et Jackson, 1998) authors developed a finite-reaching-time continuous SMC. In this study, a special function is used instead of a discontinuous component of SMC. When the dynamic states cross the sliding surface, the continuous power function makes the discontinuous component smooth and thus the chattering will be attenuated. In (Fallaha et al., 2011) authors have designed a nonlinear Exponential Reaching Law (ERL) by using an exponential function that dynamically adapt the discontinuous component of the control law to the variations of the controlled system. ERL allows chattering reduction on control input while keeping high tracking performance of the controller in steady-state regime. In (Shin, Moon et Kim, 2005) authors introduced a power rate reaching law of the discontinued component of the control law to improve the reaching speed and reduce chattering.

In (Corradini, Orlando et Parlangeli, 2006) and (Wang, 2012) authors designed an AFTC system using the SMC technique and applied it to a linear model. The FDD process uses the designed sliding surfaces as an indicator to detect a fault. In the case when dynamics states leave the sliding hyperplane, the value of sliding surface increased and a fault is detected in the correspondent actuators. After getting faults information the control law will be automatically reconfigured. Unlike previous methods, this method can deal with stuck actuator failure which is considered as totally loss fault. The main drawback of these works is the assumption that the existing redundant actuators are a perfect duplication of the faulty actuators which is not available in most real systems.

A multiple time scale reconfigurable SMC system based on backstepping control concept is developed by (Shtessel et Shkolnikov, 2003). The discontinuous control is replaced with a boundary layer continuous approximation. Totally and severe partial loss faults are not handled using this concept because of actuators' mechanical limits constraints. The performance is also degraded in the normal condition.

1.8 Summary

In the above literature review, the new development in AFTC systems has been outlined. The existing methods used in the design of FDD process as those used in the design of RC are summarized. However, there are some important topics that have not yet received the required attention. They are listed below:

The first topic that still needs to be considered in an AFTC systems design is the nonlinear dynamic systems. The presented works consider often a linear system in their controller development. However, physical systems are always nonlinear. Moreover, the assumption that a linear model accurately describes the dynamic behavior of a physical system in a wide range of operating conditions is not always true. In this thesis, linear as well as nonlinear aircraft models are considered in the design of the proposed AFTC system.

The second topic that still needs to be considered is multiple fault scenarios. This leads to the design of a FDD process that had a capacity of handle multiple actuators' faults. Handle multiple actuators' faults means the detection, the isolation and the identification of these faults. Indeed, the major of the above works don't deal with simultaneous faults and the designs proposed are always based on the assumption that a simple fault occurs at a time. Some of the above works, mainly which use the robust AC techniques, treat simultaneous faults but no development on detection and diagnosis is done. Those that use residual approaches don't treat this topic because they need to design a restructured residual signal which is difficult for many practical systems. In this thesis, a FDD process based on the geometric approach is developed. It is proved that multiple actuators' faults can be handled with the designed FDD process.

The third topic is the total actuator faults. The above works focused on the partial loss of effectiveness of actuator which is considered as a partial fault. In this thesis, an AFTC system is developed based on a reconfigurable controller that can deal with not only partial actuator faults but also total actuator faults so-called failures. Furthermore, unlike in the above works,

the accuracy faults parameters estimated by the FDD process converged to real faults parameters.

The fourth topic is the FDD process's delay. Indeed, after fault occurrence and before getting faults information from FDD process, the system operates in a faulty condition but no reconfiguration action is activated yet. The system may lose the control and leads to degradable performances and even the system may become or tend to become unstable. Hence, AFTC systems must have the capability to preserve the faulty system stability during this critical delay. In this thesis, a RSMC is developed based on faults parameters given by an FDD based on the geometric approach. As the RSMC can accommodate significant uncertainties without losing of performance in normal conditions, it can preserve faulty system stability since actuators' faults are considered as a type of uncertainties. The Lyapunov (1857-1918) stability of the proposed controller is proved.

CHAPTER 2

STANDARD AIRCRAFT DYNAMIC MODELING

In conventional control systems in which the controlled systems used are relatively simple with single input single output, the control system can be developed without need of the mathematical model of controlled systems. Unlike conventional control systems, modern control systems are more complex and are designed for multi-input multi-output systems. Such control systems require a better comprehension of the controlled system behavior. In general, these systems are modeled by using differential equations, Laplace transforms or state space representation. The performance of modern control systems depends on the accuracy of the mathematical model used in the design of these systems.

Aircrafts are multi-input multi-output systems. So modeling aircraft is very important in the design of FTC systems. Aircraft models are obtained by applying Newton's laws on a rigid body. The term rigid implies that all points of the aircraft body remain fixed in their relative positions in space at each time (McLean, 1990), (Etkin et Reid, 1996), (Nelson, 1998), (Stevens et Lewis, 2003) and (Bates et Hagström, 2007).

In the first section of the chapter, the equations of forces and moments that characterize a nonlinear standard aircraft motions used in chapter four are developed and the differential equations of the rigid body used in chapter four are defined. In the second section, the linear model of the AFTI-F16 aircraft used in chapter three, as well as the linear model of the Boeing 767 used in chapter five, are introduced.

2.1 Reference frames

Several frames are required to describe the motion and the behavior of a standard aircraft. These reference frames are orthogonal systems and designed based on the rule of the right-hande as shown in Figure 2.1. The most important reference frames are:

- The inertial reference frame $\mathcal{F}_I$;
- The navigation reference frame $\mathcal{F}_N$;
- The fixed-body reference frame $\mathcal{F}_B$;
- The wind reference frame $\mathcal{F}_W$.

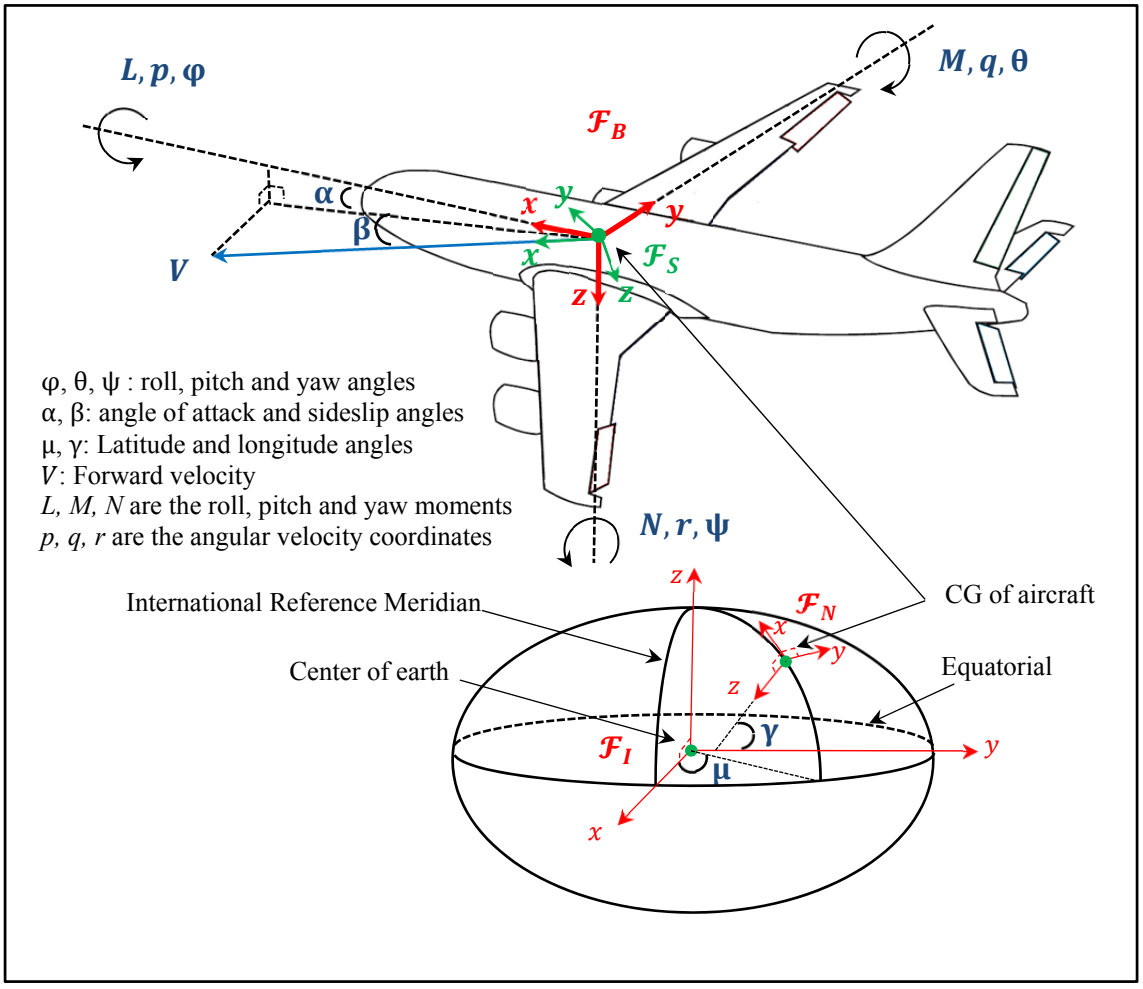

Figure 2.1 The aerodynamic reference frames
Adapted from McLean (1990)

2.1.1 The inertial reference frame

The inertial reference frame $\mathcal{F}_I$, known also as the Earth-Centered, Earth-Fixed reference frame $\mathcal{F}_{ECEF}$, describes the Cartesian coordinates $(x \quad y \quad z)^T$ of the position of the center of

gravity (CG) of the aircraft relative to the center of the earth. As shown in Figure 2.1, the origin of $\mathcal{F}_I$ is fixed to the origin of earth. The z axis coincides with the earth rotation axis and points to the north. The x axis coincides with the International Reference Meridian (IRM). The y axis coincides with the earth equatorial. The position of the CG of the aircraft can be also described via the geodesic coordinates $(\gamma \quad \mu \quad h)^T$, known also as Longitude, Latitude and Altitude (LLA) coordinates. Conversion between the two coordinates can be realized as follows (NIMA, 2000):

$$\begin{cases} x = \left(\dfrac{a}{\sqrt{1 - e^2 sin^2(\mu)}} + h\right) cos(\mu) cos(\gamma) \\ y = \left(\dfrac{a}{\sqrt{1 - e^2 sin^2(\mu)}} + h\right) cos(\mu) sin(\gamma) \\ z = \left(\dfrac{b^2}{a\sqrt{1 - e^2 sin^2(\mu)}} + h\right) sin(\gamma) \end{cases} \tag{2.1}$$

where:

$$e = \sqrt{\frac{a^2 - b^2}{a^2}} \tag{2.2}$$

a is the dimension of the equatorial axis and b is the dimension of the vertical axis. They are equal to 6 378 137,0 m and 6 356 753,314 245 m respectively.

2.1.2 The navigation reference frame

The navigation reference frame $\mathcal{F}_N$, known also as the North, East, Down (NED) reference frame, describes the aircraft navigation trajectories. As shown in Figure 2.1, the origin of $\mathcal{F}_N$ is the perpendicular projection of the CG of the aircraft on the surface of earth. The x axis coincides with the geographic north, the y axis coincides with the east, and the z axis points to center of earth.

2.1.3 The fixed-body reference frame

The fixed-body reference frame $\mathcal{F}_B$ is consolidated to the aircraft fuselage. As shown in Figure 2.1, the origin of $\mathcal{F}_B$ is fixed on the CG of the aircraft. The x axis coincides with the nose of the aircraft, the y axis coincides with the right win, and the z axis points down.

2.1.4 The wind reference frame

The wind reference frame $\mathcal{F}_W$, known also as the stability frame is similar to the body-fixed reference frame $\mathcal{F}_B$. As shown in Figure 2.1, the origin of $\mathcal{F}_W$ is fixed on the CG of the aircraft. The x axis coincides with the forward velocity vector V on the xy plan of $\mathcal{F}_B$. The y axis remains in the xy plane of the body frame $\mathcal{F}_B$, it is orthogonal to the x axis and it points toward the right wing. Finally, the z axis is orthogonal to the x and y axes and it points down.

2.2 Transformation between reference frames

The three matrices used for transformations as follows (McLean, 1990), (Nelson, 1998):

$$R_N^I = \begin{pmatrix} -s(\mu)c(\gamma) & -s(\mu)s(\gamma) & c(\mu) \\ -s(\gamma) & c(\gamma) & 0 \\ -c(\mu)c(\gamma) & -c(\mu)s(\gamma) & -s(\mu) \end{pmatrix} \tag{2.3}$$

$$R_B^N = \begin{pmatrix} c(\theta)c(\psi) & c(\theta)s(\psi) & -s(\theta) \\ -c(\varphi)s(\psi) + s(\varphi)s(\theta)c(\psi) & c(\varphi)c(\psi) + s(\varphi)s(\theta)s(\psi) & s(\varphi)c(\theta) \\ s(\varphi)s(\psi) + c(\varphi)s(\theta)c(\psi) & -s(\varphi)c(\psi) + c(\varphi)s(\theta)s(\psi) & c(\varphi)c(\theta) \end{pmatrix} \tag{2.4}$$

$$R_B^W = \begin{pmatrix} c(\alpha)c(\beta) & -c(\alpha)s(\beta) & -s(\alpha) \\ s(\beta) & c(\beta) & 0 \\ s(\alpha)c(\beta) & -s(\alpha)s(\beta) & c(\alpha) \end{pmatrix} \tag{2.5}$$

where $c(\cdot)$ and $s(\cdot)$ design $cos(\cdot)$ and $sin(\cdot)$ respectively.

Figure 2.2 illustrates the most three important transformations between reference frames used for modeling a standard nonlinear aircraft model.

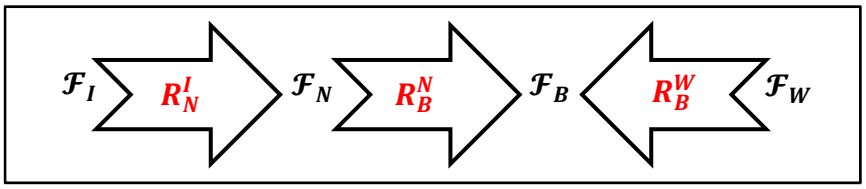

Figure 2.2 The transformation matrices between reference frames

2.3 Nonlinear standard aircraft model

A standard aircraft is represented with three usual primary control surfaces, namely elevator, ailerons, and rudder. The nonlinear dynamics of a standard aircraft dynamics can be developed based on the second Newton law. To make Newton's laws applicable, the following assumptions are to be considered (McLean, 1990), (Etkin et Reid, 1996), (Stevens et Lewis, 2003), (Bates et Hagström, 2007):

- The inertial reference frame is a topocentric coordinate system: the origin is fixed at the center of the Earth;
- The origin of the aircraft frame (body frame) is located identically at the center of gravity of the aircraft;
- The aircraft is flying over a few minutes (the path is rectilinear);
- The Centripetal and Coriolis accelerations of the earth are neglected compared to the earth gravity field;
- The aircraft is considered as a rigid body;
- The earth is considered to be a fixed body in space.

2.3.1 Equations of rigid-body for a translation motion

The Newton's second law, relating forces acting on the aircraft as shown in Figure 2.3, expressed in $\mathcal{F}_B$ is given in (Nelson, 1998) as follows:

$$F_g^B + F_{Th}^B + F_A^B = m\left(\frac{d}{dt}V^B\right) + \Omega^B \times V^B \tag{2.6}$$

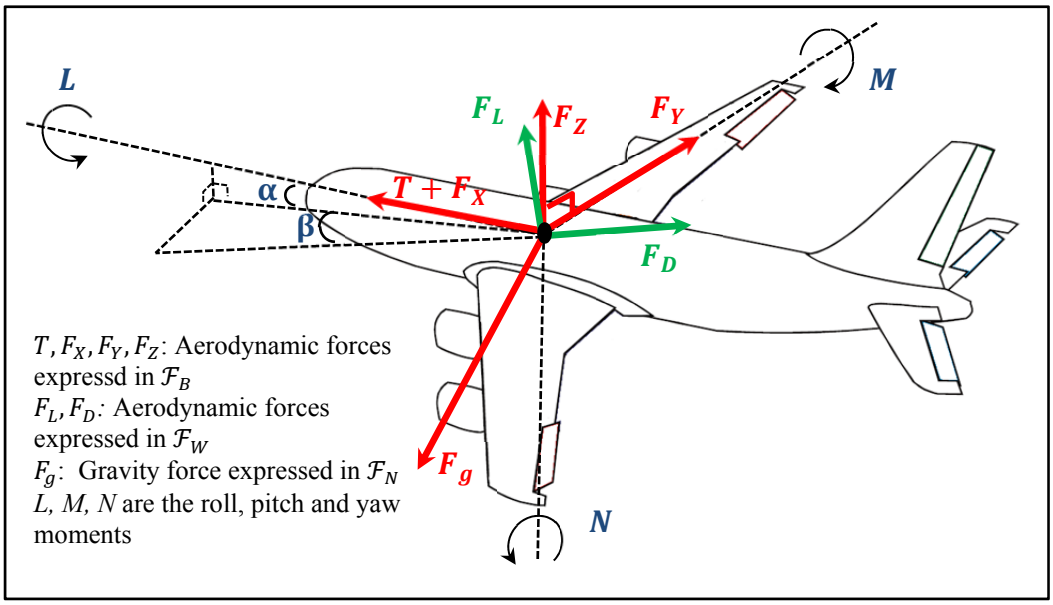

Figure 2.3 Forces and moments acting on the aircraft
Adapted from Etkin et Reid (1996)

where:

× is the cross product operator.

$V^B = \begin{pmatrix} V_x \\ V_y \\ V_z \end{pmatrix} = \begin{pmatrix} V cos\alpha cos\beta \\ V sin\beta \\ V sin\alpha cos\beta \end{pmatrix}$ is the velocity of the aircraft expressed in $\mathcal{F}_B$.

$\Omega^B = \begin{pmatrix} p \\ q \\ r \end{pmatrix}$ is the angular velocity of the aircraft expressed in $\mathcal{F}_B$.

$F_g^B = R_B^N F_g^N = R_B^N \begin{pmatrix} 0 \\ 0 \\ mg \end{pmatrix} = mg \begin{pmatrix} -sin\theta \\ sin\varphi cos\theta \\ cos\varphi cos\theta \end{pmatrix}$ is the force of gravity expressed in $\mathcal{F}_B$.

$F_{Th}^B = \begin{pmatrix} T \\ 0 \\ 0 \end{pmatrix}$ is the force of the engine thrust expressed in $\mathcal{F}_B$. This force is taken assuming that the thrust acts only on the longitudinal axis.

$F_A^B = \begin{pmatrix} F_X \\ F_Y \\ F_Z \end{pmatrix} = \begin{pmatrix} C_X \overline{q} S_w \\ C_Y \overline{q} S_w \\ C_Z \overline{q} S_w \end{pmatrix}$ are the aerodymamic forces expressed in $\mathcal{F}_B$.

m (kg): The mass of the aircraft which is assumed to be constant.

$g = 9{,}80\ 665$ (m/s^2): gravitational acceleration.

F_X, F_Y and F_Z are longitudinal, lateral and vertical forces respectively.

T is the engine thrust.

$\bar{q}$ (lb/ft): Dynamic pressure.

S_w (ft^2 or m^2): Total wing area.

V (ft/s or m/s): is the longitudinal velocity.

α (rad or deg): is the angle of attack.

β (rad or deg): is the sideslip angle.

φ (rad or deg): is the roll angle

θ (rad or deg): is the pitch angle.

C_X, C_Y, C_Z are the aerodynamic coefficients and are defined later in section 2.3.3.

Hence, the equations for the translation motion are defined as follows:

$$mg \begin{pmatrix} -sin\theta \\ sin\varphi cos\theta \\ cos\varphi cos\theta \end{pmatrix} + \begin{pmatrix} T \\ 0 \\ 0 \end{pmatrix} + \begin{pmatrix} F_x \\ F_y \\ F_z \end{pmatrix} = m \begin{pmatrix} \dot{V}_x \\ \dot{V}_y \\ \dot{V}_z \end{pmatrix} + \begin{pmatrix} p \\ q \\ r \end{pmatrix} \times \begin{pmatrix} V_x \\ V_y \\ V_z \end{pmatrix} \tag{2.7}$$

Then:

$$m \begin{pmatrix} \dot{V}_x \\ \dot{V}_y \\ \dot{V}_z \end{pmatrix} = mg \begin{pmatrix} -sin\theta \\ sin\varphi cos\theta \\ cos\varphi cos\theta \end{pmatrix} + \begin{pmatrix} T \\ 0 \\ 0 \end{pmatrix} + \begin{pmatrix} C_X \overline{q} S_w \\ C_Y \overline{q} S_w \\ C_Z \overline{q} S_w \end{pmatrix} - \begin{pmatrix} p \\ q \\ r \end{pmatrix} \times \begin{pmatrix} V_x \\ V_y \\ V_z \end{pmatrix} \tag{2.8}$$

The translation equations defined by (2.8) are generally chosen to be expressed in $\mathcal{F}_W$ because the aerodynamic forces and moments are more naturally expressed in terms of the forward velocity V, the angle of attack α and the sideslip angle β. These terms are also known as wind parameters. In addition, the aerodynamic forces are easier to define in $\mathcal{F}_W$ in terms of the lift force, the drag force and the lateral force, see Figure (2.3). Using the matrix conversion from $\mathcal{F}_B$ to $\mathcal{F}_W$, equation (2.8) becomes:

$$m(R_B^W)^{-1}\begin{pmatrix}\dot{V}_x\\ \dot{V}_y\\ \dot{V}_z\end{pmatrix} = mg(R_B^W)^{-1}\begin{pmatrix}-sin\theta\\ sin\varphi cos\theta\\ cos\varphi cos\theta\end{pmatrix} + (R_B^W)^{-1}\begin{pmatrix}T\\ 0\\ 0\end{pmatrix} + (R_B^W)^{-1}\begin{pmatrix}C_X\overline{q}S_w\\ C_Y\overline{q}S_w\\ C_Z\overline{q}S_w\end{pmatrix} - (R_B^W)^{-1}\begin{pmatrix}p\\ q\\ r\end{pmatrix}\times(R_B^W)^{-1}\begin{pmatrix}V_x\\ V_y\\ V_z\end{pmatrix} \quad (2.9)$$

The final form of the translation equations in $\mathcal{F}_W$ takes the form:

$$m\begin{pmatrix}\dot{V}\\ Vcos\beta\dot{\alpha}\\ V\dot{\beta}\end{pmatrix} = mg\begin{pmatrix}-c\alpha c\beta s\theta + s\varphi c\theta s\beta + c\varphi c\theta s\alpha c\beta\\ s\alpha s\beta c\varphi c\theta\\ c\alpha s\beta s\theta + c\beta s\varphi c\theta - s\alpha s\beta c\varphi c\theta\end{pmatrix} + \begin{pmatrix}Tsin\alpha cos\beta\\ -Tsin\alpha\\ -Tcos\alpha sin\beta\end{pmatrix} + \begin{pmatrix}C_D\overline{q}S_w sin\alpha cos\beta\\ -C_Y\overline{q}S_w cos\alpha sin\beta\\ C_L\overline{q}S_w cos\alpha\end{pmatrix} + mV\begin{pmatrix}0\\ -pcos\alpha tan\beta + q - rsin\alpha tan\beta\\ psin\alpha - rcos\alpha\end{pmatrix} \quad (2.10)$$

Finally, the cinematic equations for the translation motion in $\mathcal{F}_N$ are defined as follows:

$$\begin{pmatrix}\dot{x}_N\\ \dot{x}_E\\ \dot{x}_D\end{pmatrix} = (R_B^N)^{-1}\begin{pmatrix}V_x\\ V_y\\ V_z\end{pmatrix} = (R_B^N)^{-1}\begin{pmatrix}Vcos\alpha cos\beta\\ Vsin\beta\\ Vsin\alpha cos\beta\end{pmatrix} \quad (2.11)$$

where x_N, x_E, x_D are the north, east and down position respectively. Note that x_D must be negative because of the direction (down) of the z axis in the $\mathcal{F}_N$.

2.3.2 Equations of rigid-body for an angular motion

Similarly, the angular accelerations can be determined by applying Newton's second law as follows (Nelson, 1998):

$$\begin{pmatrix} L \\ M \\ N \end{pmatrix}^B = I^B \left(\frac{d}{dt} \Omega^B \right) + \Omega^B \times (I^B \Omega^B) \tag{2.12}$$

where:

$\begin{pmatrix} L \\ M \\ N \end{pmatrix}^B = \begin{pmatrix} C_l \overline{q} S_w b \\ C_m \overline{q} S_w \bar{c} \\ C_n \overline{q} S_w b \end{pmatrix}$ are the roll, pitch and yaw moments expressed in the $\mathcal{F}_B$.

$I^B = \begin{pmatrix} I_{xx} & 0 & I_{xz} \\ 0 & I_{yy} & 0 \\ I_{zx} & 0 & I_{zz} \end{pmatrix}$ is the inertia matrix of the aircraft expressed in the $\mathcal{F}_B$.

$\overline{c}$: Mean chord (ft).

b: Wing Span (ft).

C_l, C_m, C_n are the aerodynamic coefficients and are defined later in section 2.3.3.

The equations for the angular motion are then defined as follows:

$$\begin{pmatrix} \dot{p} \\ \dot{q} \\ \dot{r} \end{pmatrix} = (I^B)^{-1} \left(\begin{pmatrix} C_l \overline{q} S_w b \\ C_m \overline{q} S_w \bar{c} \\ C_n \overline{q} S_w b \end{pmatrix} - \begin{pmatrix} p \\ q \\ r \end{pmatrix} \times I^B \begin{pmatrix} p \\ q \\ r \end{pmatrix} \right) \tag{2.13}$$

The angular equations defined by (2.13) are generally chosen to be expressed in $\mathcal{F}_B$ because the aircraft inertia matrix I^B in this frame is assumed to be fixe. In the $\mathcal{F}_W$, I^B depends on α and β.

Finally, the cinematic equations for the angular motion in $\mathcal{F}_\mathrm{B}$ are defined as follows:

$$\begin{pmatrix} \dot{\varphi} \\ \dot{\theta} \\ \dot{\psi} \end{pmatrix} = \begin{pmatrix} 1 & tan\theta sin\varphi & tan\theta cos\varphi \\ 0 & cos\varphi & -sin\varphi \\ 0 & \frac{sin\varphi}{cos\theta} & \frac{cos\varphi}{cos\theta} \end{pmatrix} \begin{pmatrix} p \\ q \\ r \end{pmatrix} \tag{2.14}$$

where φ, θ, ψ are the roll, pitch and yaw angles respectively.

2.3.3 Summary of the nonlinear aircraft model

Defining C_X, C_Y, C_Z and C_l, C_m, C_n as follows (Chaib et al., 2009b):

$$\begin{cases} C_X = C_{D_0} + C_{D_\alpha}\alpha + C_{D_{i_h}} i_h + C_{D_{\delta_e}}\delta_e \\ C_Y = C_{y_\beta}\beta + C_{y_{\delta_a}}\delta_a + C_{y_{\delta_r}}\delta_r \\ C_Z = C_{L_0} + C_{L_\alpha}\alpha + C_{L_{i_h}} i_h + C_{L_{\delta_e}}\delta_e \end{cases} \tag{2.15}$$

$$\begin{cases} C_l = C_{l_\beta}\beta + C_{l_{\delta_a}}\delta_a + C_{l_{\delta_r}}\delta_r \\ C_m = C_{m_0} + C_{m_\alpha}\alpha + C_{m_{i_h}} i_h + C_{m_{\delta_e}}\delta_e \\ C_n = C_{n_\beta}\beta + C_{n_{\delta_a}}\delta_a + C_{n_{\delta_r}}\delta_r \end{cases} \tag{2.16}$$

where:

α, β (rad): angle of attack and sideslip angle.

i_h(rad or deg): horizontal stabilizer incidence angle.

$\delta_e, \delta_a, \delta_r$ (rad): elevator, aileron, rudder deflections.

C_{ij}, $i = D, Y, L, l, m, n$ and $j = 0, M, p, q, r, \alpha, \beta, i_h, \delta_a, \delta_e, \delta_r$ are the aerodynamic coefficients and are modelled in Appendix I.

By replacing (2.15) and (2.16) in (2.10) and (2.13) respectively and by adding (2.11) and (2.14), the set of first-order nonlinear differential equations $\dot{x} = f(x, u)$, where $x(t) = [V\ \alpha\ \beta\ p\ q\ r\ \varphi\ \theta\ \psi]^{\mathrm{T}}$ and $u(t) = [\delta_a\ \delta_r\ \delta_e\ T]^{\mathrm{T}}$ are state and control vectors respectively, is described as follows (Chaib et al., 2009b):

$$\dot{V} = \frac{sin\beta}{m}\bar{q}S_w C_{Y\beta}\beta - \frac{cos\alpha cos\beta}{m}\bar{q}S_w\left(C_{D_0} + C_{D_\alpha}\alpha + C_{D_{i_h}} i_h\right) - \frac{sin\alpha cos\beta}{m}\bar{q}S_w\left(C_{L_0} + C_{L_\alpha}\alpha + C_{L_{i_h}} i_h\right) + g(-cos\alpha cos\beta sin\theta + sin\beta sin\varphi cos\theta + sin\alpha cos\beta cos\varphi cos\theta) + \frac{sin\beta}{m}\bar{q}S_w C_{Y\delta_a}\delta_a + \frac{sin\beta}{m}\bar{q}S_w C_{Y\delta_r}\delta_r - \left(\frac{cos\alpha cos\beta}{m}\bar{q}S_w C_{D\delta_e} + \frac{sin\alpha cos\beta}{m}\bar{q}S_w C_{L\delta_e}\right)\delta_e + \frac{cos\alpha cos\beta}{m}T \tag{2.17}$$

$$\dot{\alpha} = -cos\alpha tan\beta p + q - sin\alpha tan\beta r + \frac{sin\alpha}{mVcos\beta}\bar{q}S_w\left(C_{D_0} + C_{D_\alpha}\alpha + C_{D_{i_h}} i_h\right) - \frac{cos\alpha}{mVcos\beta}\bar{q}S_w\left(C_{L_0} + C_{L_\alpha}\alpha + C_{L_{i_h}} i_h\right) + \frac{g}{Vcos\beta}(sin\alpha sin\theta + cos\alpha cos\varphi cos\theta) + \left(\frac{sin\alpha}{mVcos\beta}\bar{q}S_w C_{D\delta_e} - \frac{cos\alpha}{mVcos\beta}\bar{q}S_w C_{L\delta_e}\right)\delta_e - \frac{sin\alpha}{mVcos\beta}T \tag{2.18}$$

$$\dot{\beta} = sin\alpha p - cos\alpha r + \frac{cos\alpha sin\beta}{mV}\bar{q}S_w\left(C_{L_0} + C_{L_\alpha}\alpha + C_{L_{i_h}} i_h\right) + \frac{cos\beta}{mV}\bar{q}S_w C_{Y\beta}\beta + \frac{sin\alpha sin\beta}{mV}\bar{q}S_w\left(C_{L_0} + C_{L_\alpha}\alpha + C_{L_{i_h}} i_h\right) + \frac{g}{V}(cos\beta cos\theta sin\varphi + cos\alpha sin\beta sin\theta - sin\alpha sin\beta cos\varphi cos\theta) + \frac{cos\beta}{mV}\bar{q}S_w C_{Y\delta_a}\delta_a + \frac{cos\beta}{mV}\bar{q}S_w C_{Y\delta_r}\delta_r + \left(\frac{cos\alpha sin\beta}{mV}\bar{q}S_w C_{D\delta_e} + \frac{sin\alpha sin\beta}{mV}\bar{q}S_w C_{L\delta_e}\right)\delta_e - \frac{cos\alpha sin\beta}{mV}T \tag{2.19}$$

$$\dot{p} = I_1 qr + I_2 pq + \left(I_3\bar{q}S_w C_{l\beta} + I_4\bar{q}S_w C_{n\beta}\right)\beta + \left(I_3\bar{q}S_w C_{l\delta_a} + I_4\bar{q}S_w bC_{n\delta_a}\right)\delta_a + \left(I_3\bar{q}S_w bC_{l\delta_r} + I_4\bar{q}S_w bC_{n\delta_r}\right)\delta_r \tag{2.20}$$

$$\dot{q} = I_5 pr - I_6(p^2 - r^2) + I_7 \bar{q} S_w \bar{c} \left(C_{m_0} + C_{m_\alpha} \alpha + C_{m_{i_h}} i_h \right) + I_7 \bar{q} S_w \bar{c} C_{m\delta_e} \delta_e \tag{2.21}$$

$$\dot{r} = -I_2 qr + I_8 pq + \left(I_4 \bar{q} S_w b C_{l\beta} + I_9 \bar{q} S_w b C_{n\beta} \right) \beta + \left(I_4 \bar{q} S_w b C_{l\delta_a} + I_9 \bar{q} S_w b C_{n\delta_a} \right) \delta_a + \left(I_4 \bar{q} S_w b C_{l\delta_r} + I_9 \bar{q} S_w b C_{n\delta_r} \right) \delta_r \tag{2.22}$$

$$\dot{\varphi} = p + (qsin\varphi + rcos\varphi)tan\theta \tag{2.23}$$

$$\dot{\theta} = qcos\varphi - rsin\varphi \tag{2.24}$$

$$\dot{\psi} = \frac{qsin\varphi + rcos\varphi}{cos\theta} \tag{2.25}$$

$$\dot{x}_N = Vcos\alpha cos\beta \cos\theta \cos\psi - Vsin\beta(\cos\varphi \sin\psi - \sin\varphi \sin\theta \cos\psi) + Vsin\alpha cos\beta(\sin\varphi \sin\psi + \cos\varphi \sin\theta \cos\psi) \tag{2.26}$$

$$\dot{x}_E = Vcos\alpha cos\beta \cos\theta \sin\psi - Vsin\beta(\cos\varphi \cos\psi + \sin\varphi \sin\theta \sin\psi) - Vsin\alpha cos\beta(\sin\varphi \cos\psi - \cos\varphi \sin\theta \sin\psi) \tag{2.27}$$

$$\dot{x}_D = -Vcos\alpha cos\beta \sin\theta - Vsin\beta \sin\varphi \cos\theta - Vsin\alpha cos\beta \cos\varphi \cos\theta \tag{2.28}$$

$I_i, i = 1,9$ (kgm^2) are the moment's inertia and are defined in Appendix I.

2.4 Decoupling aircraft model

The nonlinear six degrees of freedom motion of the nonlinear aircraft model can be decoupled into a longitudinal and a lateral-directional set of equations assuming the following assumptions (McLean, 1990), (Etkin et Reid, 1996), (Stevens et Lewis, 2003), (Bates et Hagström, 2007):

- The aircraft is a rigid body and symmetric;
- Constant mass, constant engine thrust, constant aerodynamics' parameters;
- The atmosphere is assumed fixed with respect to the earth;
- There is a flat Earth (The Earth's curvature is zero);
- There is a non-rotating Earth (No Coriolis accelerations and such are present);
- No lateral slip ($\beta = \dot{\beta} = 0$);
- No roll ($\dot{\varphi}_0 = \varphi = 0$);
- The flight is straight ($\dot{\psi}_0 = 0$);
- The flight is not accelerated ($p_0 = r_0 = 0$);
- The angular velocities p and r are assumed to be very small ($pr = p^2 = r^2 = 0$).

Consider that the forward velocity is expressed in the fixed-body reference frame $\mathcal{F}_B$ by $V = \begin{pmatrix} V_{x_0} + V_x \\ V_{y_0} + V_y \\ V_{z_0} + V_z \end{pmatrix}$, the angular velocity by $\Omega = \begin{pmatrix} p_0 + p \\ q_0 + q \\ r_0 + r \end{pmatrix}$ and the Euler angles $\begin{pmatrix} \varphi_0 + \varphi \\ \theta_0 + \theta \\ \psi_0 + \psi \end{pmatrix}$ where: $\begin{pmatrix} V_{x_0} \\ V_{y_0} \\ V_{z_0} \end{pmatrix}$, $\begin{pmatrix} p_0 \\ q_0 \\ r_0 \end{pmatrix}$ and $\begin{pmatrix} \varphi_0 \\ \theta_0 \\ \psi_0 \end{pmatrix}$ are the component of the trim values. The longitudinal and the lateral models are presented in the next subsections.

2.4.1 Longitudinal model

Considering these assumptions, the longitudinal motion can be described by a system of first order linear differential equations as follows (Nelson, 1998):

$$\dot{V}_x = X_u V_x + X_w V_z - (g cos\theta_0)\theta + X_{\delta_e}\delta_e + X_{\delta_{Th}} T \tag{2.29}$$

$$\dot{V}_z = Z_u V_x + Z_w V_z + V_{x_0} q + -(g sin\theta_0)\theta Z_{\delta_e}\delta_e + Z_{\delta_{Th}} T \tag{2.30}$$

$$\dot{q} = (M_u + M_{\dot{w}}Z_u)V_x + (M_w + M_{\dot{w}}Z_w)V_z + \left(M_q + M_{\dot{w}}V_{x_0}\right)q + \left(M_{\delta_e} + M_{\dot{w}}Z_{\delta_e}\right)\delta_e + \left(M_{\delta_{Th}} + M_{\dot{w}}Z_{\delta_{Th}}\right)\delta_{Th} \quad (2.31)$$

$$\dot{\theta} = q \quad (2.32)$$

2.4.2 Lateral model

Considering these assumptions, the first order linear differential equations for the lateral motion equations are defined as follows (Nelson, 1998), (McLean, 1990):

$$\dot{\beta} = \frac{Y_\beta}{\mu_0}\beta + \frac{Y_p}{\mu_0}p - \left(1 - \frac{Y_r}{\mu_0}\right)r + \left(\frac{gcos\theta_0}{\mu_0}\right)\varphi + \frac{Y_{\delta_r}}{\mu_0}\delta_r \quad (2.33)$$

$$\dot{p} = L_\beta\beta + L_p p + L_r r + L_{\delta_a}\delta_a + L_{\delta_r}\delta_r \quad (2.34)$$

$$\dot{r} = N_\beta\beta + N_p p + N_r r + N_{\delta_a}\delta_a + N_{\delta_r}\delta_r \quad (2.35)$$

$$\dot{\varphi} = p \quad (2.36)$$

The Aerodynamic coefficients for the longitudinal and lateral models can be found in Appendix I.

The resulting models can be written in state-space form $\dot{x}(t) = Ax(t) + Bu(t)$ where $x(t)$ and $u(t)$ are respectively the state and control vectors. Matrices A and B are respectively dynamic and input matrices. In the next two sections of this chapter, the linear model of the AFTI-F16 used in chapter 3 as well as that of the Boeing 767 used in chapter 5 will be described.

2.5 The AFTI-F16 linear aircraft model

The Advanced Fighter Technology Integration (AFTI) aircraft is a modified model of the original F-16 aircraft. The major external modification related to the context of the FTC systems is the addition of symmetric twin vertical canards located on both sides under the engine. However, the original F-16 sensors are maintained (Pawlowski, 1989), (Barfield et D'Azzo, 1983), (Ishmael, Regenie et Mackall, 1984), (Ishmael et McMonagle, 1983), (Fossen, 2011). Figure 2.3 illustrates the AFTI-F16 aircraft and its control surfaces (Ishmael, Regenie et Mackall, 1984).

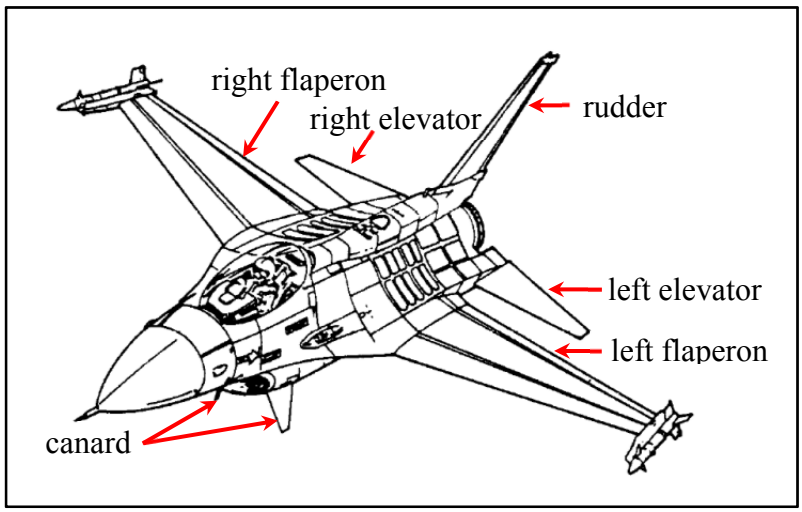

Figure 2.4 The AFTI-F16 and its control surfaces
Adapted from Ishmael, Regenie et Mackall (1984)

AFTI-F16 control surfaces consist of right and left elevators, right and left flaperons, rudder and canards. Elevators are located on the horizontal tail unit and can be deflected symmetrically for pitch control. Flaperons, so-called ailerons, are located on the trailing edge of each wing and can be deflected asymmetrically for roll control. The rudder is located on the vertical tail unit and it can be deflected from side to side for yaw control. The added canards are located under the engine and are used for side force control and for minimum yaw moment control. At the equilibrium point defined by:

- Trim velocity V_T=596.91 ft/s;
- Altitude h=30 000 ft;
- Mass m=9 533,604 433 kg;
- Mach number Mac=0.6.

The state and control vectors are respectively $x(t) = [\alpha\ \beta\ \varphi\ p\ q\ r\ V\ \theta]^T$ and $u(t) = \left[\delta_{eR}\ \delta_{eL}\ \delta_{fR}\ \delta_{fL}\ \delta_c\ \delta_r\right]^T$. A and B are described as below (Shin, Moon et Kim, 2005):

$$A = \begin{pmatrix} Z_\alpha & 0 & 0 & 0 & Z_q & 0 & Z_u & Z_\theta \\ 0 & Y_\beta & Y_\varphi & Y_p & 0 & Y_r & 0 & 0 \\ 0 & 0 & 0 & 1 & 0 & 0 & 0 & 0 \\ 0 & L_\beta & 0 & L_p & 0 & L_r & 0 & 0 \\ M_\alpha & 0 & 0 & 0 & M_q & 0 & M_u & M_\theta \\ 0 & N_\beta & 0 & N_p & 0 & N_r & 0 & 0 \\ X_\alpha & 0 & 0 & 0 & X_q & 0 & X_u & X_\theta \\ 0 & 0 & 0 & 0 & 1 & 0 & 0 & 0 \end{pmatrix} \tag{2.37}$$

$$B = \begin{pmatrix} 0.5Z'_{\delta_e} & 0.5Z'_{\delta_e} & 0.5Z'_{\delta_f} & 0.5Z'_{\delta_f} & 0 & 0 \\ 0.5Y'_{\delta_{DT}} & -0.5Y'_{\delta_{DT}} & 0.5Y'_{\delta_a} & -0.5Y'_{\delta_a} & Y_{\delta_c} & Y_{\delta_r} \\ 0 & 0 & 0 & 0 & 0 & 0 \\ 0.5L'_{\delta_{DT}} & -0.5L'_{\delta_{DT}} & 0.5L'_{\delta_a} & -0.5L'_{\delta_{DT}} & L_{\delta_c} & L_{\delta_r} \\ 0.5M'_{\delta_e} & 0.5M'_{\delta_e} & 0.5M'_{\delta_f} & 0.5M'_{\delta_f} & 0 & 0 \\ 0.5N'_{\delta_{DT}} & -0.5N'_{\delta_{DT}} & 0.5N'_{\delta_a} & 0.5N'_{\delta_a} & N_{\delta_c} & N_{\delta_r} \\ 0.5X'_{\delta_e} & 0.5X'_{\delta_e} & 0.5X'_{\delta_{ef}} & 0.5X'_{\delta_f} & 0 & 0 \\ 0 & 0 & 0 & 0 & 0 & 0 \end{pmatrix} \tag{2.38}$$

In this thesis, the linear dynamic motion described by $\dot{x}(t) = Ax(t) + Bu(t)$ is decoupled in two ways. The first decoupling is used for the design of the Reconfigurable Controller (RC), and the second is used for the design of the detection process and defect diagnosis (FDD). Both decoupling are presented in the following sections.

2.5.1 The decoupling model used for RC

The linear dynamic motion described by $\dot{x}(t) = Ax(t) + Bu(t)$ can be divided into two state spaces, as described previously (Shin, Moon et Kim, 2005):

$$\begin{cases} \dot{x}_1(t) = A_{11}x_1(t) + A_{12}x_2(t) \\ \dot{x}_2(t) = A_{21}x_1(t) + A_{22}x_2(t) + B_2u(t) \end{cases} \tag{3.39}$$

where $x_1(t) = [\alpha\ \beta\ \varphi]^T$ and $x_2(t) = [p\ q\ r]^T$. A_{11}, A_{12}, A_{21}, A_{22} and B_2 are described as below:

$$A_{11} = \begin{pmatrix} Z_\alpha & 0 & 0 \\ 0 & Y_\beta & Y_\varphi \\ 0 & 0 & 0 \end{pmatrix} \tag{2.40}$$

$$A_{12} = \begin{pmatrix} 0 & Z_q & 0 \\ Y_p & 0 & Y_r \\ 1 & 0 & 0 \end{pmatrix} \tag{2.41}$$

$$A_{21} = \begin{pmatrix} 0 & L_\beta & 0 \\ M_\alpha & 0 & 0 \\ 0 & N_\beta & 0 \end{pmatrix} \tag{2.42}$$

$$\mathrm{A}_{22} = \begin{pmatrix} L_p & 0 & L_r \\ 0 & M_q & 0 \\ N_p & 0 & N_r \end{pmatrix} \tag{2.43}$$

$$B_2 = \begin{pmatrix} 0.5L'_{\delta_{DT}} & -0.5L'_{\delta_{DT}} & 0.5L'_{\delta_a} & -0.5L'_{\delta_{DT}} & L_{\delta_c} & L_{\delta_r} \\ 0.5M'_{\delta_e} & 0.5M'_{\delta_e} & 0.5M'_{\delta_f} & 0.5M'_{\delta_f} & 0 & 0 \\ 0.5N'_{\delta_{DT}} & -0.5N'_{\delta_{DT}} & 0.5N'_{\delta_a} & 0.5N'_{\delta_a} & N_{\delta_c} & N_{\delta_r} \end{pmatrix} \tag{2.44}$$

2.5.2 The decoupling model used for FDD

The linear dynamic motion described by $\dot{x}(t) = Ax(t) + Bu(t)$ is decoupled into a longitudinal motion described by $\dot{x}_{long}(t) = A_{long}x_{long}(t) + B_{long}u_{long}(t)$ and a lateral motion described by $\dot{x}_{lat}(t) = A_{lat}x_{lat}(t) + B_{lat}u_{lat}(t)$. The longitudinal and lateral state vectors are respectively $x_{long}(t) = [\theta\ V\ \alpha\ q]^T$ and $x_{lat}(t) = [\varphi\ \beta\ p\ r]^T$. The longitudinal

and lateral input vectors are respectively $u_{long}(t) = [\delta_{eR}\ \delta_{eL}]^T$ and $u_{lat}(t) = \left[\delta_{fR}\ \delta_{fL}\ \delta_c\ \delta_r\right]^T$. A_{long}, B_{long}, A_{lat} and B_{lat} are described as below (Barfield et D'Azzo, 1983):

$$A_{long} = \begin{pmatrix} 0 & 0 & 0 & 1 \\ X_\theta & X_u & X_\alpha & X_q \\ Z_\theta & Z_u & Z_\alpha & Z_q \\ M_\theta & M_u & M_\alpha & M_q \end{pmatrix} \tag{2.45}$$

$$B_{long} = \begin{pmatrix} 0 & 0 \\ X'_{\delta_e} & X'_{\delta_f} \\ Z'_{\delta_e} & Z'_{\delta_f} \\ M'_{\delta_e} & M'_{\delta_f} \end{pmatrix} \tag{2.46}$$

$$A_{lat} = \begin{pmatrix} 0 & 0 & 1 & 0 \\ Y_\varphi & Y_\beta & Y_p & Y_r \\ 0 & L_\beta & L_p & L_r \\ 0 & N_\beta & N_p & N_r \end{pmatrix} \tag{2.47}$$

$$B_{lat} = \begin{pmatrix} 0 & 0 & 0 \\ Y'_{\delta_a} & Y'_{\delta_r} & Y'_{\delta_c} \\ L'_{\delta_a} & L'_{\delta_r} & L'_{\delta_c} \\ N'_{\delta_a} & N'_{\delta_r} & N'_{\delta_c} \end{pmatrix} \tag{2.48}$$

The flight conditions, Aerodynamic coefficients modeling and other details can be found in chapter 3 and in Appendix II.

2.6 The Boeing 767 aircraft linear model

The Boeing 767 is a commercial aircraft which has two turbo engines with a capacity of 181 to 375 passengers. It has a range of 3850 to 6385 nautical miles (Garvin, 1988). The state and control vectors are respectively $x(t) = [V\ \alpha\ \beta\ p\ q\ r\ \varphi\ \theta\ \psi]^T$ and $u(t) = [\delta_a\ \delta_e\ \delta_r\ \delta_{Th}]^T$ (Tao et al., 2013). Given the assumption listed below, the linear dynamic motion can be decoupled into a longitudinal motion described by $\dot{x}_{long}(t) = A_{long}x_{long}(t) + B_{long}u_{long}(t)$ and a lateral motion described by $\dot{x}_{lat}(t) = A_{lat}x_{lat}(t) + B_{lat}u_{lat}(t)$. The

longitudinal and lateral state vectors are respectively $x_{long}(t) = [\theta\ V\ \alpha\ q]^T$ and $x_{lat}(t) = [\varphi\ \beta\ p\ r]^T$. The longitudinal and lateral input vectors are respectively $u_{long}(t) = [\delta_e\ \delta_{Th}]^T$ and $u_{lat}(t) = [\delta_a\ \delta_r]^T$. At the equilibrium point defined by:

- Trim velocity V_T=890 ft/s;
- Altitude h=35 000 ft;
- Mass m=83 460,9 961 kg;
- Mach number Mac=0.8.

Matrices A_{long}, B_{long}, A_{lat} and B_{lat} are described in (Wang, 2012) and (Fossen, 2011). Other details can be found in chapter 5 and in Appendix IV.

2.7 Description of the manuscript-based chapters

In this section, developed AFTC systems in this thesis are presented in the following three subsections. After a summary and a brief introduction and identification of the contribution of the manuscripts, the faults' modeling are presented. Then, the FDD processes, as well as the reconfigurable controllers designed, are detailed. The integration of the overall systems completes the theoretical phase of the manuscripts. In the validation phase of the developed AFTC systems, simulations are performed on a selected aircraft models and the controller's performances are illustrated. In the simulations, the types of actuator faults, as well as the fault scenarios, are carefully chosen to much as possible real flight situations. At the end, conclusions discuss the objectives achieved in the manuscripts.

2.7.1 Manuscript-based chapter 3: Design of a tolerant flight control system in response to multiple actuator control signal faults induced by cosmic rays

This manuscript presents the design of an active tolerant flight control (AFTC) system in response to multiple actuator control signal faults induced by cosmic rays. The manuscript proposes a novel architecture for a fault-tolerant flight control system able to detect and

compensate for a new type of faults. The faults are the cause of cosmic-ray-induced multiple-bit upsets that affect actuator control signals in modern Fly-By-Wire (FBW) avionics systems. In this type of faults, the actuator itself remains healthy.

A fault detection and diagnosis process is designed using a geometric approach combined with an extended multiple model adaptive estimation (EMMAE) technique. The geometric approach handles the lateral model and the EMMAE technique handles the longitudinal model. This procedure is able to process multiple faulty actuator control signals and identify their parameters. The parameters thus obtained are then used with a reconfigurable sliding mode control to compensate for such errors by mobilizing the remaining actuators' healthy control signals. Lyapunov stability theory is used to analyze the closed-loop system stability.

A triple fault scenario is considered. The faults considered representing three cosmic-ray-induced fault types from among those published previously (Hobeika et al., 2013). The first fault is a lock-in-place of the right flaperon. The second fault is canard oscillation. The third fault is another lock-in-place of the left elevator.

The simulation scenario is taken under the assumption that the redundant actuators control signals must not be faulty at the same time. In the longitudinal model of the AFTI/F-16 aircraft, the left and right elevators are considered as redundant actuators for each other. In the lateral model, the left flaperon and canards are considered as redundant actuators for the right flaperon and for the rudder respectively.

The proposed AFTC system is applied to the linear military Advanced Fighter Technology Integration (AFTI-F16) aircraft model (Barfield et D'Azzo, 1983) using Matlab®/Simulink® simulations. FlightGear software simulator is used to show the performance and the behavior of the AFTI-F16 aircraft on a Graphical User Interface (GUI).

2.7.2 Manuscript-based chapter 4: Applied actuator fault accommodation in flight control systems using fault reconstruction-based FDD and SMC reconfiguration

This manuscript presents an applied actuator fault accommodation in flight control systems using fault reconstruction based FDD and SMC reconfiguration. The Geometric approach is used for cosmic ray fault reconstruction, while Sliding Mode Control, based on Lyapunov stability theory, is designed for the reconfiguration of the controller in order to compensate for the fault effect.

Given the lack of redundant actuators, a simple rudder fault scenario is considered. It is modeled as oscillations around zero. The fault model used in the simulation is one of the cosmic rays faults models cited in (Hobeika et al., 2013). For realistic situations, the fault model considered is corrupted by a zero-mean white Gaussian noise.

The designed AFTC system is applied on a non-linear 6 degrees of freedom (DOF) standard aircraft model generated from the Aero Data Model In a Research Environment (ADMIRE) (Forssell et Nilsson, 2005), (Bates et Hagström, 2007), using Matlab®/Simulink® platforms. The FlightGear software simulator is used to show the performance and the behavior of the 6 DOF aircraft on a Graphical User Interface (GUI).

2.7.3 Manuscript-based chapter 5: Reconfigurable flight control system using multi-projector-based geometric approach and sliding mode technique

This manuscript presents the simultaneous fault reconfigurable flight control system using a multi-projector based geometric approach and an Extended Kalman Filter (EKF) for data fusion (Jassemi-Zargani et Necsulescu, 2001). This manuscript treats the case where the number of sensors is greater than the number of control surfaces. In such case, a multi-projector geometric approach based on several sub-projectors combined with an EKF filter is used to design the fault detection and diagnosis process. The idea is to design a multi-

projector system and to use the reconstructed fault inputs given by each sub-projector. The optimal reconstruction fault inputs are then designed by using an Extended Kalman Filter (EKF) algorithm for signal data fusion. The reconfigurable flight control then uses these parameters with a sliding mode control law to carry out an online reconfiguration of the remaining healthy actuators for fault compensation. The Lyapunov theory is used to analyze the closed-loop system stability.

A double fault scenario is considered. The faults considered are derived from (Hobeika et al., 2013). The right thrust responds at only 400 lbs. of the control generated by the controller. For the lateral model, the fault considered is the actuator oscillation. The rudder oscillates close to zero degrees.

The proposed approach is applied to the linear model of the two turbo engines Boeing 767 commercial aircraft. Matlab®/Simulink® numerical simulations are performed to carry out comparisons with a conventional controller simulations, and to demonstrate the effectiveness and robustness of such a controller. FlightGear software simulator is used to show the performance and the behavior of the Boeing 767 aircraft on a Graphical User Interface.

2.8 Summary

In this chapter, the nonlinear model of the standard 6DOF aircraft, as well as, the linear models of the AFTI-F16 and Boeing 767 were introduced. These high-fidelity models are used for the design of FDD processes and control algorithms in this thesis. The types and modeling of actuator failures, as well as the modeling of the system with faults and failures in actuators, are introduced in the next three manuscript-based chapters.

CHAPTER 3

DESIGN OF A TOLERANT FLIGHT CONTROL SYSTEM IN RESPONSE TO MULTIPLE ACTUATOR CONTROL SIGNAL FAULTS INDUCED BY COSMIC RAYS

A. Ghodbane [a], M. Saad [b], C. Hobeika [c], J.–F. Boland [d] and C. Thibeault [e],

[a, b, c, d, e] Department of Electrical Engineering, École de technologie supérieure,
1100 Notre-Dame West, Montreal, Quebec, Canada H3C 1K3

This paper has been published
in the IEEE Transaction on Aerospace and Electronic Systems
Volume 52, Issue 2, April 2016

Abstract

Due to continued miniaturization, semiconductor-based components used in high-performance digital microelectronics are becoming increasingly sensitive to cosmic rays and solar particle events. In the context of high-altitude flight control systems based on fly-by-wire techniques, this may produce sensor noise or affect actuator control signals. Although the consequences so far have been simply reductions in aircraft performance, catastrophic scenarios may be envisioned. In this paper, we propose a novel architecture for a fault-tolerant flight control system able to detect and compensate for cosmic-ray-induced multiple-bit upsets that affect actuator control signals in modern fly-by-wire avionics systems, while assuming that the actuator itself remains healthy. A fault detection and diagnosis procedure was designed using a geometric approach combined with an extended multiple model adaptive estimation technique. This procedure is able to process multiple faulty actuator control signals and identify their parameters. The parameters thus obtained are then used with a reconfigurable sliding mode control to compensate for such errors by mobilizing the remaining actuators' healthy control signals. Lyapunov stability theory is used to analyze the closed-loop system stability. Simulation results using Matlab®/Simulink® showed the effectiveness of the proposed approach in the case of a system challenged with double faults.

FlightGear software simulator is used to show the performance and the behavior of the AFTI-F16 aircraft on a Graphical User Interface.

Keywords: Cosmic ray fault emulation, geometric fault reconstruction, extended multiple model adaptive estimation, extended Kalman filter, reconfigurable flight control, sliding mode control, Lyapunov stability.

3.1 Introduction

A multitude of solar and cosmic rays cause semiconductor devices to experience long-term and single-event effects. These effects produce soft errors such as upsets or transients, or destructive hard errors such as latch-up, burnout, or gate rupture (Maurer et al., 2008). In 1992, Taber and Normand (Taber et Normand, 1995) found that neutrons generated by cosmic rays are capable of causing single-event upsets (SEUs) in electronic systems responsible for producing actuator control signals during flight. The resulting inappropriate actuator deflection affects aircraft dynamics and stability. Recent experiments on flash-based field-programmable-gate-array (FPGA) integrated circuits at different altitudes tend to confirm the initial research. At 40 degrees latitude north, the fault rate of an FPGA may reach 2×10^{-4} per hour at an altitude of 30,000 feet and 7×10^{-4} per hour at 60,000 feet (Brogley, 2009).

An unprecedented and very disturbing incident has confirmed these findings. In October 2008, an Airbus A330 operated by an Australian airline suffered a fault described as rare and unique. During a flight in cruise mode at an altitude of 37,000 feet, one of the three inertial reference data units began to report incorrect values for angle of attack, causing the primary flight control computer to command the aircraft to pitch downwards for 2 seconds, which resulted in injuries to 110 of the 303 passengers. The Aviation Safety Investigation and Report (ASIR) concluded that the failure was most likely due to cosmic rays (Bureau, 2008). The last revelation states that flight control systems should establish rather severe requirements since flight safety is a paramount issue. The current conventional avionics

control system should be redesigned to operate even after several faults. They should absolutely be enhanced to handle these kinds of faults.

Because of the extra weight that would be required, shielding microelectronics against such radiation effects is not feasible. The cost of using radiation hardened (rad-hard) circuits would be prohibitive, due to the number of integrated circuits in an avionics control system. For example, the Airbus A380 has more than 700 FPGA integrated circuits on board (Asadi et Tahoori, 2005), (Hu et Zain, 2010). So far, the problem has been addressed using hardware redundancy to replicate critical components two, three or even four times (Collinson, 2013).

Recent research focused on designing systems to respond appropriately to spontaneous faults is leading to the development of light-weight and cost-effective fault-tolerant flight control (FTFC) systems. The FTFC approach includes processes for fault detection and diagnosis (FDD) and compensation by adjusting on-line flight control (reconfigurable flight control or RFC). Using a mathematical model of aircraft in flight, FDD logs the time, location and form of actuator control signal fault as it occurs, while RFC compensates for it in real time based on the FDD output parameters.

Over the past 20 years, different approaches to the design of mathematical-model-based FDD processes have been developed (Isermann, 2006). The most often cited and used are the residual-generator-based and observer-based approaches (Ducard, 2009). The observer-based approach is also popular for the fault detection problem (Beard, 1971), (Jones, 1973). In these studies, linear systems were used in order to force the fault residual to belong to a different output mode. Massoumnia (Massoumnia, 1986) extended the application to a geometric case and De Persis and Isidori later generalized it to nonlinear systems (De Persis et Isidori, 2001). The potential of the geometric approach for use in avionic systems has been demonstrated (Chaib et al., 2009a), (Chaib et al., 2009b).

RFC research has focused on a wide range of design methodologies usable when tolerance to damage or structural failure is required. These include among others model reference

adaptive control (MRAC) (Tao et al., 2013), feedback linearization (Calise, Lee et Sharma, 2001), adaptive control (Kim, Lee et Kim, 2003), multiple-model control (MMC) (Morse et Ossman, 1990), eigenstructure assignment (EA) (Zhang et Jiang, 2001), robust control (Castillo, Munoz et Santos, 2014), model predictive control (MPC) (Kale et Chipperfield, 2005), (Bemporad et Morari, 1999) and non-linear dynamics inversion (NDI) (Li, Jing et Liu, 2014). Their limitations are described below.

The MRAC controller is defined as a controller that has adjustable parameters in order to force the system output to follow the dynamics of a given reference model. Although designing the control law is simple, this approach has two major limitations. The first is the suitability of the reference model while the second is system stability even with the best reference model. The adaptive control law may be used for indirect design by estimating plant parameters and using these estimates to compute controller parameters or for direct design by estimating the controller parameters. Although this ensures stability and tracking, it does not ensure exact matching of parameters (Tao et al., 2013).

The so-called multi-model switching and tuning (MMST) method is a MMC method based on a finite set of linear models that describe the system under different failure conditions (Morse et Ossman, 1990). A controller is designed for each model. The overall control is a weighted combination of that provided by the designed controllers. The weights are determined using Kalman filters designed for each model. This type of controller requires prior knowledge of the different types of faults that can occur, making it unreliable in real situations.

EA is designed to maintain flight stability and maximize system performance using a control law that recovers eigenvalues and eigenvectors. This assumes a linear model of FDD. The goal is to obtain a new own closed-loop structure that is as close as possible to the original closed-loop system. The advantage of this method is that in addition to ensuring stability, it maximizes the performance of the eigenvectors by placing them as closely as possible to those of the original system. However, this requires linear system dynamics and perfect

knowledge of the time of the fault as well as a dynamic post-fault model (Zhang et Jiang, 2001).

The MPC technique uses an explicit model of plant control to predict future output behavior. Using this prediction, it is possible to solve optimal control problems online, where tracking error between the predicted output and the desired reference is minimized over a future horizon. Fundamental limitations of the MPC method are its lack of robustness due to model uncertainty and its sensitivity to noise perturbation (Kale et Chipperfield, 2005).

NDI uses a simple dynamic inversion process to determine the inputs that will yield desired outputs. The advantage of its control law is the ability to control specific state variables directly. However, NDI systems are sensitive to faults in plant modeling and to errors arising from the inversion of plant dynamics. The assumption that dynamics are invertible for all state values is not always true (Li, Jing et Liu, 2014).

SMC has proven robust for uncertain systems and abrupt faults that lead to major changes in flight dynamics and even aircraft instability (Shin, Moon et Kim, 2005), (Fallaha et al., 2011), (Slotine et Li, 1991). This robustness has been studied thoroughly in the literature, making it an appealing feature for fault-tolerant flight control systems. A detailed study on the robustness of the control law under conditions of bounded uncertainties has been published (Slotine et Li, 1991).

The SMC technique utilizes essentially a discontinuous control law to drive the aircraft state trajectory onto a specified surface called the sliding surface, and to keep the state trajectory on this surface for all subsequent time frames. However, SMC is subject to a well-known chattering problem that causes high-frequency vibration of the system. Various techniques have been developed in order to reduce the effect of this problem, including the exponential reaching law (Fallaha et al., 2011).

The novelty of our approach is that multiple actuator faults caused by cosmic rays are diagnosed via a FDD process designed based on the combination of a geometric approach and an extended multiple model adaptive estimation (EMMAE) technique. The fault compensation is ensured in real time using a RSMC based on accurate faults' parameters estimation provided by the FDD process via a reconfiguration mechanism. To the best of our knowledge, these three techniques have never been integrated into a main flight control system. This integration is critical since fault detection and compensation must be very fast. The FDD process must be completed in real time (generally less than 300 ms) in order to allow the RSMC controller to produce an appropriate and effective actuator response. The proposed fault-tolerant flight control technique was applied to compensate for triple actuator faults under the assumption that their exact nature remains unknown. To demonstrate the performance of the proposed control law, numerical simulations were performed using a model of the AFTI/F-16 jet fighter aircraft.

The study presented below is organized as follows. We first describe in Section 3.2 the origin of cosmic rays and how an actuator control signal fault is emulated using a SEU controller. The geometric approach to fault reconstruction is presented in Section 3.3. In Section 3.4, we present an overview of the EMMAE theory. In Section 3.5, the RFC based on RSMC is proposed. In Section 3.6, the numerical simulations carried out to demonstrate the performance of the proposed FTFC system is presented. We state our conclusions in Section 3.7.

3.2 Faults Induced By Cosmic Rays

Avionic systems' designs based on semiconductor devices are more subject to failures caused by radiation. These failures have been an area of interest since the beginning of the 21st century when the first failures were observed in space and avionic applications.

3.2.1 Origins of cosmic rays

High-energy solar and galactic primary cosmic rays generate high-energy particles when they interact with atoms of nitrogen and oxygen in the Earth's atmosphere. At terrestrial flight altitudes, the main particle generated is the high-energy neutron (Ziegler, 1998). These collide with Si nuclei in the semiconductor substrate material and generate charges. If the charge accumulation exceeds the logical threshold of a digital circuit, the result is a current pulse that manifests itself as an electrical noise usually referred to as a single-event effect (SEE) (Asadi et Tahoori, 2005). This phenomenon is illustrated in Figure 3.1.

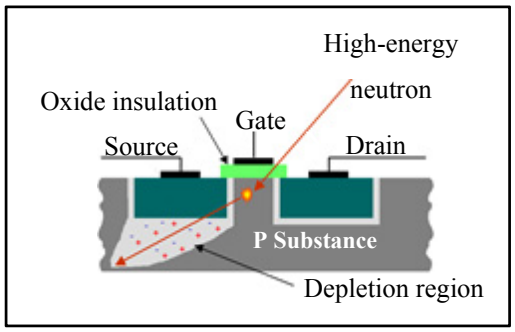

Figure 3.1 Interaction of a high-energy neutron with a silicon-based integrated circuit
Adapted from Asadi et Tahoori (2005)

Such effects on semiconductor devices can assume many forms and are classified as destructive or non-destructive. Destructive effects are called hard errors and may render the device useless. They often can be cleared by a power reset if devices have not been permanently damaged. Non-destructive effects can be of two types.

A single-event transient (SET) can manifest itself in combinational logic, in the global clock line or in control lines. A single-event upset (SEU) causes a change in the state of a memory cell. A single high-energy neutron can also induce a multiple-bit upset (MBU). Data errors that occur as a result of a radiation-induced SET, SEU or MBU are called soft errors, because of their temporary nature (they cause no permanent change in the physical characteristics of the circuit). Memories are among the digital circuits most vulnerable to soft errors (Baumann, 2005). SRAM memories are particularly vulnerable compared to other electronic

devices, due to their limited charge-holding capacity and relatively large critical area. In addition, they may convert a transient into an error, depending on the polarity of the signal they hold. Soft errors in modern sub-65-nm technologies are becoming an increasing nuisance (Shivakumar et al., 2002). MBUs are observed with increasing frequency in devices built using newer technologies (Quinn et al., 2005).

3.2.2 Xilinx-ISE® SEU Controller

Radiation testing is the usual method of evaluating sensitivity to SEEs and analyzing their effects on the behavior of a device. The device is exposed to bombardment with heavy ions and protons in a particle accelerator and induction of SEEs is evaluated. This very expensive testing method does not allow any control over where and when the SEE is induced. In addition, the experiment cannot be repeated.

The sensitivity of FPGA design to radiation depends greatly on the application to be implemented. More affordable fault emulation systems have become popular in recent years to help FPGA designers investigate, evaluate and mitigate radiation effects (Quinn et al., 2013). Fault injection is a technique in which the SEU effect of radiation is emulated using instrumented designs. The SEU controller (Chapman et Jones, 2010) is based on such a technique. It contains an IP core designed by Xilinx® to emulate the effects of SEU-type radiation on SRAM-based FPGA by injecting errors into the configuration memory in a controlled and predictable manner, specifically by forcing bit flips at the chosen location. The SEU controller macro should be implemented within the device and can be controlled via a Universal Asynchronous Receiver Transmitter (UART) interface.

3.2.3 Emulation of actuator faults induced by cosmic rays

Actuators are very important components of aircraft. Aircraft response to their activation is direct. For this reason, recent aircraft are designed with redundant control surfaces, in order to tolerate the loss of some or all of the responsiveness of a given control surface. Cosmic-

ray-induced faults affecting actuator signals can be emulated on a FPGA using the SEU controller. The methodology used to evaluate and quantify radiation effects on actuator control systems on the basis of fault emulation has been described previously (Hobeika et al., 2013). The output data are analyzed to build a model of design susceptibility to SEU and behavior in the presence of radiation. High-level designers can then use the model to develop detection and correction methodologies in order to build robust flight control systems. The proposed procedure can be described in four principal steps, as shown in Figure 3.2.

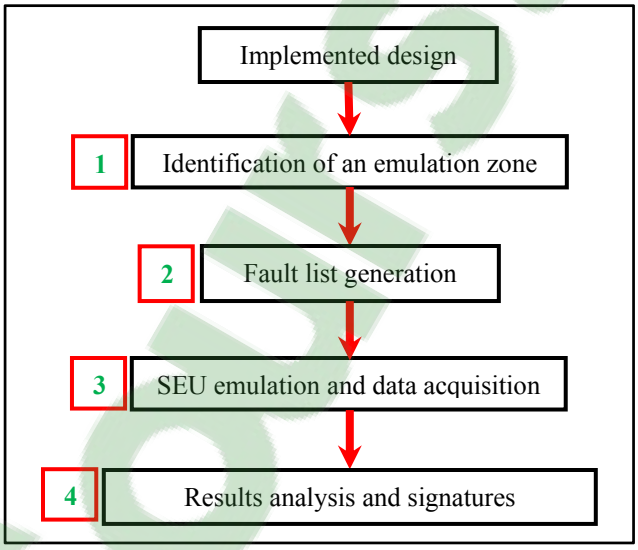

Figure 3.2 The proposed fault emulation methodology
Adapted from Hobeika et al. (2013)

A. Identification of an emulation zone

In the proposed methodology, fault emulation focuses on specific parts of the design to exclude those that will not be affected by radiation. Emulating a bit flip for every cell in the configuration memory would be very time-consuming. In the present case, the part of interest is the designed controller. Figure 3.3 describes the design implemented on FPGA with the SEU controller.

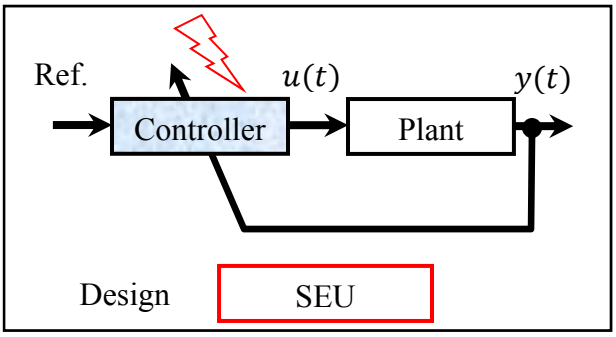

Figure 3.3 Description of the system implemented on FPGA and used for SEU emulation Adapted from Hobeika et al. (2013)

The designed controller represents the emulation zone of interest. The plant and the SEU controller should not be affected when emulating the SEUs. This will reduce the number of bits to emulate and give a representative and accurate results of the controller output $u(t)$ faults only.

B. Fault list generation

The fault list is the list of bit positions to be involved. An in-house tool generates the list of addresses based on the results of step 1. This list still contains some unwanted bits that can cause multiple bit errors. The final list of the bits that can interrupt the test and cause it to fail needs to be edited using a semi-automated process. This edited list of bit addresses is used for emulation.

C. SEU emulation

Fault emulation is based mainly on the use of the SEU controller. Since a large number of emulations are required, this step is fully automated based on the setup described in Figure 3. 4. PC-based software controls the whole experiment so that automated stimulus/response testing can be performed. The software controls the SEU controller on the FPGA via a UART interface as well as the logic analyzer used for data acquisition. Each bit defining the system is flipped. Output acquisition follows each fault injection. The flipped bit is then

corrected and a new emulation is done until all identified bits have been flipped. Figure 3.4 illustrates the experimental setup designed.

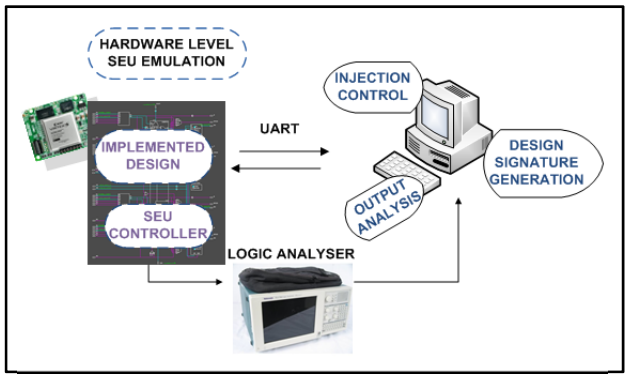

Figure 3.4 The experimental setup
Adapted from Hobeika et al. (2013)

D. Results analysis

The final step consists of analyzing the data obtained in the emulation step and building a model of design susceptibility to SEU and its behavior when it is affected. An in-house tool was developed to perform much of the analysis automatically. The tool allows:

- Automatic comparison of the design outputs with the reference model outputs to compute the corresponding failure rate;
- Separation of the faulty outputs into different groups based on system behavior and calculation of the probability of occurrence of each;
- Generation of comparison graphs for all faulty output groups with the reference behavior in Matlab.

3.2.4 Modeling of actuator faults induced by cosmic rays

Categorization of actuator flight control system faults due to radiation effects was based on automated primary analysis. About 10 % of the faulty outputs fit existing models such as locked in place, loss of effectiveness, floating around trim and hard over. The other 90 %

displayed behaviors described more recently. These are listed in Table 3.1 and illustrated in Figure 3.5 (Hobeika et al., 2013).

Table 3.1 New Control Signal Fault Models (See Figure (3.5) For Description)
Adapted from Hobeika et al. (2013)

Model	Fault Behavior
1	Amplification
2	Sign inversion
3	Locked in place with sudden pulses
4	Oscillation
5	Positive or negative displacement
6	Reflection symmetry around an axis
7	Punctual change of values at time t_0

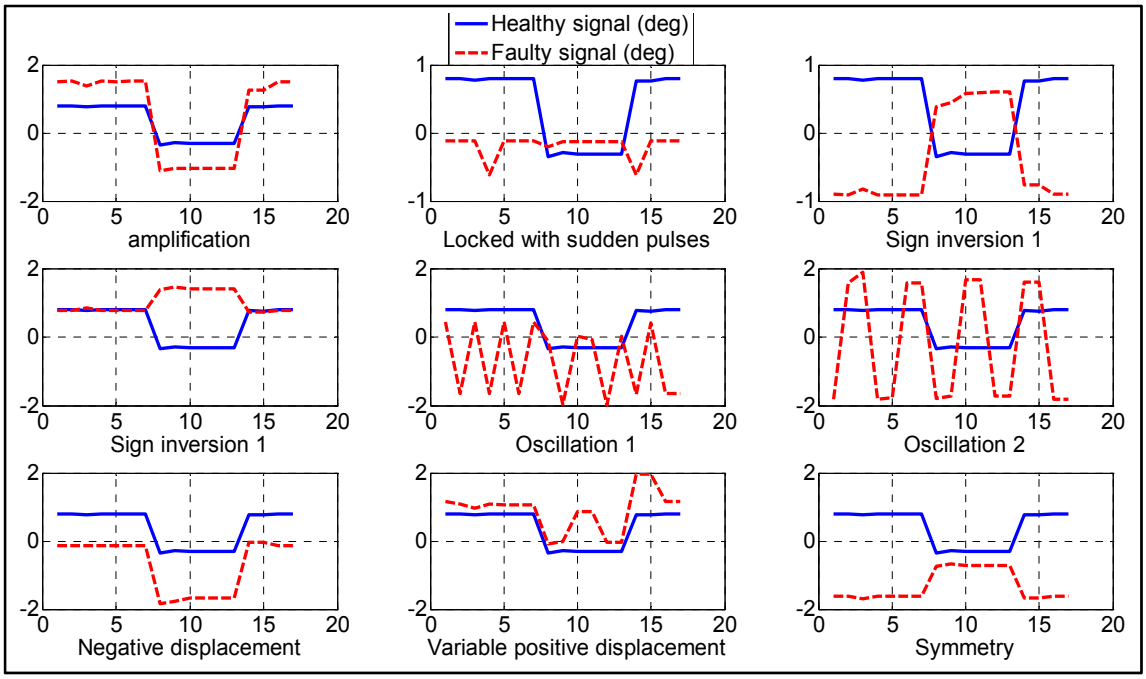

Figure 3.5 Examples of control signal time-varying faulty behavior
Adapted from Hobeika et al. (2013)

Figure 3.6 illustrates the mathematical modeling of neutron-radiation-induced faults as considered in this article. For a surface control signal k affected by a faulty control signal $\bar{u}_k$, we can write (Tao et al., 2013):

$$u_f(t) = Fu(t) + (I_{m\times m} - F)\bar{u}(t) \tag{3.1}$$

$$F = diag\{f_i\}, \quad f_i = \begin{cases} 1, & i \neq k \\ 0, & i = k \end{cases} \tag{3.2}$$

$$\bar{u}(t) = [0 \ldots \bar{u}_k \ldots 0]^T \tag{3.3}$$

where $\bar{u}_1(t), \ldots, \bar{u}_i(t), \ldots, \bar{u}_m(t)$ are the actuator faulty signals and $u_1(t), \ldots, u_i(t), \ldots, u_m(t)$ are the actuator non-faulty control signals obtained from the controller.

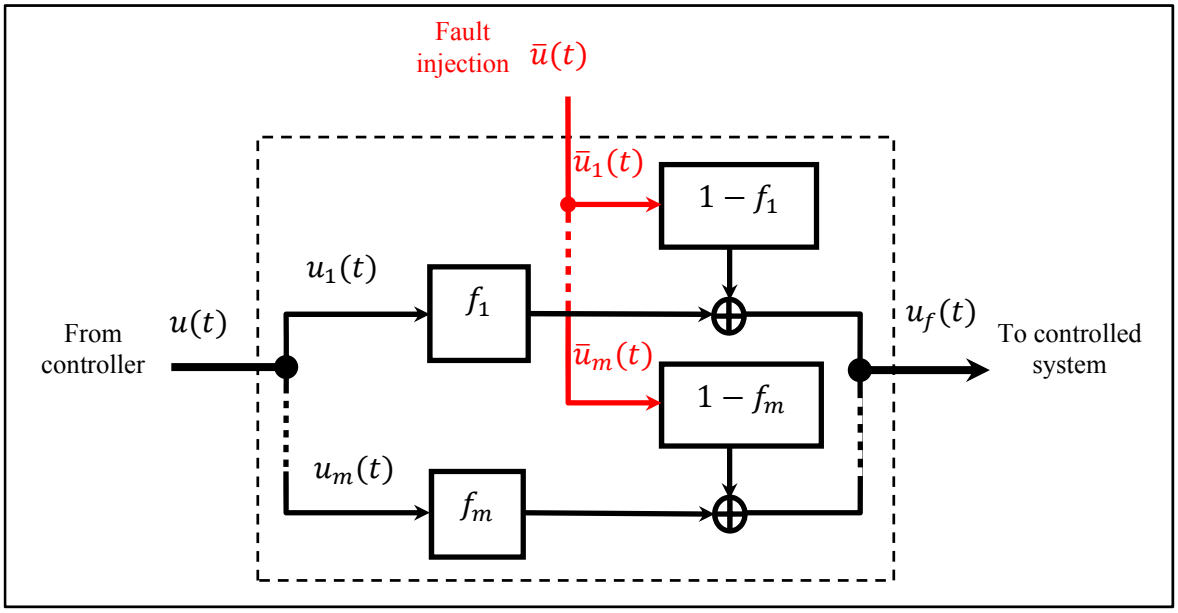

Figure 3.6 Mathematical modeling of neutron-induced radiation faults
Adapted from Tao et al. (2013)

3.3 Geometric Approach to Fault Reconstruction

The geometric reconstruction mechanism considered in this article is described below. We begin by considering linear system dynamics represented by the following state space equations:

$$\begin{cases} \dot{x}(t) = Ax(t) + Bu(t) \\ y(t) = Cx(t) \end{cases} \tag{3.4}$$

where $x \in \mathbb{R}^{n\times 1}$ is the state vector, $u(t) = (u_1\, u_2 \ldots u_m)^T \in \mathbb{R}^{m\times 1}$ is the input vector and $A \in \mathbb{R}^{n\times n}$, $B = (b_1\, b_2 \ldots b_m) \in \mathbb{R}^{n\times m}$ and $C = \left(C_1 \ldots C_i \ldots C_p\right)^T \in \mathbb{R}^{n\times p}$ are respectively the system, input and output matrices.

The main objective of this approach is to design a projector $\Pi(x)$ that decomposes the aircraft state space along a sub-manifold surface S_b into two planes, the first of which is tangent to the faulty inputs and the second is transverse, Figure 3.7 illustrates this projector.

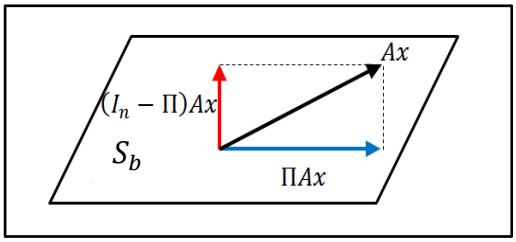

Figure 3.7 Decomposition and projection of Ax using the projector $\Pi(x)$
Adapted from Chaib et al. (2009)

The faulty unknown inputs $u_f(t)$ are then recovered from known outputs $y(t)$, known part of states $x(t)$ and known initial states $x(0)$. This process is called the minimal invertibility concept, and it exists by respecting two conditions. These conditions can be traduced by two theorems:

Theorem 1: *Consider the dynamical system in (3.4), and let* $\mathcal{W}(\ker C)$ *denote the largest controlled-invariant subspace contained in* $\ker C$. *Then the system is left-invertible if and only if:* $\mathcal{W}(\ker C) \cap \mathcal{R}(B) = \{0\}$.

Theorem 2: *If* B *is monic and* $\dim \mathcal{R}(B) = 1$, *then (3.4) is left-invertible if and only if:* $\langle \ker C \,|A\rangle \cap \mathcal{R}(B) = \{0\}$.

where $\mathcal{R}(B)$ denotes the column space (range space) of B and $\ker C$ denotes the kernel function of C, also known as the null space of C. The subspace $\mathcal{W} \subseteq \mathbb{R}^n$ is called controlled

invariant if for any $x_0 \in \mathcal{W}$, there exists an input function u such that the solution of $\dot{x}(t) = Ax(t) + Bu(t)$ satisfies $x(t) \in \mathcal{W}$, for all $t \geq 0$.
The following statements are equivalent:

- $\mathcal{W}$ is controlled invariant;
- $A\mathcal{W} \subseteq \mathcal{W} + \mathcal{R}(B)$;
- There exists a linear map F_M such that $(A + BF_M)\mathcal{W} \subseteq \mathcal{W}$.

More details can be found in (Chaib et al., 2009b) and (Chaib et al., 2009a).

3.3.1 Formulation of the geometric approach

Assuming the same number of inputs m and outputs p, a geometric projector $\Pi(x)$ can be designed as described previously (Chaib et al., 2009b), (Chaib et al., 2009a):

$$\Pi(x) = I_{m\times m} - B{A_{proj}}^{-1}\nabla\sigma^T \tag{3.5}$$

where $I_{m\times m}$ is the identity matrix. The A_{proj} and $\nabla\sigma^T$ matrices are described in greater detail in Appendix V. Using (5), the dynamic vector $Ax(t)$ can be decomposed into a tangent and a transverse components along the sub-manifold S_b as follows:

$$Ax(t) = \Pi(x)Ax(t) + \big(I_{m\times m} - \Pi(x)\big)Ax(t),\ \forall x \in S_b \tag{3.6}$$

The term $\Pi(x)Ax(t)$ represents the tangential component, while the term $\big(I_{m\times m} - \Pi(x)\big)Ax(t)$ represents the transverse component. The definition of the sub-manifold S_b and the details of the approach are shown in Appendix V.

3.3.2 Fault Reconstruction

Once the projector $\Pi(x)$ has been designed, the minimal invertibility concept can be applied to compensate for the faulty inputs using the following equations:

$$\begin{cases} \dot{x}(t) = \Pi(x)Ax(t) + BA_{proj}{}^{-1}\dot{y}(t) \\ u_f(t) = A_{proj}{}^{-1}(\dot{y}(t) - \nabla\sigma^T Ax(t)) \end{cases} \tag{3.7}$$

The proof of equation (3.7) has been published previously (Chaib et al., 2009a). Using (3.6) and (3.7), the system represented in equation (3.4) will take the form:

$$\dot{x}(t) = \Pi(x)Ax(t) + BA_{proj}{}^{-1}\nabla\sigma^T Ax(t) + Bu_f(t) \tag{3.8}$$

The general structure of the geometric approach is illustrated in Figure 3.8.

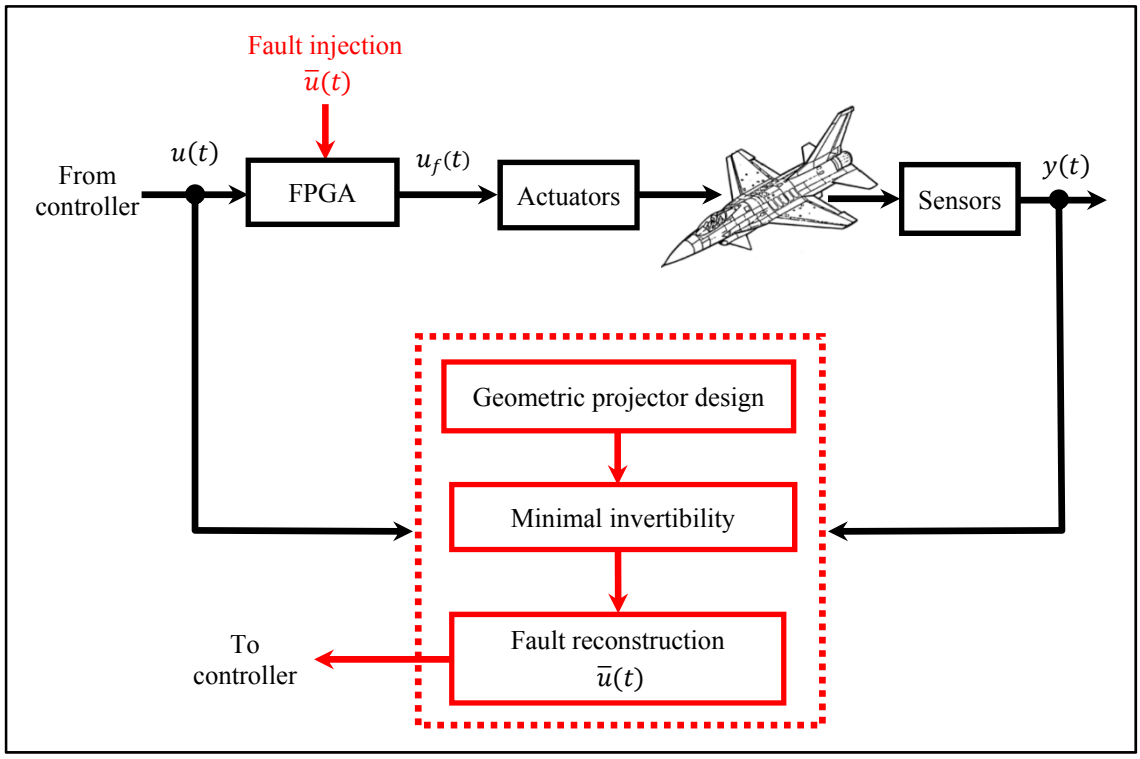

Figure 3.8 General structure of the geometric projector approach
Adapted from Chaib et al. (2009)

3.4 Extended Multiple-Model Adaptive Estimation Theory

This approach uses a bank of $(m+1)$ extended Kalman filters (EKFs) for estimating both the state vector and the fault parameters, with m being the number of actuators. Each EKF_i controls its assigned actuator i for each fault scenario. The $(m+1)^{th}$ filter is added to

control the non-faulty case. Actuator health can be supervised and faults can be detected and isolated as they occur. Figure 3.9 illustrates this method (Ducard, 2009).

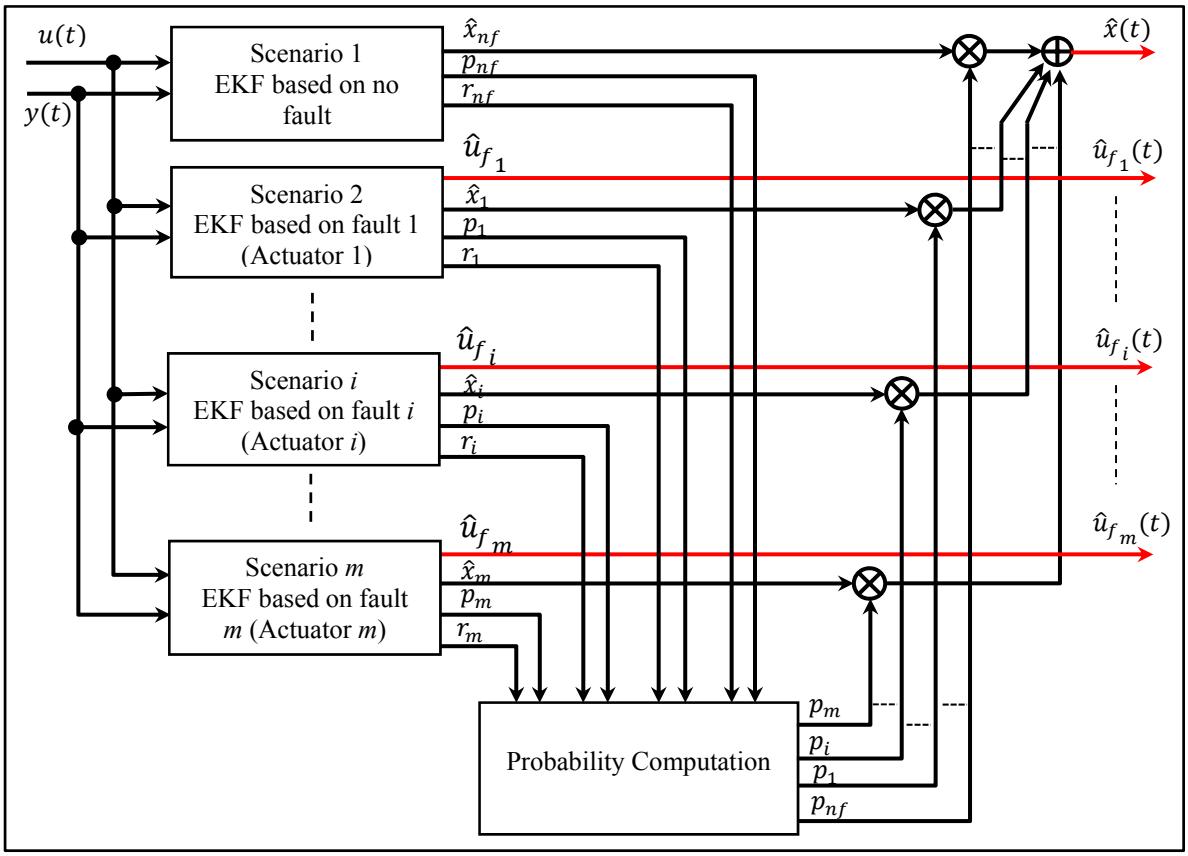

Figure 3.9 General structure of the EMMAE approach
Adapted from Ducard (2009)

3.4.1 Formulation of the extended multiple model adaptive estimation approach

Consider the linear system dynamics represented by the state space equations described in (3.4). To define the matrix that describes a failure of the i^{th} actuator, the i^{th} column of the control input matrix B is zeroed, thus becoming $B_{0,i}$. The state vector $x(t)$ is augmented with the i^{th} faulty actuator deflection $u_{f_i}(t)$ and becomes $z_i(t) = \begin{pmatrix} x & u_{f_i} \end{pmatrix}^T$. The dynamics matrix A will be also augmented with the original i^{th} column of the control input matrix B

noted B_i, becoming $\begin{pmatrix} A & B_i \\ 0 & 1 \end{pmatrix}$. After these modifications, for each EKF_i the system will be as described below (Ducard, 2009):

$$\begin{cases} \dot{z}_i(t) = \begin{pmatrix} \dot{x} \\ \dot{u}_{f_i} \end{pmatrix} = \begin{pmatrix} A & B_i \\ 0 & 1 \end{pmatrix} \begin{pmatrix} x \\ u_{f_i} \end{pmatrix} + \begin{pmatrix} B_{0,i} \\ 0 \end{pmatrix} u(t) \\ y_i(t) = (C \quad 0) \begin{pmatrix} x \\ u_{f_i} \end{pmatrix} \end{cases} \tag{3.9}$$

3.4.2 Fault identification and isolation

The faulty deflection $u_{f_i}(t)$ will be estimated constantly from the EMMAE process in the state vector. The $\hat{u}_{f_i}(t)$ estimate will contribute to determining the new dynamics of the aircraft model using the i^{th} filter. The EKF that matches the occurring fault then produces a residual signal $r_i(t)$, the smallest among the residuals produced by the other EKFs. The residual signal $r_i(t)$ and state vector covariance matrix $R_i(t)$ of each filter EKF_i are used to assign a conditional probability $p_i(t)$ to each fault scenario. The estimated state vector $\hat{x}(t)$ is the sum of the state vector of each EKF $\hat{x}_i(t)$ weighted by its corresponding probability $p_i(t)$.

$$\hat{x}(t) = \sum_i \hat{x}_i(t)\, p_i(t) \tag{3.10}$$

where $\hat{x}_i(t)$ is the state estimate computed by the EKF that assumes the fault scenario θ_i, which is given by Bayes' law as follows (Ducard, 2009):

$$p_i = p_{i,t}[(\theta = \theta_i)/Y_t] = \frac{p[y=y_t/(\theta=\theta_i, Y_{t-T_s})]p_{i,t-T_s}}{\sum_{j=1}^{p+1} p[y=y_t/(\theta=\theta_j, Y_{t-T_s})]p_{j,t-T_s}} \tag{3.11}$$

The probability density is chosen to be a Gaussian function, which is defined as follows (Ducard, 2009):

$$p\big[y = y_t/\big(\theta = \theta_i, Y_{t-T_s}\big)\big] = \frac{1}{(2\pi)^{\frac{p}{2}}|R_{i,t}|^{\frac{1}{2}}} exp\big(-r_{i,t}^T R_{i,t}^{-1} r_{i,t}/2\big) \tag{3.12}$$

where p is the number of outputs, $|R_{i,t}|$ is the determinant of the residual covariance matrix $R_i(t)$ calculated by EKF_i at the time step t, $r_{i,t}$ is the residual signal generated by EKF_i at

the time step t, T_s is the sampling time and $Y_t = \{y_1, y_2, \dots, y_t\}$. The healthiness of the i^{th} actuator status can be determined via the probabilities computed using (3.12). The filter that corresponds to the fault scenario produces a residual signal $r_{i,t}$ that will be small and close to zero and leads to the highest corresponding probability $p_i(t)$. The equations used in each EKF are shown in Appendix VI.

3.5 Reconfigurable Flight Control Design

Among the existing methods, the sliding mode control (SMC) technique is characterized by simplicity and robustness. This technique essentially uses a discontinuous control law to drive the aircraft state trajectory onto a specified surface $S(t)$ called the sliding surface. The aircraft state stays on the surface $S(t)$ for all subsequent time increments. The design steps for the sliding surface, the SMC and the reconfiguration mechanism are described below.

3.5.1 Sliding surface design

Designing the sliding surface is the first step in SMC. The objective of such a design is to obtain the sliding mode dynamics that match the desired trajectories and mismatch uncertainties. Let us consider the general linear system of the form:

$$x^{(n)} = Ax(t) + Bu(t) \tag{3.13}$$

where $x(t)$ is the state vector and $u(t)$ is the control input. Superscript n corresponds to the order of differentiation, while A and B are matrices representing respectively the system and the input. If $n \geq 2$, the sliding surface is a time-varying surface $S(t) \in \mathbb{R}^n$ defined with a vector s such as described previously (Slotine et Li, 1991):

$$s(x,t) = \left(\frac{d}{dt} + \lambda\right)^{(n-1)} \tilde{x}(t) = 0,\ \lambda > 0 \tag{3.14}$$

where $\tilde{x}(t) = x(t) - x_d(t)$ is the output state error and $x_d(t)$ is the desired state. The integral form can be also considered, as follows:

$$s(x,t) = \left(\frac{d}{dt} + \lambda\right)^{(n)} \int_0^t \tilde{x}(t)dt = 0,\ \lambda > 0 \tag{3.15}$$

Equations (3.14) and (3.15) thus define what is called the sliding surface $S(t)$. The system behavior once the aircraft trajectory is on this surface is called the sliding mode or sliding regime. The simplified first-order problem of keeping the scalar $s(x,t)$ at zero can now be defined by choosing the control law $u(t)$ for the system of (3.13) such that when the system is outside of the limits of $S(t)$ we have:

$$\frac{1}{2}\frac{d}{dt}s^2 \leq -\eta|s|,\ \eta > 0 \tag{3.16}$$

When $s(t=0) \neq 0$, the state trajectories require designing a control law to reach $S(t)$ in a finite time. Satisfying (16) guarantees that this requirement will be met. A graphical illustration of (3.14) and (3.15) for $n = 1, 2$ is shown in Figure 3.10.

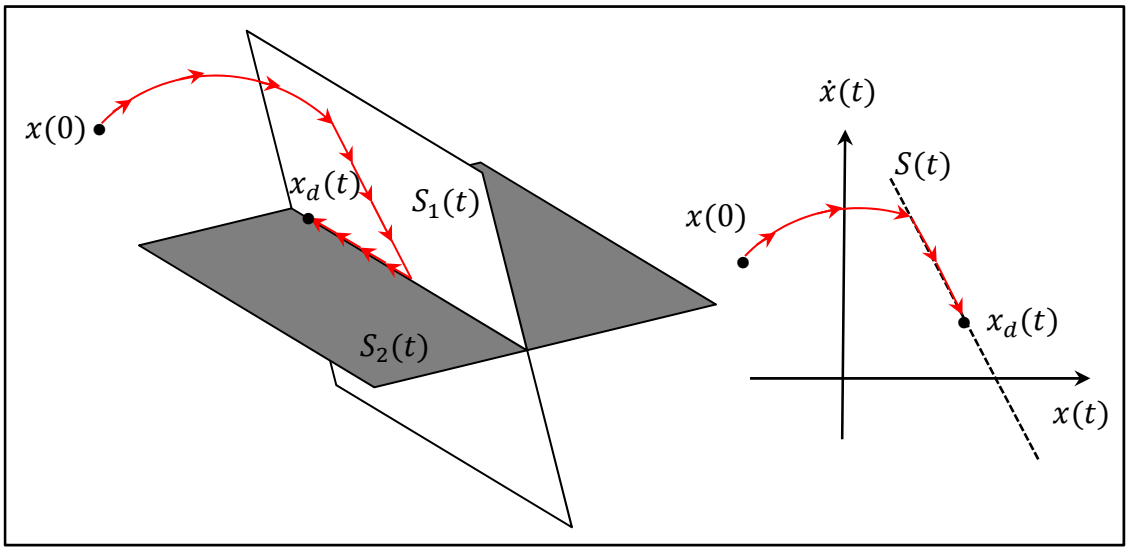

Figure 3.10 Graphical interpretation of the sliding mode equation
Adapted from Slotine et Li (1991) and Utkin (1992)

The time required to reach the surface, t_{reach}, is then defined as follows:

$$t_{reach} \leq \frac{|s(t=0)|}{\eta} \tag{3.17}$$

We conclude that starting from any initial condition, the state trajectories reach the time-varying surface $S(t)$ in a finite time smaller than $\frac{|s(t=0)|}{\eta}$, and then slide along the surface to converge towards $x_d(t)$ exponentially, with a time constant equal to $\frac{1}{\lambda}$ (Slotine et Li, 1991).

3.5.2 Design of the sliding mode control law

Since the case studied in this paper is an aircraft modeled by a first order system, in this section a simple first-order system described by (3.18) is considered:

$$\dot{x}(t) = Ax(t) + Bu(t) \tag{3.18}$$

The sliding vector will take the following form:

$$s(x,t) = \left(\frac{d}{dt} + \lambda\right) \int_0^t \tilde{x}(t)dt = \tilde{x}(t) + \lambda \int_0^t \tilde{x}(t)dt \tag{3.19}$$

Differentiation of (3.19) yields:

$$\dot{s}(x,t) = \dot{x}(t) - \dot{x}_d(t) + \lambda\tilde{x}(t) \tag{3.20}$$

Substituting (3.18) in (3.20), we obtain:

$$\dot{s}(x,t) = Ax(t) + Bu(t) - \dot{x}_d(t) + \lambda\tilde{x}(t) \tag{3.21}$$

Let us choose the Lyapunov candidate function $V_L = \frac{1}{2}s^T s$. Stability will be ensured if the time variation of V_L is a decreasing function. Thus $\dot{V}_L < 0 \Rightarrow s^T\dot{s} < 0$. By specifying:

$$\dot{s}(x,t) = -K.sign(s),\ k > 0, sign(s) = \begin{cases} -1 & if \quad s < 0 \\ 0 & if \quad s = 0 \\ +1 & if \quad s > 0 \end{cases} \tag{3.22}$$

We obtain:

$$\dot{V}_L = -K.s^T.sign(s) < 0,\ \forall s \tag{3.23}$$

Combining (3.18) and (3.22), if B is invertible, then the control law will be as follows:

$$u(t) = B^*[\dot{x}_d(t) - \lambda\tilde{x}(t) - Ax(t)] - B^{-1}Ksign(s) \tag{3.24}$$

where B^* denotes the Moore–Penrose pseudo inverse of B matrix.

Using (3.24), we ensure that the system trajectories will take a finite time to reach the sliding surface $S(t)$, after which the error will approach zero exponentially. The first term of (3.24) is called $u_{eq}(t)$ and represents the continuous control law that drives state trajectories on $S(t)$ and maintains the sliding condition $\dot{s} = 0$, while the second term is called $u_{disc}(t)$ and represents the discrete control law required to push the state trajectories towards $S(t)$. One can note the use of derivate term $\dot{x}_d(t)$ of (3.24). Since it is the desired term, it can be easily generated using simple methods as the 3rd degree polynomial trajectory generator.

3.5.3 Reconfiguration mechanism

The faulty actuator control signal thus takes the form:

$$u_f(t) = Fu(t) + (I_{m\times m} - F)\bar{u}(t) \tag{3.25}$$

In real situations, terms F and $\bar{u}(t)$, so-called fault parameters, are unknown and must be estimated in real time by comparing the faulty input $u_f(t)$ to the computed control input $u(t)$ in the reconfiguration mechanism at each step time. Using fault parameters thus obtained and sensor measurements, the RSMC reconfigures signals for the remaining healthy actuators in order to compensate on line for the faulty actuator signal. After the occurrence of faults, the system dynamics take the form:

$$\begin{cases} \dot{x}(t) = Ax(t) + B[Fu(t) + (I_{m\times m} - F)\bar{u}(t)] \\ y(t) = Cx(t) \end{cases} \tag{3.26}$$

By choosing $U(t) = Fu(t)$ to be the reconfigurable flight control, the control law $U(t)$ will take the form:

$$U(t) = B^*[(\dot{x}_d(t) - \lambda\tilde{x}(t) - Ax(t)) - B(I_{m\times m} - F)\bar{u}(t)] - B^*(Ksign(s)) \tag{3.27}$$

3.6 Case study

The proposed approach was applied to the military aircraft AFTI/F-16 (Advanced Fighter Technology Integration) illustrated in Figure 3.11, a new version of the F-16 with the addition of symmetric actuators called canards. The addition of canards provides more lateral acceleration, which can enhance lateral aerodynamics provided by the rudder. This addition also provides aerodynamic redundancy to the rudder. This redundancy present a positive impact in the design of a reconfigurable fault-tolerant flight control system, since they reconfigure online the remaining redundant healthy actuators to compensate for the faulty actuators (Morse et Ossman, 1990), (Shin, Moon et Kim, 2005), (Barfield et D'Azzo, 1983) and (Wu, 2002). In this section, the FDD process based on the geometric approach for the lateral model and on EMMAE for the longitudinal model is tested using a realistic flight scenario. The aircraft follows a predefined trajectory using a reference altitude and speed profile. The simulation is conducted using sensor noise and wind gusts to test the robustness of the FTFC system in the presence of low-cost sensors and external disturbances.

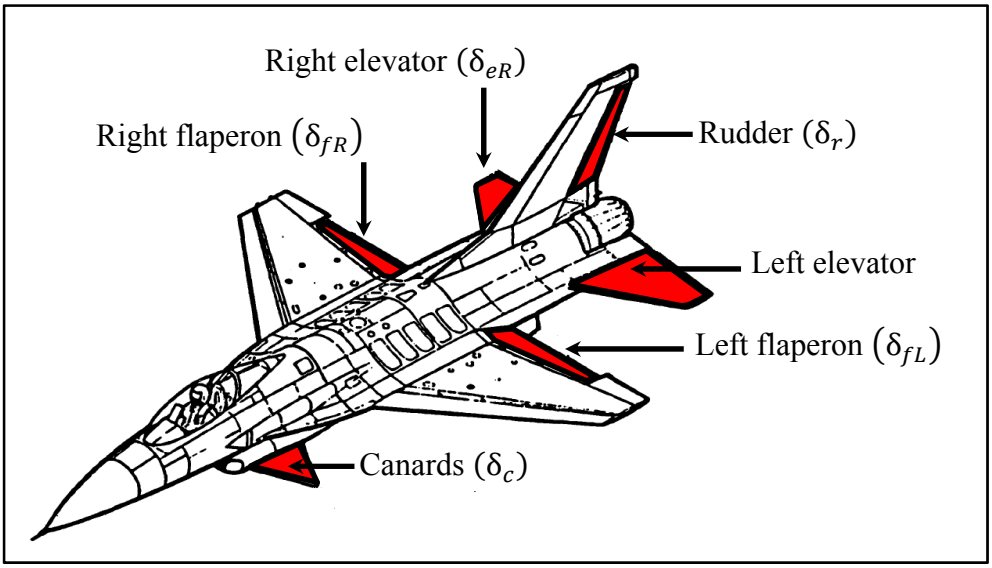

Figure 3.11 The AFTI/F-16 aircraft and its actuators
Adapted from Wu (2002)

3.6.1 The linear model of the AFTI/F-16 aircraft

As described previously in (Morse et Ossman, 1990), (Shin, Moon et Kim, 2005) and (Barfield et D'Azzo, 1983), the linear model of the AFTI/F-16 aircraft is based on two flight conditions, shown in Table II. It is defined here as follows:

$$\dot{x}(t) = Ax(t) + Bu(t) \tag{3.28}$$

where matrices A and B are defined as below:

$$A = \begin{pmatrix} Z_\alpha & 0 & 0 & 0 & Z_q & 0 & Z_u & Z_\theta \\ 0 & Y_\beta & Y_\varphi & Y_p & 0 & Y_r & 0 & 0 \\ 0 & 0 & 0 & 1 & 0 & 0 & 0 & 0 \\ 0 & L_\beta & 0 & L_p & 0 & L_r & 0 & 0 \\ M_\alpha & 0 & 0 & 0 & M_q & 0 & M_u & M_\theta \\ 0 & N_\beta & 0 & N_p & 0 & N_r & 0 & 0 \\ X_\alpha & 0 & 0 & 0 & X_q & 0 & X_u & X_\theta \\ 0 & 0 & 0 & 0 & 1 & 0 & 0 & 0 \end{pmatrix} \tag{3.29}$$

$$B = \begin{pmatrix} 0.5Z'_{\delta_e} & 0.5Z'_{\delta_e} & 0.5Z'_{\delta_f} & 0.5Z'_{\delta_f} & 0 & 0 \\ 0.5Y'_{\delta_{DT}} & -0.5Y'_{\delta_{DT}} & 0.5Y'_{\delta_a} & -0.5Y'_{\delta_a} & Y_{\delta_c} & Y_{\delta_r} \\ 0 & 0 & 0 & 0 & 0 & 0 \\ 0.5L'_{\delta_{DT}} & -0.5L'_{\delta_{DT}} & 0.5L'_{\delta_a} & -0.5L'_{\delta_{DT}} & L_{\delta_c} & L_{\delta_r} \\ 0.5M'_{\delta_e} & 0.5M'_{\delta_e} & 0.5M'_{\delta_f} & 0.5M'_{\delta_f} & 0 & 0 \\ 0.5N'_{\delta_{DT}} & -0.5N'_{\delta_{DT}} & 0.5N'_{\delta_a} & 0.5N'_{\delta_a} & N_{\delta_c} & N_{\delta_r} \\ 0.5X'_{\delta_e} & 0.5X'_{\delta_e} & 0.5X'_{\delta_{ef}} & 0.5X'_{\delta_f} & 0 & 0 \\ 0 & 0 & 0 & 0 & 0 & 0 \end{pmatrix} \tag{3.30}$$

$x(t) = [\alpha\ \beta\ \varphi\ p\ q\ r\ V\ \theta]^T$ and $u(t) = \left[\delta_{eR}\ \delta_{eL}\ \delta_{fR}\ \delta_{fL}\ \delta_c\ \delta_r\right]^T$ are respectively the state and control vector variables listed in Tables 3.2 and 3.3. The numerical aerodynamic parameters of matrices A (dynamics) and B (input) used to define the system in (3.28) are obtained by a general dynamic program and differ depending on flight conditions. They have been described previously in (Morse et Ossman, 1990) and (Barfield et D'Azzo, 1983) and are listed in Appendix II.

Table 3.2 AFTI/F-16 flight conditions
Adapted from Shin, Moon et Kim (2005) and Barfield et D'Azzo (1983)

Parameters	**Flight Condition**
Mach number	0.6
Altitude	30 000 ft.
Dynamic pressure	158.81 lbs./ft^2
Trim Velocity	596.91 ft./s
Trim angle of attack	4.705 degrees

Given the flight parameters listed in Table 3.2, the linear dynamic motion of (3.28) can be divided into longitudinal and lateral motions and a controller can be designed for each mode separately (Barfield et D'Azzo, 1983). Tables 3.3 and 3.4 illustrate state vector and control surfaces for each of these models. Although in this paper one controller is designed for the global system, the separate models are used to prove that even in the case of two separate controllers the proposed method remain applicable, since every controller need to have its own FDD process. To test the processing of simultaneous faults, faulty actuators are chosen on both lateral and longitudinal motions. Choosing the triple fault on both lateral and longitudinal motions ensures that multiple faults are processed.

3.6.2 The reconfigurable mechanism

For the linear system of the AFTI/F-16, the vector *s* was defined otherwise than in section (3.5.1). Indeed, the state space aircraft model can be reduced and divided into two state spaces, as described previously (Shin, Moon et Kim, 2005):

$$\begin{cases} \dot{x}_1(t) = A_{11}x_1(t) + A_{12}x_2(t) \\ \dot{x}_2(t) = A_{21}x_1(t) + A_{22}x_2(t) + B_2u(t) \end{cases} \tag{3.31}$$

where $x_1(t) = [\alpha\ \beta\ \varphi]^T$ and $x_2(t) = [p\ q\ r]^T$. A_{11}, A_{12}, A_{21}, A_{22} and B_2 can be found in chapter 2 and in (Shin, Moon et Kim, 2005). The vector $s(x,t)$ considered in this article is the same as previously considered in (Shin, Moon et Kim, 2005) with the following form:

$$s(x,t) = (s_1 \quad s_2) \times \begin{pmatrix} x_1 \\ x_2 \end{pmatrix} = 0 \tag{3.32}$$

Table 3.3 State vector variables and control surfaces of the AFTI/F-16 longitudinal model Adapted from Barfield et D'Azzo (1983)

State vector variables		Control surfaces	
$\boldsymbol{\theta}$	Pitch angle, rad	$\boldsymbol{\delta_e = \frac{1}{2}(\delta_{eR} + \delta_{eL})}$	Right and left Elevators, rad
$\boldsymbol{V}$	Long. Velocity, ft./s		
$\boldsymbol{\alpha}$	Angle of attack, rad	$\boldsymbol{\delta_f = \frac{1}{2}(\delta_{fR} + \delta_{fL})}$	Right and left flaperon, rad
$\boldsymbol{q}$	Pitch rate, rad/s		

Table 3.4 State vector and control surfaces of the AFTI/F-16 lateral model Adapted from Barfield et D'Azzo (1983)

State vector variables		Control surfaces	
$\boldsymbol{\varphi}$	Roll angle, rad	$\boldsymbol{\delta_f = \frac{1}{2}(\delta_{fR} - \delta_{fL})}$	Right and Left Flaperon, rad
$\boldsymbol{\beta}$	Side slip angle, rad	$\boldsymbol{\delta_c}$	Canards, rad
$\boldsymbol{p}$	Roll rate, rad/s	$\boldsymbol{\delta_r}$	Rudder, rad
$\boldsymbol{r}$	Yaw rate, rad/s		

Without loss of generality, $s_2 = I$ and s_1 is computed using the LQR method. Equations (3.32) and (3.27) are then used to design the sliding surface and the sliding control law respectively. F and $\overline{u}(t)$ can be derived from the FDD process.

3.6.3 Algorithm implementation

The geometric, as well as, the EMMAE methods are both used for the design of the FDD process. Although they have different formulations, they ensure the same roles: detect and diagnose the faults and then transfer faults' parameters to the reconfigurable flight controller. Since the geometric approach has the ability to handle simultaneous faults, it is used for the lateral motion. Indeed, this motion is controlled via four actuators, and the case of a simultaneous fault is highly realistic. The EMMAE approach is used for the longitudinal motion which is controlled by only two actuators. As these two actuators are redundant for each other and they cannot become faulty simultaneously, the EMMAE approach is used

since it has the ability to handle only the single fault. Figure 3.12 illustrates the steps followed for the implementation of the proposed algorithm. The algorithm starts by initializing the fault parameters by setting matrix F at identity ($F = I_{m\times m}$) and zeroing all faults ($\bar{u}_i(t) = 0, i = 1, \dots, m$). Then for each step time, the longitudinal sensor measurements illustrated in Table (3.3) are used to compute the assigned probabilities using (3.11) and (3.12) and the lateral sensor measurements illustrated in Table (3.4) are used to design the geometric projector $\Pi(x)$ using (3.5).

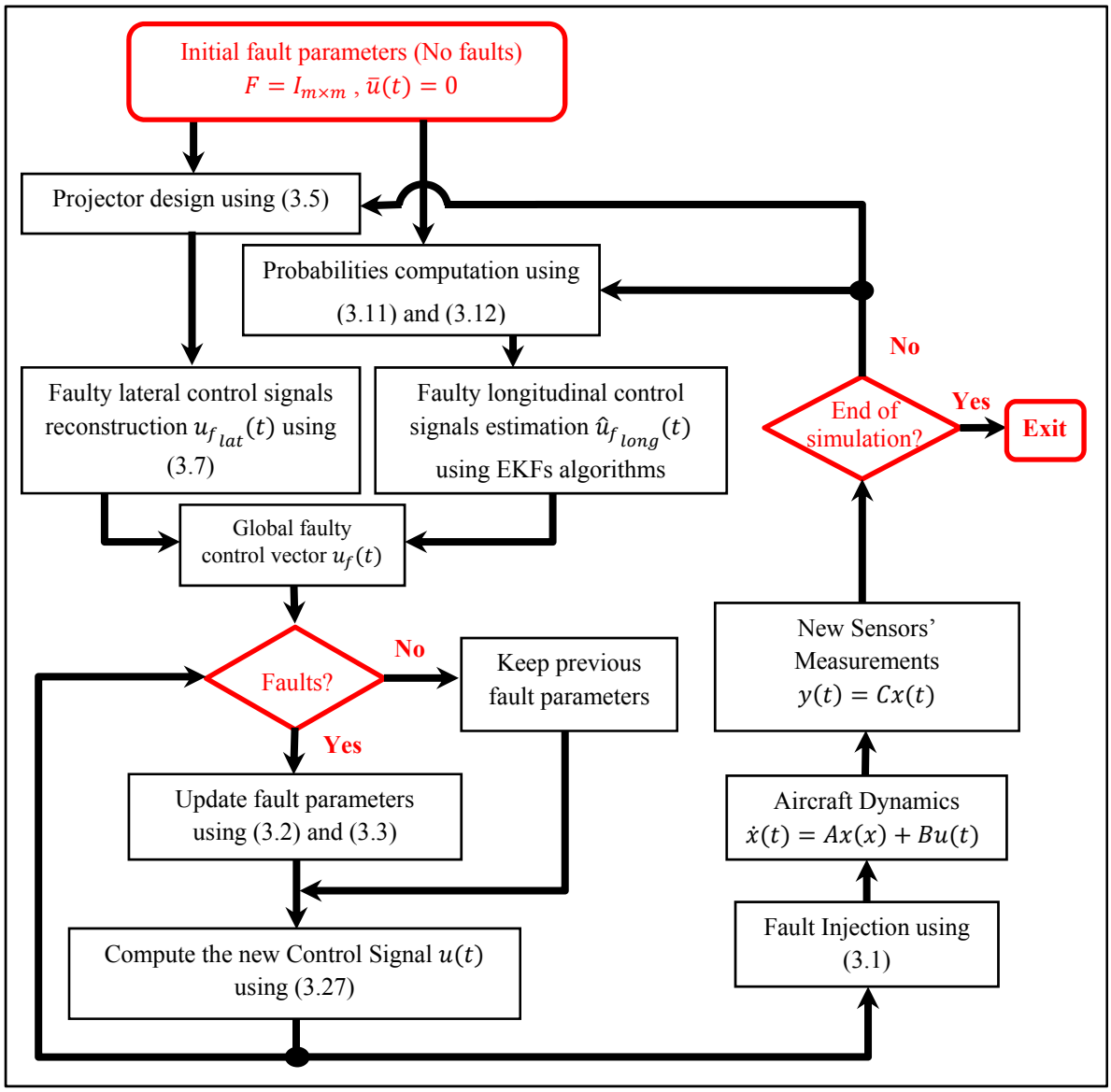

Figure 3.12 Steps followed for implementation of the reconfiguration algorithm

After designing the projector and the probabilities, the unknown lateral control signals $u_{f_{lat}}(t)$ are then reconstructed using (3.7) and the unknown longitudinal control signals $u_{f_{long}}(t)$ are then estimated using EKFs algorithms. The global faulty input $u_f(t)$ and the computed control input $u(t)$ are then compared to compute the fault value $\bar{u}(t)$ and to make the fault decision. Depending on whether or not there is a fault, fault parameters are updated using (3.2) and (3.3) and the new control law is then computed using (3.27). The simulated faults are then injected and finally the sensor measurements are used for the next time step. The overall scheme of the controller designed using the geometric approach, the EMMAE and the RSMC is shown in Figure 3.13.

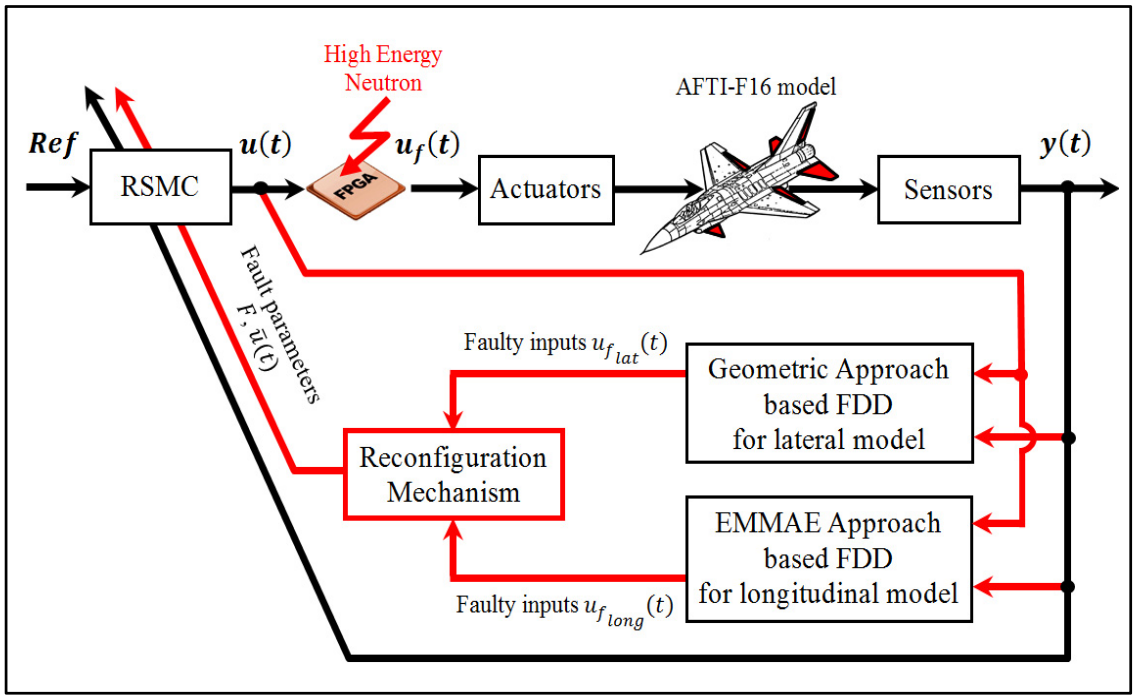

Figure 3.13 FTFC scheme using the Geometric-based FDD (lateral model), EMMAE-based FDD (longitudinal model) and the RSMC

3.6.4 Simulation scenario

Matlab®/Simulink® was used to run simulations of the AFTI/F-16 overall linear model described by (3.28) in a triple fault scenario over a period of 200 seconds. The simulation

scenario is taken under the assumption that the redundant actuators control signals must not be faulty at the same time. In the longitudinal model of the AFTI/F-16 aircraft, the left and right elevators are considered as redundant actuators for each other. In the lateral model, the left flaperon and canards are considered as redundant actuators for the right flaperon and for the rudder respectively. That said, the eight possible scenario combinations of the triple fault are illustrated in Table 3.5.

Table 3.5 Possible Fault Scenarios Combinations

1	**2**	**3**	**4**	**5**	**6**	**7**	**8**
δ_{fR} (Lat.)	δ_{fR} (Lat.)	δ_{fR} (Lat.)	δ_{fR} (Lat.)	δ_{fL} (Lat.)	δ_{fR} (Lat.)	δ_{fL} (Lat.)	δ_{fL} (Lat.)
δ_{c} (Lat.)	δ_{c} (Lat.)	δ_{r} (Lat.)	δ_{r} (Lat.)	δ_{c} (Lat.)	δ_{c} (Lat.)	δ_{r} (Lat.)	δ_{r} (Lat.)
δ_{eL} (Long.)	δ_{eR} (Long.)	δ_{eL} (Long.)	δ_{eR} (Long.)	δ_{eL} (Long.)	δ_{eR} (Long.)	δ_{eL} (Long.)	δ_{eR} (Long.)

The faults considered represent three cosmic-ray-induced fault types from among those published previously (Hobeika et al., 2013). The first fault is a lock-in-place of the right flaperon δ_{fR} at 5^{o} occurring at t = 20–125 s. The second fault is canard oscillation δ_{c} between -5^{o} and $+5^{o}$ occurring at t = 50–150 s. The right flaperon δ_{fR} and the canard δ_{c} both act on the lateral motion. The third fault is another lock-in-place of the left elevator δ_{eL} at -1^{o} occurring at t = 75–180 s. The left elevator δ_{eL} acts on the longitudinal motion. After t = 180 s no more faults were introduced. The double fault thus occurred at t = 50–75 s and at t = 125–150 s, while the triple fault occurred at t = 75–125 s. The simulation thus included six fault activation or deactivation events, at t = 20 s, 50 s, 75 s, 125 s, 150 s, and 180 s. Table 3.6 summarizes the fault scenarios considered in the simulations.

In order to produce data resembling those from actual flight situations, the sensor measurements were corrupted with zero-mean white Gaussian noise corresponding to typical specifications of low-cost sensors. The deviation is taken as $\sigma = 2^{\circ}$, which corresponds to an error covariance matrix ($0.012 \times \mathrm{I}[\mathrm{rad}^2]$). The control signals became noisy as well. Wind gusts are included in the simulation to test the robustness of the FDD system in the presence of external disturbances.

Table 3.6 Fault Scenarios Considered in Simulations

Time	Single fault	Double fault	Triple fault
20–50 s	δ_{fR} stuck at 5° (Lat.)		
50–75 s		δ_{fR} stuck at 5° (Lat.) δ_c oscillates between $-5°$ and $+5°$ (Lat.)	
75–125 s			δ_{fR} stuck at 5° (Lat.) δ_c oscillates between $-5°$ and $+5°$ (Lat.) δ_{eL} stuck at $-1°$ (Long.)
125–150 s		δ_c oscillates between $-5°$ and $+5°$ (Lat.) δ_{eL} stuck at $-1°$ (Long.)	
150–180 s	δ_{eL} stuck at $-1°$ (Long.)		

In order to test the time available constraint and the performance of the proposed controller in terms of interaction between the FDD and the RSMC blocks, the simulation time-frame was set at twice the speed of a real fly-by-wire flight control system. The dynamic and input matrices A_{lat} and B_{lat} of the lateral model (Barfield et D'Azzo, 1983) used for the geometric approach based-FDD process are as follows:

$$A_{lat} = \begin{pmatrix} 0 & 0 & 1 & 0 \\ Y_\varphi & Y_\beta & Y_p & Y_r \\ 0 & L_\beta & L_p & L_r \\ 0 & N_\beta & N_p & N_r \end{pmatrix} \tag{3.33}$$

$$B_{lat} = \begin{pmatrix} 0 & 0 & 0 \\ Y'_{\delta_f} & Y'_{\delta_r} & Y'_{\delta_c} \\ L'_{\delta_f} & L'_{\delta_r} & L'_{\delta_c} \\ N'_{\delta_f} & N'_{\delta_r} & N'_{\delta_c} \end{pmatrix} \tag{3.34}$$

For the geometric approach, the following set of outputs was used: $y_1 = x_1 = \varphi, y_2 = x_2 = \beta, y_3 = x_4 = r$. The corresponding relative degrees are (2,1,1), which yield the sub-manifold $S_b = \{p = \beta = r = 0\}$. Using the approach presented in section (3.3), the associated projector Π was obtained using equation (3.5):

$$\Pi = \begin{pmatrix} 1 & 0 & 0 & 0 \\ 0 & 0 & 0 & 0 \\ 0 & 0 & 0 & 0 \\ 0 & 0 & 0 & 0 \end{pmatrix} \tag{3.35}$$

The inverse dynamics and the fault input reconstruction are provided in the following specifications:

$$\begin{cases} \dot{\varphi} = p \\ \delta_f = -0.4434\varphi + 0.2359\beta - 0.7303p + 8.2461r \\ \qquad -0.0568\dot{\varphi} + 8.2487\dot{\beta} - 0.0245\dot{p} \\ \delta_c = -1.7262\varphi + 5.3670\beta - 2.6428p + 32.0107r \\ \qquad +0.0031\dot{\varphi} + 32.1092\dot{\beta} - 0.1568\dot{p} \\ \delta_r = -2.3268\varphi + 5.5108\beta - 3.5708p + 43.33637r \\ \qquad -0.0061\dot{\varphi} + 43.2806\dot{\beta} + 0.4537\dot{p} \end{cases} \tag{3.36}$$

For the EMMAE approach, a bank of three EKFs was used. The left elevator faulty signal δ_{eL} was estimated via (3.10) and the assigned probability was computed using (3.11) and (3.12). The dynamic and input matrices A_{long} and B_{long} of the longitudinal model (Barfield et D'Azzo, 1983) are as follows:

$$A_{long} = \begin{pmatrix} 0 & 0 & 0 & 1 \\ X_\theta & X_u & X_\alpha & X_q \\ Z_\theta & Z_u & Z_\alpha & Z_q \\ M_\theta & M_u & M_\alpha & M_q \end{pmatrix} \tag{3.37}$$

$$B_{long} = \begin{pmatrix} 0 & 0 \\ X'_{\delta_e} & X'_{\delta_f} \\ Z'_{\delta_e} & Z'_{\delta_f} \\ M'_{\delta_e} & M'_{\delta_f} \end{pmatrix} \tag{3.38}$$

3.6.5 Simulation results

Figure 3.14 illustrates the aircraft health monitoring. The aircraft operates healthy until t = 20 s when it becomes affected by a single fault and compromised until t = 50 s. At t = 50 s the aircraft becomes affected by a double fault and further compromised until t = 75 s. At t = 75 s the aircraft becomes affected by a triple fault and yet further compromised until t = 125 s. At t = 125 s, one fault is removed and the aircraft remains compromised by a double fault until t = 150 s. At t = 150 s, another fault is removed and the aircraft remains compromised by a simple fault until t = 180 s. Finally, at t = 180 s, the last fault is removed and the aircraft re-establishes its healthy status and no more faults are introduced for the rest of the simulation.

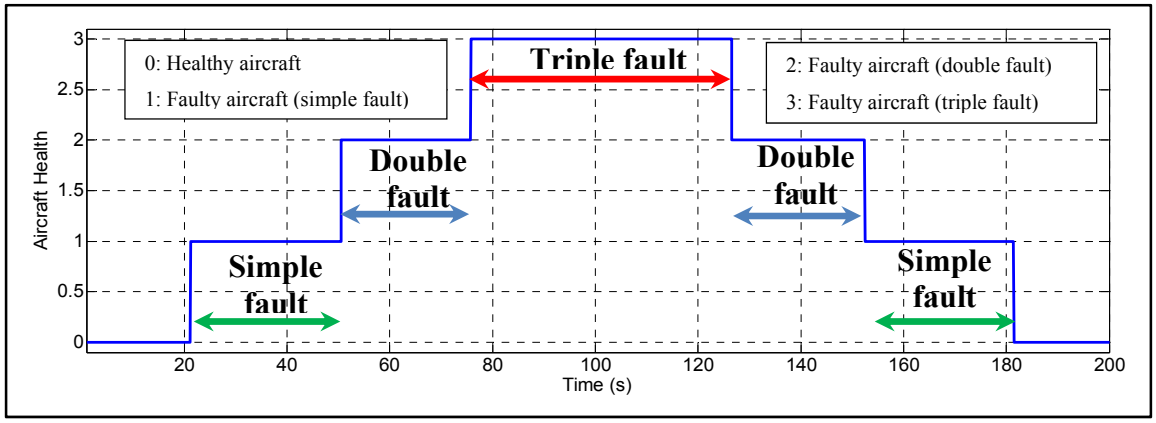

Figure 3.14 Health monitoring of the AFTI/F-16 aircraft

Figure 3.15 illustrates the fault isolation process results, which allow identification of the actuator that is acting erroneously. During the interval t = 20–125 s, the right flaperon (δ_{fR}) is in error. The next actuators in error are the canards (δ_c), during the interval t = 50–150 s. The third actuator error takes place during the interval t = 75–180 s and involves the left elevator (δ_{eL}). The delay in fault decision-making (less than 300 ms) at this stage is due to the oscillations generated by the FDD process. Minimizing these oscillations can improve fault detection and isolation results.

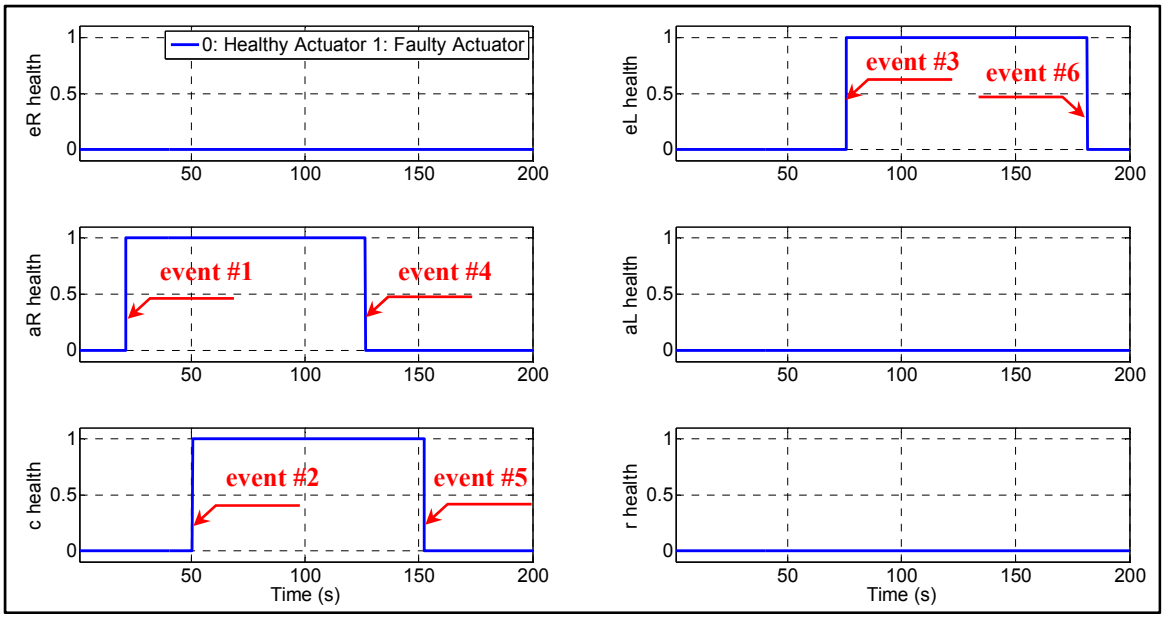

Figure 3.15 Monitoring AFTI/F-16 actuator status

Figure 3.16 shows the detection time zone between 200 and 300 ms, which can be considered as acceptable regarding the time available constraint existing in the real fly-by-wire flight control system which is usually less than 300 ms.

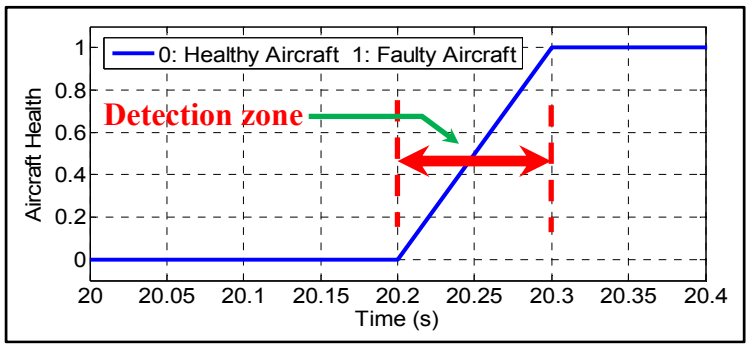

Figure 3.16 Time frame of fault detection

Figure 3.17 illustrates the aircraft state vector variables during the simulation. All states were affected first by the simple fault at t = 20 s (event #1), then twice by the double fault at t = 50 s (event #2), and then three times by the triple fault at t = 75 s (event #3). In each case, the reconfigurable control law compensated for the effect within a few seconds. At t = 125 s (event #4), the states were affected for the fourth time when the first fault was removed.

Again the control law was reconfigured to adapt to the new condition. Another reconfiguration was required in order to compensate for the fifth behavioral variation at t = 150 s (event #5). At this moment, the second fault was removed. Finally, the last reconfiguration was required in order to compensate for the sixth and last behavior variation at t = 180 s (event #6). At this time, the third fault was removed and the initial health of the aircraft was restored. The figure shows also that the tracking performances are satisfactory using the proposed approach compared to the conventional one. It should be noted that corruption of all sensor measurement signals by noise was very apparent.

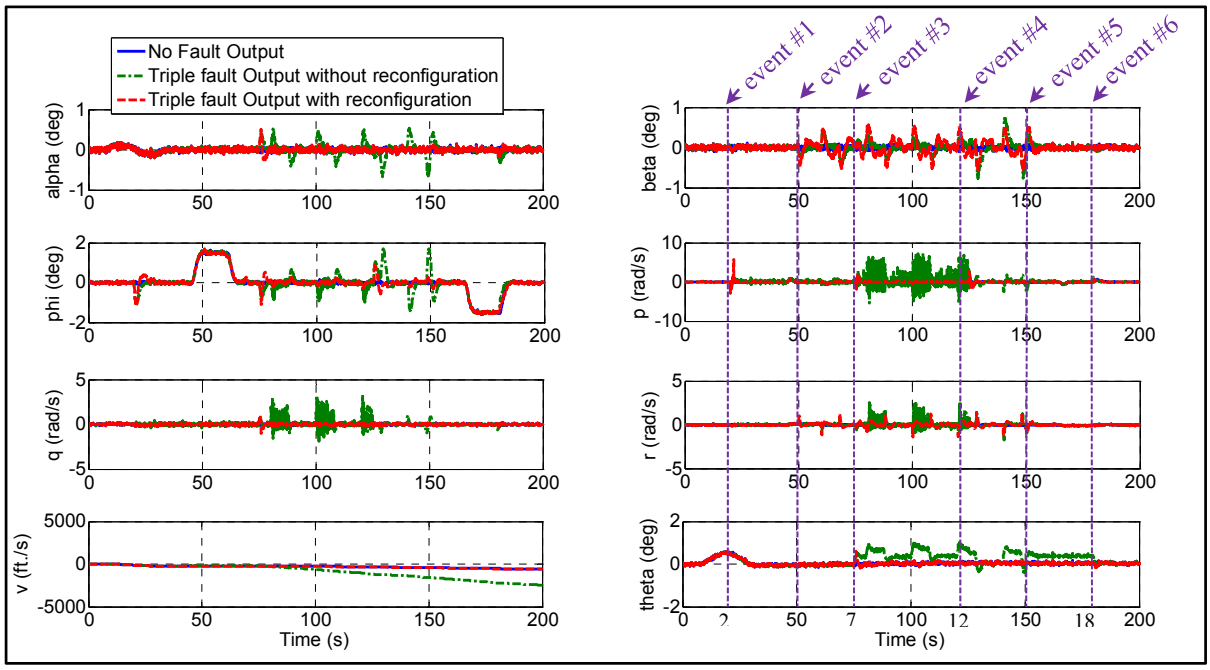

Figure 3.17 AFTI/F-16 state vector variables

Figure 3.18 illustrates the control signals of the six actuators. The faulty signals for the lateral motion (δ_{fR} and δ_c) were reconstructed from the minimal inverse using the geometric projector, and the faulty signal of the longitudinal motion (δ_{eL}) was estimated using the EMMAE approach. The other actuator control signals (δ_{fL}, δ_{eR} and δ_r) remained correct. Note that oscillations are minimized when using the proposed approach in comparison with the conventional approach.

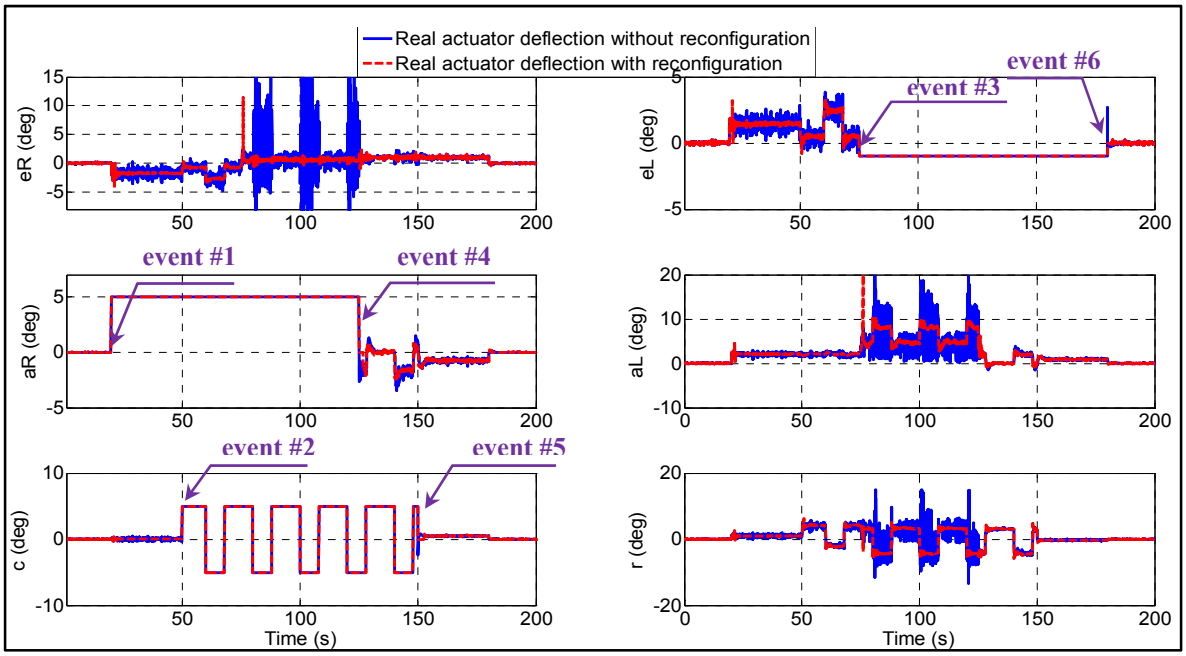

Figure 3.18 AFTI/F-16 control signals

Figure 3.19 illustrates the real actuator deflection and the actuator control signals estimated and reconstructed using the FDD process. From t = 20–125 s, the right aileron is affected and locks at 5°. The geometric approach reconstructs the fault perfectly. For t = 50–150 s, the canards are floating between the two positions 5° and -5° in a square-wave fashion. Here again, the geometric approach was able to reconstruct this fault. Finally, for t = 75–180 s, the left elevator is affected and locks at -1°. Here the fault was estimated accurately via the EMMAE approach.

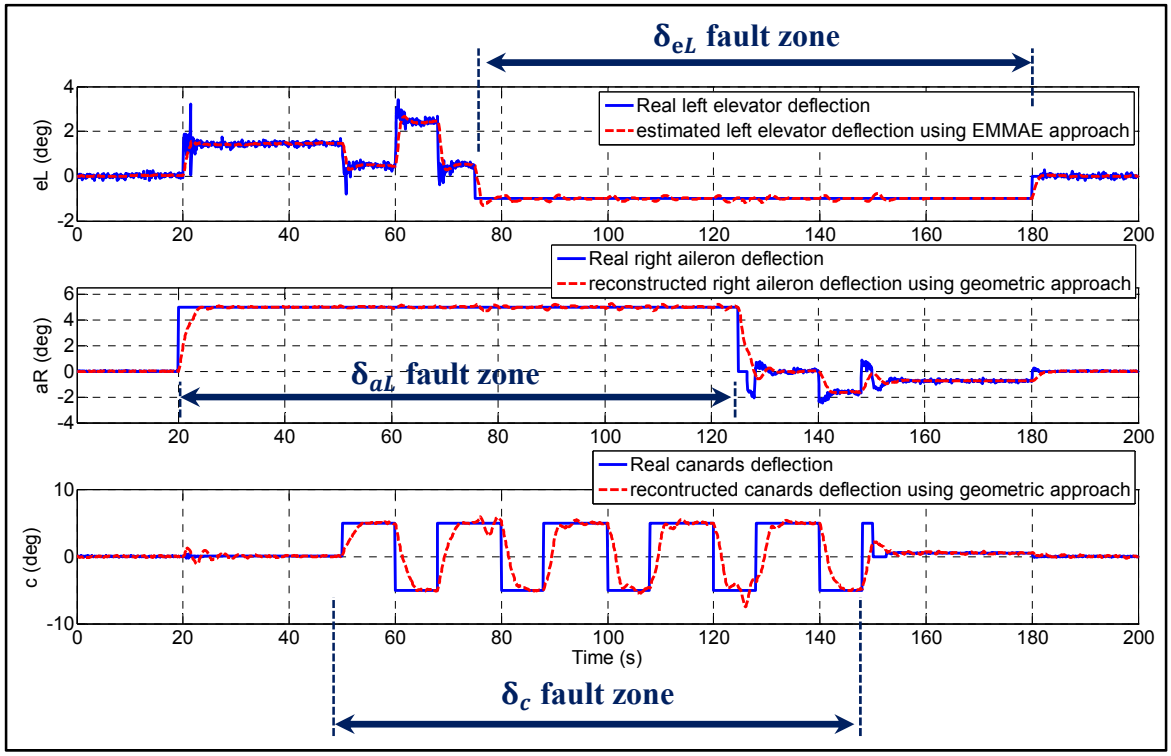

Figure 3.19 AFTI/F-16 control signals, estimated and reconstructed

Figure 3.20 illustrates the aircraft attitude, the so-called Euler angles (φ, θ and ψ). The roll and the pitch angles (φ, θ) are among the state vector variables. The yaw angle (ψ) at the bottom of the figure is not among the state vector variables and is computed via kinematic equations as defined below:

$$\begin{cases} \dot{\varphi} = p + (qsin\varphi + rcos\varphi)tan\theta \\ \dot{\theta} = qcos\varphi - rsin\varphi \\ \dot{\psi} = \frac{qsin(\varphi)+rcos(\varphi)}{\cos(\theta)} \end{cases} \tag{3.39}$$

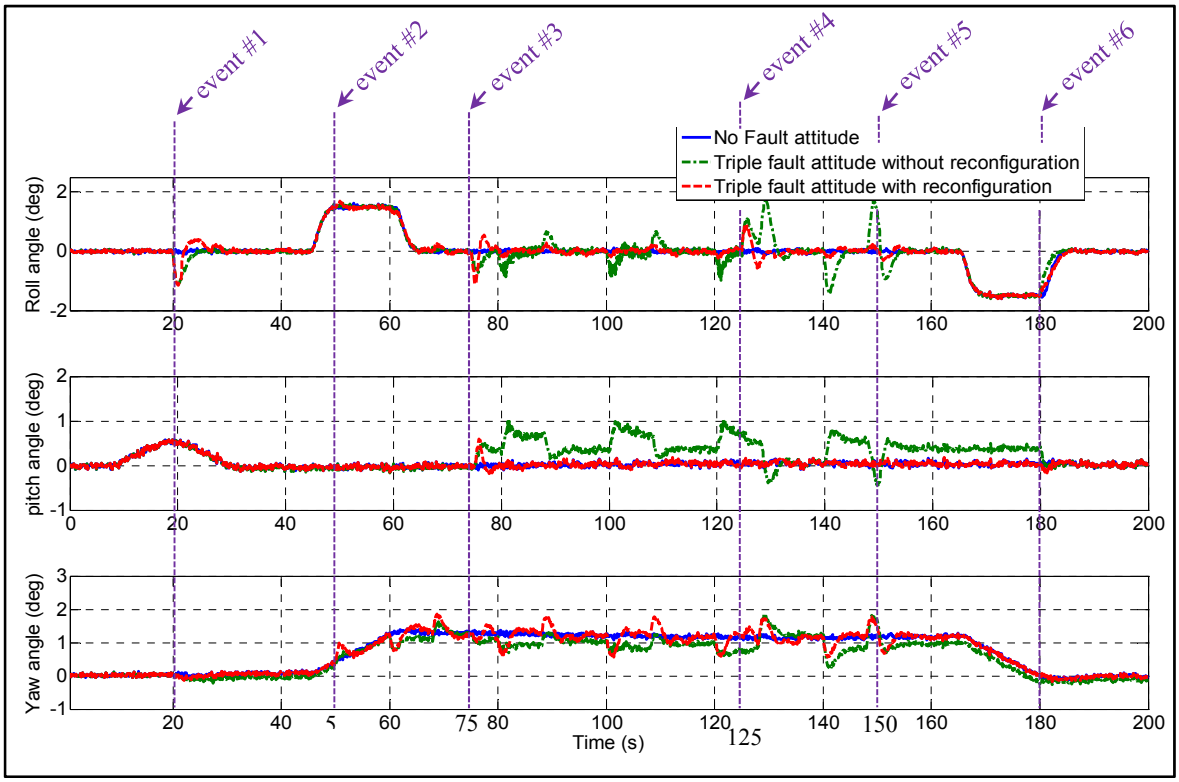

Figure 3.20 AFTI/F-16 attitude

Figure 3.21 illustrates the aircraft northeast path using the navigation equations. The left of Figure 3.21 illustrates that the triple fault led to a degradable northeast tracking error. This is because the fault on the left elevator affected the forward velocity $V(t)$ directly. The reconfigurable controller compensated for the actuator fault but did not eliminate it entirely. However, compared to conventional controller (without reconfiguration) illustrated in the right of Figure 3.21, the aircraft path remained closed to the desired path, the aircraft stability was preserved and the aircraft performances were maintained. In spite of the sequence of the generated faults, the aircraft continued to fly straight and level.

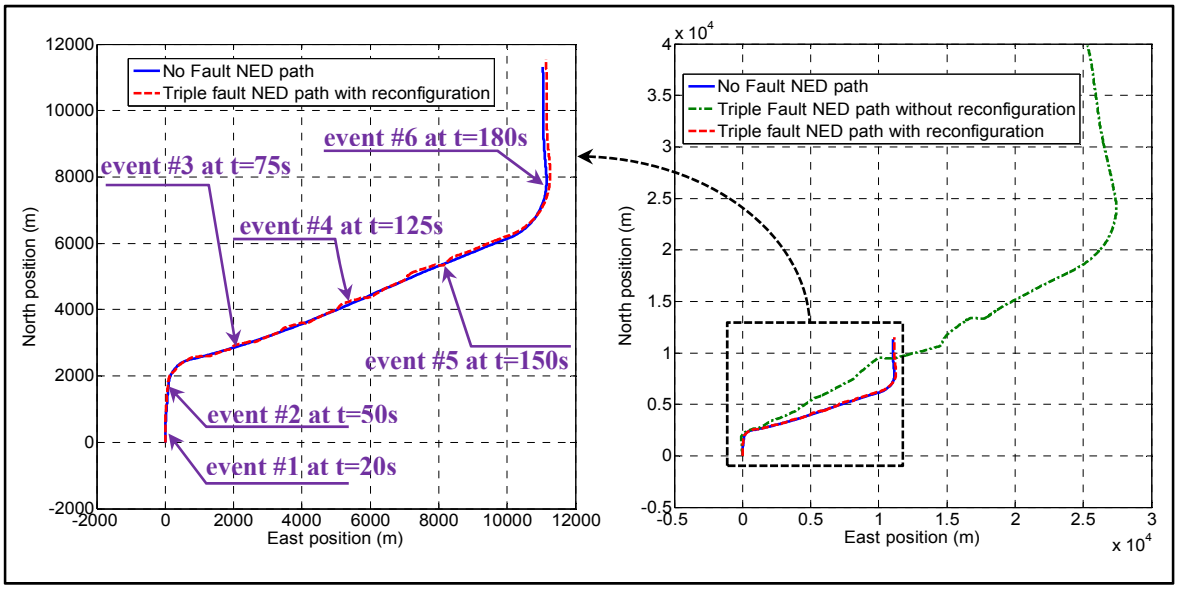

Figure 3.21 The northeast path of the AFTI/F-16

Figure 3.22 shows the AFTI-F16 behavior and tracking trajectory on the FlightGear simulator GUI and a 3D animation at t = 50 s.

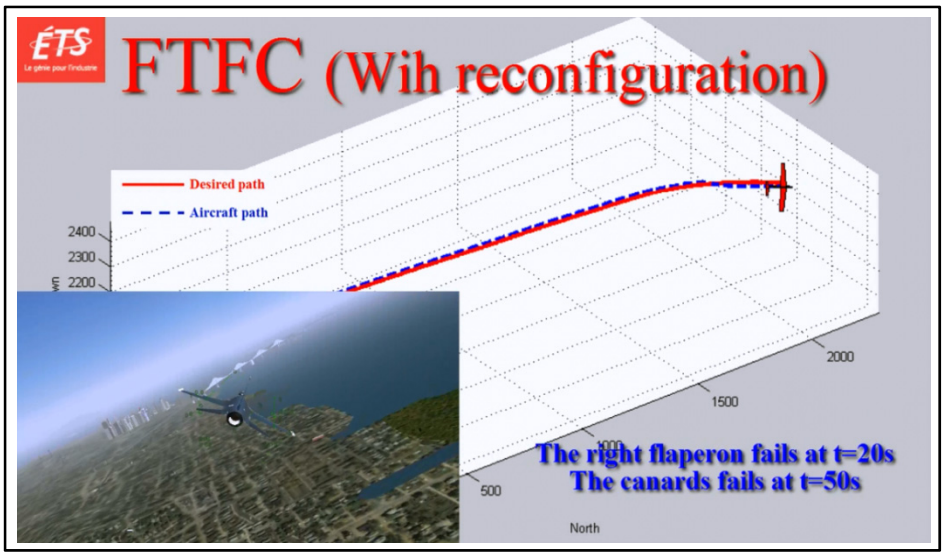

Figure 3.22 Screenshot of FlightGear simulator and 3D animation at t = 50 s

3.7 Conclusion

The multiple fault-tolerant flight control system proposed in this article can detect and compensate in real time for multiple abrupt actuator control signal faults caused by cosmic rays. Based on the geometric approach to fault reconstruction and on extended multiple model adaptive estimation, the described fault detection and diagnosis process is fast (requiring less than 300 ms) and accurate. These characteristics make the method applicable to real aircraft.

The geometric approach and the extended multiple model adaptive estimation combined with the reconfigurable sliding mode technique make it possible to determine fault parameters and compensate for them within a short delay so that aircraft stability will be preserved and acceptable performance will be maintained, even when actuator faults occur simultaneously.

The results obtained using linear simulations of a realistic flight scenario show the robustness of this controller, even in the presence of uncertainties such as wind disturbances and measurement noise. It has thus been shown that the proposed fault-tolerant flight control method is capable of adjusting to three simultaneous actuator control signal failures caused by radiation. It has been shown also that the fault detection and diagnosis process, as well as the reconfigurable sliding mode control, have been integrated into an overall flight control system.

It has been demonstrated further that the performance of the proposed controller in terms of interaction between the FDD and the RSMC blocks is well respected. The faults' parameters are identified and injected in a very small delay which corresponds to the real fly-by-wire flight control system delay. For the inputs generated by the controller, the results showed the effectiveness and robustness of the designed controller, in spite of errors in deflection. They were always within the mechanical limits and rates of the aircraft.

It has been shown that when an actuator control signal is faulty, actuator control signals reconstructed via the geometric-based FDD or estimated via extended multiple model adaptive estimation can be used advantageously to reconfigure online the unaffected actuator control signals. This technique adjusts only the reconfigurable sliding mode controller so that aircraft stability will be preserved and performance will be maintained. The proposed control system algorithm is thus capable of processing triple faults, without any change to the initial controller and without any additional actuator position sensor.

CHAPTER 4

APPLIED ACTUATOR FAULT ACCOMMODATION IN FLIGHT CONTROL SYSTEMS USING FAULT RECONSTRUCTION-BASED FDD AND SMC RECONFIGURATION

A. Ghodbane [a], M. Saad [b], J.–F. Boland [c] and C. Thibeault [d],

[a, b, c, d] Department of Electrical Engineering, École de technologie supérieure,
1100 Notre-Dame West, Montreal, Quebec, Canada H3C 1K3

This paper has been published
in the International Journal of Computer, Information, Systems and Control Engineering
Volume 8, Issue 7, July 2014

Abstract

Historically, actuator redundancy has been used to handle faults occurring suddenly in flight systems. This technique was generally expensive, time-consuming, and involved increased weight and space in the system. Today, therefore, the online fault diagnosis of actuators and accommodation play a major role in the design of avionic systems. These approaches, which are the root of Fault-Tolerant Flight Control systems, are able to adapt to such sudden faults while keeping avionics systems lighter and less expensive. In this paper, a Fault-Tolerant Flight Controller based on the Geometric Approach and a Reconfigurable Flight Control is presented. The Geometric approach is used for cosmic ray fault reconstruction, while Sliding Mode Control, based on Lyapunov stability theory, is designed for the reconfiguration of the controller in order to compensate for the fault effect. Matlab®/Simulink® simulations are performed to illustrate the effectiveness and robustness of the proposed flight control system against the faulty signal of actuators caused by cosmic rays. The results demonstrate the successful real-time implementation of the proposed controller on a non-linear aircraft model. FlightGear software simulator is used to show the performance and the behavior of the aircraft on a Graphical User Interface.

Keywords: Actuator faults, Fault detection and diagnosis, Fault-tolerant flight control, Sliding mode control, Geometric approach for fault reconstruction, Lyapunov stability.

4.1 Introduction

The safety of flight control systems is a key issue for the aerospace industry. The challenge of maintaining acceptable performances and preserving aircraft stability when unexpected scenarios occur requires other strategies than just using simple conventional controllers, designed only on the basis of the sensors' actual measurements. Indeed, FTFC systems are crucial for increasing the reliability of an aircraft when actuators fail, possibly leading to a loss of control during a flight. These strategies allow the aircraft to land safety and help avoid serious accidents and disasters.

Generally, FTFC systems react instantly to the occurrence of actuator faults by using the faults' parameters provided by a Fault Detection and Diagnosis (FDD) process. Then, the remaining healthy actuators are reconfigured to compensate for the effect the faulty actuator has on the aircraft behavior. The reconfiguration of the controller is usually necessary for the event of severe actuator faults, such as total actuator loss. A wide survey on FTFC and FDD systems can be found in (Isermann, 2006), (Edwards, Lombaerts et Smaili, 2010), (Meskin et Khorasani, 2011), (Alwi, Edwards et Tan, 2011), (Hajiyev et Caliskan, 2013) and (Isidori, 1995).

A reliable FDD process is assumed to provide accurate information about the aircraft's health status in order to prevent false alarms. This ensures robustness against external disturbances, model uncertainties, and sensor noise measurements. Model-based FDD processes can be classified into two major categories: residual generation-based FDD and fault reconstruction-based FDD (Isermann, 2006). In residual-generation based FDD, a residual signal is formed by comparing the mathematical model outputs with the sensor measurements. Thus, in normal conditions, the residual signal is supposed to be close to zero, and will be nonzero when faults occur. In fault-reconstruction based FDD, the process estimates and reconstructs

the actuator deflection. This reconstruction can be used directly to correct the faulty actuator before it is used by the controller. Among the methods used for the design of such FDD processes, the geometric approach has been selected, and will be considered later in this paper (De Persis et Isidori, 2001), (Chaib et al., 2009b) and (Chaib et al., 2009a). The fundamental characteristic of this approach is that it handles simultaneous faults more accurately than other approaches. It consists of a decomposition of the aircraft state space into two planes: one being tangent to the faulty signal, and the other being transverse. The input signals are then constructed using the minimum invertibility concept.

Once the geometric-based FDD process detects, locates and identifies the source of the fault, the fault parameter information is then used by a reconfiguration mechanism. This mechanism tries to adapt and to compensate for the effect of the fault by using the remaining healthy actuator signals, therefore preserving the entire stability and maintaining acceptable performances. Just like the FDD process, the reconfigurable controller needs to be robust against external uncertainties and disturbances. Recent research on reconfigurable flight controls used specifically for FTFC systems includes a focus on the Sliding Mode Control (SMC) (Slotine et Li, 1991), (Fridman, Davila et Levant, 2011), (Bandyopadhyay, Janardhanan et Spurgeon, 2013), (Shin, Moon et Kim, 2005), (Hamayun, Edwards et Alwi, 2012) and (Fallaha et al., 2011). The SMC controller design depends primarily on the design of a so-called ‘sliding surface’ and the trajectory of the states will be driven towards this surface. Once they have reached their destination, the states are forced to remain on it, ensuring it is robust to uncertainties and to the stability of the system. This makes it a strong candidate for the design of the FTFC systems to handle actuator faults.

This paper is organized as follows. In Section 4.2, the actuator fault models are defined and described. Then, the origins of radiation faults and their emulation using Xilinx-ISE® and mathematical modeling are explained. Section 4.3 presents the geometric fault reconstruction-based FDD formulation. Section 4.4 presents the reconfigurable sliding mode control design. Section 4.5 briefly presents the integration between FDD and SMC. To demonstrate the performances of the proposed system, Matlab®/Simulink® numerical

simulations are performed on the nonlinear 6 DOF aircraft model in Section 4.6. Section 4.7 concludes the paper.

4.2 Actuator fault modeling

According to Isermann's definition of fault (Isermann, 2006), an actuator fault corresponds to any abnormal system behavior. The fault may be small or hidden, and may thus be hard to diagnose. In the literature, several types of actuator faults are listed (Isermann, 2006), (Edwards, Lombaerts et Smaili, 2010) and (Meskin et Khorasani, 2011). The actuator may be stuck and motionless, it may move freely without providing any aerodynamic moment to the aircraft or it may lose some effectiveness or totally hard over. When a fault occurs in the actuator, the first step should be to diagnose the kind of fault, and then decide how to deal with it. It must be detected, isolated and identified. The fault detection consists in monitoring the system health and determining the time of fault occurrence, the fault isolation determines the kind and location of such fault, and the fault identification determines the form and the time varying of the fault.

In the last decade, new types of faults affecting aircrafts have been a topic of interest. The neutrons generated by cosmic rays could cause Single-Event Upsets (SEUs) in avionic systems at high flight altitudes (Taber et Normand, 1995). Indeed, because of the high technology used to fabricate integrated circuits, semiconductor-based components are becoming increasingly sensitive to cosmic ray events, as well as the target of many such faults. These types of faults can be emulated on a Field-Programmable Gate Array (FPGA) device using the soft error mitigation (SEM) IP core provided by Xilinx® (Hobeika et al., 2013). In the remainder of this paper, one type of cosmic ray fault model, previously published in (Hobeika et al., 2013), is used. It is illustrated in Figure 4.1.

Equations (4.1), (4.2) and (4.3) define the faulty control signal $u_f(t)$ of the k^{th} actuator affected by a faulty input signal $\bar{u}_k(t)$.

$$u_f(t) = Fu(t) + (I_{m\times m} - F)\bar{u}(t) \tag{4.1}$$

$$F = diag\{f_i\}, \quad f_i = \begin{cases} 1, & i \neq k \\ 0, & i = k \end{cases} \tag{4.2}$$

$$\bar{u}(t) = [0 \ldots \bar{u}_k \ldots 0]^T \tag{4.3}$$

where $\bar{u}_1, \ldots, \bar{u}_i, \ldots, \bar{u}_m$ are the actuator faulty signals and $u_1, \ldots, u_i, \ldots, u_m$ are the actuator non-faulty control signals obtained from the controller.

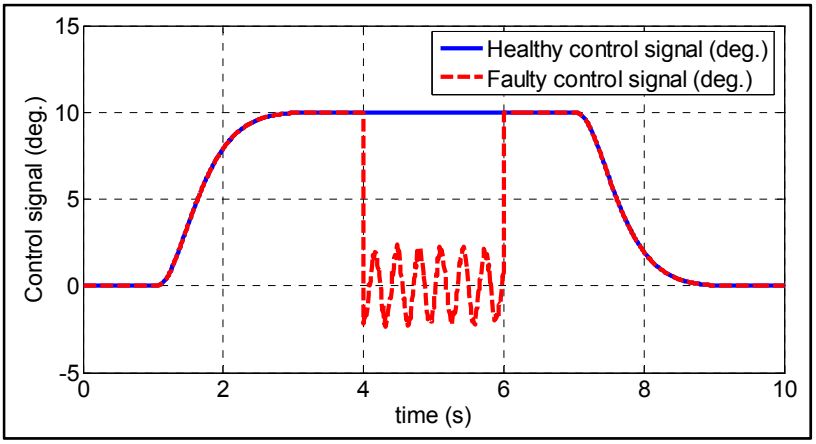

Figure 4.1 Cosmic rays fault: Noisy oscillations around zero between t = 4 s and t = 6 s

Figure 4.2 illustrates the mathematical model of such an actuator fault (Tao et al., 2013).

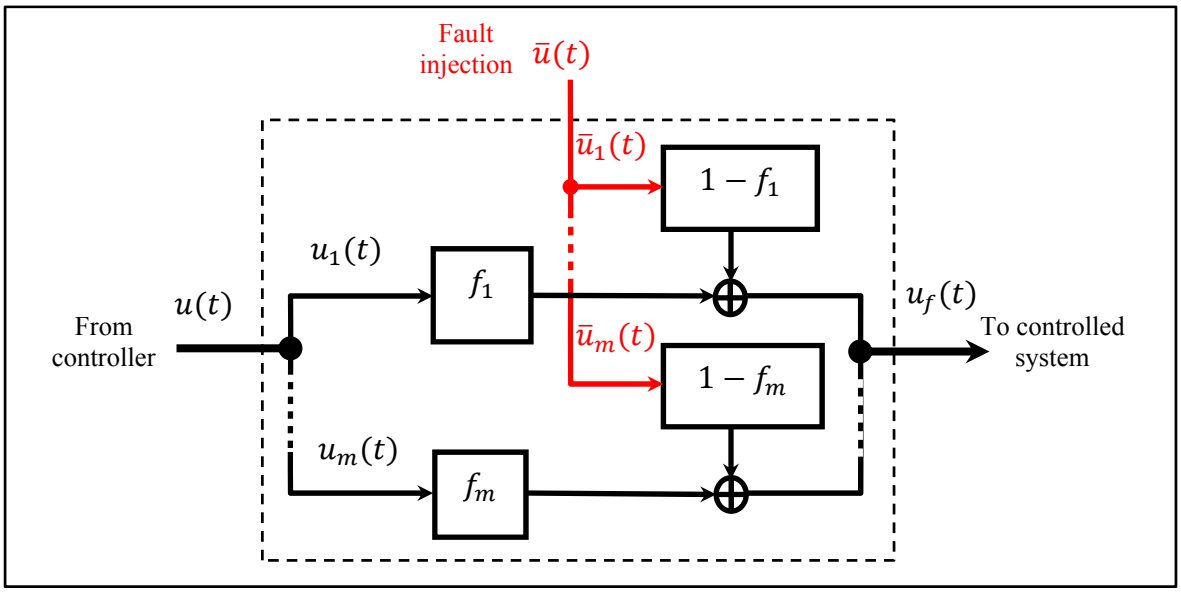

Figure 4.2 Mathematical modeling of neutron-induced radiation faults
Adapted from Tao et al. (2013)

4.3 Geometric fault reconstruction based-FDD

In this section, a non-linear dynamic system for a 6 DOF aircraft model is considered. Equation (4.4) presents the state space of the non-linear dynamic system.

$$\begin{cases} \dot{x}(t) = f(x) + g(x)u(t) \\ y(t) = h(x) \end{cases} \tag{4.4}$$

where f, g and h are respectively the system, input and output functions. $x(t) \in \mathbb{R}^{n\times 1}, y(t) \in \mathbb{R}^{p\times 1}$ and $u(t) \in \mathbb{R}^{m\times 1}$ represent the state vector variables, the output vector variables and the control input variables, respectively.

Figure 4.3 illustrates the general concept of the geometric fault reconstruction-based FDD.

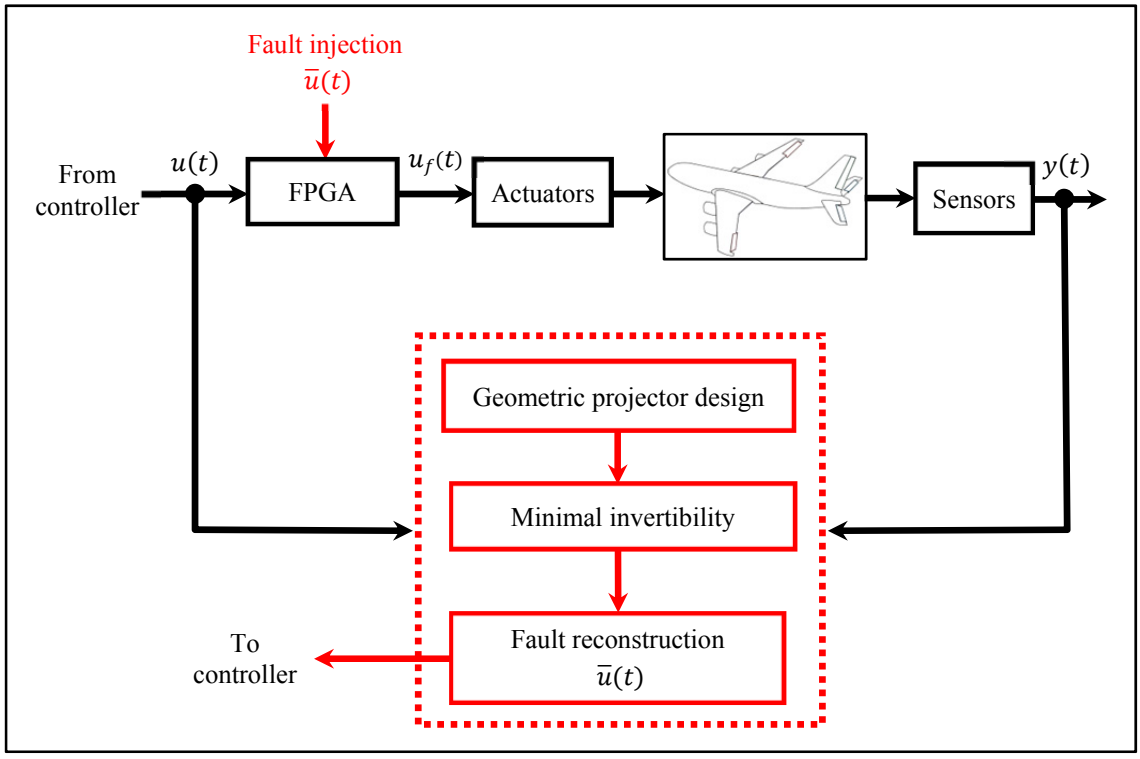

Figure 4.3 General structure of the geometric fault reconstruction-based FDD
Adapted from Chaib et al. (2009)

The main objective of this approach is to design a geometric projector $\Pi(x)$ as presented below (Chaib et al., 2009a):

$$\Pi(x) = I_{m\times m} - g{A_{proj}}^{-1}\nabla\sigma^{T} \tag{4.5}$$

where details on A_{proj} and $\nabla\sigma^{T}$ matrices can be found in Appendix V, $I_{m\times m}$ is the identity matrix and m is the output vector size. Using (4.5), the dynamic vector $f(x)$ can be decomposed into tangent and transverse parts along a so-called sub-manifold S_b as presented below (Chaib et al., 2009a):

$$f(x) = \Pi(x)f(x) + \big(I_{m\times m} - \Pi(x)\big)f(x),\ \forall x \in S_b \tag{4.6}$$

The terms $\Pi(x)f(x)$ and $\big(I_{m\times m} - \Pi(x)\big)f(x)$ represent the tangent part and the transverse part, respectively. The projector $\Pi(x)$ is then used to reconstruct the faulty inputs by using the minimum invertibility system concept illustrated by the following (Chaib et al., 2009a):

$$\begin{cases} \dot{x}(t) = \Pi(x)f(x) + g{A_{proj}}^{-1}\dot{y}(t) \\ u_f(t) = {A_{proj}}^{-1}(\dot{y}(t) - \nabla\sigma^{T}f(x)) \end{cases} \tag{4.7}$$

In the case when $p > m$ (similarly as the case treated in this paper), a set of dummy directions $G = \{g_i\}, 1 \le i \le p - m$ must be added such that:

$$\begin{cases} g_i L_{Ax}^{r_j-1} h_j(x) = 1,\ j = m + i \\ g_i L_{Ax}^{r_k} h_j(x) = 0,\ 1 \le k \le r_j - 1, j \ne m + i \end{cases} \tag{4.8}$$

Then g will be $\overline{g}$ and will be expressed as follows:

$$\bar{g} = (g|G) \tag{4.9}$$

And A_{proj} will be $\bar{A}_{proj}$ and will be expressed as follows:

$$\bar{A}_{proj} = \big(A_{proj}\big|\nabla\sigma^{T}G\big) \tag{4.10}$$

If $\bar{A}_{proj}$ has a rank equal to p, then the projector $\Pi(x)$ can be designed.

$$\Pi(x) = I_{m\times m} - \bar{g}{\bar{A}_{proj}}^{-1}\nabla\sigma^{\mathrm{T}} \tag{4.11}$$

The faulty inputs are then reconstructed by using the minimum invertibility concept illustrated by the following:

$$\begin{cases} \dot{x}(t) = \Pi f(x) + \bar{g}\bar{A}_{proj}{}^{-1}\dot{y}(t) \\ u_f(t) = \Gamma\bar{A}_{proj}{}^{-1}\left(\dot{y}(t) - \nabla\sigma^T f(x)\right) \end{cases} \tag{4.12}$$

where: $\Gamma = \begin{pmatrix} I_{m\times m} & 0_{m\times(p-m)} \\ 0_{(p-m)\times m} & 0_{(p-m)\times(p-m)} \end{pmatrix}$.

4.4 Reconfigurable Sliding Mode Control design

The SMC design process starts by defining a so-called sliding surface $S(t)$. Then, a first control law is designed to drive the trajectory of the states towards this surface. Once the surface is reached, a second control law is then designed to force the trajectory to remain on the surface. The sliding surface is defined for a second-order system by a vector $s(x,t)$, as shown below (Slotine et Li, 1991):

$$s(x,t) = \left(\frac{d}{dt} + \lambda\right)\int \tilde{x}(t) = 0,\ \lambda > 0 \tag{4.13}$$

where $\tilde{x}(t) = x(t) - x_d(t)$ is the state error and $x_d(t)$ is the desired state. Once the sliding surface is designed, the stability based on the Lyapunov approach is used to ensure the design of the sliding control law, assuming that $g(x)$ is invertible, as follows (Slotine et Li, 1991):

$$u(t) = g(x)^{-1}\left[\left(\dot{x}_d(t) - \lambda\tilde{x}(t) - f(x)\right)\right] - g(x)^{-1}[Ksign(s)] \tag{4.14}$$

The first term of (4.14) represents the continuous control law and is defined by $u_{eq}(t)$. The second term represents the discrete one, and is defined by $u_{disc}(t)$. In the case where the inverse cannot be calculated, the pseudo-inverse function can be used.

4.5 FDD process and FTFC integration mechanism

When a sudden fault occurs, the terms F and $\overline{u}(t)$ in (4.1), are unknown. The vector $\overline{u}(t)$ is reconstructed by the geometric fault reconstruction-based FDD process, and the matrix F is designed in the reconfiguration mechanism. By using fault parameters F and $\overline{u}(t)$, and

sensor measurements $y(t)$, the SMC controller reconfigures the remaining healthy actuator signals online to compensate for the faulty actuator signal. Using (4.1), (4.4) and (4.14), and by choosing $U(t) = Fu(t)$ to be the reconfigurable flight control law, $U(t)$ will take the form:

$$U(t) = g(x)^{-1}[(\dot{x}_d(t) - \lambda\tilde{x}(t) - f(x)) - g(x)(I - F)\overline{u}(t)] - g(x)^{-1}(Ksign(s)) \qquad (4.15)$$

4.6 Case study

In this section, the approach presented below is applied on a general 6 DOF nonlinear aircraft model, using Matlab®/Simulink® simulations. First, the fault reconstruction-based process is designed using minimal inverse dynamics. Then, based on FDD information, a sliding mode control is designed to compensate for the effect of the fault occurring on the aircraft behavior. The flight dynamic equations of a general nonlinear aircraft model can be rewritten as in (4.4), where $x(t)$, $u(t)$ and $y(t)$ are defined in Table 4.1, illustrated below, and $f(x)$, $g(x)$ and $h(x)$ are deduced using the aerodynamic equations of forces and moments described in chapter 2, section 2.3.3. Numerical aerodynamics parameters used in this paper can be found in Appendix III and in (Roskam, 2003). Figure 4.4 shows the overall scheme of the designed controller.

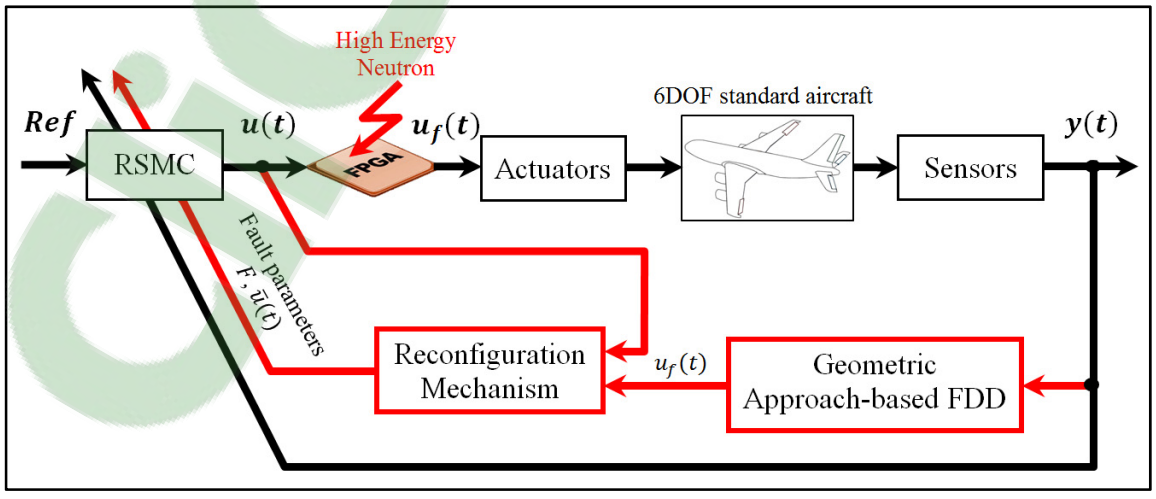

Figure 4.4 FTFC scheme using a geometric fault reconstruction-based FDD and a reconfigurable SMC

4.6.1 Simulation scenario

The fault model used in the simulation is one of the cosmic ray faults models cited in (Hobeika et al., 2013). It is modeled as oscillations around zero. For realistic situations, the fault model considered is corrupted by a zero-mean white Gaussian noise. The simulation runs for over 10 s, and the rudder surface fails between t = 4 s and t = 6 s, and then it becomes healthy until the end of the simulation. The sensors' measurements are corrupted with zero-mean white Gaussian noise with an error covariance matrix ($0.012 \times \mathrm{I}[\mathrm{rad}^2]$). This specification corresponds to low-cost sensors.

Table 4.1 State Vectors and Control Surfaces
of the General Nonlinear 6 DOF Aircraft Model

State vector $\boldsymbol{x(t)}$		**Control surface $\boldsymbol{u(t)}$**	
$\boldsymbol{V}$	Longitudinal velocity, m/s	$\boldsymbol{\delta_a}$	Aileron, rad
$\boldsymbol{\alpha}$	Angle of attack, rad	$\boldsymbol{\delta_e}$	Elevator, rad
$\boldsymbol{\beta}$	Side slip angle, rad	$\boldsymbol{\delta_r}$	Rudder, rad
$\boldsymbol{p}$	Roll rate, rad/s		
$\boldsymbol{q}$	Pitch rate, rad/s		
$\boldsymbol{r}$	Yaw rate, rad/s		
$\boldsymbol{\varphi}$	Roll angle, rad		
$\boldsymbol{\theta}$	Pitch angle, rad	Output vector $y(t)$	
$\boldsymbol{\psi}$	Yaw angle, rad	$\boldsymbol{y(t)}$	$[V\ \alpha\ \beta\ p\ q\ r]^{\mathrm{T}}$

4.6.2 Algorithm implementation

The geometric is used for the design of the FDD process. Figure 4.5 illustrates the steps followed for the implementation of the proposed algorithm. The algorithm starts by initializing the fault parameters. Then for each step time, the sensor measurements are used to design the geometric projector $\Pi(x)$ using (4.11). Next, the unknown control signals $u_f(t)$ are then reconstructed using (4.12). The faulty input $u_f(t)$ and the computed control

input $u(t)$ are then compared to compute the fault value $\bar{u}(t)$ and to make the fault decision, and then fault parameters are updated using (4.2). The new control law is then computed using (4.15). The simulated faults are then injected and finally the sensor measurements are used for the next time step.

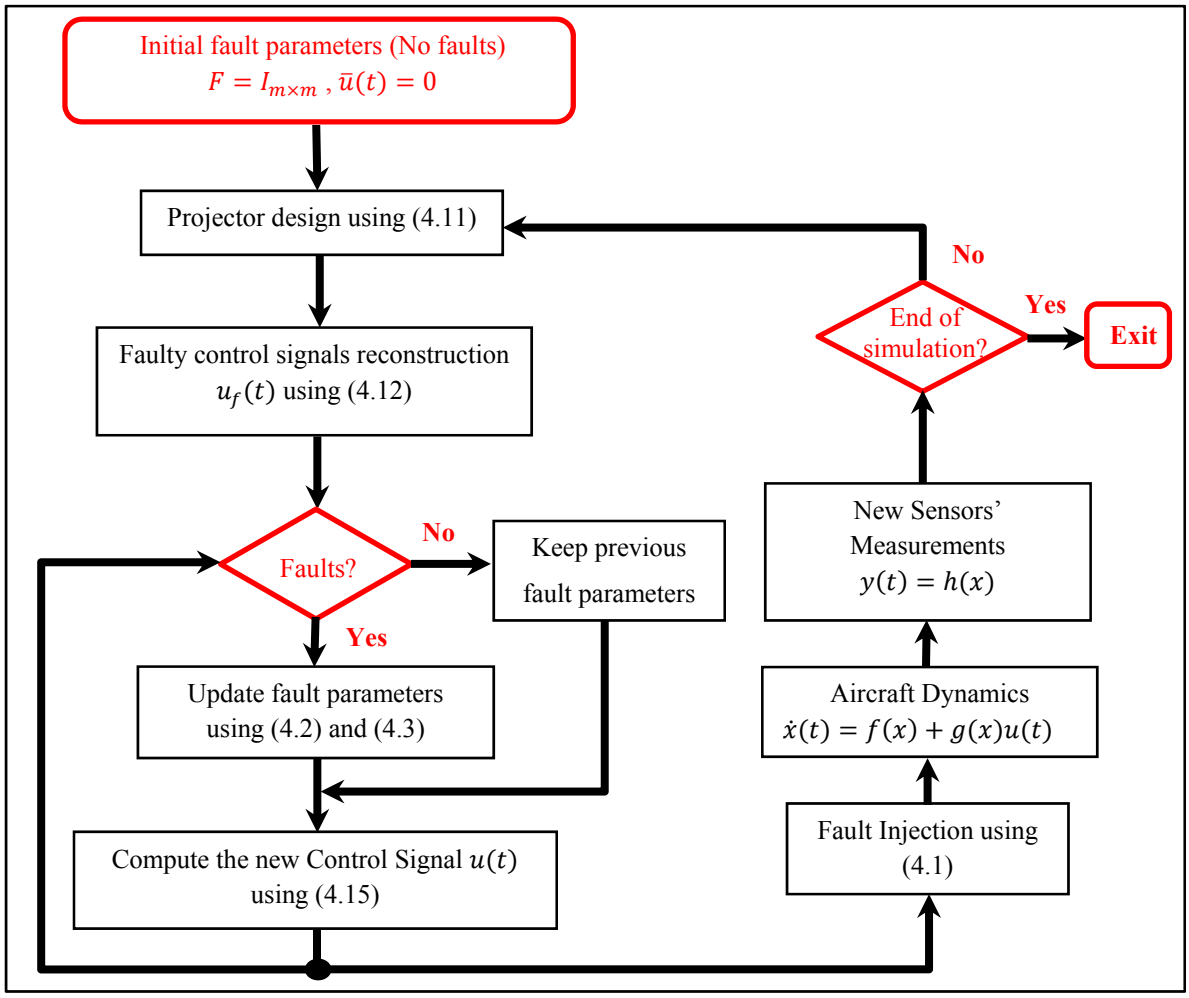

Figure 4.5 Steps followed for implementation of the reconfiguration algorithm

4.6.3 Simulation results

Figure 4.6 illustrates the geometric fault reconstruction-based FDD process detection and isolation results. A value of 1 means that the actuator is in the healthy state, while a value of zero means that the actuator fails. Notice that the FDD reacts instantly to the occurrence of

the fault. Indeed, the rudder fails at t = 4 s, and after less than 0.1 s, the health status monitor changes from 1 to 0, indicating that a fault occurs at this time on the rudder. On the other hand, the FDD process also takes 0.1 s to detect the disappearance of the fault.

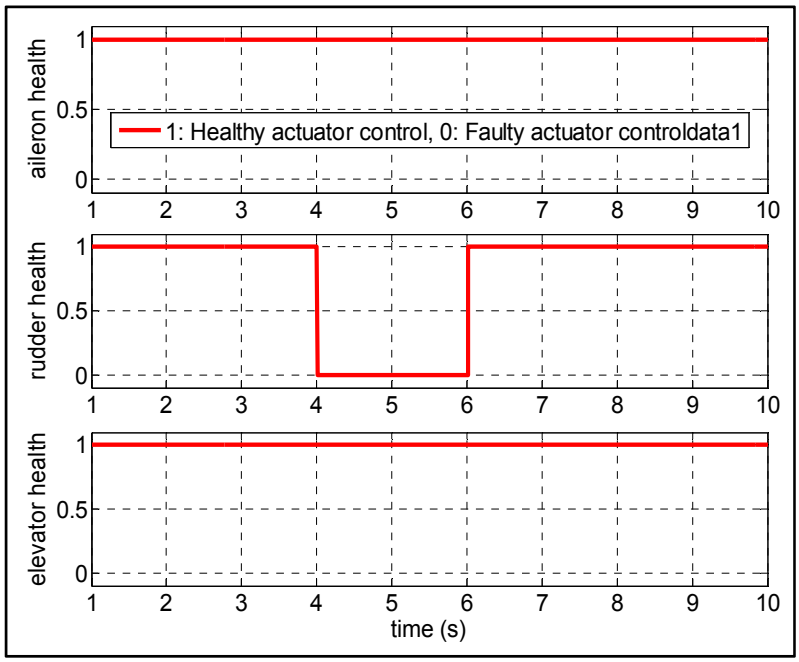

Figure 4.6 FDD Detection and Isolation for the rudder fault

Figure 4.7 illustrates the SMC outputs in both healthy and faulty states, as well as those reconstructed using the geometric fault reconstruction-based FDD process. The reconstructed control output of the rudder is close to the actuator deflection in both states (faulty and healthy).

Figure 4.8 illustrates the geometric fault reconstruction error and shows the fault reconstruction performance better. It can be seen that even the remaining two actuators are still healthy and that their geometric reconstruction is perfect. Notice that the SMC outputs do not suffer from the chattering problem, and they do not exceed the actuator mechanical and rate limits.

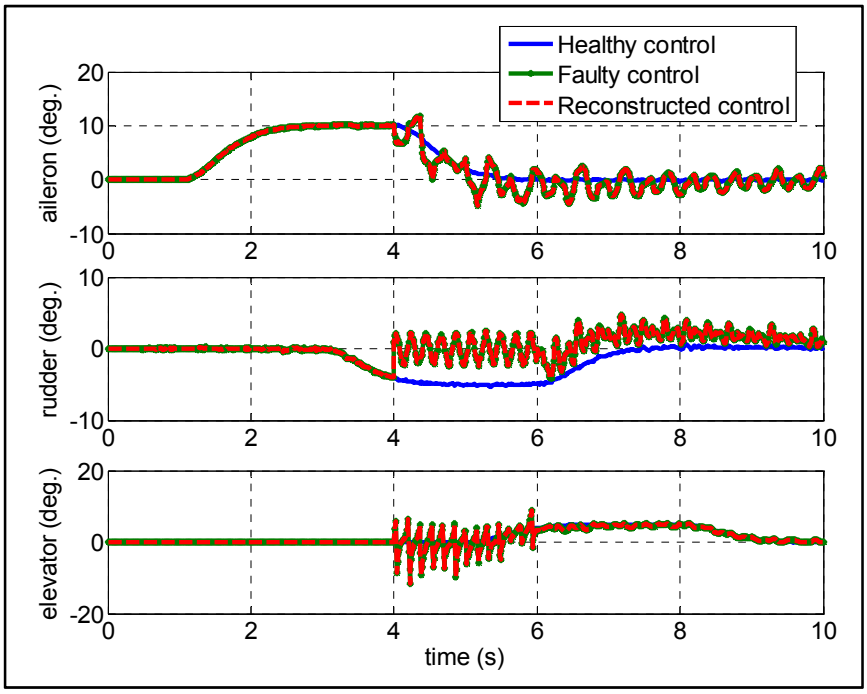

Figure 4.7 SMC outputs time history

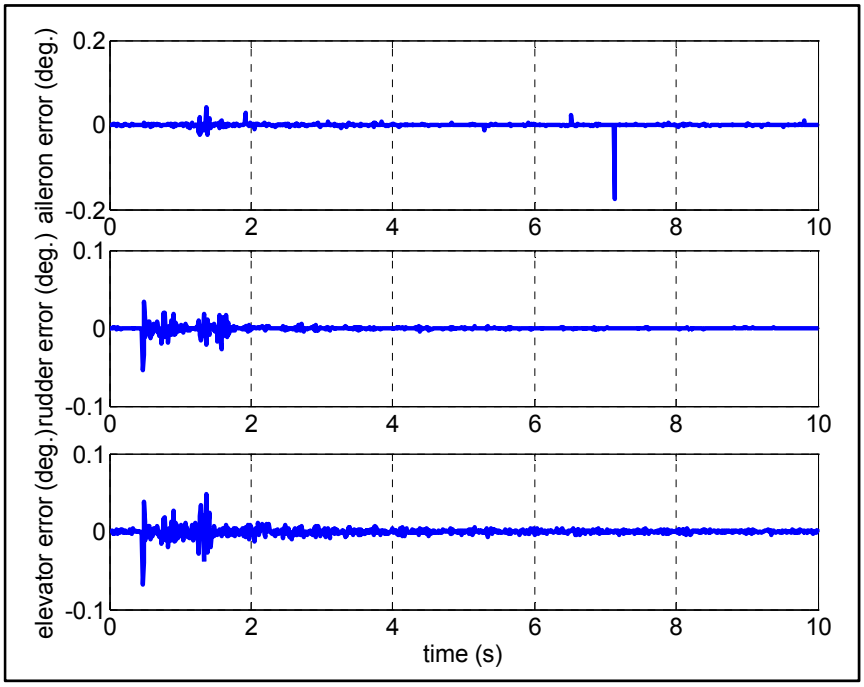

Figure 4.8 Comparison between SMC outputs and FDD reconstruction

Figure 4.9 illustrates the aircraft's attitude angles φ, θ and ψ. The roll angle φ has not been affected by the fault. That is because the rudder does not act on the roll angle directly. The

pitch and yaw angles θ and ψ show a minimal degradation when the fault occurs, but the whole stability is still preserved.

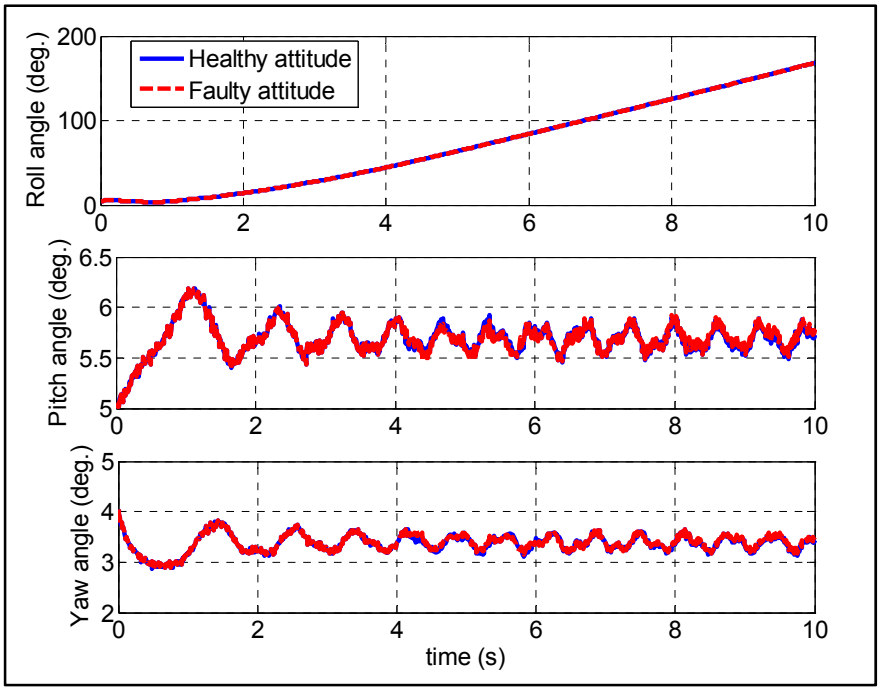

Figure 4.9 Attitude time history

Figure 4.10 illustrates the aircraft's omega rates. Unlike the roll and yaw rates p and r, which do not present any trace of the effect of the fault, the pitch q is affected by the fault, and suffers from some degradation. The reason is that the reconfigurable control requests the elevator actuator, which acts directly on q, to compensate for the rudder's fault and to minimize its effect. Note that due to the FTFC system design, the fault impact still remains so minimal that the aircraft's stability is preserved and the performances are maintained close to those desired by the pilot.

Figure 4.11 illustrates the aircraft's wind parameters: the forward velocity $V(t)$, the angle of attack α and the sideslip angle β. It can easily be seen that the parameters have not been affected by the rudder fault. This can be explained by the fact that reconfiguring the remaining healthy actuators compensated for the rudder fault effect without affecting the

acceptable performances. Here again, the FTFC system designed was able to compensate for the effect of the fault and preserve the aircraft's stability.

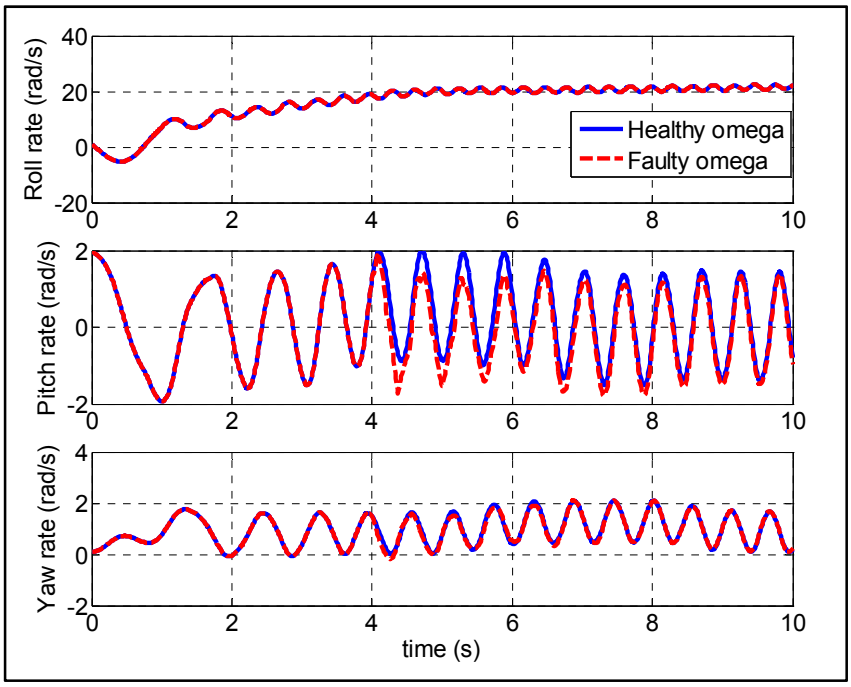

Figure 4.10 Omega time history

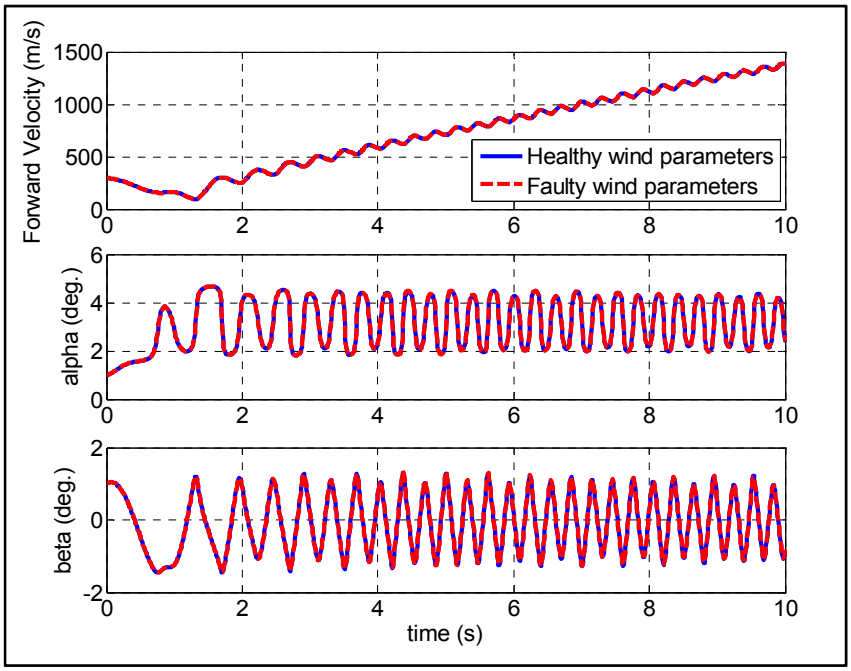

Figure 4.11 Wind parameters time history

Figure 4.12 illustrates the state of the aircraft's northeast path trajectory, in both cases, namely, when the controller used is based on a conventional technique, and when it is used with the reconfiguration technique proposed in this paper. The rudder fault degrades the tracking error to a greater extent than is seen in the second case. Here again, the actuators' redundancy plays a major role in the fault compensation and helps minimize the tracking error more and to get better performances.

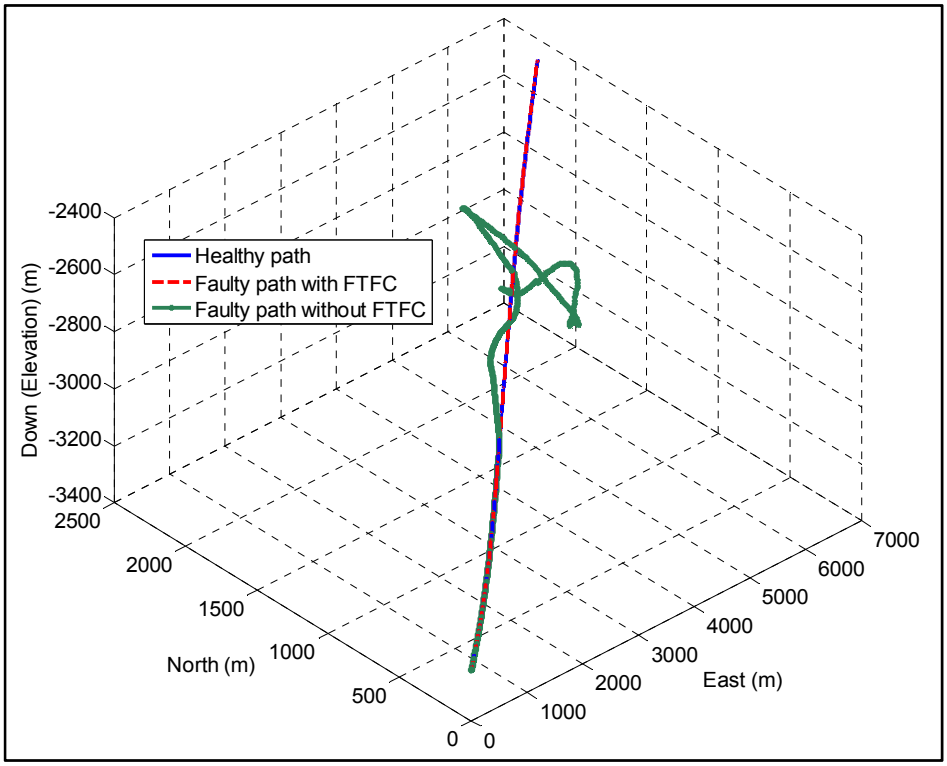

Figure 4.12 NED trajectory path

The figure also shows that compensation provides better results than in the case without reconfiguration, where the aircraft stability and performance are totally lost. One can see a minimal degradation in the tracking error, and this can be avoided or at least attenuated by adding redundant actuators, which will provide aerodynamic redundancy to the existing three actuators, and the compensation effect will then be more accurate.

Figure 4.13 shows the Boeing 737 aircraft behavior and tracking trajectory on the FlightGear simulator GUI and a 3D animation at t = 8 s.

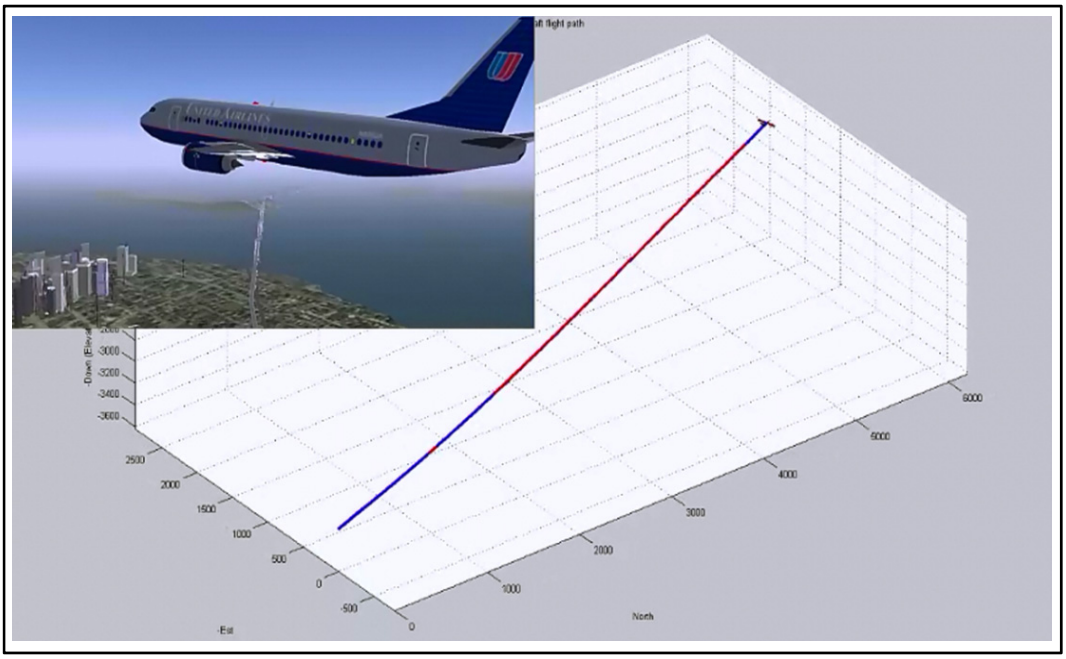

Figure 4.13 Screenshot of FlightGear simulator and 3D animation at t = 8 s

4.7 Conclusion

In this paper, an FTFC system was proposed to detect and compensate for cosmic ray faults affecting actuators of a nonlinear 6 DOF aircraft. It was shown that the fault reconstruction-based FDD, integrated into the SMC technique, ensures higher performance, even in the presence of sudden faults, compared to a conventional controller. The aircraft preserves its stability and maintains acceptable performances until the end of the flight mission.

The fault detection and reconstruction-based FDD system designed shows good performance as well. It can accurately reconstruct the controller outputs. Even if the actuator faults are time-varying and corrupted, the FDD process error is maintained close to zero.

The FDD results allow the SMC controllers to provide an accurate idea of the faults' parameters. The controllers then reconfigure the remaining actuators to compensate for the effect of the fault on the aircraft behavior, on safe navigation and on landing.

The two processes have a complementary role in the success of the entire FTFC system, with each needing the other. By exchanging accurate data at specific times, they ensure a reliable solution for the actuators' faults in avionics, even in the presence of different type of faults, including those caused by radiation in high flight altitudes.

CHAPTER 5

RECONFIGURABLE FLIGHT CONTROL SYSTEM USING MULTI-PROJECTOR-BASED GEOMETRIC APPROACH AND SLIDING MODE TECHNIQUE

A. Ghodbane [a], M. Saad [b], J.–F. Boland [c] and C. Thibeault [d],

[a, b, c, d] Department of Electrical Engineering, École de technologie supérieure,
1100 Notre-Dame West, Montreal, Quebec, Canada H3C 1K3

This paper has been submitted for publication
in the Journal of The Franklin Institute - Elsevier
on May 2016

Abstract

To preserve aircraft stability and maintain the best target performances, flight control systems require continually accurate measurements of the positions and rates of actuators. This information cannot always be ensured since, in addition to the presence of the measurement noise and modeling uncertainties, actuators are also subject to malfunction caused by sudden abrupt faults. This paper proposes a new method for the design of an online fault-tolerant flight control system, which can be able to detect and compensate for such faults. A multi-projector geometric approach is used to design the fault detection and diagnosis process, which can detect and identify the actuator fault occurring and reproduce the parameters of the faults. The reconfigurable flight control then uses these parameters with a sliding mode control law to carry out an online reconfiguration of the remaining healthy actuators for fault compensation. The Lyapunov theory is used to analyze the closed-loop system stability. Matlab®/Simulink® numerical simulations are performed to carry out comparisons with a conventional controller simulations, and to demonstrate the effectiveness and robustness of such a controller in preserving stability and maintaining acceptable flight performances in the presence of such faults. FlightGear software simulator is used to show the performance and the behavior of the Boeing 767 aircraft on a Graphical User Interface.

Keywords: Actuator faults, Fault detection and diagnosis, Fault-tolerant flight control, Sliding mode control, Geometric approach for fault reconstruction, Multi-Projector, Extended Kalman Filter, Lyapunov stability.

5.1 Introduction

Actuator faults can cause severe performance degradation and even lead to catastrophic instability in aircraft. Therefore, to preserve safety and avoid disasters, such faults must be appropriately compensated for since they are critical issues during a flight mission. Moreover, actuator fault behaviors are uncertain in nature, since it is impossible to predict which of them may fail in flight, or the time of the occurrence of such failure.

Depending on the severity of actuator faults, conventional flight control systems are not reliable in terms of facing the associated risks. Different means can be adapted to accommodate such faults. One involves using hardware redundancy, which consists in comparing the outputs of identical hardware and performing consistency cross-checks. This solution results in extra weight and costs, and thus affects the overall space, weight and power (SWAP). Therefore, to improve the system's robustness against such actuator failures, recent research approaches have been focused on new methods, collectively known in the literature as analytical redundancy, to design fault-tolerant control systems capable of adapting to such sudden faults while keeping avionics systems lighter and less expensive (Isermann, 2006). These systems are known as Fault-Tolerant Flight Control (FTFC) systems.

FTFC systems are classified into two main categories: Passive Fault-Tolerant Flight Control (PFTFC) systems and Active Fault-Tolerant Flight Control (AFTFC) systems. PFTC systems are generally based on robust techniques and do not require any information on fault parameters or controller reconfiguration or adaptation. These types of FTFC systems are reliable only for a closed class of faults and they degrade system performance even when no faults occur. However, AFTFC systems depend on explicit online knowledge of fault

parameters. These parameters are generated from the Fault Detection and Diagnosis (FDD) process, which operates as a health supervision module of the system, and makes decisions regarding the reconfiguration of the flight controller when faults occur. During the FDD process, three semi-processes are undertaken, namely, fault detection, fault identification and fault isolation. Based on the aircraft mathematical model, the FDD process is able to monitor the aircraft health status by detecting and identifying simple or simultaneous faults.

In addition to the FDD process, AFTFC systems include an online Reconfigurable Flight Controller (RFC). The RFC compensates for the faults in real time using fault parameters provided by the FDD process by reconfiguring the remaining redundant healthy actuators. When such actuators are not available, the challenge then becomes accommodating faulty actuators in order to completely or partially compensate for fault effects. The main critical drawback in AFTFC systems is the FDD process delay constraint. This delay can be defined by the time required to detect and diagnose a fault. A key problem in AFTFC systems is the combination of these two parts in an overall real-time environment.

Considerable efforts which have been put into developing FTFC systems in several applications, including RFC controllers and FDD processes, can be found in (Hwang et al., 2010), (Noura et al., 2009), (Witczak, 2007), (Zolghadri et al., 2014), (Li et al., 2013), (Zhang et Jiang, 2008) and (Zhang et al., 2013). Many methods have been developed to design the FDD process in (Thumati et Halligan, 2013), (Meskin, Naderi et Khorasani, 2013), (Meskin et Khorasani, 2011), (Mechhoud et al., 2015), (Zhang et Pisu, 2014), (Sharma et Aldeen, 2011), (Fan, Zhang et Zheng, 2013), (Isidori, 1995), (Chaib et al., 2009b) and (Chaib et al., 2009a), and they can be classified into two main categories: residual generation methods and geometric methods. Residual generation methods limit the FDD process to the detection function only. The isolation and identification functions are not handled using such methods. However, the geometric methods, which are based on a geometric projector and developed previously in (Isidori, 1995), (Chaib et al., 2009b) and (Chaib et al., 2009a), are widely used in the design of FDD processes. The main objective of the geometric methods is the decomposition of the system dynamics into two parts

(tangential and transverse dynamics), which results in an inverse dynamic computation. Such methods can easily handle a large class of single, as well as, simultaneous actuator faults.

In some practical situations, a multi-projector based on a set of sub-projectors is needed. In such a situation, a data fusion algorithm is used to estimate the accuracy of fault reconstruction based on each of the sub-projector's outputs. The algorithm based on the Extended Kalman Filter (EKF) (Kalman, 1960), (Liu, He et Sun, 2016), (Roshany-Yamchi et al., 2013), (Jassemi-Zargani et Necsulescu, 2001), (Ducard, 2009) can be considered a potential challenge to data fusion.

RFC controllers are developed using several methods. Among them, the Sliding Mode Control (SMC) technique is widely used because of its simplicity and robustness (Muske et al., 2012), (Bandyopadhyay, Janardhanan et Spurgeon, 2013), (Ghodbane et al., 2014), (Shen et al., 2015), (Zheng et Park, 2016), (Shah, Samar et Bhatti, 2015), (Hamayun, Edwards et Alwi, 2014), (Hess et Wells, 2003), (Wang et Adeli, 2012), (Fallaha et al., 2011), (Slotine et Li, 1991), (Fridman, Davila et Levant, 2011), (Utkin, 1992). SMC is used in the design of systems presenting highly uncertain dynamics and requiring high performances. However, the technique has been criticized for its consequent chattering effect. This effect decreases control accuracy and leads to damage to electrical and mechanical components. However, such damage can be attenuated using certain techniques, such as the exponential reaching law technique (Fallaha et al., 2011), the high order sliding mode (Fridman, Davila et Levant, 2011), etc.

This paper presents a novel methodology for designing an FTFC controller, combining the geometric approach for online simultaneous faults detection, the extended Kalman filter for data fusion and the sliding mode technique for the controller design. To the best of our knowledge, the integration and coordination of these techniques in a flight control system have never been done before now. The main contributions of the paper are therefore listed as follows:

- Double fault compensation using multi-projector geometric approach based-FDD;
- Accurate fault parameter identification;
- Faulty signals fusion using an EKF algorithm;
- Delay constraint accommodation using the SMC technique.

The rest of the paper is organized as follows. The fault modeling is described in section 5.2. Section 5.3 presents the geometric approach for fault reconstruction used for the design of the FDD process. Section 5.4 presents the reconfigurable flight controller based on the sliding mode approach, and the section is concluded with the reconfiguration mechanism. In section 5.5, the algorithm implemented to design the overall AFTFC system is presented. Matlab®/Simulink® numerical simulations are performed in section 5.6 to illustrate the performances of the proposed approach. Section 5.7 concludes this paper.

5.2 Actuator faults modeling

Isermann (Isermann, 2006) defined a fault as "*an unpermitted deviation of at least one characteristic property (feature) of the system from the acceptable, usual, standard condition*." At any time, faults may be present as they can occur suddenly. They can be introduced by design errors, the wrong operation or components aging. In this paper, only actuator faults are considered. Several actuator fault models have been proposed in the literature, such as floating around trim value or around zero, hard-over, loss of effectiveness, and stuck at some unknown fixed or varying value. The latter type of fault is considered very significant and is often encountered in many safety-critical control systems (Isermann, 2006).

Figure 5.1 illustrates a block diagram of the mathematical modeling of an actuator fault (Tao et al., 2013).

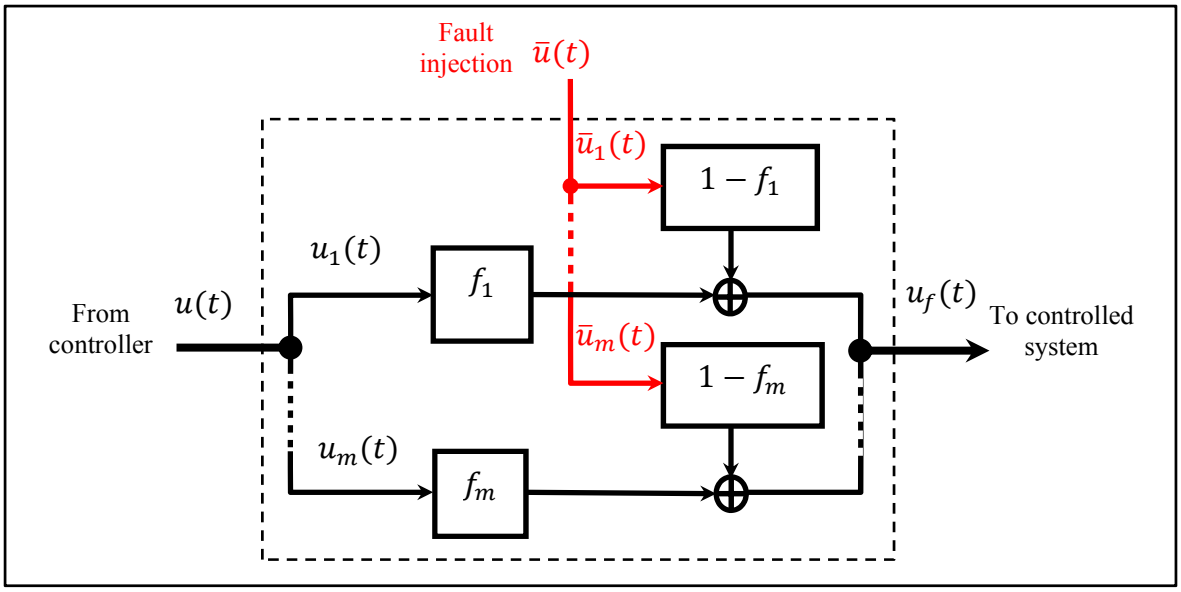

Figure 5.1 Block diagram of the mathematical modeling of actuator faults
Adapted from Tao et al. (2013)

In the presence of a fault, the faulty signal $u_f(t)$ takes the form:

$$u_f(t) = Fu(t) + (I_{m\times m} - F)\bar{u}(t) \tag{5.1}$$

where $u_f = [u_{f1}, \dots, u_{fm}]^T$ are the faulty actuators' input signals, $\bar{u} = [\bar{u}_1, \dots, \bar{u}_m]^T$ are the fault signals, $u = [u_1, \dots, u_m]^T$ are the computed control signals, and m is the number of actuators. Assuming the k^{th} actuator to be the target of the fault $\bar{u}_k(t)$, the F matrix and $\bar{u}(t)$ are then designed as follows:

$$F = diag\{f_i\}, \quad f_i = \begin{cases} 1, & i \neq k \\ 0, & i = k \end{cases} \tag{5.2}$$

$$\bar{u}(t) = [0 \dots \bar{u}_k(t) \dots 0]^T \tag{5.3}$$

In an AFTFC system, any actuator fault occurring must be detected at each time step. In addition, it must be identified and isolated. Fault identification determines the variation of the form of the fault with time, while fault isolation determines the actuator that failed. These three tasks are performed using the FDD process. In this paper, the FDD is designed based on the geometric approach for fault reconstruction which will be developed in the next section.

5.3 Geometric approach for fault reconstruction

The main objective of the geometric approach is to reconstruct the actuator input signals affecting the aircraft dynamics. This technique decomposes the state space of the aircraft into two planes, using a so-called geometric projector. The first plane is tangential to the defective signal, and the second is transverse. Actuator input signals are then constructed according to the minimum invertibility theorem (Isidori, 1995), (Chaib et al., 2009b) and (Chaib et al., 2009a). If the number of actuators available is less than the number of available outputs, as is the case in this paper, more than one geometric projector is needed. Then, a geometric multi-projector, which includes a set of sub-projectors, is designed, and several forms of faults are reconstructed from each sub-projector. The optimal reconstruction fault inputs are then given by using the reconstructed fault inputs obtained from each sub-projector using a selected data fusion algorithm.

To better illustrate the approach, and without loss of generality, a nonlinear dynamic system is considered in this paper as follows:

$$\begin{cases} \dot{x}(t) = f(x) + g(x)u(t) \\ y(t) = h(x) \end{cases} \tag{5.4}$$

where $f(x) \in \mathbb{R}^{n\times 1}, g(x) \in \mathbb{R}^{n\times m}$ and $h(x) \in \mathbb{R}^{p\times 1}$ are respectively the system, input and output nonlinear functions of appropriate dimensions. $x(t) \in \mathbb{R}^{n\times 1}, y(t) \in \mathbb{R}^{p\times 1}$ and $u(t) \in \mathbb{R}^{m\times 1}$ represent the state vector variables, the output vector variables and the control inputs variables, respectively.

5.3.1 Multi-projector design

When the number of outputs is greater than the number of inputs $(p > m)$, a multi-projector should be considered. The multi-projector-based fault is designed using k possible subsets. Each subset includes $m = p$ independent outputs. The idea is to design a sub-projector associated to each subset. The multi-projector-based FDD approach for fault reconstruction using k sub-projectors is illustrated in Figure 5.2.

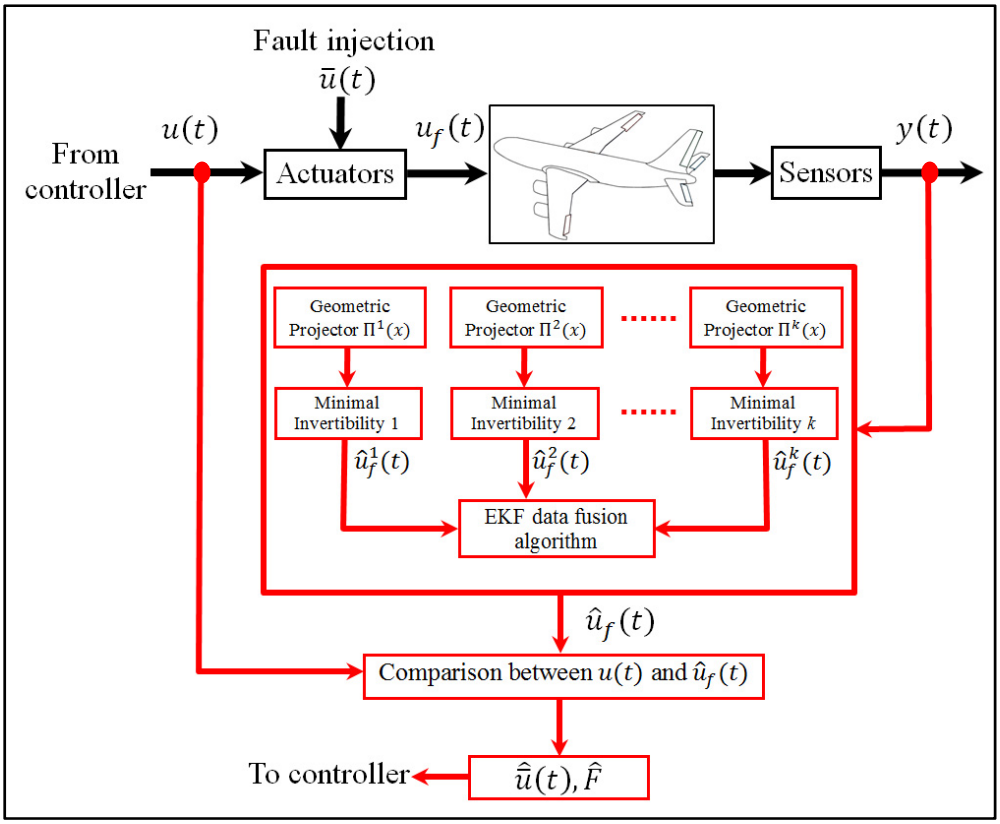

Figure 5.2 General structure of the geometric multi-projector approach using k sub-projectors
Adapted from Chaib et al. (2009)

Each sub-projector $\Pi^i(x)$ is designed as follows (Chaib et al., 2009b) and (Chaib et al., 2009a):

$$\Pi^i(x) = I_{m\times m} - L^i {A^i_{proj}}^{-1} \nabla\sigma^{T^i}, i = 1, \dots, k \tag{5.5}$$

where $I_{m\times m}$ is the identity matrix, L^i, A^i_{proj} and $\nabla\sigma^{T^i}$ are associated to the m independent output set i. More details can be found in Appendix V. Each sub-projector $\Pi^i(x)$ decomposes the aircraft state space, along a sub-manifold surface S_b^i, into two planes. The first one is tangent to the faulty inputs and the second one is transverse. The sub-manifold surface S_b^i is defined as follows:

$$S_b^i = \left\{x := L_{f(x)}^{r_j-1} h_j(x) = 0, for\ 1 \le j \le p\right\}, i = 1, \dots, k \tag{5.6}$$

where the term $L_{f(x)}^{r_j-1}h_j(x)$, with $1 \leq i \leq p$, are called the $(r_j - 1)^{\text{th}}$ Lie Derivative of $h_j(x)$ in the direction of the vector field $f(x)$.

Using (5), the dynamic vector $f(x)$ can be decomposed into tangent and transverse parts along the sub-manifold S_b^i as follows:

$$f(x) = \Pi^i(x)f(x) + \left(I_{m\times m} - \Pi^i(x)\right)f(x), \ \forall x \in S_b^i \tag{5.7}$$

The term $\Pi^i(x)f(x)$ represents the tangent part, while the term $\left(I_{m\times m} - \Pi^i(x)\right)f(x)$ represents the transverse part. Figure 5.3 illustrates the interpretation of one sub-projector.

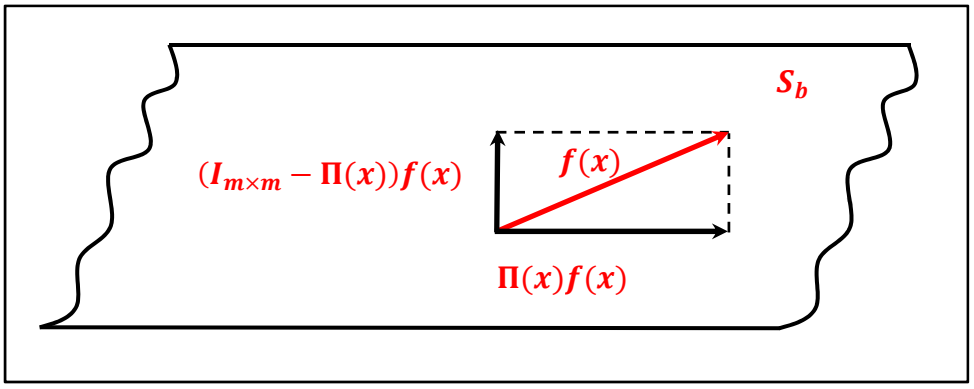

Figure 5.3 Decomposition and projection of $f(x)$
Adapted from Chaib et al. (2009)

5.3.2 Faulty inputs reconstruction

Once the sub-projector $\Pi^i(x)$ is designed, the faulty inputs $u_f^i(t)$ can be reconstructed via the minimum invertibility theorem (De Persis et Isidori, 2001), (Chaib et al., 2009b), (Chaib et al., 2009a), as follows:

$$\begin{cases} \dot{x}^i(t) = \Pi^i f(x^i) + L^i {A_{proj}^i}^{-1} \dot{y}^i(t) \\ u_f^i(t) = {A_{proj}^i}^{-1} \left(\dot{y}^i(t) - \nabla\sigma^{T^i} f(x^i)\right) \end{cases} \tag{5.8}$$

where $\dot{y}^i(t)$ is the output vector derivative associated to the m independent output set i.

Finally, using (5.7) and (5.8), the system in (5.4) will take the form:

$$\dot{x}^i(t) = \Pi^i(x) f(x^i) + L^i {A^i_{proj}}^{-1} \nabla\sigma^{T^i} f(x^i) + L^i u^i_f(t) \tag{5.9}$$

Once the faulty inputs $u^i_f(t)$ are designed using the k sub-projectors $\Pi^i(x)$, they are used in an algorithm for signal data fusion, to design the optimal reconstruction fault inputs. In this paper, the Extended Kalman Filter (EKF), which is considered a suitable method for fault signal fusion, is designed for this purpose (Kalman, 1960), (Liu, He et Sun, 2016), (Roshany-Yamchi et al., 2013), (Jassemi-Zargani et Necsulescu, 2001), (Ducard, 2009). In the multi-projector case, several forms of faults are reconstructed from each sub-projector. The optimal reconstruction fault inputs are then given by using the reconstructed fault inputs obtained from each sub-projector using the EKF data fusion algorithm, as illustrated in Figure 5.4.

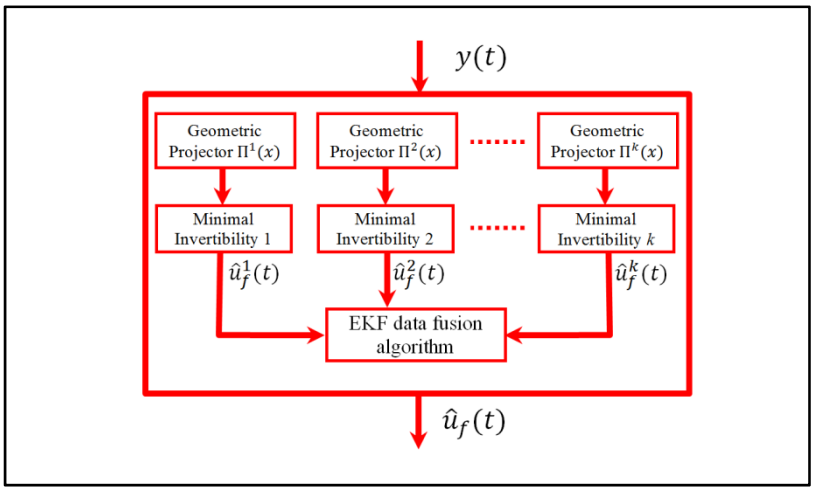

Figure 5.4 The optimal reconstruction fault using a data fusion algorithm

The EKF has been proved suitable for real-time estimation of state space variables $x(t)$. Given incomplete noisy measurement $y(t)$ and modeling uncertainties, it has also been proven to be suitable in signal fusion. The measurement noise is modeled using a Gaussian white sensor noise $\eta_v(t)$, described by its measurement noise covariance matrix $Q_n = E\{\eta_v {\eta_v}^T\}$. The modeling uncertainties are modeled using a Gaussian white noise $\eta_w(t)$,

described by its process noise covariance matrix $R_w = E\{\eta_w \eta_w{}^T\}$. Figure 5.5 illustrates these two cases of the use of the EKF.

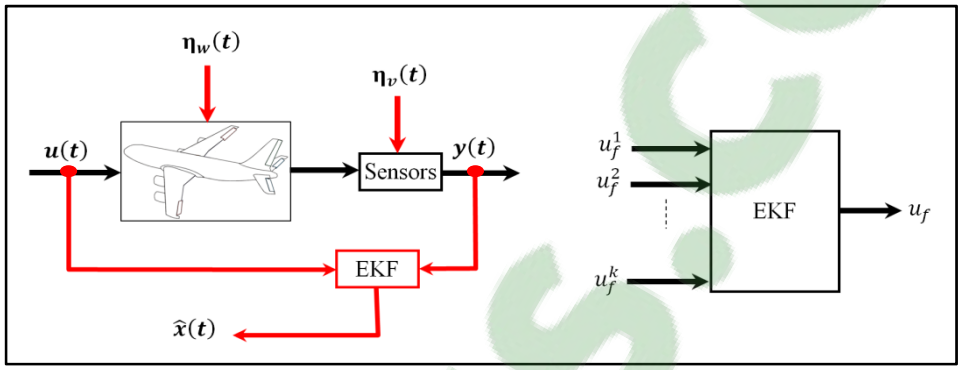

Figure 5.5 Extended Kalman Filter used for state estimate and for data fusion
Adapted from Jassemi-Zargani et Necsulescu (2001)

In order to improve the online estimation of the value of the reconstructed faulty control outputs, the EKF is used to fuse the noisy signals of the set of k sub-projector outputs $\hat{u}_f^k(t) = \{\hat{u}_f^i(t),\ i = 1, \ldots, k\}$. For the filter design, the reconstructed time-varying output is modeled as a Gaussian process $\hat{u}_f^i(t) = \eta_w(t)$. The following system is used in the data fusion algorithm:

$$\begin{cases} \hat{u}_f^k(t) = \eta_w(t) \\ \hat{u}_f(t) = I_{m\times m}\hat{u}_f^k(t) + \eta_v(t) \end{cases} \tag{5.10}$$

More details on EKF algorithm for data fusion can be found in (Jassemi-Zargani et Necsulescu, 2001).

When the occurred actuator fault is detected, identified and isolated using the designed FDD process, the fault parameters are then used to design the Reconfigurable Flight Control (RFC) system. In this paper, the Sliding Mode Control (SMC) technique is used for the design of the RFC system, which will be developed in the next section.

5.4 Reconfigurable Flight Control design

Once the faults' parameters are determined using the geometric method, they will be used in the design of Reconfigurable Flight Control (RFC) systems. The technique first designs a discontinuous control law to drive the aircraft error dynamics onto a specified surface $S(t)$ called the sliding surface. It then designs a continuous law to let the aircraft error dynamics slide on this surface for the remainder of the flight. This approach has two main advantages. Firstly, while the aircraft error dynamics are on the sliding surface, the aircraft behavior becomes a reduced order system. Secondly, the aircraft dynamics, while in sliding mode, is insensitive to modeling uncertainties and to external disturbances.

5.4.1 Sliding surface design

The first step in the design of the SMC controller involves designing the sliding surface $S(t)$. The goal here is to have a dynamic motion on this surface, which governs the error trajectory to zero. Assuming that $\tilde{x}(t) = x(t) - x_d(t)$ are the output state error and $x_d(t)$ the desired state, the sliding surface $S(t)$ is defined by a vector $s(x,t)$ such as (Slotine et Li, 1991) and (Utkin, 1992):

$$s(x,t) = \left(\frac{d}{dt} + \lambda\right)^{(n-1)} \tilde{x}(t) = 0,\ \lambda > 0 \tag{5.11}$$

The integral form can be also considered, as follows (Ghodbane et al., 2014), (Hamayun, Edwards et Alwi, 2014) :

$$s(x,t) = \left(\frac{d}{dt} + \lambda\right)^{(n)} \int \tilde{x}(t) = 0,\ \lambda > 0 \tag{5.12}$$

Figure 5.6 gives a graphical interpretation of $S(t)$ for the case of a first- and a second-order system.

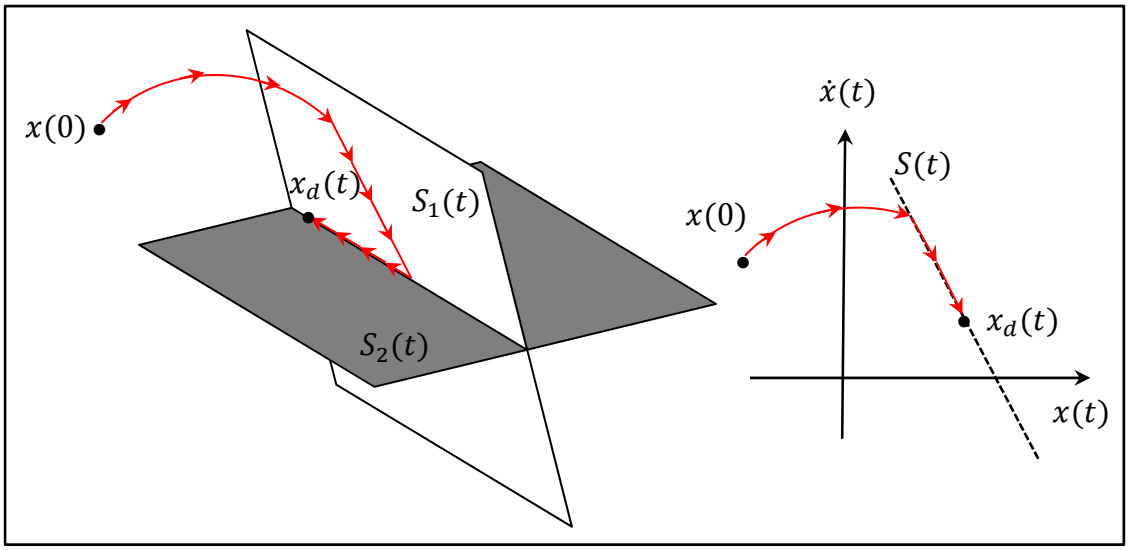

Figure 5.6 Graphical interpretation of (5.11) and (5.12) for first and second order system Adapted from Slotine et Li (1991) and Utkin (1992)

5.4.2 Sliding Mode Control law design

Referring to the stability theorem of Lyapunov (Slotine et Li, 1991), the system described by (5.4) is stable if a positive candidate function V_L exists that satisfies $\dot{V}_L < 0$ for any time t. Consider this Lyapunov function candidate:

$$V_L = \frac{1}{2} s^T s \tag{5.13}$$

System (5.4) is stable if $\dot{V}_L = s^T \dot{s} < 0$. A logical choice for $\dot{s}$ is given as:

$$\dot{s} = -Ksign(s)\ ,\ K > 0 \tag{5.14}$$

The sign function is defined as: $sign(s) = \begin{cases} +1 & \text{if } s > 0 \\ 0 & \text{if } s = 0. \\ -1 & \text{if } s < 0 \end{cases}$

Combining (5.4) and (5.14), if $g(x)$ is invertible, then the control law will take the form:

$$u(t) = g(x)^{-1}[\dot{x}_d(t) - \lambda\tilde{x}(t) - f(x)] - g(x)^{-1}[Ksign(s)] \tag{5.15}$$

where $g(x)^{-1}$ is the inverse of the $g(x)$ function. Without loss of generality, we assume that $g(x)^{-1}$ always exists. In the case where the inverse cannot be calculated, the pseudo-inverse function can be used.

The first term of equation (5.15) is called $u_{eq}(t)$ and it represents the continuous law that maintains the condition $\dot{s}(x,t) = 0$. Thus, the control law drives error trajectories towards the equilibrium point, while remaining on the surface $S(t)$. The second term is called $u_{disc}(t)$ and it represents the discrete control law required to push the error trajectories towards the sliding surface $S(t)$.

5.4.3 Reconfiguration process

Assuming that $\bar{u}(t)$ is the fault affecting the actuator, the system dynamics can be written using (5.1) and (5.4) as follows:

$$\begin{cases} \dot{x} = f(x) + g(x)[Fu(t) + (I_{m\times m} - F)\bar{u}(t)] \\ y = h(x) \end{cases} \tag{5.16}$$

By choosing $U(t) = Fu(t)$ to be the reconfigurable flight control law, and combining (5.12), (5.14), (5.15) and (5.16), the control law $U(t)$ takes the form:

$$U(t) = g(x)^{-1}[(\dot{x}_d(t) - \lambda\tilde{x}(t) - f(x)) - g(x)(I - F)\bar{u}(t)] - g(x)^{-1}(Ksign(s)) \tag{5.17}$$

The terms F and $\bar{u}(t)$ in (5.17), also called fault parameters, are unknown, and must be reconstructed in real time using the geometric projector approach. The SMC controller uses the reconstructed parameters $\hat{F}$ and $\hat{\bar{u}}(t)$ and reconfigures the remaining healthy actuator signals online to compensate for the faulty actuator signal.

5.4.4 Closed-loop stability of the whole system

For the faulty system defined by (5.16), the sliding surface is chosen based on (5.12), as follows:

$$s(x,t) = \tilde{x}(t) + \lambda \int \tilde{x}(t) = 0,\ \lambda > 0 \tag{5.18}$$

which yields to:

$$\dot{s}(x,t) = \frac{d}{dt}\tilde{x}(t) + \lambda\tilde{x}(t) = 0,\ \lambda > 0 \tag{5.19}$$

By considering the stability condition given in (5.14), and by using (5.15) and (5.19), the control law given by (5.17) will be deducted, and hence, the stability of the whole system is proved.

5.4.5 Chattering problem

Theoretically, the ideal sliding mode implies infinite switching frequency. In practical applications, the control is constant within a sampling interval, and as a result, the switching frequency cannot exceed that of sampling. This leads to the generation of undesirable oscillations having finite frequency and amplitude, and constituting what is known as the 'chattering phenomenon'. This phenomenon is considered harmful, and could represent the main obstacle for the implementation of the controller because it leads to low control accuracy, high wear of moving mechanical parts, and high heat losses in power circuits.

To reduce the chattering phenomenon, the authors in (Hess et Wells, 2003) introduced a power rate reaching law in the discrete control law given in (5.17). The idea was to improve the reaching speed. In (Fallaha et al., 2011), the authors introduced an exponential reaching law, and in that case, the idea was to let the reaching speed become inversely proportional to the distance between the sliding surface and the system trajectory. Other techniques were introduced in (Wang et Adeli, 2012), (Slotine et Li, 1991) and (Fridman, Davila et Levant, 2011).

After the required blocks for the implementation of the AFTFC system were designed, an algorithm integrating these blocks into an overall system had to be implemented. The implementation is detailed in the next section.

5.4.6 Overall algorithm of the proposed AFTFC system

Figure 5.7 illustrates the steps to be followed in implementing the proposed algorithm at each sampling time T_s.

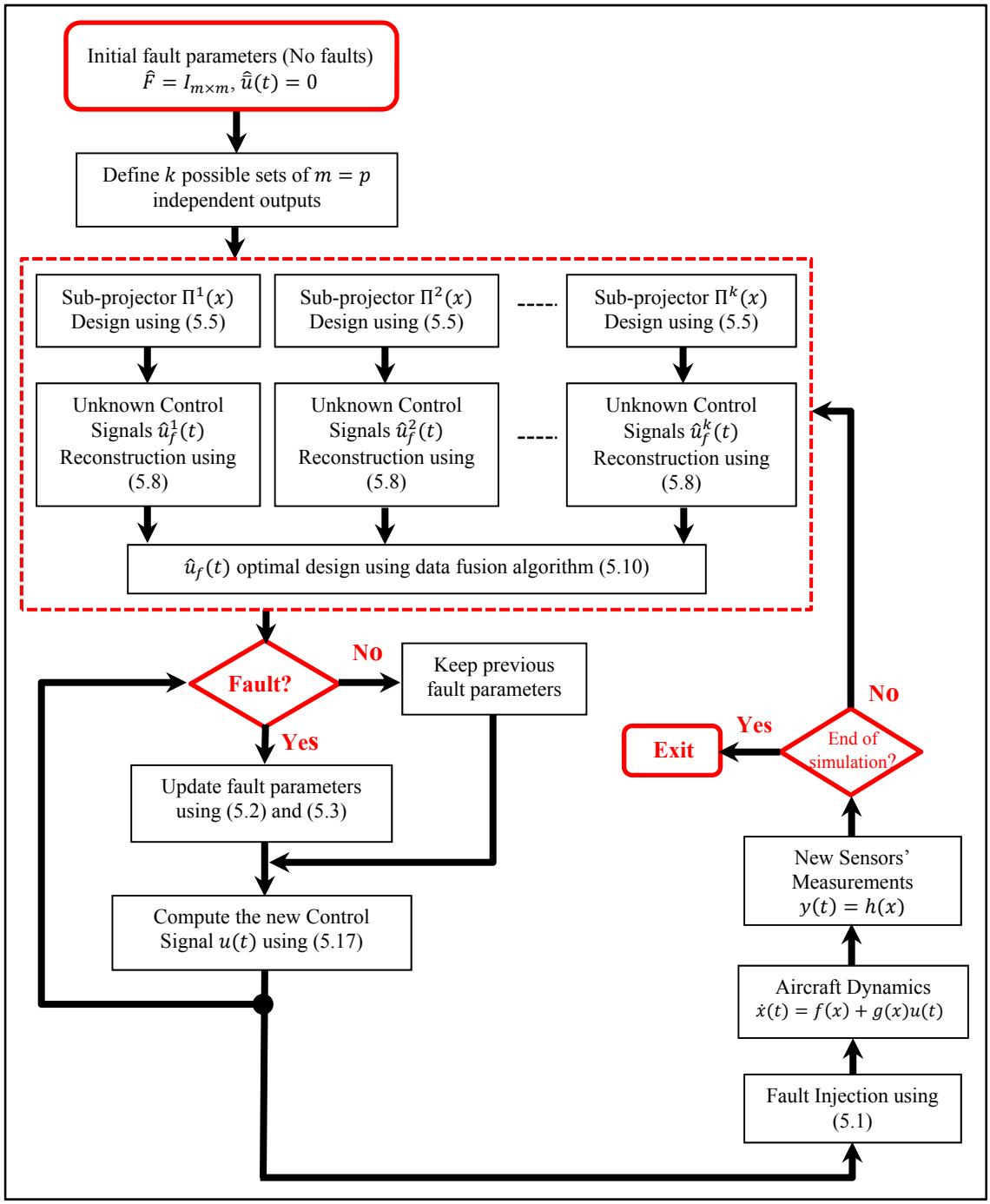

Figure 5.7 FTFC algorithm used to perform simulations

The fault parameters are initialized firstly by choosing $\hat{F} = I_{m\times m}$ and $\hat{\bar{u}}_i(t) = 0, i = 1, \dots, m$. This initialization assumes that the system state starts out healthy. Then, for each step time, the sensors' measurements of state variables are collected and the possible k outputs sets,

such as $m = p$ are defined to design the k geometric sub-projectors $\Pi^i(x)$, $i = 1, \ldots, k$ using (5.5). Next, the associated unknown faulty control signals $\hat{u}_f^i(t)$ are reconstructed using (5.8). The data fusion algorithm is then used to design the optimal faulty control signal $\hat{u}_f(t)$ using (5.10), and the fault parameters $\hat{\bar{u}}(t)$ and $\hat{F}$ are defined by a comparison between the reconstructed optimal control signal $\hat{u}_f(t)$ and the computed control $u(t)$. Based on that comparison, the fault decision is made. Fault parameters are then updated using (5.2) and (5.3), and the new control law is computed using (5.17), based on the fault decision. After that, the simulated fault is injected and finally, the sensors' measurements are collected for the next sampling time $T_s + 1$.

The overall structure of the proposed AFTFC system is depicted in Figure 5.8.

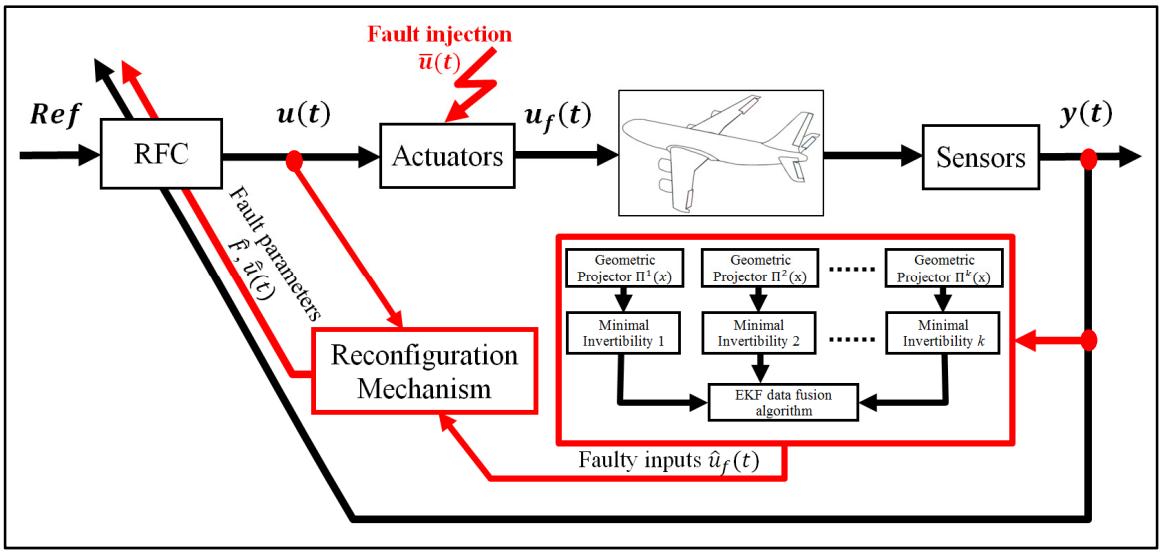

Figure 5.8 FTFC Scheme using the multi-projector geometric method, the EKF algorithm and the SMC reconfigurable flight control

5.5 Case study

The proposed approach is applied to the linear model of the Boeing 767. This commercial aircraft has two turbo engines, with a capacity of 181 to 375 passengers. It has a range of 3850 to 6385 nautical miles (Garvin, 1988).

5.5.1 System modeling

The complete nonlinear model of the Boeing 767 is described as follows:

$$\dot{x}(t) = f(x) + g(x)u(t) \tag{5.20}$$

where $f(x) \in \mathbb{R}^{9\times1}$, $g(x) \in \mathbb{R}^{9\times5}$ are respectively the dynamics and the inputs nonlinear functions. The state space variables $x(t) \in \mathbb{R}^{9\times1}$ and the primary actuator input variables $u(t) \in \mathbb{R}^{5\times1}$ are described in Table 5.1.

Table 5.1 B767 state vector and control actuators
Adapted from Fossen (2011)

State vector		**Primary control surfaces**	
$\boldsymbol{V}$	Longitudinal velocity, ft./s	$\boldsymbol{\delta_e}$	Elevator, rad
$\boldsymbol{\alpha}$	Angle of attack, rad	$\boldsymbol{\delta_a}$	Aileron, rad
$\boldsymbol{\beta}$	Side slip angle, rad	$\boldsymbol{\delta_r}$	Rudder, rad
$\boldsymbol{p}$	Roll rate, rad/s	$\boldsymbol{\delta_{RTh}}$	Right thrust, (lbs.)
$\boldsymbol{q}$	Pitch rate, rad/s	$\boldsymbol{\delta_{LTh}}$	Left thrust, (lbs.)
$\boldsymbol{r}$	Yaw rate, rad/s		
$\boldsymbol{\varphi}$	Roll angle, rad		
$\boldsymbol{\theta}$	Pitch angle, rad		
$\boldsymbol{\psi}$	Yaw angle, rad		

The linearization process can be developed on a part of the aircraft path by considering that the aircraft motion comprises two components: a mean motion which represents the trim conditions and a dynamic motion which accounts for the perturbations about the mean motion (McLean, 1990). The trim conditions used for the Boeing 767 are defined in Table 5.2. The linear model is described by the state space equation as follows:

$$\dot{x}(t) = Ax(t) + Bu(t) \tag{5.21}$$

Where $A \in \mathbb{R}^{8\times8}$ and $B \in \mathbb{R}^{8\times5}$ are respectively the dynamics and the inputs matrices.

Table 5.2 B767 flight parameters
Adapted from Fossen (2011)

Flight parameters		Flight conditions
$\boldsymbol{V_T}$	Speed, ft./s	890
$\boldsymbol{h}$	Altitude, ft.	35000
$\boldsymbol{m}$	Mass, lbs.	184000
$\boldsymbol{Mac}$	Mach Number	0.8

For the dynamic motion in (5.21), it is common to assume that the longitudinal velocity is much larger than the vertical and transversal velocities. So, the longitudinal modes can be decoupled from the lateral modes. The longitudinal motion is described by $\dot{x}_{long}(t) = A_{long}x_{long}(t) + B_{long}u_{long}(t)$, and the lateral motion is described by $\dot{x}_{lat}(t) = A_{lat}x_{lat}(t) + B_{lat}u_{lat}(t)$. The longitudinal state and input vectors are respectively $x_{long}(t) = [\theta\ V\ \alpha\ q]^T$ and $u_{long}(t) = [\delta_e\ \delta_{RTh}\ \delta_{LTh}]^T$. Table 5.3 illustrates the state variable vector and the actuator control signal for the lateral model.

Table 5.3 B767 state vector and control actuators for the lateral model
Adapted from Fossen (2011)

State space variables		Control signal variables	
$\boldsymbol{\varphi}$	Roll angle, rad	$\boldsymbol{\delta_a}$	Aileron, rad
$\boldsymbol{\beta}$	Side slip angle, rad	$\boldsymbol{\delta_r}$	Rudder, rad
$\boldsymbol{p}$	Roll rate, rad/s		
$\boldsymbol{r}$	Yaw rate, rad/s		

The lateral state and input vectors are respectively $x_{lat}(t) = [\varphi\ \beta\ p\ r]^T$ and $u_{lat}(t) = [\delta_a\ \delta_r]^T$. Table 5.4 illustrate the state variable vector and the actuator control signal for the longitudinal model.

Table 5.4 B767 state vector and control actuators for the longitudinal model
Adapted from Fossen (2011)

State space variables		Control signal variables	
θ	Pitch angle, rad	δ_e	Elevator, rad
V_x	Longitudinal velocity, ft./s	δ_{RTh}	Right thrust, (lbs.)
α	Angle of attack, rad	δ_{LTh}	Left thrust, (lbs.)
q	Pitch rate, rad/s		

According to the flight conditions illustrated in Table 5.2, matrices A and B in (5.21) are described in Appendix IV.

5.5.2 Simulation scenario

Simulations are performed using Matlab®/Simulink® on the overall FTFC control architecture for the longitudinal and lateral models separately. They run for over 100 seconds. The faults considered are derived from (Hobeika et al., 2013). The right thrust responds at only 400 lbs. of the control generated by the controller between t = 20 s and t = 50 s. For the lateral model, the fault considered is the actuator oscillation. The rudder oscillates close to zero degrees between t = 40 s and t = 60 s. Note here that between t = 40 s and t = 50 s, a simultaneous fault case is considered. Figure 5.9 shows the faults injected on the right trust and rudder actuators, respectively.

In order to obtain realistic simulations, the sensor measurement data are corrupted with zero-mean Gaussian noise corresponding to typical specifications of low-cost sensors. The deviation is taken as $\sigma = 2^{\circ}$, which corresponds to an error covariance matrix $(0.012 \times I[rad^2])$. Two separate controllers, based on the sliding mode technique and a geometric approach for fault reconstruction, are designed for each model. The numerical aerodynamics parameters of the Boeing 767 and the two linear models considered in this paper can be found in (Fossen, 2011).

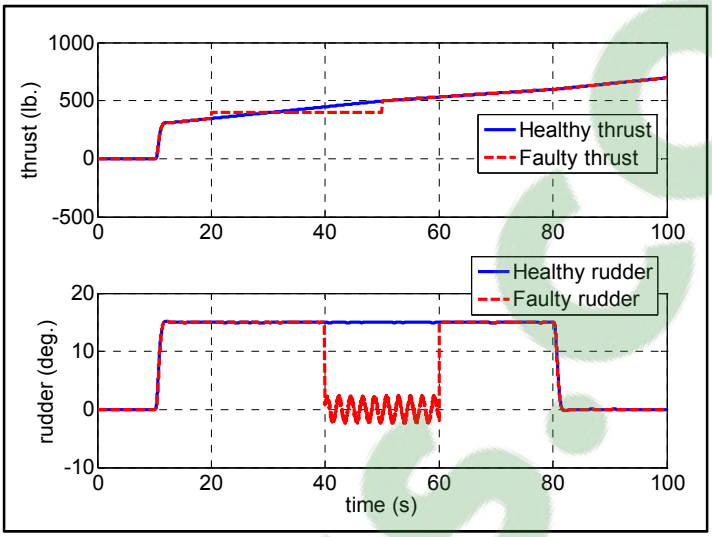

Figure 5.9 Fault models used in the simulation

5.5.3 Multi-projector design

In this study, the number of outputs is greater than the number of inputs. Therefore, a multi-projector may be designed. For the lateral model, the number of outputs is $p = 3$ and the number of actuators is $m = 2$. For the longitudinal model, the number of outputs is $p = 4$ and the number of actuators is $m = 3$. The idea is to design a multi-projector system and to use the reconstructed fault inputs given by each sub-projector. The optimal reconstruction fault inputs are then designed by using an Extended Kalman Filter (EKF) algorithm for signal data fusion.

For the lateral model, three ($k = 3$) sub-projectors are designed. The sets of all possible $y^i, i = 1,3$ outputs chosen for each sub-projector are:

$$y_{21} = \begin{pmatrix} \beta \\ p \end{pmatrix}, y_{22} = \begin{pmatrix} \beta \\ r \end{pmatrix}, y_{23} = \begin{pmatrix} p \\ r \end{pmatrix} \tag{5.22}$$

Following the approach given in section 5.3, the relative degrees (defined in Appendix V) of y^1, y^2 and y^3 are (1,1), (1,1) and (1,1), respectively. The respective sub-manifold surfaces S_b^i deduced, and the correspondent sub-projectors $\Pi^i(x)$ designed, are illustrated in Appendix IV.

Similarly, for the longitudinal model, three ($k = 3$) sub-projectors are designed. The sets of all possible $y^i, i = 1,3$ outputs chosen for each sub-projector are:

$$\mathrm{y}_{21} = \begin{pmatrix} V_x \\ \alpha \\ q \end{pmatrix}, \mathrm{y}_{22} = \begin{pmatrix} V_x \\ q \\ \theta \end{pmatrix}, \mathrm{y}_{33} = \begin{pmatrix} \alpha \\ q \\ \theta \end{pmatrix} \tag{5.23}$$

The relative degrees of y^1, y^2 and y^3 are (1,1,1), (1,1,1) and (1,1,1), respectively. The respective sub-manifold surfaces S_b^i deduced and the correspondent sub-projectors $\Pi^i(x)$ designed are illustrated in Appendix IV.

5.5.4 Inverse dynamics design

Following (5.8), the inverse dynamics $\hat{x}^i(t)$ and the fault reconstruction $\hat{u}_f^i(t)$ for each sub-projector $\Pi^i(x)$ of the lateral model are given in Appendix IV. The optimal reconstruction fault inputs $\hat{u}_f(t)$ are then given by injecting the reconstructed fault inputs $\hat{u}_f^i(t)$ obtained from each sub-projector $\Pi^i(x)$ in a selected data fusion algorithm.

Similarly, the inverse dynamics $\hat{x}^i(t)$ and the fault reconstruction $\hat{u}_f^i(t)$ for each sub-projector $\Pi^i(x)$ of the longitudinal model are illustrated in Appendix IV. The optimal reconstruction fault inputs $\hat{u}_f(t)$ are then given by injecting the reconstructed fault inputs $\hat{u}_f^i(t)$ obtained from each sub-projector $\Pi^i(x)$ in a selected data fusion algorithm. The fusion algorithm used in this paper is developed in the next sub-section.

5.5.5 EKF design for signal fusion

The fusion algorithm used in this paper is developed based on the EKF theory detailed in Appendix VI. For the lateral model, the multi-projector structure gives three ($k = 3$) different reconstructions for each faulty input $\delta_{a_f}(t)$ and $\delta_{r_f}(t)$. These three faulty input

reconstructions, $\hat{\delta}_{a_f}{}^{i}(t)$ and $\hat{\delta}_{r_f}{}^{i}(t)$, are combined in an EKF fusion algorithm to estimate the optimal faulty input reconstructions $\hat{\delta}_{a_f}(t)$ and $\hat{\delta}_{r_f}(t)$.

Faulty time-varying inputs are modeled as a Gaussian process, such as $\dot{\hat{\delta}}_{a_f}(t) = \dot{\hat{\delta}}_{r_f}(t) = \eta_w(t)$. The covariance matrices Q_n and R_w are defined as 0.02 and $0.001 \times I_{3\times3}$ respectively. The initial conditions of faulty inputs are taken, such as $\hat{\delta}_{a_f}(0) = \hat{\delta}_{r_f}(0) = 0$. The initial condition of the covariance error matrix $P_0 = 0.01$. The systems used in the data fusion algorithm are described as follows (Jassemi-Zargani et Necsulescu, 2001):

$$\begin{cases} \dot{\hat{\delta}}_{a_f}{}^{i}(t) = \eta_w(t), i = 1,2,3 \\ \hat{\delta}_{a_f}(t) = \left(\hat{\delta}_{a_f}{}^{1}(t) \quad \hat{\delta}_{a_f}{}^{2}(t) \quad \hat{\delta}_{a_f}{}^{3}(t)\right)^T \\ \hat{\delta}_{a_f}(t) = I_{3\times3}\hat{\delta}_{a_f}(t) + \eta_v(t) \end{cases} \tag{5.24}$$

$$\begin{cases} \dot{\hat{\delta}}_{r_f}{}^{i}(t) = \eta_w(t), i = 1,2,3 \\ \hat{\delta}_{r_f}(t) = \left(\hat{\delta}_{r_f}{}^{1}(t) \quad \hat{\delta}_{r_f}{}^{2}(t) \quad \hat{\delta}_{r_f}{}^{3}(t)\right)^T \\ \hat{\delta}_{r_f}(t) = I_{3\times3}\hat{\delta}_{r_f}(t) + \eta_v(t) \end{cases} \tag{5.25}$$

Figure 5.10 illustrates the estimated faulty inputs $\hat{\delta}_{a_f}(t)$ and $\hat{\delta}_{r_f}(t)$ using the EKF fusion algorithm:

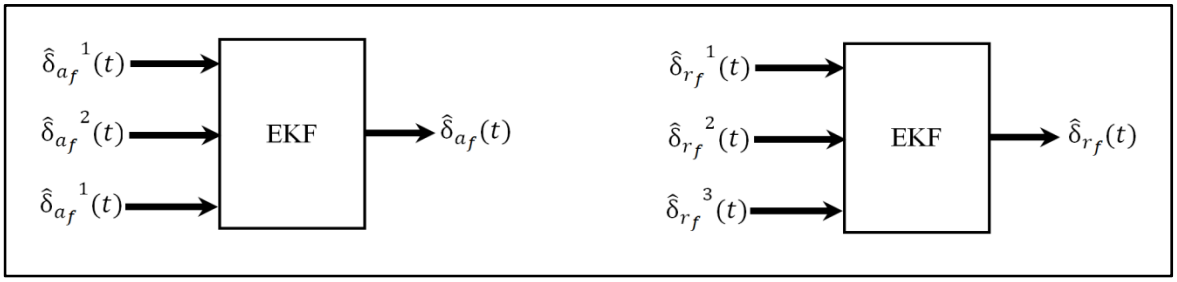

Figure 5.10 Estimated faulty inputs $\hat{\delta}_a$ and $\hat{\delta}_r$ using an EKF fusion algorithm
Adapted from Jassemi-Zargani et Necsulescu (2001)

Similarly, for the longitudinal model, the multi-projector structure gives three ($k = 3$) different reconstructions for each faulty input $\delta_{e_f}(t)$, $\delta_{RTh_f}(t)$ and $\delta_{LTh_f}(t)$. These three reconstructions, $\hat{\delta}_{e_f}{}^{i}(t)$, $\hat{\delta}_{RTh_f}{}^{i}(t)$ and $\hat{\delta}_{LTh_f}{}^{i}(t)$, are combined in an EKF fusion algorithm to produce the optimal faulty input reconstructions $\hat{\delta}_{e_f}(t)$, $\hat{\delta}_{RTh_f}(t)$ and $\hat{\delta}_{LTh_f}(t)$.

In the next sub-section, numerical simulation results for the proposed overall AFTFC system are illustrated and compared to those for a conventional controller (without fault detection and online reconfiguration).

5.5.6 Simulation results

Figure 5.11 illustrates the geometric approach-based FDD process results. A value of 1, means that the actuator is healthy and does not suffer from any fault. Note that the fault detection is instantaneous: when the right thrust δ_{RTh} fails at t = 20 s, the health status monitor changes from 1 to 0, indicating that a fault occurs at this time. At t = 50 s, the health status changes twice from 0 to 1, indicating that at this moment, the right thrust becomes healthy. The same can be seen at t = 40 s and at t = 60 s in the case of the rudder fault δ_r. The elevator δ_e, as well as the aileron δ_a and the left thrust δ_{LTh}, remain healthy. Note that because of the robustness of SMC against uncertainties, the proposed overall system handled the delay constraint.

Figure 5.12 illustrates the time response of aircraft state variables for the fault scenario considered. As shown, in spite of the multiple faults on the right thrust and on the rudder, the tracking performance of the proposed reconfigurable controller is acceptable. In the case when the reconfiguration is OFF (case of a conventional controller), the controller shows the degradation of the tracking performance after the actuator fault. However, the conventional sliding mode controller still shows some degree of tracking ability because of its robustness against uncertainties.

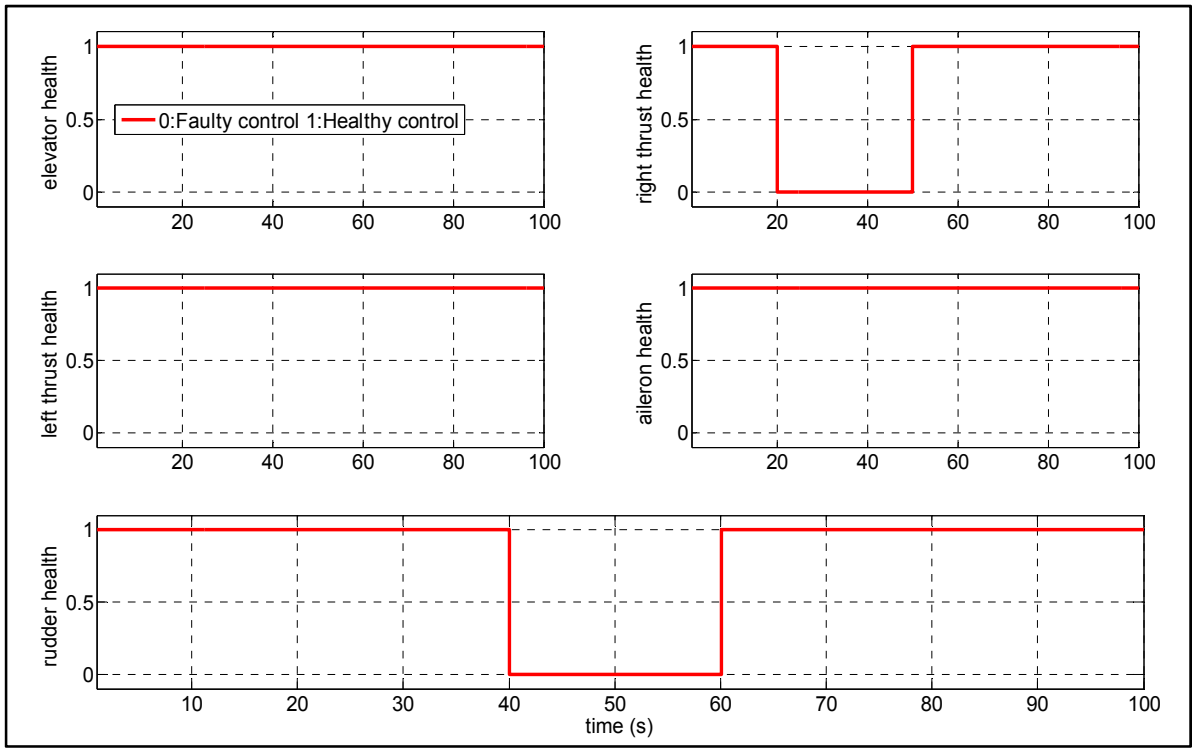

Figure 5.11 Fault detection and isolation

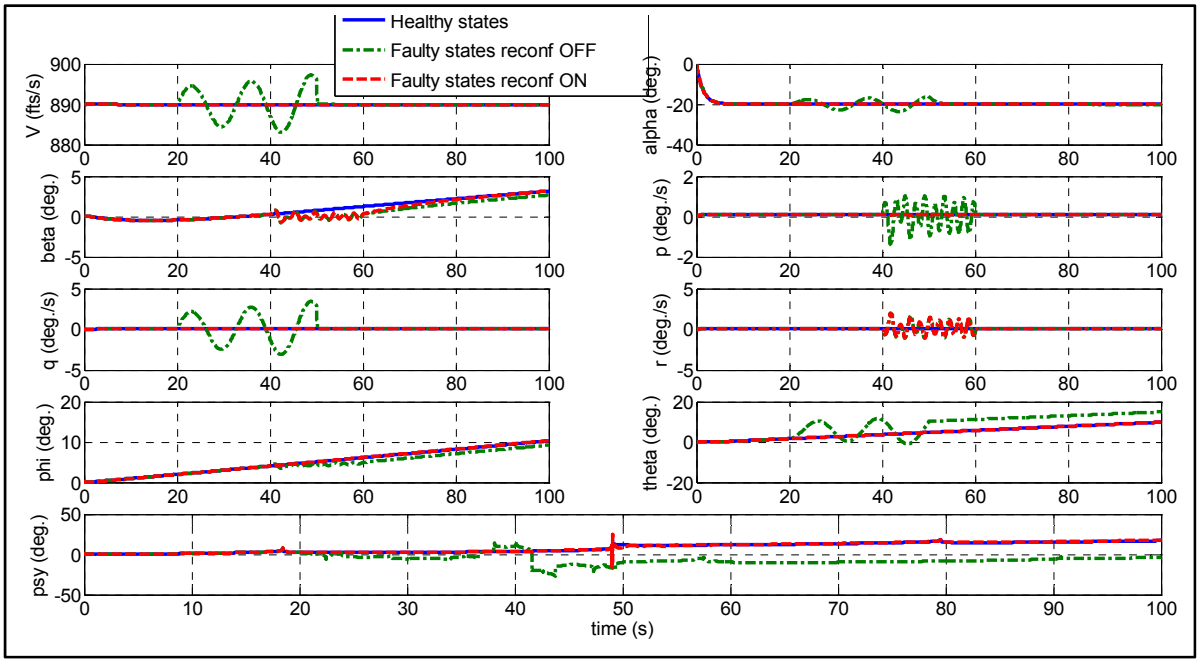

Figure 5.12 State vector variables

Figure 5.13 illustrates the time history of the control surfaces in both healthy and faulty cases. When the right thrust receives the input control δ_{RTh}, it gets stuck $\left(\delta_{RTh_f}(t) = 400 \text{ lbs.}\right)$ between t = 20 s and t = 50 s according to the fault scenarios used in the simulation. When the rudder receives the order δ_r, the time response shows oscillations of about zero $\left(\delta_{r_f}(t)\right)$ between t = 40 s and t = 60 s, according to the fault scenario.

Using fault parameters and the sensors' measurements, the proposed controller reconfigures the remaining healthy actuators (elevator δ_e, aileron δ_a and left thrust δ_{LTh}) online to compensate for the faulty actuators, right thrust $\delta_{RTh_f}(t)$ and rudder $\delta_{r_f}(t)$. As shown, the proposed reconfigurable flight controller works effectively without chattering, and within the operational control deflections limit of the B767 aircraft even though there may be some abrupt actuator faults.

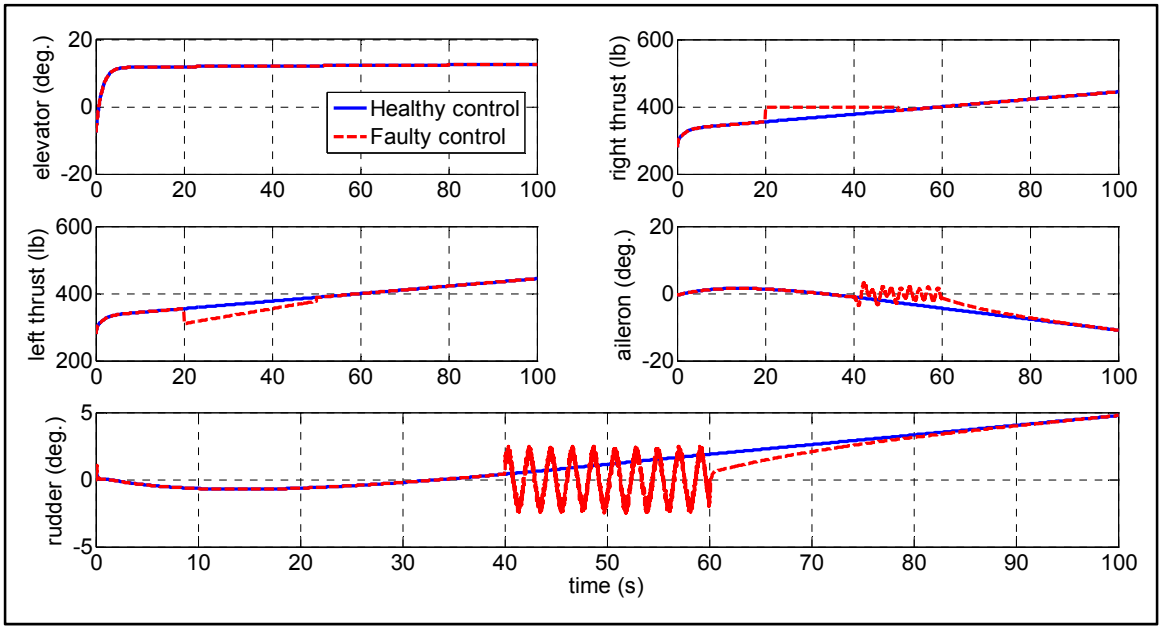

Figure 5.13 Control action

Figure 5.14 illustrates the reconstructed deflection of the failed actuators using the geometric approach technique. It can be seen that the faulty actuator reconstructions $\hat{\delta}_{RTh_f}(t)$ and $\hat{\delta}_{r_f}(t)$ are close to the values of real deflections $\delta_{RTh_f}(t)$ and $\delta_{r_f}(t)$.

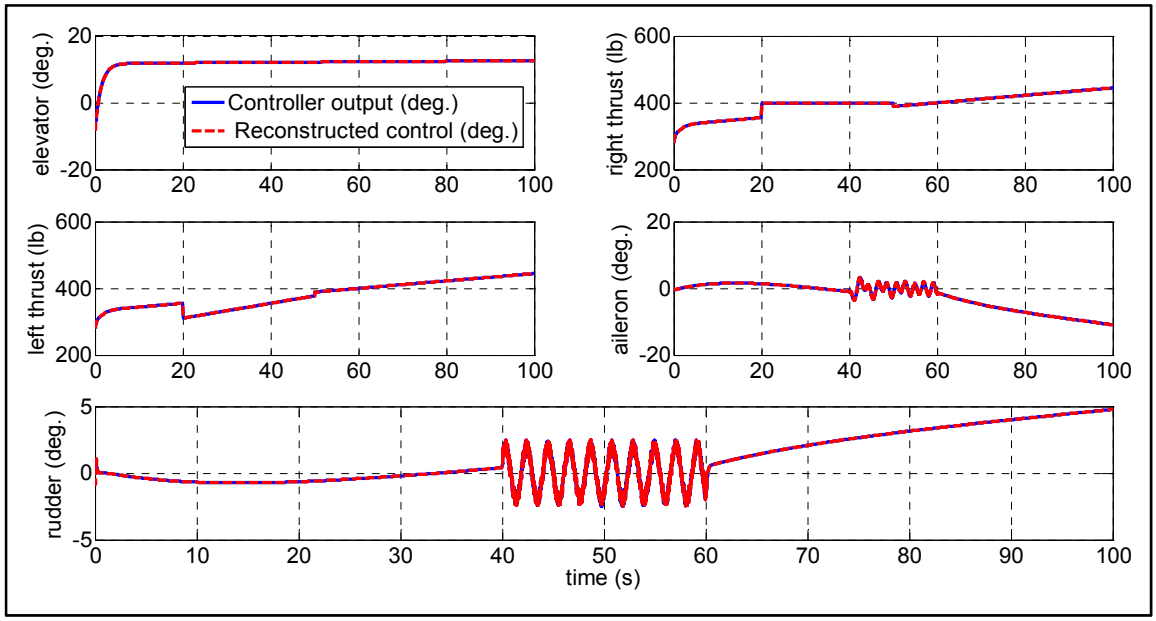

Figure 5.14 Control reconstruction: Fault diagnosis

As shown in Figure 5.15, which represents the associated fault reconstruction errors, the estimation errors are almost zero, and even the failure inputs are variable and stochastic. These results show that the proposed fault reconstruction system maintains a high precision throughout the evolution of the fault inputs.

Figure 5.16 illustrates the aircraft's northeast path trajectory, in both cases when the controller is based on a conventional technique, and when it is used with the proposed reconfiguration technique. In the first case, the multiple faults degrade the tracking error. This result shows that the fault parameters contribute to enhancing the system behavior against such abrupt faults. We should note that redundancy is very important in such controllers. Indeed, it minimizes the tracking error more pronounced, and provides better performances by compensating for fault effects using the remaining healthy redundant

actuators. This provides aerodynamic redundancy to the existing actuators, and the compensation effect is more accurate.

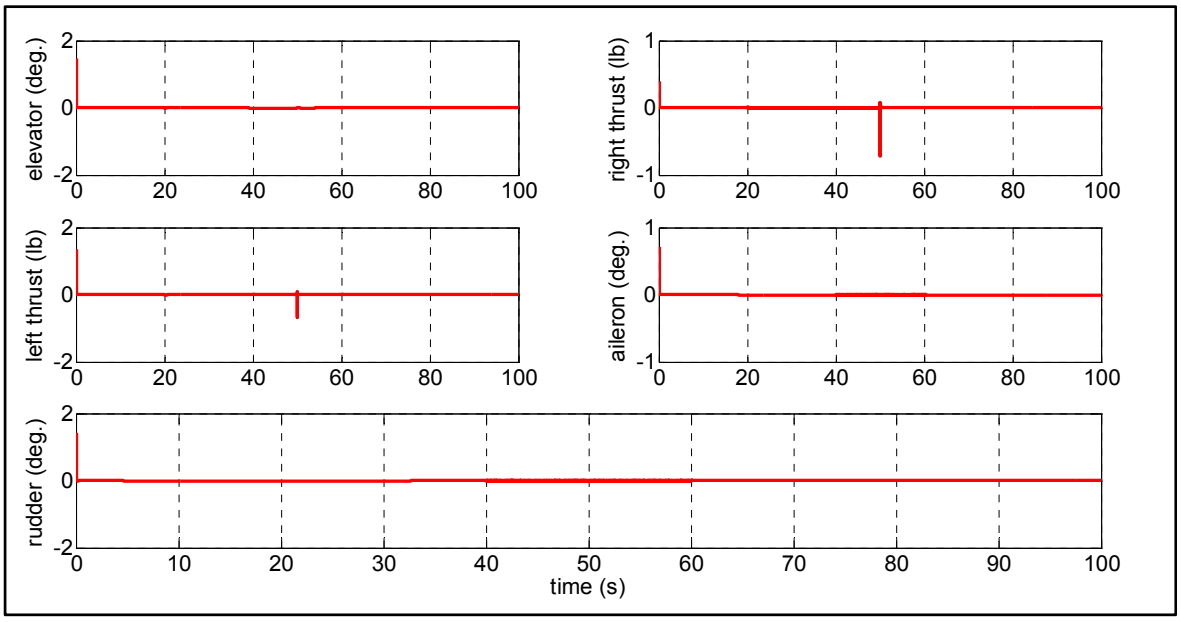

Figure 5.15 Geometric reconstruction error: FDD performance

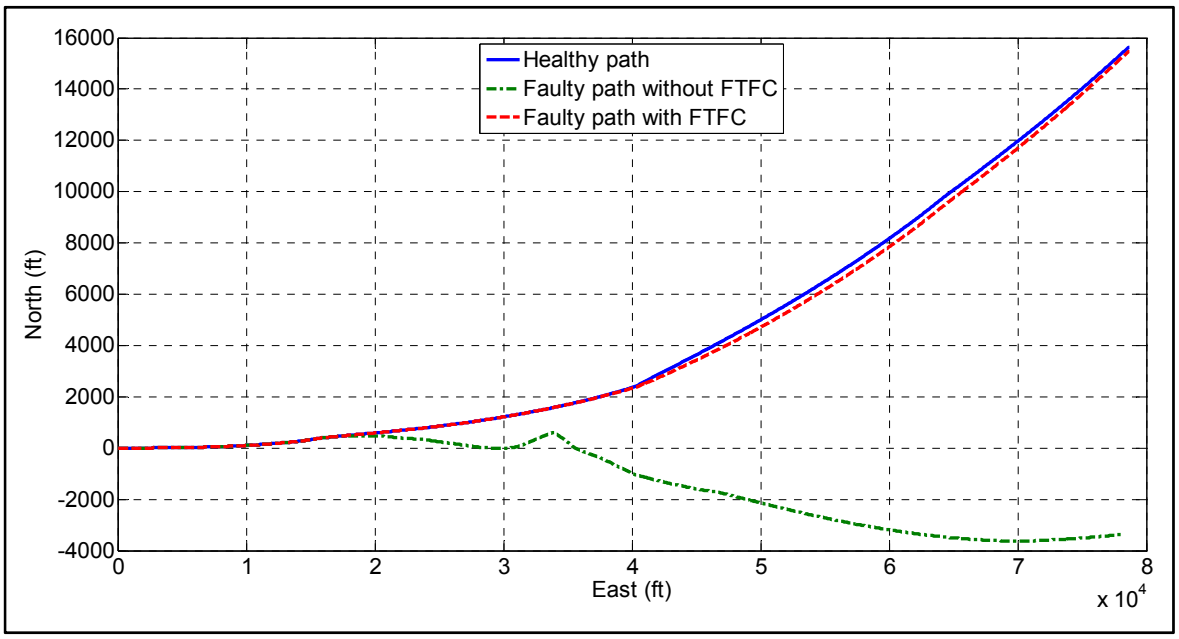

Figure 5.16 Aircraft north east tracking path

Figure 5.17 shows the Boeing 737 aircraft behaviour and tracking trajectory on the FlightGear simulator GUI and a 3D animation at t = 90 s.

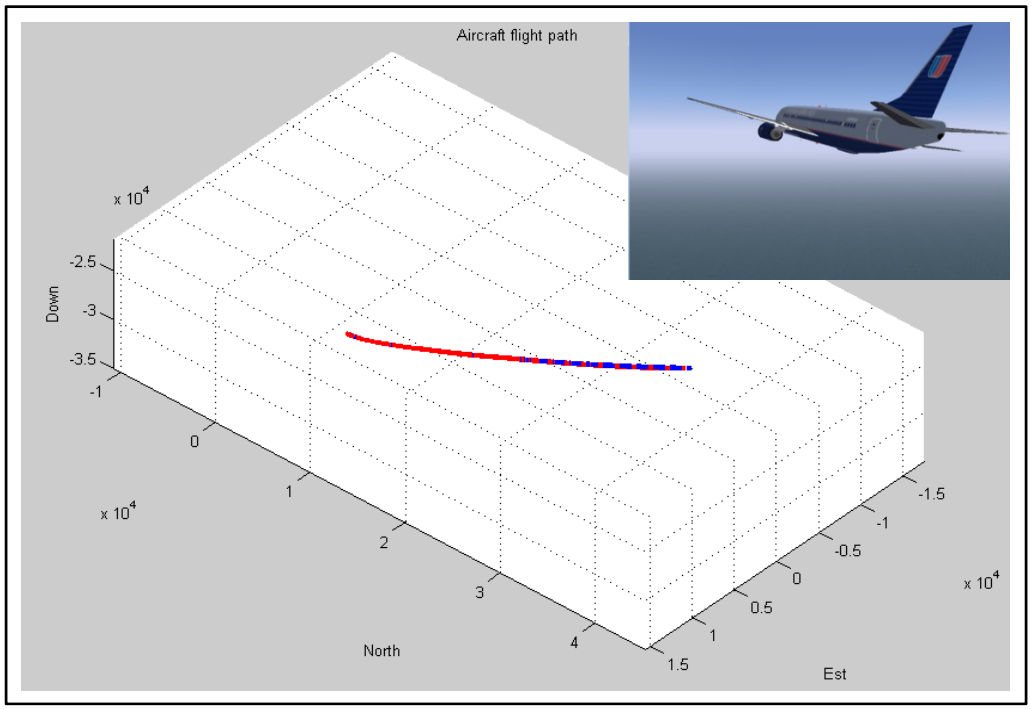

Figure 5.17 Screenshot of FlightGear simulator and 3D animation at t = 90 s

5.6 Conclusion

In this paper, a fault-tolerant flight control system for the overall linear model of the Boeing 767 aircraft was designed. A geometric approach for fault reconstruction was used to design the FDD process to detect, isolate and identify actuator faults in real time. Because the number of outputs exceeds the number of inputs, a multi-projector, as well as a fusion algorithm, were required to better carry out the fault reconstruction. Then, using the generated fault parameters, a reconfigurable flight control law based on the sliding mode technique was designed. This reconfiguration compensates for the faults online to preserve aircraft stability and maintain acceptable flight path tracking performances.

Matlab®/Simulink® simulation runs were performed to prove the effectiveness of the proposed controller on the lateral and the longitudinal linear dynamic models of the Boeing

767 aircraft. Using the proposed controller outputs, the system could track the desired input either with or without abrupt actuator faults.

Since the redundant actuators provide aerodynamic redundancy to the existing actuators, the fault effect was better compensated. Indeed, simulation results showed that the tracking error was better minimized and the performances were better maintained by compensating for the right thrust fault effect using the remaining healthy left thrust. The results obtained are expected to be further enhanced by adding a redundant rudder actuator or by segmenting the rudder itself.

For the FDD process, the results showed that actuators' faults were instantly detected as soon as they occurred. In addition, they were accurately diagnosed. Indeed, the faulty actuators were accurately isolated and their faults' behaviors were accurately identified.

For the controller outputs, the results showed the effectiveness and robustness of the reconfigurable sliding mode technique used for the designed controller. In spite of the double fault that occurred, the aircraft stability was preserved and acceptable performances were maintained without exceeding the mechanical and rate aircraft deflections limits.

CONCLUSION

The objective of the work presented in this research was the design of a fault-tolerant flight control system against multiple simultaneous actuator control signal failures caused by cosmic ray. In addition to actuators failures, the designed fault-tolerant controller must deal simultaneously with modeling uncertainties and external distributions.

In order to satisfactory achieve this objective, some background was required and several techniques were developed and combined, in order to online execute two tasks. First, actuator failures that occurred must be faster detected and diagnosed. In this thesis, this task is ensured using the geometric approach-based FDD process. Second, the fault-tolerant controller must readapt to the faulty situation so that the stability will be preserved and desired tracking error will be maintained, despite the detrimental effects of the actuator failures on the aircraft dynamics and tracking. In this thesis, this task is ensured using a reconfigurable sliding mode technique. Furthermore, the performance of the proposed fault-tolerant controller in terms of interaction between the FDD process and the RFC system must be respected. The occurred faults must be identified and diagnosed in a very small delay.

The robustness of the designed fault-tolerant controller has been checked using a single flight conditions for a linear aircraft model as well as an entire flight envelope for a nonlinear aircraft model were used. In addition, the designed fault-tolerant controller has proved its usefulness in real-world situations. For that, firstly the actuator failures used include a large class of faults with unknown time of occurrence, unknown failure patterns and unknown failed actuators. These types of faults include as well those caused by cosmic rays which were modeled in this work for the first time. Secondly, the flight environment was chosen under external disturbances, which have been simulated by including wind turbulence. Thirdly, sensors' measurements were corrupted using a zero-mean Gaussian noise, which corresponds to typical specifications of low-cost sensors.

Only two assumptions were made throughout this work. The first assumption is the availability of redundant actuators. Indeed, in case when the faulty actuator will not be capable to accommodate the fault by itself, redundant actuators are required to contribute for preserving the aircraft stability. This assumption is satisfied in most recent civil and military aircrafts. The second assumption is the existence of the aircraft inverse dynamics, to be able to compute the tolerant flight controller law. Also, this assumption is satisfied in most physical systems.

In this thesis, detecting and diagnosing multiple simultaneous actuator faults is designed using an efficient FDD process developed using the geometric approach for fault reconstruction. This technique has proved its reliability to handle three simultaneous actuator failures. Once a fault is detected, isolated and identified, the computed faulty parameters are appropriately used to online reconfigure the fault-tolerant controller. The reconfigurable fault-tolerant controller designed is based on the sliding mode technique. This technique divides the dynamic behavior of the system through control which let it simple to implement. Based on the faulty parameters given by the geometric approach-based FDD, the RSMC online compensates for the occurrence faults. The RSMC has proven its reliability in such situations because it can handle significant modeling uncertainties and external disturbance without losing desired performances.

Furthermore, the designed fault-tolerant controller has proved its performance in terms of interaction between the FDD process and the RSMC system, by refreshing simulations at twice of the speed of a real fly-by-wire flight control system. Using this speed, the FDD tasks were completed in less than 300 ms, which can be considered as acceptable regarding to the time available constraint existing in the real fly-by-wire flight control system which is usually less than 300 ms.

In summary, performed simulation results reported in this thesis show that the designed fault-tolerant controller gives satisfactory results in terms of achieving the major objective defined a priori for this research work expectations. It has accommodated three unknown

simultaneous faults taken from a large failure class and has preserved stability for the faulty system in both cases of linear and nonlinear aircraft models in the presence of external disturbances and noise measurements, while providing a fast reflex in order to preserve the stability and maintain the trajectory tracking in faulty situations. Although, this work has not been able to be experimentally validated, the simulation environments were very close to realistic flight environments.

RECOMMENDATIONS AND FUTURE WORK

At the end of this thesis here are some recommendations and suggested future works that can expand the results presented in this study.

Recommendations

In this thesis, the design of the reconfigurable flight controller was based on the SMC technique which uses the inverse of the input matrix $g(x)$ to compute the required control law. However, this inverse is not usually easy to compute accurately. Especially if the state vector size is much greater than the control vector size. This problem can be solved by using the multiple time scale approximation approach (Holzapfel et Sachs, 2004). This approach assumes that there are significant differences between the time scales of various system variables. It is considered that the state variables α, β and φ have a slow dynamics, because they are not affected immediately by the control surfaces. However, the dynamics of the state variables p, q and r is fast, because the effect of the control surfaces on these variables is very large. Several works have been done based on this approach. However, they were applied only on the non-linear dynamic inverse (NDI), and no one has applied it on the SMC technique. As part of this thesis, this approach was designed successfully on a nonlinear model of F16 by using the SMC technique. However, only the case of single fault was tested. It would be very interesting to expand the study on the case of simultaneous faults.

Sensor measurements are considered always available when designing the several controllers proposed in this thesis. It will be interesting to investigate the case of loss of one sensor or more. In such situation, the required variable must be predicted at each time. The Kalman filter (Kalman, 1960) seems to be the best candidate in such situation. In addition to be able to estimate noisy measurements, it is also able to predict some missing data.

Throughout this thesis, the environment of the performed simulations was close to realistic flight situations. Indeed, simulations were performed by considering sensor noise, process

noise, wind gusts, time constraint and mechanical actuator limits. However, the actuator rate limits were not taken into consideration. It will be interesting to investigate the effect of such limits on the performance of the designed controllers. It will be easy to model this limit by integrating a first order transfer function in the actuator design for example. The rate limits can be considered by varying the time constant parameter of the transfer function.

Another topic which will be interesting to investigate is the high order SMC technique (Fridman, Davila et Levant, 2011). In this thesis, this technique has only cited in relation to its importance to minimize the chattering phenomenon, and no analysis was done on the effect of this technique on the proposed controllers' performance.

Finally, in this thesis, controller performances are always defined comparing to healthy aircraft performance. However, in some situations, it may not be able to restore completely the healthy aircraft. It can be able to restore only a part of the healthy aircraft so called degraded performances (Zhang et Jiang, 2001). This is the case for example when a significant failure occurred on the aircraft. Again, it will be very interesting to consider such situation in the design of the proposed controllers.

Future work

The fault-tolerant control systems designed in this thesis must prove their usefulness in real flight situations. Therefore, the proposed control systems must be tested in real aircrafts. In GRÉPCI laboratory of the Department of Electrical Engineering, the quadrotor and the hexarotor platforms are about to be developed. There is another platform which was developed a few years ago. It is a fixed wing UAV called MOUETS and was designed throughout a master thesis (Landry, 2012). In the near future, the proposed algorithms can be implemented on these platforms.

Another way to test the proposed algorithms in real flight-situation will be the 6 DOF flight simulator implemented in LASSENA laboratory at the Department of Electrical Engineering.

Although the FlightGear software was used in this thesis to visualize the behavior and tracking trajectory of the aircraft on a graphical user interface (GUI), it will be also better to validate the developed algorithms in this flight simulator.

APPENDIX I

AERODYNAMIC COEFFICIENTS MODELLING FOR THE 6DOF AIRCRAFT

Equations for modelling aerodynamic parameters adapted from (McLean, 1990), (Nelson, 1998), (Etkin et Reid, 1996) and (Bates et Hagström, 2007) are:

$C_L = \frac{F_L}{\overline{q} S_w}$		$C_{n_\beta} = \frac{\partial C_n}{\partial \beta}$	(rad^{-1})	$C_{l_\beta} = \frac{\partial C_l}{\partial \beta}$	(rad^{-1})
$C_{L_M} = \frac{\partial C_L}{\partial Mac}$		$C_{D_M} = \frac{\partial C_D}{\partial Mac}$		$C_{l_p} = \frac{\partial C_l}{\partial \left({pb}/{2V_{x_0}} \right)}$	(rad^{-1})
$C_{L_{\delta_e}} = \frac{\partial C_L}{\partial \delta_e}$	(rad^{-1})	$C_{D_{\delta_e}} = \frac{\partial C_D}{\partial \delta_e}$	(rad^{-1})	$C_{l_r} = \frac{\partial C_l}{\partial \left({rb}/{2V_{x_0}} \right)}$	(rad^{-1})
$C_D = \frac{F_D}{\overline{q} S_w}$		$C_m = \frac{M}{\overline{q} S_w \overline{c}}$		$C_{n_p} = \frac{\partial C_n}{\partial \left({pb}/{2V_{x_0}} \right)}$	(rad^{-1})
$C_{D_\alpha} = \frac{\partial C_D}{\partial \alpha}$	(rad^{-1})	$C_{m_\alpha} = \frac{\partial C_m}{\partial \alpha}$	(rad^{-1})	$C_{m_M} = \frac{\partial C_m}{\partial Mac}$	
$C_{L_\alpha} = \frac{\partial C_L}{\partial \alpha}$	(rad^{-1})	$C_y = \frac{F_Y}{\overline{q} S_w}$		$C_{m_q} = \frac{\partial C_m}{\partial \left({q\bar{c}}/{2V_{x_0}} \right)}$	(rad^{-1})
$C_{l_{\delta_a}} = \frac{\partial C_l}{\partial \delta_a}$	(rad^{-1})	$C_{y_\beta} = \frac{\partial C_y}{\partial \beta}$	(rad^{-1})	$C_{n_{\delta_a}} = \frac{\partial C_n}{\partial \delta_a}$	(rad^{-1})
$C_{l_{\delta_r}} = \frac{\partial C_l}{\partial \delta_r}$	(rad^{-1})	$C_{y_{\delta_r}} = \frac{\partial C_y}{\partial \delta_r}$	(rad^{-1})	$C_{n_{\delta_r}} = \frac{\partial C_n}{\partial \delta_r}$	(rad^{-1})
$C_n = \frac{N}{\overline{q} S_w b}$		$C_l = \frac{L}{\overline{q} S_w b}$			

Equations for modelling longitudinal aerodynamic parameters:

$X_u = \frac{-(C_{D_u} + 2C_{D_0})\overline{q}S_w}{mV_{x_0}}$	(s^{-1})	$M_q = C_{m_q}\frac{\overline{q}S_w\overline{c}^2}{2I_yV_{x_0}}$	(s^{-1})
$Z_u = \frac{-(C_{L_u} + 2C_{L_0})\overline{q}S_w}{mV_{x_0}}$	(s^{-1})	$X_w = \frac{-(C_{D_\alpha} + C_{L_0})\overline{q}S_w}{mV_{x_0}}$	(s^{-1})
$Z_w = \frac{-(C_{L_\alpha} + C_{D_0})\overline{q}S_w}{mV_{x_0}}$	(s^{-1})	$Z_{\dot{w}} = -C_{Z_{\dot{\alpha}}}\frac{\overline{q}S_w\overline{c}}{2m{V_{x_0}}^2}$	
$Z_\alpha = V_{x_0}Z_w$	(ft/s^2) or (m/s^2)	$Z_{\dot{\alpha}} = V_{x_0}Z_{\dot{w}}$	(ft/s) or (m/s)
$Z_q = -C_{Z_q}\frac{\overline{q}S_w\overline{c}}{2mV_{x_0}}$	(ft/s) or (m/s)	$Z_{\delta_e} = -C_{Z_{\delta_e}}\frac{\overline{q}S_w}{m}$	(ft/s^2) or (m/s^2)
$M_u = C_{m_u}\frac{\overline{q}S_w\overline{c}}{I_yV_{x_0}}$	$(ft\text{-}s)^{-1}$ or $(m\text{-}s)^{-1}$	$M_{\dot{w}} = C_{m_{\dot{\alpha}}}\frac{\overline{q}S_w\overline{c}^2}{2I_y{V_{x_0}}^2}$	(ft^{-1})
$M_w = C_{m_\alpha}\frac{\overline{q}S_w\overline{c}}{I_yV_{x_0}}$	$(ft\text{-}s)^{-1}$ or $(m\text{-}s)^{-1}$	$M_{\dot{\alpha}} = V_{x_0}M_{\dot{w}}$	(s^{-1})
$M_\alpha = V_{x_0}M_w$	(s^{-2})	$M_{\delta_e} = C_{m_{\delta_e}}\frac{\overline{q}S_w\overline{c}}{I_y}$	(s^{-2})

Equations for modelling lateral aerodynamic parameters:

$Y_\beta = \frac{\overline{q}S_wC_{y_\beta}}{m}$	(ft/s^2) or (m/s^2)	$N_r = \frac{\overline{q}S_wb^2C_{n_r}}{2mV_{x_0}}$	(s^{-1})
$Y_p = \frac{\overline{q}S_wbC_{y_p}}{2mV_{x_0}}$	(ft/s) or (m/s)	$Y_{\delta_r} = \frac{\overline{q}S_wC_{y_{\delta_r}}}{m}$	(ft/s^2) or (m/s^2)
$Y_r = \frac{\overline{q}S_wbC_{y_r}}{2mV_{x_0}}$	(ft/s) or (m/s)	$N_{\delta_r} = \frac{\overline{q}S_wbC_{n_{\delta_r}}}{I_z}$	(s^{-2})
$Y_{\delta_a} = \frac{\overline{q}S_wC_{y_{\delta_a}}}{m}$	(ft/s^2) or (m/s^2)	$N_{\delta_r} = \frac{\overline{q}S_wbC_{l_{\delta_r}}}{I_x}$	(s^{-2})
$N_{\delta_a} = \frac{\overline{q}S_wbC_{n_{\delta_a}}}{I_z}$	(s^{-2})	$L_\beta = \frac{\overline{q}S_wbC_{l_\beta}}{I_x}$	(s^{-2})
$L_{\delta_a} = \frac{\overline{q}S_wbC_{l_{\delta_a}}}{I_x}$	(s^{-2})	$L_p = \frac{\overline{q}S_wb^2C_{l_p}}{2I_xV_{x_0}}$	(s^{-1})
$N_\beta = \frac{\overline{q}S_wbC_{n_\beta}}{I_z}$	(s^{-2})	$L_r = \frac{\overline{q}S_wb^2C_{l_r}}{2mV_{x_0}}$	(s^{-1})
$N_p = \frac{\overline{q}S_wb^2C_{n_p}}{2I_xV_{x_0}}$	(s^{-1})	$C_{D_u} = Mac\frac{\partial C_D}{\partial Mac}$	
$C_{m_u} = Mac\frac{\partial C_m}{\partial Mac}$	$C_{Z_q} = -C_{L_q} = -\frac{\partial C_L}{\partial q}$	$C_{L_u} = Mac\frac{\partial C_L}{\partial Mac}$	

Inertias equations

$I_1 = -\frac{I_x(I_z-I_y)+I_{xy}^2}{I_xI_z-I_{xz}^2}$, $I_2 = \frac{I_{xz}(I_x-I_y+I_z)}{I_xI_z-I_{xz}^2}$, $I_3 = \frac{I_z}{I_xI_z-I_{xz}^2}$

$I_4 = \frac{I_{xz}}{I_xI_z-I_{xz}^2}$, $I_5 = \frac{I_z-I_x}{I_y}$, $I_6 = \frac{I_{xz}}{I_y}$

$I_7 = \frac{1}{I_y}$, $I_8 = \frac{I_x(I_x-I_y)+I_{xy}^2}{I_xI_z-I_{xz}^2}$, $I_9 = \frac{I_x}{I_xI_z-I_{xz}^2}$

where:

b: Wing Span (ft)

$\overline{c}$: Mean chord (ft)

Mac: Flight Mach number

m: Mass of the aircraft (kg)

I_x, I_y, I_z,: Rolling, pitching and yawing moments of inertia (slug-ft^2)

I_{xz}: Inertia product (slug-ft^2)

$\overline{q}$: Dynamic pressure (lb/ft^2)

S_w: Wing planform area (ft^2)

$V = \left[V_x\ V_y\ V_z\right]^T$: Forward velocity (ft/s)

p, q, r: Angular velocities (rad/s)

V_{x_0}: Reference flight speed in the x direction (ft/s)

F_L, F_D, M: Lift and drag forces (N)

M: Pitching moment (N.m)

F_Y: Aerodynamic force in the y direction (N)

C_y: Coefficients inducing a force along the y axis of the aircraft frame

C_{y_β}, $C_{y_{\delta_r}}$: C_y coefficient derivative with respect to β, δ_r

C_L, C_D: Lift and drag coefficients

C_{L_0}, C_{D_0}: Lift and drag reference coefficients

C_{L_u}, C_{L_q}, C_{L_M}, C_{L_α}, $C_{L_{i_h}}$, $C_{L_{\delta_e}}$: Lift coefficient derivative with respect to V_x, q, Mac, α, i_h, δ_e

C_{D_u}, C_{D_α}, C_{D_M}, $C_{D_{i_h}}$, $C_{D_{\delta_e}}$: Drag coefficient derivative with respect to V_x, α, Mac, i_h, δ_e

C_l, C_m, C_n: Rolling, pitching and yawing moments coefficients

C_{l_β}, C_{l_p}, C_{l_r}, $C_{l_{\delta_a}}$, $C_{l_{\delta_r}}$: Rolling moment coefficient derivative with respect to β, p, r, δ_a, δ_r

C_{m_M}, C_{m_q}, C_{m_u}, C_{m_α}: Pitching moment coefficient derivative with respect to Mac, q, V_x, α

C_{n_β}, C_{n_p}, $C_{n_{\delta_a}}$, $C_{n_{\delta_r}}$: Yawing moment coefficient derivative with respect to β, p, δ_a, δ_r

APPENDIX II

AERODYNAMIC PARAMETERS FOR THE AFTI-F16

Flight conditions of the AFTI/F-16 (Barfield et D'Azzo, 1983)

Mac (flight Mach number): 0.6

h (altitude) :30 000 (ft)

$\overline{q}$ (dynamics pressure): 158.81 (lb/ft^2)

V_T (trim velocity): 596.91 (ft/s)

α_T (trim angle of attack): 4.705 (deg)

S_w (wing reference area): 300 (ft^2)

$\overline{c}$ (wing mean aerodynamic chord): 11.32 (ft)

b (wing span): 30 (ft)

W (weight): 21 018 (lb)

I_x (x direction inertia): 10 033.4 (slug-ft^2)

I_y (y direction inertia): 10 876.3 (slug-ft^2)

I_z (z direction inertia): 10 033.4 (slug-ft^2)

I_{xz} (xz inertia): 282.132 (slug-ft^2)

Aerodynamic coefficients of the AFTI/F-16 (Barfield et D'Azzo, 1983)

$C_L = 0.439013$		$C_m = 0$		$C_D = 0.044151$	
$C_{L_\alpha} = 0.073559$	(rad^{-1})	$C_{m_\alpha} = 0.004356$	(rad^{-1})	$C_{D_\alpha} = 0.008210$	(rad^{-1})
$C_{l_{\delta_e}} = 0.009473$	(rad^{-1})	$C_{m_{\delta_e}} = -0.010229$	(rad^{-1})	$C_{D_{\delta_e}} = 0.000019$	(rad^{-1})
$C_{l_{\delta_f}} = 0.015850$	(rad^{-1})	$C_{m_{\delta_f}} = -0.000383$	(rad^{-1})	$C_{D_{\delta_f}} = 0.001808$	(rad^{-1})

$C_{L_q} = 2.437286$	(rad^{-1})	$C_{m_q} = -2.859448$	(rad^{-1})		
$C_{L_{\dot{\alpha}}} = -1.029896$	(rad^{-1})	$C_{m_{\dot{\alpha}}} = -0.747194$	(rad^{-1})		
$C_{L_{V_x}} = 0.000158$	(ft^{-1}s)	$C_{m_{V_x}} = -0.000106$	(ft^{-1}s)	$C_{D_{V_x}} = 0.000050$	(ft^{-1}s)
$C_{y_p} = 0.132102$	(rad^{-1})	$C_{n_p} = -0.013813$	(rad^{-1})	$C_{l_p} = -0.243246$	(rad^{-1})
$C_{y_\beta} = -0.021995$	(deg^{-1})	$C_{n_\beta} = 0.001972$	(deg^{-1})	$C_{l_\beta} = -0.002209$	(deg^{-1})
$C_{y_{\delta_r}}$ =0.003021	(deg^{-1})	$C_{n_{\delta_r}} = -0.001520$	(deg^{-1})	$C_{l_{\delta_r}} = 0.000364$	(deg^{-1})
$C_{y_r} = 0.536904$	(rad^{-1})	$C_{n_r} = -0.484330$	(rad^{-1})	$C_{l_r} = 0.071941$	(rad^{-1})
$C_{y_{\delta_a}}$ =0.000051	(deg^{-1})	$C_{n_{\delta_a}} = 0.000035$	(deg^{-1})	$C_{l_{\delta_a}} = -0.002141$	(deg^{-1})
$C_{y_{DT}}$ =0.002059	(deg^{-1})	$C_{n_{DT}} = -0.000940$	(deg^{-1})	$C_{l_{DT}} = -0.001742$	(deg^{-1})
$C_{y_{\delta_c}} = 0.001047$	(deg^{-1})	$C_{n_{\delta_c}} = 0.001121$	(deg^{-1})	$C_{l_{\delta_c}} = 0.000138$	(deg^{-1})

Lateral aerodynamic parameters of the AFTI/F-16

Lateral motion					
$\boldsymbol{Y_\varphi}$	0.05376	$\boldsymbol{L_\beta}$	-19.2246	$\boldsymbol{N_\beta}$	-0.998322
$\boldsymbol{Y_\beta}$	-0.154099	$\boldsymbol{L_p}$	-0.893601	$\boldsymbol{N_p}$	2.29583
$\boldsymbol{Y_p}$	0.082387	$\boldsymbol{L_r}$	0.318845	$\boldsymbol{N_r}$	-0.000888
$\boldsymbol{Y_r}$	-0.278676	$\boldsymbol{L'_{\delta_{DT}}}$	-13.5832	$\boldsymbol{N'_{\delta_{DT}}}$	-1.50547
$\boldsymbol{Y'_{\delta_{DT}}}$	0.014398	$\boldsymbol{L'_{\delta_a}}$	-17.4468	$\boldsymbol{N'_{\delta_a}}$	-0.2684403
$\boldsymbol{Y'_{\delta_a}}$	0.000357	$\boldsymbol{L'_{\delta_c}}$	0.414519	$\boldsymbol{N'_{\delta_c}}$	1.51008
$\boldsymbol{Y'_{\delta_c}}$	0.007335	$\boldsymbol{L'_{\delta_r}}$	3.92325	$\boldsymbol{N'_{\delta_r}}$	-1.96651
$\boldsymbol{Y'_{\delta_r}}$	0.021165				

Longitudinal aerodynamic parameters of the AFTI/F-16

Longitudinal motion					
X_{θ}	-32.0915	Z_{θ}	-0.004425	M_{θ}	0.000313
X_{u}	0.005142	Z_{u}	-0.000109	M_{u}	-0.000337
X_{α}	23.0402	Z_{α}	-0.526422	M_{α}	2.52708
X_{q}	-48.8785	Z_{q}	0.997184	M_{q}	-0.341902
X'_{δ_e}	3.17035	Z'_{δ_e}	-0.066156	M'_{δ_e}	-5.86214
X'_{δ_f}	-2.09855	Z'_{δ_f}	-0.111711	M'_{δ_f}	-0.211773

Mechanical limits of the AFTI/F-16

Control surface	**Rate limit deg/sec**	**Lower mechanical stop, deg**	**Upper mechanical Stop, deg**
Elevators	60	-25	+25
Flaperons	52	-23	+20
Canards	108	-27	+27
Rudder	120	-30	+30

APPENDIX III

AERODYNAMICS PARAMETERS FOR THE STANDARD 6DOF AIRCRAFT

Flight conditions of the standard 6DOF aircraft (Roskam, 2003):

h (altitude): 20 000 (ft)

$\overline{q}$ (dynamics pressure): 287.2 (lb/ft^2)

S_w (wing reference area): 5500 (ft^2)

$\overline{c}$ (wing mean aerodynamic chord): 27.3 (ft)

b (wing span): 196 (ft)

m (mass): 636 636 (lbs)

I_x (x direction inertia): 18200000 (slug-ft^2)

I_y (y direction inertia): 33100000 (slug-ft^2)

I_z (z direction inertia): 49700000 (slug-ft^2)

I_{xz} (xz inertia): 970000 (slug-ft^2)

T (Thrust engine):100 000 (N)

$C_{L_0} = 0.21$		$C_{m_0} = 0$		$C_{D_0} = 0.0164$	
$C_{L_{ih}} = 0.7$	(rad^{-1})	$C_{m_\alpha} = -1$	(rad^{-1})	$C_{D_{ih}} = 0$	(rad^{-1})
$C_{l_{\delta_e}} = 0.32$	(rad^{-1})	$C_{m_{\delta_e}} = -1.3$	(rad^{-1})	$C_{D_{\delta_e}} = 0$	(rad^{-1})
$C_{l_{\delta_a}} = 0.013$	(rad^{-1})	$C_{m_{ih}} = -2.7$	(rad^{-1})	$C_{D_\alpha} = 0.2$	(rad^{-1})
$C_{y_\beta} = -0.9$	(deg^{-1})	$C_{n_\beta} = 0.16$	(deg^{-1})	$C_{l_\beta} = -0.16$	(deg^{-1})
$C_{y_{\delta_r}}$ =0.12	(deg^{-1})	$C_{n_{\delta_r}} = -0.1$	(deg^{-1})	$C_{l_{\delta_r}} = 0.008$	(deg^{-1})
$C_{y_{\delta_a}}$ =0	(deg^{-1})	$C_{n_{\delta_a}} = 0.0018$	(deg^{-1})	$C_{l_\alpha} = 4.4$	(deg^{-1})

APPENDIX IV

AERODYNAMICS PARAMETERS FOR THE B767 AIRCRAFT AND THE GEOMETRIC APPROACH RESULTS

According to the flight conditions illustrated in Table 5.2, matrices A and B in (5.20) are described as follows (Garvin, 1988):
For the lateral model:

$$A_{lat} = \begin{pmatrix} -0.1245 & 0.0350 & 0.0414 & -0.9962 \\ -15.2138 & -2.0587 & 0.0032 & 0.6458 \\ 0 & 1 & 0 & 0.0357 \\ 1.6447 & -0.0447 & -0.0022 & -0.1416 \end{pmatrix} \quad \text{(A IV–1)}$$

$$B_{lat} = \begin{pmatrix} -0.0049 & 0.0237 \\ -4.0379 & 0.9613 \\ 0 & 0 \\ -0.0568 & -1.2168 \end{pmatrix} \quad \text{(A IV–2)}$$

For the longitudinal model:

$$A_{long} = \begin{pmatrix} -0.0168 & 0.1121 & 0.0003 & -0.5608 \\ -0.0164 & -0.7771 & 0.9945 & 0.0015 \\ -0.0417 & -3.6595 & -0.9544 & 0 \\ 0 & 0 & 1 & 0 \end{pmatrix} \quad \text{(A IV–3)}$$

$$B_{long} = \begin{pmatrix} -0.0243 & 0.03595 & 0.01595 \\ -0.0634 & -0.00015 & -0.00035 \\ -3.6942 & 0.01115 & 0.01315 \\ 0 & 0.01 & -0.01 \end{pmatrix} \quad \text{(A IV–4)}$$

Possible sets of outputs and their matching projectors
and sub-manifold surfaces for the lateral model

Possible outputs set	**Matching projectors**	**Sub-manifold surfaces**
$\boldsymbol{y_{21}} = \begin{pmatrix} \boldsymbol{\beta} \\ \boldsymbol{p} \end{pmatrix}$	$\begin{pmatrix} 0 & 0 & 0 & 0 \\ 0 & 0 & 0 & 0 \\ 0 & 0 & 1 & 0 \\ 54.5998 & -0.0803 & 0 & 1 \end{pmatrix}$	$S_b^{(\beta,p)} = \{x \in \mathbb{R}^4 : \beta = 0, p = 0\}$
$\boldsymbol{y_{22}} = \begin{pmatrix} \boldsymbol{\beta} \\ \boldsymbol{r} \end{pmatrix}$	$\begin{pmatrix} 0 & 0 & 0 & 0 \\ -679.7472 & 1 & 0 & -12.4496 \\ 0 & 0 & 1 & 0 \\ 0 & 0 & 0 & 0 \end{pmatrix}$	$S_b^{(\beta,r)} = \{x \in \mathbb{R}^4 : \beta = 0, r = 0\}$
$\boldsymbol{y_{23}} = \begin{pmatrix} \boldsymbol{p} \\ \boldsymbol{r} \end{pmatrix}$	$\begin{pmatrix} 1 & -0.0015 & 0 & 0.0183 \\ 0 & 0 & 0 & 0 \\ 0 & 0 & 1 & 0 \\ 0 & 0 & 0 & 0 \end{pmatrix}$	$S_b^{(p,r)} = \{x \in \mathbb{R}^4 : p = 0, r = 0\}$

Possible sets of outputs and their matching projectors
and sub-manifold surfaces for the longitudinal model

Possible outputs set	**Matching projectors**	**Sub-manifold surfaces**
$\mathbf{y_{31}} = \begin{pmatrix} \boldsymbol{V_x} \\ \boldsymbol{\alpha} \\ \boldsymbol{q} \end{pmatrix}$	$\begin{pmatrix} 0 & 0 & 0 & 0 \\ 0 & 0 & 0 & 0 \\ 0 & 0 & 0 & 0 \\ -6.0179 & -339.5382 & 5.8668 & 1 \end{pmatrix}$	$S_b^{(V_x,\alpha,q)} = \{x \in \mathbb{R}^4 : V_x = 0, \alpha = 0, q = 0\}$
$\mathbf{y_{32}} = \begin{pmatrix} \boldsymbol{V_x} \\ \boldsymbol{q} \\ \boldsymbol{\theta} \end{pmatrix}$	$\begin{pmatrix} 0 & 0 & 0 & 0 \\ 0 & 0 & 0 & 0 \\ -1.0258 & -57.8750 & 1 & 0.1705 \\ 0 & 0 & 0 & 0 \end{pmatrix}$	$S_b^{(V_x,q,\theta)} = \{x \in \mathbb{R}^4 : V_x = 0, q = 0, \theta = 0\}$
$\mathbf{y_{33}} = \begin{pmatrix} \boldsymbol{\alpha} \\ \boldsymbol{q} \\ \boldsymbol{\theta} \end{pmatrix}$	$\begin{pmatrix} 1 & 56.4210 & -0.9749 & -0.1662 \\ 0 & 0 & 0 & 0 \\ 0 & 0 & 0 & 0 \\ 0 & 0 & 0 & 0 \end{pmatrix}$	$S_b^{(\alpha,q,\theta)} = \{x \in \mathbb{R}^4 : \alpha = 0, q = 0, \theta = 0\}$

Possible sets of outputs and their matching inverse dynamics for the lateral model

Possible set	Matching inverse dynamics
$\boldsymbol{y_{21}} = \begin{pmatrix}\boldsymbol{\beta}\\ \boldsymbol{p}\end{pmatrix}$	$\begin{cases}\begin{pmatrix}\dot{\varphi}_{11}\\ \dot{r}_{11}\end{pmatrix} = \begin{pmatrix}0 & 1 & 0 & 0.0357\\ -3.9309 & 2.0316 & 2.2579 & -54.5857\end{pmatrix}\begin{pmatrix}\beta\\ p\\ \varphi\\ r\end{pmatrix} + \begin{pmatrix}0 & 0\\ -54.5997 & 0.0803\end{pmatrix}\begin{pmatrix}\dot{\beta}\\ \dot{p}\end{pmatrix}\\ \begin{pmatrix}\delta_{a_{11}}\\ \delta_{r_{11}}\end{pmatrix} = \begin{pmatrix}-2.6474 & -0.9060 & -0.4365 & 10.6931\\ 4.7058 & -1.6641 & -1.8370 & 44.2445\end{pmatrix}\begin{pmatrix}\beta\\ p\\ \varphi\\ r\end{pmatrix} + \begin{pmatrix}10.5651 & -0.2604\\ 44.3784 & -0.0538\end{pmatrix}\begin{pmatrix}\dot{\beta}\\ \dot{p}\end{pmatrix}\end{cases}$
$\boldsymbol{y_{22}} = \begin{pmatrix}\boldsymbol{\beta}\\ \boldsymbol{r}\end{pmatrix}$	$\begin{cases}\begin{pmatrix}\dot{p}_{12}\\ \dot{\varphi}_{12}\end{pmatrix} = \begin{pmatrix}48.9388 & -25.2933 & -28.1109 & 679.5727\\ 0 & 1 & 0 & 6.8856\end{pmatrix}\begin{pmatrix}\beta\\ p\\ \varphi\\ r\end{pmatrix} + \begin{pmatrix}679.7471 & 12.449\\ 0 & 0\end{pmatrix}\begin{pmatrix}\dot{\beta}\\ \dot{r}\end{pmatrix}\\ \begin{pmatrix}\delta_{a_{12}}\\ \delta_{r_{12}}\end{pmatrix} = \begin{pmatrix}-15.3947 & 5.6822 & 6.8856 & -166.3180\\ 2.0702 & -0.3019 & -0.3232 & 7.6473\end{pmatrix}\begin{pmatrix}\beta\\ p\\ \varphi\\ r\end{pmatrix} + \begin{pmatrix}-166.4915 & -3.2428\\ 7.7717 & -0.6704\end{pmatrix}\begin{pmatrix}\dot{\beta}\\ \dot{r}\end{pmatrix}\end{cases}$
$\boldsymbol{y_{23}} = \begin{pmatrix}\boldsymbol{p}\\ \boldsymbol{r}\end{pmatrix}$	$\begin{cases}\begin{pmatrix}\dot{\beta}_{13}\\ \dot{\varphi}_{13}\end{pmatrix} = \begin{pmatrix}-0.0719 & 0.0372 & 0.0413 & -0.9997\\ 0 & 1 & 0 & 0.0357\end{pmatrix}\begin{pmatrix}\beta\\ p\\ \varphi\\ r\end{pmatrix} + \begin{pmatrix}0.0014 & -0.1935\\ 0 & 0\end{pmatrix}\begin{pmatrix}\dot{p}\\ \dot{r}\end{pmatrix}\\ \begin{pmatrix}\delta_{a_{13}}\\ \delta_{r_{13}}\end{pmatrix} = \begin{pmatrix}-3.4080 & -0.5128 & 3.5807 & 0.1307\\ 1.5107 & -0.0127 & -0.0018 & -0.1224\end{pmatrix}\begin{pmatrix}\beta\\ p\\ \varphi\\ r\end{pmatrix} + \begin{pmatrix}-0.2449 & -0.1935\\ 0.0114 & -0.8127\end{pmatrix}\begin{pmatrix}\dot{p}\\ \dot{r}\end{pmatrix}\end{cases}$

Possible sets of outputs and their matching inverse dynamics for the longitudinal model

Possible set	Matching inverse dynamics
$\boldsymbol{y_{31}} = \begin{pmatrix}\boldsymbol{V_x}\\ \boldsymbol{\alpha}\\ \boldsymbol{q}\end{pmatrix}$	$\begin{cases}\dot{\theta}_{31} = \begin{pmatrix}5.4249 & 2417.1 & -342.2218 & 2.8658\end{pmatrix}\begin{pmatrix}V_x\\ \alpha\\ q\\ \theta\end{pmatrix} + \begin{pmatrix}6.0179 & 339.5382 & -5.8668\end{pmatrix}\begin{pmatrix}\dot{V}_x\\ \dot{\alpha}\\ \dot{q}\end{pmatrix}\\ \begin{pmatrix}\delta_{e_{31}}\\ \delta_{RTh_{31}}\\ \delta_{LTh_{31}}\end{pmatrix} = \begin{pmatrix}-0.0929 & -4.7372 & 5.0370 & 0.0271\\ 16.9521 & 738.4531 & -1052.6 & 19.6245\\ -37.2968 & -1678.79 & 2380.12 & -9.0309\end{pmatrix}\begin{pmatrix}V_x\\ \alpha\\ q\\ \theta\end{pmatrix} + \begin{pmatrix}0.0343 & -5.2386 & -0.1810\\ 37.7783 & 1041.02 & -18.1146\\ -22.4011 & -2354.36 & 40.5529\end{pmatrix}\begin{pmatrix}\dot{V}_x\\ \dot{\alpha}\\ \dot{q}\end{pmatrix}\end{cases}$
$\boldsymbol{y_{32}} = \begin{pmatrix}\boldsymbol{V_x}\\ \boldsymbol{q}\\ \boldsymbol{\theta}\end{pmatrix}$	$\begin{cases}\dot{q}_{32} = \begin{pmatrix}0.9247 & 41.2002 & -58.3409 & -0.0613\end{pmatrix}\begin{pmatrix}V_x\\ \alpha\\ q\\ \theta\end{pmatrix} + \begin{pmatrix}1.0258 & 57.8750 & -0.1705\end{pmatrix}\begin{pmatrix}\dot{V}_x\\ \dot{\alpha}\\ \dot{q}\end{pmatrix}\\ \begin{pmatrix}\delta_{e_{32}}\\ \delta_{RTh_{32}}\\ \delta_{LTh_{32}}\end{pmatrix} = \begin{pmatrix}-0.2603 & -12.1950 & 15.5976 & -0.0613\\ 0.2018 & -7.8697 & 4.2239 & 10.7767\\ 0.2018 & -7.8697 & 14.2239 & 10.7767\end{pmatrix}\begin{pmatrix}V_x\\ \alpha\\ q\\ \theta\end{pmatrix} + \begin{pmatrix}-0.1514 & -15.7148 & 0.0309\\ 19.1969 & -7.3578 & 3.0877\\ 19.1969 & -7.3578 & -6.9123\end{pmatrix}\begin{pmatrix}\dot{V}_x\\ \dot{\alpha}\\ \dot{q}\end{pmatrix}\end{cases}$
$\boldsymbol{y_{33}} = \begin{pmatrix}\boldsymbol{\alpha}\\ \boldsymbol{q}\\ \boldsymbol{\theta}\end{pmatrix}$	$\begin{cases}\dot{V}_{x_{33}} = \begin{pmatrix}-0.9015 & -40.1651 & 56.8752 & -0.4762\end{pmatrix}\begin{pmatrix}V_x\\ \alpha\\ q\\ \theta\end{pmatrix} + \begin{pmatrix}-56.4210 & 0.9749 & 0.1662\end{pmatrix}\begin{pmatrix}\dot{V}_x\\ \dot{\alpha}\\ \dot{q}\end{pmatrix}\\ \begin{pmatrix}\delta_{e_{33}}\\ \delta_{RTh_{33}}\\ \delta_{LTh_{33}}\end{pmatrix} = \begin{pmatrix}-0.1238 & -6.1142 & 6.9870 & 0.0108\\ -17.1033 & -778.9164 & 1096.1 & 1.6357\\ -17.1033 & -778.9164 & 1096.1 & 1.6357\end{pmatrix}\begin{pmatrix}V_x\\ \alpha\\ q\\ \theta\end{pmatrix} + \begin{pmatrix}-7.1730 & -0.1476 & 0.0057\\ -1090.5 & 18.7147 & 6.2776\\ -1090.5 & 18.7147 & -3.7224\end{pmatrix}\begin{pmatrix}\dot{V}_x\\ \dot{\alpha}\\ \dot{q}\end{pmatrix}\end{cases}$

APPENDIX V

GEOMETRIC APPROACH FORMULATION

Considering the system described by:

$$\begin{cases} \dot{x}(t) = f(x) + g(x)u(t) \\ y(t) = h(x) \end{cases} \quad \text{(A V–1)}$$

And assuming that a set of numbers $\{r_i\}$ called relative degrees exists such that for $1 \leq i \leq p$ outputs and $1 \leq j \leq m$ inputs, the following conditions then apply (De Persis et Isidori, 2001), (Chaib et al., 2009b) and (Chaib et al., 2009a):

$$\begin{cases} dL_{f(x)}^{r_i-1} h_i(b_j) \neq 0 \\ dL_{f(x)}^{k-1} h_i(b_s) = 0, \forall s \neq j \; and \; 1 \leq k \leq r_i \end{cases} \quad \text{(A V–2)}$$

The term $L_{f(x)}^{r_i-1} h_i(b_j)$ is called the $(r_i - 1)^{\text{th}}$ Lie Derivative of $h_i(x)$ in the direction of the vector field $f(x)$. The sub-manifold surface S_b is expressed as follows:

$$S_b = \left\{ x \coloneqq L_{f(x)}^{r_i-1} h_i(x) = 0, for \; 1 \leq i \leq p \right\} \quad \text{(A V–3)}$$

The matrix σ is defined as follows:

$$\sigma = \begin{pmatrix} L_{f(x)}^{r_1-1} h_1(x) \\ \vdots \\ L_{f(x)}^{r_p-1} h_p(x) \end{pmatrix} \quad \text{(A V–4)}$$

The gradient of σ determined by ∇σ will take the following form:

$$\nabla\sigma^T = \begin{pmatrix} dL_{f(x)}^{r_1-1} h_1(x) \\ \vdots \\ dL_{f(x)}^{r_p-1} h_p(x) \end{pmatrix} = \begin{pmatrix} \frac{\partial}{\partial x_1} L_{f(x)}^{r_1-1} h_1(x) & \cdots & \frac{\partial}{\partial x_n} L_{f(x)}^{r_1-1} h_1(x) \\ \vdots & \ddots & \vdots \\ \frac{\partial}{\partial x_1} L_{f(x)}^{r_p-1} h_p(x) & \cdots & \frac{\partial}{\partial x_n} L_{f(x)}^{r_p-1} h_p(x) \end{pmatrix} \quad \text{(A V–5)}$$

If $p = m$, then the form of matrix A_{proj} is as follows:

$$A_{proj} = \nabla\sigma^T g = \begin{pmatrix} g_1 \frac{\partial}{\partial x_1} L_{f(x)}^{r_1-1} h_1(x) & \cdots & g_m \frac{\partial}{\partial x_n} L_{f(x)}^{r_1-1} h_1(x) \\ \vdots & \ddots & \vdots \\ g_1 \frac{\partial}{\partial x_1} L_{f(x)}^{r_p-1} h_p(x) & \cdots & g_m \frac{\partial}{\partial x_n} L_{f(x)}^{r_p-1} h_p(x) \end{pmatrix} \quad \text{(A V–6)}$$

To construct the projector Π, two conditions must be met:

- The rank of A_{proj} must be equal to m
- $dL_{f(x)}^{r_i-1} h_i(x),\ 1 \le i \le p$ must be linearly independent

The projector Π is defined as follows:

$$\Pi(x) = I_{m\times m} - g{A_{proj}}^{-1} \nabla\sigma^T \quad \text{(A V–7)}$$

$\Pi(x)$ must satisfy three characteristics:

$$\begin{cases} \Pi^2(x) = \Pi(x) \\ \Pi(x) g = 0 \\ \Pi(x)^T \nabla\sigma = 0 \end{cases} \quad \text{(A V–8)}$$

Once the projector designed, the aircraft dynamics is decomposed as follows:

$$\dot{x}(t) = \Pi(x) f(x) + g{A_{proj}}^{-1} \nabla\sigma^T f(x) + g(x) u_f(t) \quad \text{(A V–9)}$$

where $u_f(t)$ is the faulty inputs vector which can be reconstructed via the minimum inverse dynamics as follows:

$$\begin{cases} \dot{x}(t) = \Pi f(x) + g{A_{proj}}^{-1} \dot{y} \\ u_f(t) = {A_{proj}}^{-1} (\dot{y} - \nabla\sigma^T f(x)) \end{cases} \quad \text{(A V–10)}$$

If $p > m$, two approaches are suggested. The first approach consists in adding a set of dummy directions, $G = \{g_i\}, 1 \le i \le p - m$ such that:

$$\begin{cases} g_i dL_{f(x)}^{r_j-1} h_j(x) = 1, \ j = m + i \\ g_i dL_{f(x)}^{r_k} h_j(x) = 0, \ 1 \leq k \leq r_j - 1, j \neq m + i \end{cases} \quad \text{(A V–11)}$$

Then, the projector $\Pi(x)$ will be expressed as follows:

$$\Pi(x) = I_{m\times m} - \bar{g}{\bar{A}_{proj}}^{-1} \nabla\sigma^T \quad \text{(A V–12)}$$

where:

$$\bar{A}_{proj} = \left(A_{proj} \middle| \nabla\sigma^T g\right) \quad \text{(A V–13)}$$

Another way to obtain $\bar{A}_{proj}$ is to use the augmented matrix $\bar{g} = [g \ G]$; in that case, $\bar{A}_{proj}$ is expressed as follows:

$$\bar{A}_{proj} = \nabla\sigma^T \bar{g} \quad \text{(A V–14)}$$

where $\bar{A}_{proj}$ has a rank equal to p.

Once the projector is designed, the aircraft dynamics can be decomposed as follows:

$$\dot{x}(t) = \Pi(x) f(x) + \bar{g}(x){\bar{A}_{proj}}^{-1} \nabla\sigma^T f(x) + \bar{g}(x)\bar{u}_f(t) \quad \text{(A V–15)}$$

such that $\bar{u}_f = \left({u_f}^T \ 0_{(p-m)\times 1}^{\mathrm{T}}\right)$ and $0_{(p-m)\times 1}^T$ is the null vector of dimension $p - m$. The minimum inverse dynamics are then defined as follows:

$$\begin{cases} \dot{x}(t) = \Pi(x) f(x) + \bar{g}(x){\bar{A}_{proj}}^{-1} \dot{y}(t) \\ u_f(t) = \Gamma{\bar{A}_{proj}}^{-1} \left(\dot{y}(t) - \nabla\sigma^T f(x)\right) \end{cases} \quad \text{(A V–16)}$$

where: $\Gamma = \begin{pmatrix} I_{m\times m} & 0_{m\times(p-m)} \\ 0_{(p-m)\times m} & 0_{(p-m)\times(p-m)} \end{pmatrix}$.

The second approach involves designing a multi projector using k possible output subsets. Each subset comprises m independent outputs. The reconstructed fault inputs are provided by each sub-projector $\Pi^i(x)$.

The projector $\Pi^i(x)$ is defined as follows:

$$\Pi^i(x) = I_{m\times m} - g(x){A^i_{proj}}^{-1}\nabla\sigma^{T^i}, i = 1, \dots, k \qquad \text{(A V–17)}$$

Once the projector is designed, the aircraft dynamics can be decomposed as follows:

$$\dot{x}^i(t) = \Pi^i(x)f(x) + g(x){A^i_{proj}}^{-1}\nabla\sigma^{T^i}f(x) + g(x)u^i_f(t) \qquad \text{(A V–18)}$$

To optimize the fault reconstruction, appropriate fusion algorithms such as those based on EKF theory can be used.

Additional details are provided elsewhere in (Chaib et al., 2009b) and (Chaib et al., 2009a).

APPENDIX VI

EXTENDED KALMAN FILTER THERORY

In real situation, dynamic equation is described as follows (Kalman, 1960):

$$\begin{cases} \dot{x}(t) = f(x) + g(x)u(t) + \eta_w(t) \\ y(t) = h(x) + \eta_v(t) \end{cases} \quad \text{(A VI–1)}$$

where, $\eta_w(t)$ is the process noise vector, described by its process noise covariance matrix $R_W = E\{\eta_w {\eta_w}^T\}$, and $\eta_v(t)$ is the measurements noise vector, described by its measurement noise covariance matrix $R_V = E\{\eta_v {\eta_v}^T\}$. T_s is defined as the sampling time of the system. The control input vector at time step $t_i = iT_s$ is defined as u_i. For one step time $t_i = iT_s, i = 1, \dots, n$, equations used in EKF are described as follows:

Step 1: Define the initial state estimate $\hat{x}_{i/i-1} = \hat{x}_{0/-1}$ and the initial state error covariance matrix $P_{i/i-1} = P_{0/-1}$ and enter the sensors' measurements y_i.

Step 2: Design of the continuous dynamics and output matrices F_i and H_i

$$\begin{cases} F_i = \left.\frac{\partial f(x)}{\partial x}\right|_{x=\hat{x}_{i/i}, u=u_i} \\ H_i = \left.\frac{\partial h(x)}{\partial x}\right|_{x=\hat{x}_{i/i}, u=u_i} \end{cases} \quad \text{(A VI–2)}$$

Step 3: Design of the transition matrix ϕ_i

$$\phi_i \approx I_{n\times n} + T_s F_i \quad \text{(A VI–3)}$$

Step 4: Gain matrix computation K_{EKF_i} **:** It is a function of the last propagated state error covariance matrix $P_{i/i-1}$, and of the measurement noise covariance matrix R_V.

$$K_{EKF_i} = P_{i/i-1} H_i^T \left(H_i^T P_{i/i-1} H_i^T + R_V\right)^{-1} \quad \text{(A VI–4)}$$

Step 5: Measurement update

5.1 State estimation update: It is a function of the Kalman gain K_{EKF_i}, the measurement vector y_i, the estimated measurement vector $h(\hat{x}_{i/i-1})$ and the last extrapolated state estimate $\hat{x}_{i/i-1}$.

$$\hat{x}_{i/i} = \hat{x}_{i/i-1} + K_{EKF_i}\left(y_i(t) - h(\hat{x}_{i/i-1})\right) \quad \text{(A VI–5)}$$

5.2 State error covariance matrix update: It is recursively computed as a function of the last predicted state error covariance matrix $P_{i/i-1}$ and the last computed Kalman gain matrix K_{EKF_i}.

$$P_{i/i} = \left(I_{n\times n} - K_{EKF_i}H_i^T\right)P_{i/i-1} \quad \text{(A VI–6)}$$

Step 6: Measurements forward propagation

6.1 State vector forward propagation**:** The state vector is evaluated at the discrete time step $t_i = iT_s$.

$$\hat{x}_{i+1/i} = \hat{x}_{i/i} + \left(f(\hat{x}_{i/i}) + g(\hat{x}_{i/i})u_i(t)\right)T_s \quad \text{(A VI–7)}$$

6.2 State error covariance matrix forward propagation: It is computed as a function of the last state error covariance matrix updated $P_{i/i}$, the discrete process noise $\eta_w(t)$ acting on the elements of the state vector and the discrete transition matrix ϕ_i.

$$R_{W_i} = G_i R_W G_i^T \quad \text{(A VI–8)}$$

$$G_i = T_s \frac{\partial g(x)}{\partial x}\Big|_{x=\hat{x}_{i/i},u=u_i} \quad \text{(A VI–9)}$$

$$P_{i+1/i} = \phi_i P_{i/i}\phi_i^T + R_{W_i} \quad \text{(A VI–10)}$$

LIST OF PUBLICATIONS

Papers published in refereed journals

Ghodbane, Azeddine, Maarouf Saad, Jean-François Boland et Claude Thibeault. 2014. « Applied Cosmic Rays Fault Accommodation in Flight Control Systems using Fault Reconstruction based FDD and SMC Reconfiguration ». *International Journal of Computer, Information, Systems and Control Engineering,* vol. 8, n^{o} 7, p. 1141-1146.

Ghodbane, Azeddine, Maarouf Saad, Christelle Hobeika, Jean-François Boland et Claude Thibeault. 2016. « Design of a Tolerant Flight Control System Capable of Reconfiguring in Response to Multiple Faults Induced by Cosmic Rays ». *IEEE Transactions on Aerospace and Electronic Systems,* vol. 52, n^{o} 2, p. 981-697.

Papers submitted to refereed journals

Ghodbane, Azeddine, Maarouf Saad, Jean-François Boland et Claude Thibeault. « Reconfigurable Flight Control System Using Multi-Projector-Based Geometric Approach and Sliding Mode technique ». *Journal of the Franklin Institute, Elsevier,* submitted on May 2016.

Papers published in refereed conference proceedings:

Ghodbane, Azeddine, Maarouf Saad, Jean-François Boland et Claude Thibeault. 2012. « Fault-Tolerant Flight Control System using EMMAE method and reconfiguration with Sliding Mode Technique ». In *IN: 2012 Electrical & Computer Engineering (CCECE 2012), 25th IEEE Canadian Conference, Montreal, Canada, April 29-May 2, 2012, Proceedings.* DOI 10.1109/CCECE.2012.6335041.

Ghodbane, Azeddine, Maarouf Saad, Jean-François Boland et Claude Thibeault. 2013. « Design of an Actuator Fault-Tolerant Flight Control System Using Fault Detection and Diagnosis ». In *IN: 2013 AeroTech Congress and Exhibition (SAE 2013), Montreal, Canada, September 24-26, 2013, Proceedings.* DOI 10.4271/2013-01-2138.

Ghodbane, Azeddine, Maarouf Saad, Jean-François Boland et Claude Thibeault. 2014. « Applied Cosmic Rays Fault Accommodation in Flight Control Systems using Fault Reconstruction based FDD and SMC Reconfiguration ». In *IN: 2014 International Conference on Modelling, Identification and Control Engineering, (ICMICE 2014), Prague, Czech Republic, July 10-11, 2014, Proceedings.*

Ghodbane, Azeddine, Maarouf Saad, Jean-François Boland et Claude Thibeault. 2014. « Sliding Mode Reconfigurable Control for Cosmic Rays Faults in Flight Systems ». In *IN: 2014 International Mechanical Engineering Congress & Exposition, (ASME*

2014), Montreal, Canada, November 14-20, 2014, Proceedings. DOI:10.1115/IMECE2014-38118.

Ghodbane, Azeddine, Maarouf Saad, Jean-François Boland et Claude Thibeault. 2014. « Fault-Tolerant Control System Using a Multiple Time Scale SMC technique and a Geometric Approach ». In *IN: 2016 International Conference on Control, Dynamic Systems, and Robotics, (ICCDSR 2016), Amsterdam, The Netherlands, August 4-5, 2016, Proceedings*.

Posters in refereed conferences

Ghodbane, Azeddine, Maarouf Saad, Jean-François Boland et Claude Thibeault. 2015. « Design of an Actuator Fault-Tolerant Flight Control System Using Fault Detection and Diagnosis. Case studied: AFTI-F16, Triple actuator fault ». In *IN: 2015 Regroupement Stratégique en Microsystèmes à Québec (ReSMiQ), Association Francophone pour le savoir ACFAS Congres, (ACFAS 2015), Rimouski, Canada, May 25-29, 2015.*

Ghodbane, Azeddine, Maarouf Saad, Jean-François Boland et Claude Thibeault. 2014. « Design of Actuator's Faults Tolerant Flight Control Systems Using Fault Detection and Diagnosis Process ». In *IN: 2014 7th Forum of the Consortium de recherche et d'innovation en aérospatiale au Québec, (CRIAQ 2015), Montreal, Canada, April 16-17, 2014.*

Ghodbane, Azeddine, Maarouf Saad, Jean-François Boland et Claude Thibeault. 2013. « Design of an Actuator Fault-Tolerant Flight Control System Using Fault Detection and Diagnosis ». In *IN: 2013 2013 AeroTech Congress and Exhibition (SAE 2012), Montreal, Canada, September 24-26, 2013.*

BIBLIOGRAPHY

Abdolhosseini, Mahyar, Youmin M Zhang et Camille Alain Rabbath. 2012. « Trajectory tracking with model predictive control for an unmanned quad-rotor helicopter: theory and flight test results ». In *Intelligent Robotics and Applications*. p. 411-420. Springer.

Abzug, Malcolm J, et E Eugene Larrabee. 2005. *Airplane stability and control: a history of the technologies that made aviation possible*, 14. Cambridge University Press.

Alexander, BXS, Richard Rarick et Lili Dong. 2008. « A novel application of an extended state observer for high performance control of NASA's HSS flywheel and fault detection ». In *American Control Conference*. p. 5216-5221.

Alwi, Halim, et Christopher Edwards. 2005. « Fault tolerant control of a civil aircraft using a sliding mode based scheme ». In *Decision and Control, 2005 and 2005 European Control Conference. CDC-ECC'05. 44th IEEE Conference on*. p. 1011-1016. IEEE.

Alwi, Halim, et Christopher Edwards. 2006. « Sliding mode FTC with on-line control allocation ». In *Decision and Control, 2006 45th IEEE Conference on*. p. 5579-5584. IEEE.

Alwi, Halim, et Christopher Edwards. 2008. « Fault tolerant control using sliding modes with on-line control allocation ». *Automatica,* vol. 44, n° 7, p. 1859-1866.

Alwi, Halim, Christopher Edwards et Chee Pin Tan. 2011. *Fault detection and fault-tolerant control using sliding modes*. Springer Science & Business Media.

Asadi, Ghazanfar, et Mehdi B Tahoori. 2005. « Soft error rate estimation and mitigation for SRAM-based FPGAs ». In *Proceedings of the 2005 ACM/SIGDA 13th international symposium on Field-programmable gate arrays*. p. 149-160. ACM.

Atul Garg, Rezawana Islam Linda, Tonoy Chowdhury. 2013. « Evolution of Aircraft Flight Control System and Fly-By-Light Flight Control System ». *International Journal of Emerging technology and advanced Engineering,* vol. 3, n° 12, p. 5.

Bandyopadhyay, Bijnan, Fulwani Deepak et Kyung-Soo Kim. 2009. *Sliding mode control using novel sliding surfaces*, 392. springer.

Bandyopadhyay, Bijnan, Sivaramakrishnan Janardhanan et Sarah K Spurgeon. 2013. *Advances in sliding mode control: concept, theory and implementation*, 440. Springer.

Barfield, A Finley, et JJ D'Azzo. 1983. « Multivariable control laws for the AFTI/F-16 ». Air University.

Barnett, Arnold, John Menighetti et Matthew Prete. 1992. « The Market Response to the Sioux City DC-10 Crash ». *Risk Analysis,* vol. 12, n° 1, p. 45-52.

Bartolini, Giorgio, Leonid Fridman, Alessandro Pisano et Elio Usai. 2008. « Modern sliding mode control theory ». *Lecture Notes in Control and Information Sciences,* vol. 375, n° 7, p. 23-49.

Bates, D., et M. Hagström. 2007. *Nonlinear Analysis and Synthesis Techniques for Aircraft Control*. Springer Berlin Heidelberg.

Baumann, Robert C. 2005. « Radiation-induced soft errors in advanced semiconductor technologies ». *Device and Materials Reliability, IEEE Transactions on,* vol. 5, n° 3, p. 305-316.

Beard, Richard Vernon. 1971. « Failure accomodation in linear systems through self-reorganization ». Massachusetts Institute of Technology.

Belcastro, Celeste M, Kenneth Eure et Richard Hess. 2006. « Testing a flight control system for neutron-induced disturbances ». *Los Alamos Science,* vol. 30, p. 104.

Bemporad, Alberto, et Manfred Morari. 1999. « Robust model predictive control: A survey ». In *Robustness in identification and control*. p. 207-226. Springer.

Benoit, William L, et Anne Czerwinski. 1997. « A critical analysis of USAir's image repair discourse ». *Business Communication Quarterly,* vol. 60, n° 3, p. 38-57.

Benosman, Mouhacine, Fang Liao, Kai-Yew Lum et Jian Liang Wang. 2009. « Nonlinear control allocation for non-minimum phase systems ». *Control Systems Technology, IEEE Transactions on,* vol. 17, n° 2, p. 394-404.

Blanke, Mogens, Roozbeh Izadi-Zamanabadi, Søren A Bøgh et Charlotte P Lunau. 1997. « Fault-tolerant control systems—a holistic view ». *Control Engineering Practice,* vol. 5, n° 5, p. 693-702.

Boiko, Igor, Leonid Fridman, Alessandro Pisano et Elio Usai. 2009. « On the transfer properties of the “generalized sub-optimal” second-order sliding mode control algorithm ». *Automatic Control, IEEE Transactions on,* vol. 54, n° 2, p. 399-403.

Bonfe, Marcello, Paolo Castaldi, Silvio Simani et Matteo Benini. 2009. « Nonlinear Geometric Approach-Based Filtering Methods for Aircraft Actuator FDI ». In *Fault Detection, Supervision and Safety of Technical Processes*. p. 639-644.

Boškovic, Jovan D, et Raman K Mehra. 2002. « Multiple-model adaptive flight control scheme for accommodation of actuator failures ». *Journal of Guidance, Control, and Dynamics,* vol. 25, n° 4, p. 712-724.

Brambilla, Daniele, Luca Massimiliano Capisani, Antonella Ferrara et Pierluigi Pisu. 2008. « Fault detection for robot manipulators via second-order sliding modes ». *Industrial Electronics, IEEE Transactions on,* vol. 55, n° 11, p. 3954-3963.

Brogley, M. 2009. « FPGA reliability and the sunspot cycle ». *White Paper, Actel*.

Bureau, Australian Transport Safety. 2008. *AO-2008-070: In-flight upset, 154 km west of Learmonth, WA, 7 October 2008, VH-QPA*. airbus a330-303. Technical report.

Calise, Anthony J, Seungjae Lee et Manu Sharma. 2001. « Development of a reconfigurable flight control law for tailless aircraft ». *Journal of Guidance, Control, and Dynamics,* vol. 24, n° 5, p. 896-902.

Castillo, Pedro, Laura E Munoz et Omar Santos. 2014. « Robust Control Algorithm for a Rotorcraft Disturbed by Crosswind ». *IEEE Transactions on Aerospace and Electronic Systems,* vol. 1, n° 50, p. 756-763.

Chaib, S, D Boutat, A Benali et F Kratz. 2007. « A foliation for unknown inputs reconstruction ». In *Nonlinear Control Systems*. Vol. 7, p. 810-815.

Chaib, S, D Boutat, A Benali et F Kratz. 2009a. « Failure detection and reconstruction in switched nonlinear systems ». *Nonlinear Analysis: Hybrid Systems,* vol. 3, n° 3, p. 225-238.

Chaib, S, M Saad, SC Abou et D Boutat. 2009b. « Detection of actuator faults in flight control systems ». *Canadian Aeronautics and Space Journal,* vol. 55, n° 3, p. 133-143.

Chapman, Ken, et Les Jones. 2010. « SEU strategies for Virtex-5 devices ». *Xilinx Corporation,* vol. 20.

Chen, Robert H, et Jason L Speyer. 2004. « Sensor and actuator fault reconstruction ». *Journal of Guidance, Control, and Dynamics,* vol. 27, n° 2, p. 186-196.

Chen, Shuhao, Gang Tao et Suresh M Joshi. 2004. « Adaptive actuator failure compensation designs for linear systems ». *International Journal of Control Automation and Systems,* vol. 2, p. 1-14.

Cheng, Qi, Pramod K Varshney et CM Belcastro. 2008. « Fault detection in dynamic systems via decision fusion ». *Aerospace and Electronic Systems, IEEE Transactions on,* vol. 44, n° 1, p. 227-242.

Chow, Edward Y, et Alan S Willsky. 1984. « Analytical redundancy and the design of robust failure detection systems ». *Automatic Control, IEEE Transactions on,* vol. 29, n° 7, p. 603-614.

Chowdhary, Girish, et Ravindra Jategaonkar. 2010. « Aerodynamic parameter estimation from flight data applying extended and unscented Kalman filter ». *Aerospace science and technology,* vol. 14, n° 2, p. 106-117.

Christopher, E, L Thomas et S Hafid. 2010. « Fault tolerant flight control–a benchmark challenge ». *Lecture Notes in Control and Information Sciences,* vol. 399.

Ciubotaru, Bogdan, Marcel Staroswiecki et Cyrille Christophe. 2006. « Fault tolerant control of the Boeing 747 short-period mode using the admissible model matching techn ». In *Fault Detection, Supervision and Safety of Technical Processes*. Vol. 6, p. 819-824.

Collinson, Richard PG. 2013. *Introduction to avionics systems*. Springer Science & Business Media.

Corradini, ML, G Orlando et G Parlangeli. 2006. « Actuator failures compensation: a sliding mode control approach ». In *Control and Automation, 2006. MED'06. 14th Mediterranean Conference on*. p. 1-6. IEEE.

Danecek, Vit, et Pavel Silhavy. 2011. « The Fault-tolerant control system based on majority voting with Kalman filter ». In *Telecommunications and Signal Processing (TSP), 2011 34th International Conference on*. p. 472-477. IEEE.

De Persis, C, et A Isidori. 2000. « On the observability codistributions of a nonlinear system ». *Systems & control letters,* vol. 40, n° 5, p. 297-304.

De Persis, Claudio, Raffaella De Santis et Alberto Isidori. 2001. « Nonlinear actuator fault detection and isolation for a VTOL aircraft ». In *IN: 2001 American Control Conference, Arlington, VA, June 25-27, 2001, Proceedings.* Vol. 6, p. 4449-4454. Citeseer.

De Persis, Claudio, et Alberto Isidori. 2001. « A geometric approach to nonlinear fault detection and isolation ». *Automatic Control, IEEE Transactions on,* vol. 46, n° 6, p. 853-865.

Ducard, G, et HP Geering. 2006. « A reconfigurable flight control system based on the EMMAE method ». In *American Control Conference, 2006*. p. 6 pp.: IEEE.

Ducard, Guillaume JJ. 2009. *Fault-tolerant flight control and guidance systems: Practical methods for small unmanned aerial vehicles*. Springer Science & Business Media.

Edwards, Christopher, Enric Fossas Colet et Leonid Fridman. 2006. *Advances in variable structure and sliding mode control*. Springer Verlag.

Edwards, Christopher, Thomas Lombaerts et Hafid Smaili. 2010. « Fault tolerant flight control ». *Lecture Notes in Control and Information Sciences,* vol. 399.

Edwards, Christopher, et Sarah Spurgeon. 1998. *Sliding mode control: theory and applications*. CRC Press.

Eslinger, Capt Robert A, et Phillip R Chandler. 1988. « Self-repairing flight control system program overview ». In *Aerospace and Electronics Conference, 1988. NAECON 1988., Proceedings of the IEEE 1988 National*. p. 504-511. IEEE.

Etkin, Bernard, et Lloyd Duff Reid. 1996. *Dynamics of flight: stability and control*, 3. Wiley New York.

Fallaha, Charles J, Maarouf Saad, Hadi Youssef Kanaan et Kamal Al-Haddad. 2011. « Sliding-mode robot control with exponential reaching law ». *Industrial Electronics, IEEE Transactions on,* vol. 58, n^{o} 2, p. 600-610.

Fan, Jinhua, Youmin Zhang et Zhiqiang Zheng. 2013. « Adaptive observer-based integrated fault diagnosis and fault-tolerant control systems against actuator faults and saturation ». *Journal of Dynamic Systems, Measurement, and Control,* vol. 135, n^{o} 4, p. 041008.

Fisher, James Robert. 2005. « Aircraft control using nonlinear dynamic inversion in conjunction with adaptive robust control ». Texas A&M University.

Forssell, Lars, et Ulrik Nilsson. 2005. *Admire the aero-data model in a research environment version 4.0, model description*. FOI-Totalförsvarets forskningsinstitut.

Fossen, Thor I. 2011. « Mathematical models for control of aircraft and satellites ». *Department of Engineering Cybernetics Norwegian University of Science and Technology*.

Fridman, Leonid, Jorge Davila et Arie Levant. 2011. « High-order sliding-mode observation for linear systems with unknown inputs ». *Nonlinear Analysis: Hybrid Systems,* vol. 5, n^{o} 2, p. 189-205.

Gao, Zhiqiang, et Panos J Antsaklis. 1991. « Stability of the pseudo-inverse method for reconfigurable control systems ». *International Journal of Control,* vol. 53, n^{o} 3, p. 717-729.

Gao, Zhiqiang, et Panos J Antsaklis. 1992. « Reconfigurable control system design via perfect model following ». *International Journal of Control,* vol. 56, n^{o} 4, p. 783-798.

Garvin, David A. 1988. « Boeing 767: From Concept to Production (A) ».

Gertler, Janos. 1991. « Analytical redundancy methods in fault detection and isolation ». In *Preprints of IFAC/IMACS Symposium on Fault Detection, Supervision and Safety for Technical Processes SAFEPROCESS'91*. p. 9-21.

Gertler, Janos. 1998. *Fault detection and diagnosis in engineering systems*. CRC press.

Ghodbane, A, M Saad, JF Boland et C Thibeault. 2014. « Applied Actuator Fault Accommodation in Flight Control Systems Using Fault Reconstruction Based FDD and SMC Reconfiguration ». *International Journal of Computer, Control, Quantum and Information Engineering,* vol. 8.

Hajiyev, Chingiz, et Fikret Caliskan. 2013. *Fault diagnosis and reconfiguration in flight control systems*, 2. Springer Science & Business Media.

Hamayun, Mirza Tariq, Chris Edwards et Halim Alwi. 2012. « Design and analysis of an integral sliding mode fault-tolerant control scheme ». *Automatic Control, IEEE Transactions on,* vol. 57, n° 7, p. 1783-1789.

Hamayun, Mirza Tariq, Chris Edwards et Halim Alwi. 2014. « Augmentation scheme for fault-tolerant control using integral sliding modes ». *Control Systems Technology, IEEE Transactions on,* vol. 22, n° 1, p. 307-313.

Hammouri, Hassan, Michel Kinnaert et EH El Yaagoubi. 1999. « Observer-based approach to fault detection and isolation for nonlinear systems ». *Automatic Control, IEEE Transactions on,* vol. 44, n° 10, p. 1879-1884.

Hess, RA, et SR Wells. 2003. « Sliding mode control applied to reconfigurable flight control design ». *Journal of Guidance, Control, and Dynamics,* vol. 26, n° 3, p. 452-462.

Hobeika, Christelle, Simon Pichette, Azeddine Ghodbane, Claude Thibeault, Yves Audet, Jean-François Boland et Maarouf Saad. 2013. *Flight Control Fault Models Based on SEU Emulation*. SAE Technical Paper.

Holzapfel, Florian, et Gottfried Sachs. 2004. « Dynamic inversion based control concept with application to an unmanned aerial vehicle ». In *AIAA Guidance, Navigation, and Control Conference and Exhibit*. p. 16-19.

Hsieh, Chien-Shu. 2000. « Robust two-stage Kalman filters for systems with unknown inputs ». *Automatic Control, IEEE Transactions on,* vol. 45, n° 12, p. 2374-2378.

Hsu, Liu, et Ramon R Costa. 1989. « Variable structure model reference adaptive control using only input and output measurements: Part 1 ». *International Journal of control,* vol. 49, n° 2, p. 399-416.

Hsu, Liu, et Ramon R Costa. 1990. « A binary control approach to design globally exponentially stable systems ». In *Proceedings of the 7 th International Conference on Systems Engineering, Las Vegas, July.[Links]*.

Hsu, Liu, Aldayr Dantas de Araújo et Ramon R Costa. 1994. « Analysis and design of I/O based variable structure adaptive control ». *Automatic Control, IEEE Transactions on,* vol. 39, n° 1, p. 4-21.

Hsu, Liu, Fernando Lizarralde et Aldayr D De Araújo. 1997. « New results on output-feedback variable structure model-reference adaptive control: Design and stability analysis ». *Automatic Control, IEEE Transactions on,* vol. 42, n° 3, p. 386-393.

Hu, Ching, et Suhail Zain. 2010. « NSEU mitigation in avionics applications ». *Xilinx Application Note XAPP1073 v1. 0*.

Hwang, Inseok, Sungwan Kim, Youdan Kim et Chze Eng Seah. 2010. « A survey of fault detection, isolation, and reconfiguration methods ». *Control Systems Technology, IEEE Transactions on,* vol. 18, n° 3, p. 636-653.

Isermann, Rolf. 2006. *Fault-diagnosis systems: an introduction from fault detection to fault tolerance*. Springer Science & Business Media.

Isermann, Rolf, et Peter Ballé. 1997. « Trends in the application of model-based fault detection and diagnosis of technical processes ». *Control engineering practice,* vol. 5, n° 5, p. 709-719.

Ishmael, Stephen D, Victoria A Regenie et Dale A Mackall. 1984. *Design Implications From AFTI/F-16 Flight Test*. National Aeronautics and Space Administration, Ames Research Center, Dryden Flight Research Facility.

Ishmael, Steven D, et Donald R McMonagle. 1983. *AFTI/F-16 flight test results and lessons*. National Aeronautics and Space Administration, Ames Research Center, Dryden Flight Research Facility.

Isidori, Alberto. 1995. *Nonlinear control systems*. Springer Science & Business Media.

Ito, Daigoro. 2001. *Robust dynamic inversion controller design and analysis (using the X-38 vehicle as a case study)*.

Jassemi-Zargani, Rahim, et DS Necsulescu. 2001. *Extended Kalman Filter Sensor Fusion Signals of Nonlinear Dynamic Systems*. DTIC Document.

Jones, Harold Lee. 1973. « Failure detection in linear systems ». Massachusetts Institute of Technology.

Kale, MM, et AJ Chipperfield. 2004. « Robust and stabilized MPC formulations for fault tolerant and reconfigurable flight control ». In *Intelligent Control, 2004. Proceedings of the 2004 IEEE International Symposium on*. p. 222-227. IEEE.

Kale, MM, et AJ Chipperfield. 2005. « Stabilized MPC formulations for robust reconfigurable flight control ». *Control Engineering Practice,* vol. 13, n° 6, p. 771-788.

Kalman, Rudolph Emil. 1960. « A new approach to linear filtering and prediction problems ». *Journal of Fluids Engineering,* vol. 82, n° 1, p. 35-45.

Kim, Ki-Seok, Keum-Jin Lee et Youdan Kim. 2003. « Reconfigurable flight control system design using direct adaptive method ». *Journal of Guidance, Control, and Dynamics,* vol. 26, n° 4, p. 543-550.

Kinnersley, Steve, et Alfred Roelen. 2007. « The contribution of design to accidents ». *Safety Science,* vol. 45, n° 1, p. 31-60.

Konstantopoulos, Ioannis K, et Panos J Antsaklis. 1996. « Eigenstructure assignment in reconfigurable control systems ». *ISIS,* vol. 96, p. 001.

Landry, Mario. 2012. « Commande de vol non-linéaire en temps réel d'un drone à voilure fixe ». École de technologie supérieure.

Lemaignan, Benoit. 2005. « Flying with no flight controls: Handling qualities analyses of the baghdad event ». In *AIAA Atmospheric Flight Mechanics Conference, AIAA-2005-5907*.

Li, Qingdong, Zhang Ren, Shicong Dai et Wei Wang. 2013. « A new robust fault-tolerant controller for self-repairing flight control system ». *Journal of the Franklin Institute,* vol. 350, n° 9, p. 2509-2518.

Li, Yuankai, Zhongliang Jing et Guangjun Liu. 2014. « Maneuver-Aided Active Satellite Tracking Using Six-DOF Optimal Dynamic Inversion Control ». *Aerospace and Electronic Systems, IEEE Transactions on,* vol. 50, n° 1, p. 704-719.

Liu, Jun S, et Rong Chen. 1998. « Sequential Monte Carlo methods for dynamic systems ». *Journal of the American statistical association,* vol. 93, n° 443, p. 1032-1044.

Liu, Wei, Hongwen He et Fengchun Sun. 2016. « Vehicle State Estimation Based on Minimum Model Error Criterion Combining with Extended Kalman Filter ». *Journal of the Franklin Institute*.

Lombaerts, TJJ, QP Chu, JA Mulder et DA Joosten. 2007. « Real time damaged aircraft model identification for reconfiguring flight control ». In *AIAA Atmospheric Flight Mechanics Conference and Exhibit, Hilton Head, SC, USA*. p. 1207-1231.

Maciejowski, Jan, et Colin Jones. 2003. « MPC fault-tolerant flight control case study: Flight 1862 ». In *Proceedings of the International Federation of Automatic Control on Safeprocess Sympoisum*. p. 119-124.

Maciejowski, Jan M, et Mihai Huzmezan. 1997. « Predictive control ». In *Robust Flight Control*. p. 125-134. Springer.

Magni, J, S Bennani et J Terlouw. 1997. « Robust Flight Control: A Design Challenge, Vol. 224 (Lecture notes in Control and Information Sciences) ». In.: Springer, Berlin.

Marcos, Andres, Subhabrata Ganguli et Gary J Balas. 2005. « An application of H∞ fault detection and isolation to a transport aircraft ». *Control Engineering Practice,* vol. 13, n^{o} 1, p. 105-119.

Massoumnia, Mohammad-Ali. 1986. « A geometric approach to the synthesis of failure detection filters ». *Automatic Control, IEEE Transactions on,* vol. 31, n^{o} 9, p. 839-846.

Maurer, Richard H, Martin E Fraeman, Mark N Martin et David R Roth. 2008. « RHarsh Environments: Space Radiation ». *Johns Hopkins APL technical digest,* vol. 28, n^{o} 1, p. 17.

McLean, Donald. 1990. *Automatic flight control systems(Book)*. Coll. « Englewood Cliffs, NJ, Prentice Hall, 1990, 606 ».

Mechhoud, Sarah, Emmanuel Witrant, Luc Dugard et Didier Moreau. 2015. « Estimation of heat source term and thermal diffusion in tokamak plasmas using a Kalman filtering method in the early lumping approach ». *Control Systems Technology, IEEE Transactions on,* vol. 23, n^{o} 2, p. 449-463.

Meskin, Nader, et Khashayar Khorasani. 2011. *Fault Detection and Isolation: Multi-Vehicle Unmanned Systems*. Springer Science & Business Media.

Meskin, Nader, E Naderi et Khashayar Khorasani. 2013. « A multiple model-based approach for fault diagnosis of jet engines ». *Control Systems Technology, IEEE Transactions on,* vol. 21, n^{o} 1, p. 254-262.

Montoya, R Jorge, WE Howell, WT Bundick, AJ Ostroff, RM Hueschen et Christine M Belcastro. 1983. *Restructurable controls*, 2277. National Aeronautics and Space Administration, Scientific and Technical Information Branch Washington, DC and Springfield, VA.

Morse, WD, et A Ossman. 1990. « Model following reconfigurable flight control system for the AFTI/F-16 ». *Journal of Guidance, Control, and Dynamics,* vol. 13, n° 6, p. 969-976.

Muske, Kenneth R, Hashem Ashrafiuon, Sergey Nersesov et Mehdi Nikkhah. 2012. « Optimal sliding mode cascade control for stabilization of underactuated nonlinear systems ». *Journal of Dynamic Systems, Measurement, and Control,* vol. 134, n° 2, p. 021020.

Narendra, Kumpati S, Osvaldo A Driollet, Matthias Feiler et Koshy George. 2003. « Adaptive control using multiple models, switching and tuning ». *International journal of adaptive control and signal processing,* vol. 17, n° 2, p. 87-102.

Nelson, Robert C. 1998. *Flight stability and automatic control*, 2. WCB/McGraw Hill.

NIMA. 2000. « Department of Defense World Geodetic System 1984, Its Definition and Relationships With Local Geodetic Systems ». *Technical report*.

Noura, Hassan, Didier Theilliol, Jean-Christophe Ponsart et Abbas Chamseddine. 2009. *Fault-tolerant control systems: Design and practical applications*. Springer Science & Business Media.

NTSB/AAR-03/02. 2003. *Loss of Pitch Control on Takeoff Emery Worldwide Airlines, Flight 17 McDonnell Douglas DC-8-71F, N8079U Rancho Cordova, California February 16, 2000*. PB2003-910302. Washington, D.C.: National Transportation Safety Board.

NTSB/AAR-04/01. 2004. *Loss of Pitch Control During Takeoff Air Midwest Flight 5481 Raytheon (Beechcraft) 1900D, N233YV Charlotte, North Carolina January 8, 2003*. PB2004-910401. Washington, D.C.: National Transportation Safety Board.

Oliveira, TR, AJ Peixoto, EVL Nunes et L Hsu. 2007. « Control of uncertain nonlinear systems with arbitrary relative degree and unknown control direction using sliding modes ». *International Journal of Adaptive Control and Signal Processing,* vol. 21, n° 8-9, p. 692-707.

Pastor, Enric, Juan Lopez et Pablo Royo. 2007. « UAV payload and mission control hardware/software architecture ». *Aerospace and Electronic Systems Magazine, IEEE,* vol. 22, n° 6, p. 3-8.

Patton, RJ, et J Chen. 1991. « Robust fault detection using eigenstructure assignment: a tutorial consideration and some new results ». In *Decision and Control, 1991., Proceedings of the 30th IEEE Conference on*. p. 2242-2247. IEEE.

Patton, Ron J, et Jie Chen. 1994. « Review of parity space approaches to fault diagnosis for aerospace systems ». *Journal of Guidance, Control, and Dynamics,* vol. 17, n° 2, p. 278-285.

Patton, Ron J, Paul M Frank et Robert N Clark. 2013. *Issues of fault diagnosis for dynamic systems*. Springer Science & Business Media.

Pawlowski, Brian J. 1989. *Multivariable Flight Control Design with Parameter Uncertainty for the AFTI/F-16*. DTIC Document.

Perruquetti, Wilfrid, et Jean-Pierre Barbot. 2002. *Sliding mode control in engineering*. CRC Press.

Pitt, Michael K, et Neil Shephard. 1999. « Filtering via simulation: Auxiliary particle filters ». *Journal of the American statistical association,* vol. 94, n° 446, p. 590-599.

Qinglei, HU, Youmin Zhang, HUO Xing et XIAO Bing. 2011. « Adaptive integral-type sliding mode control for spacecraft attitude maneuvering under actuator stuck failures ». *Chinese Journal of Aeronautics,* vol. 24, n° 1, p. 32-45.

Qiu, HZ, HY Zhang et XF Sun. 2005. « Solution of two-stage Kalman filter ». *IEE Proceedings-Control Theory and Applications,* vol. 152, n° 2, p. 152-156.

Quinn, Heather, Paul Graham, Jim Krone, Michael Caffrey et Sana Rezgui. 2005. « Radiation-induced multi-bit upsets in SRAM-based FPGAs ». *IEEE Transactions on Nuclear Science,* vol. 52, n° 6, p. 2455-2461.

Quinn, Heather M, Dolores A Black, William H Robinson et Stephen P Buchner. 2013. « Fault simulation and emulation tools to augment radiation-hardness assurance testing ». *Nuclear Science, IEEE Transactions on,* vol. 60, n° 3, p. 2119-2142.

Ren, Zhang, Wei Wang et Zhen Shen. 2011. « New robust fault-tolerant controller for self-repairing flight control systems ». *Systems Engineering and Electronics, Journal of,* vol. 22, n° 1, p. 77-82.

Roshany-Yamchi, Samira, Marcin Cychowski, Rudy R Negenborn, Bart De Schutter, Kieran Delaney et Joe Connell. 2013. « Kalman filter-based distributed predictive control of large-scale multi-rate systems: Application to power networks ». *Control Systems Technology, IEEE Transactions on,* vol. 21, n° 1, p. 27-39.

Roskam, Jan. 2003. *Airplane Flight Dynamics and Automatic Flight Controls*. DARcorporation.

Rupp, D, G Ducard, E Shafai et HP Geering. 2005. « Extended multiple model adaptive estimation for the detection of sensor and actuator faults ». In *Decision and Control,*

2005 and 2005 European Control Conference. CDC-ECC'05. 44th IEEE Conference on. p. 3079-3084. IEEE.

Shah, Muhammad Zamurad, Raza Samar et Aamer Iqbal Bhatti. 2015. « Guidance of air vehicles: A sliding mode approach ». *Control Systems Technology, IEEE Transactions on,* vol. 23, n° 1, p. 231-244.

Sharma, R, et M Aldeen. 2011. « Fault, State, and Unknown Input Reconstruction in Nonlinear Systems Using Sliding Mode Observers ». *Journal of Dynamic Systems, Measurement, and Control,* vol. 133, n° 5, p. 051013.

Shen, Qiang, Danwei Wang, Senqiang Zhu et Eng Kee Poh. 2015. « Integral-Type Sliding Mode Fault-Tolerant Control for Attitude Stabilization of Spacecraft ». *Control Systems Technology, IEEE Transactions on,* vol. 23, n° 3, p. 1131-1138.

Shijie, Jin Lei Xu. 2008. « Extended state observer-based fault detection and recovery for flywheels [J] ». *Journal of Beijing University of Aeronautics and Astronautics,* vol. 11, p. 007.

Shin, D, G Moon et Y Kim. 2005. « Design of reconfigurable flight control system using adaptive sliding mode control: actuator fault ». *Proceedings of the Institution of Mechanical Engineers, Part G: Journal of Aerospace Engineering,* vol. 219, n° 4, p. 321-328.

Shin, Jong-Yeob, Christine Belcastro et Thuan Khong. 2006. « Closed-loop evaluation of an integrated failure identification and fault tolerant control system for a transport aircraft ». In *AIAA Guidance, Navigation and Control Conference*. Vol. 9.

Shivakumar, Premkishore, Michael Kistler, Stephen W Keckler, Doug Burger et Lorenzo Alvisi. 2002. « Modeling the effect of technology trends on the soft error rate of combinational logic ». In *Dependable Systems and Networks, 2002. DSN 2002. Proceedings. International Conference on*. p. 389-398. IEEE.

Shtessel, Yuri B, et Ilia A Shkolnikov. 2003. « Aeronautical and space vehicle control in dynamic sliding manifolds ». *International Journal of Control,* vol. 76, n° 9-10, p. 1000-1017.

Shtessel, Yuri, James McDuffie et Mark Jackson. 1998. « Sliding mode control of the X-33 vehicle in launch and re-entry modes ». In *Proceedings of the AIAA guidance, navigation, and control conference and exhibit*. p. 1352-1362.

Slotine, Jean-Jacques E, et Weiping Li. 1991. *Applied nonlinear control*, 199. 1. Prentice-hall Englewood Cliffs, NJ.

Smaili, MH, Jan Breeman, TJJ Lombaerts et DA Joosten. 2006. « A simulation benchmark for integrated fault tolerant flight control evaluation ». In *AIAA modeling and simulation technologies conference and exhibit*. p. 21-24.

Staroswiecki, M. 2003. « Fault tolerant control ». In *Aalborg seminar*.

Staroswiecki, M. 2005. « Fault tolerant control: the pseudo-inverse method revisited ». In *16th IFAC World Congress*.

Stevens, Brian L, et Frank L Lewis. 2003. *Aircraft control and simulation*. John Wiley & Sons.

Taber, Allen H, et Eugene Normand. 1995. *Investigation and Characterization of SEU Effects and Hardening Strategies in Avionics*. DTIC Document.

Tan, Chee Pin, et Christopher Edwards. 2002. « Sliding mode observers for robust fault detection & reconstruction ». In *Proceedings of the 1FAC World Congress, Barcelona*.

Tandale, MD, et J Valasek. 2005. « Issues on integration of fault diagnosis and reconfigurable control in active fault-tolerant control systems ». In *Proceedings of the 2005 American Control Conference*.

Tao, Gang, Shuhao Chen et Suresh M Joshi. 2002. « An adaptive control scheme for systems with unknown actuator failures ». *Automatica,* vol. 38, n^{o} 6, p. 1027-1034.

Tao, Gang, Shuhao Chen, Xidong Tang et Suresh M Joshi. 2013. *Adaptive control of systems with actuator failures*. Springer Science & Business Media.

Thumati, Balaje T, et Gary R Halligan. 2013. « A novel fault diagnostics and prediction scheme using a nonlinear observer with artificial immune system as an online approximator ». *Control Systems Technology, IEEE Transactions on,* vol. 21, n^{o} 3, p. 569-578.

Tomayko, James E, et Christian Gelzer. 2003. *The Story of Self-Repairing Flight Control Systems*. NASA Dryden Flight Research Center.

Utkin, VI. 1992. *Sliding modes in optimization and control problems*. Springer Verlag, New York.

Venkata, M, et Raghu Chaitanya. 2009. « Model Based Aircraft Control System Design and Simulation ».

Vetter, TK, SR Wells et Ronald A Hess. 2003. « Designing for damage—robust flight control design using sliding mode techniques ». *Proceedings of the Institution of*

Mechanical Engineers, Part G: Journal of Aerospace Engineering, vol. 217, n° 5, p. 245-261.

Wang, An-Ping, et Sheng-Fuu Lin. 2000. « The parametric solutions of eigenstructure assignment for controllable and uncontrollable singular systems ». *Journal of mathematical analysis and applications,* vol. 248, n° 2, p. 549-571.

Wang, Nengmou, et Hojjat Adeli. 2012. « Algorithms for chattering reduction in system control ». *Journal of the Franklin Institute,* vol. 349, n° 8, p. 2687-2703.

Wang, Tao. 2012. « Sliding Mode Fault Tolerant Reconfigurable Control against Aircraft Control Surface Failures ». Concordia University.

Wells, Scott R. 2002. *Application of sliding mode methods to the design of reconfigurable flight control systems*. DTIC Document.

White, John E, et Jason L Speyer. 1987. « Detection filter design: Spectral theory and algorithms ». *Automatic Control, IEEE Transactions on,* vol. 32, n° 7, p. 593-603.

Witczak, Marcin. 2007. *Modelling and estimation strategies for fault diagnosis of non-linear systems: from analytical to soft computing approaches*, 354. Springer Science & Business Media.

Wu, N Eva. 2002. « Reliability analysis for AFTI-F16 SRFCS using ASSIST and SURE ». In *American Control Conference, 2002. Proceedings of the 2002*. Vol. 6, p. 4795-4800. IEEE.

Xiong, Yi, et Mehrdad Saif. 2000. « Robust fault detection and isolation via a diagnostic observer ». *International Journal of Robust and Nonlinear Control,* vol. 10, n° 14, p. 1175-1192.

Xu, Yunjun. 2008. « Chattering free robust control for nonlinear systems ». *Control Systems Technology, IEEE Transactions on,* vol. 16, n° 6, p. 1352-1359.

Yang, Hanlong, et Mehrdad Saif. 1995. « Fault detection in a class of nonlinear systems via adaptive sliding observer ». In *Systems, Man and Cybernetics, 1995. Intelligent Systems for the 21st Century., IEEE International Conference on*. Vol. 3, p. 2199-2204. IEEE.

Yang, Zhenyu, Mogens Blanke et Michel Verhaegen. 2007. « Robust control mixer method for reconfigurable control design using model matching ». *Control Theory & Applications, IET,* vol. 1, n° 1, p. 349-357.

Yen, Gary G, et Liang-Wei Ho. 2003. « Online multiple-model-based fault diagnosis and accommodation ». *Industrial Electronics, IEEE Transactions on,* vol. 50, n° 2, p. 296-312.

Yoney, D. 2010. *Cessna Developing Electric-Powered 172 Skyhawk, 2010*.

Zhang, Qinghua, Fabien Campillo, Frédéric Cerou et François LeGland. 2005. « Nonlinear system fault detection and isolation based on bootstrap particle filters ». In *Decision and Control, 2005 and 2005 European Control Conference. CDC-ECC'05. 44th IEEE Conference on*. p. 3821-3826. IEEE.

Zhang, Xian, et Pierluigi Pisu. 2014. « Sliding Mode Observer and State-Machine-Based Fault Diagnosis With Application in a Vehicle Chassis Steering System ». *Journal of Dynamic Systems, Measurement, and Control,* vol. 136, n° 4, p. 041026.

Zhang, Xiaodong, Thomas Parisini et Marios M Polycarpou. 2004. « Adaptive fault-tolerant control of nonlinear uncertain systems: an information-based diagnostic approach ». *Automatic Control, IEEE Transactions on,* vol. 49, n° 8, p. 1259-1274.

Zhang, YM, A Chamseddine, CA Rabbath, BW Gordon, C-Y Su, S Rakheja, C Fulford, J Apkarian et P Gosselin. 2013. « Development of advanced FDD and FTC techniques with application to an unmanned quadrotor helicopter testbed ». *Journal of the Franklin Institute,* vol. 350, n° 9, p. 2396-2422.

Zhang, YM, et Jin Jiang. 2002. « Active fault-tolerant control system against partial actuator failures ». *IEE proceedings-Control Theory and applications,* vol. 149, n° 1, p. 95-104.

Zhang, Youmin, et Jin Jiang. 2001. « Fault tolerant control systems design with consideration of performance degradation ». In *American Control Conference, 2001. Proceedings of the 2001*. Vol. 4, p. 2694-2699. IEEE.

Zhang, Youmin, et Jin Jiang. 2008. « Bibliographical review on reconfigurable fault-tolerant control systems ». *Annual reviews in control,* vol. 32, n° 2, p. 229-252.

Zhang, Youmin, et Didier Theilliol. 2007. « Reconfigurable control allocation against partial control effector faults in aircraft ». In *3rd International Conference on Advances in Vehicle Control and Safety, AVCS 2007*. p. CDROM.

Zheng, Bo-Chao, et Ju H Park. 2016. « Sliding mode control design for linear systems subject to quantization parameter mismatch ». *Journal of the Franklin Institute,* vol. 353, n° 1, p. 37-53.

Zhou, Kemin, et John Comstock Doyle. 1998. *Essentials of robust control*, 180. Prentice hall Upper Saddle River, NJ.

Zhou, Qing-Li, YM Zhang, Camille-Alain Rabbath et Jacob Apkarian. 2010. « Two reconfigurable control allocation schemes for unmanned aerial vehicle under stuck actuator failures ». In *Proceedings of AIAA Guidance, Navigation, and Control Conference, AIAA*.

Ziegler, J. F. 1998. « Terrestrial cosmic ray intensities ». *Ibm Journal of Research and Development,* vol. 42, n° 1, p. 117-139.

Zolghadri, Ali, David Henry, Jérôme Cieslak, D Efimov et Philippe Goupil. 2014. « Fault diagnosis and fault-tolerant control and guidance for aerospace vehicles ». *Advances in Industrial Control. Springer Edts: London, Heidelberg, New York, Dordrecht*.